Università degli Studi di Sassasi

Doctoral Thesis

Quantifying the dynamics of Root Distribution and Root Reinforcement of Forest Tree Species and their Applications in Forest Management

Author:
Ha My NGO
Matricola no.
50050273

Supervisor:
Prof. Filippo Giadrossich
Prof. Massimiliano Schwarz

A thesis submitted in fulfillment of the requirements for the degree of Doctor of Philosophy in Agriculture

Curriculum of Monitoring and control of agricultural and forest ecosystems in the Mediterranean environment
Department of Agricultural Sciences - XXXVII Cycle

September 10, 2025

Declaration of Authorship

I, Ha My NGO, declare that this thesis titled, “Quantifying the dynamics of Root Distribution and Root Reinforcement of Forest Tree Species and their Applications in Forest Management” and the work presented in it are my own. I confirm that:

- This work was done entirely or mainly while in candidature for a research degree at the University of Sassari, Italy.
- Where any part of this thesis has previously been submitted for a degree or any other qualification at the University of Sassari, Italy or any other institution, this has been clearly stated.
- Where I have consulted the published work of others, this is always clearly attributed.
- Where I have quoted from the work of others, the source is always given. With the exception of such quotations, this thesis is entirely my own work.
- I have acknowledged all main sources of help.
- Where the thesis is based on work done by myself jointly with others, I have made clear exactly what was done by others and what I have contributed myself.

Signed: 

Date: 09/09/2025

"*It always seems impossible until it's done.*"

Nelson Mandela

UNIVERSITÀ DEGLI STUDI DI SASSASI

Abstract

Curriculum of Monitoring and control of agricultural and forest ecosystems in the Mediterranean environment
Department of Agricultural Sciences - XXXVII Cycle

Doctor of Philosophy in Agriculture

Quantifying the dynamics of Root Distribution and Root Reinforcement of Forest Tree Species and their Applications in Forest Management

by Ha My NGO

Tree roots play a vital role in ecosystem services, including soil stabilization, erosion control, and carbon sequestration. However, quantifying root distribution, root reinforcement, and belowground biomass remains a major scientific challenge, given complexity of root systems, high variability in site conditions, and lack of spatially explicit field data. The thesis addresses these challenges by combining fieldwork data and advanced modeling techniques to evaluate ecological role of tree roots in stabilizing slopes and sequestering carbon. The work focuses on "Tasman" poplar in New Zealand and *Cryptomeria japonica* in Switzerland and Japan. For poplars, fieldwork was carried out around 4 trees and 10 pits from sparse to dense planting zones. Root properties were assessed through laboratory and field pullout tests. Root Distribution Model predicted well root spatial patterns, particularly in sparse zone and mature individuals whereas overestimated roots in dense zone. Root Reinforcement Model underestimated root force in a single tree root system but performed better in pits in sparse zone. Poplars need at least 20 years for minimal lateral root reinforcement at the stand scale and 30 years for effective shallow landslide stabilization depending on their disposition. A single mature tree can store over 170 kg of carbon in its roots, highlighting its significant potential for climate change mitigation. For *Cryptomeria japonica*, coarse root distribution was consistent between Switzerland and Japan while basal root reinforcement differed, with Swiss stand exhibited stronger reinforcement in the upper soil layer while Japanese stand showed a deeper root anchorage. This work provides a unique and comprehensive dataset on root distribution and reinforcement of poplar and cryptomeria. Developed models support slope stability assessments, planning of bioengineering interventions, and carbon accounting frameworks in forestry and land management.

Keywords: Root Reinforcement; Root Distribution; Shallow Landslides; Carbon storage; Forestry Management

Acknowledgements

I would like to express my deepest heartfelt gratitude to all those who have supported me with enthusiasm and kindness throughout my academic journey, leading to this significant achievement.

First and foremost, I am wholeheartedly thankful to my two supervisors, Professor Filippo Giadrossich and Professor Massimiliano Schwarz. I extend my sincerest thanks to Professor Giadrossich for granting me this one-of-a-kind opportunity, for his unwavering belief in me, and for his warm and continuous support throughout my entire PhD. His sincere guidance, generous advice, constant encouragement, and genuine kindness gave me strength and direction in shaping my work. I am also deeply thankful to him for offering me the opportunity to continue working with him beyond my PhD and for placing his trust in me to contribute to his ongoing research projects. His confidence in my abilities means a lot and has been a significant source of my motivation and professional growth.

I am truly grateful to Professor Massimiliano Schwarz for the academic independence he entrusted to me in pursuing this research. His insightful guidance, constructive feedback, patience, and encouragement to thinking critically have had a lasting impact on my academic and professional growth. I sincerely appreciate him for offering me the opportunity to continue working alongside him even before completing my PhD. I am especially pleased that we successfully got a bilateral research project between Switzerland and Vietnam, which I will carry forward in the coming years. This opportunity has given me the valuable chance to further collaborate and continue learning under his mentorship.

I would also like to express my sincere appreciation to Professor Severino Zara for his kind support with administrative documentation and for always taking the time to answer my questions related to it, to Professor Angelo for providing me an accommodation at the UNISS guesthouse during short stays, and to Dr. Mao Zhun for initially connecting me with this PhD opportunity.

Being part of a collaborative PhD project has given me the incredible privilege of having two more families in two countries. Whether in Italy or Switzerland, my colleagues and friends have always made me feel at home.

To my Italian family, a special mention goes to Dr. Hassan Awada for his sincere and thoughtful advice. Thank you, Dr. Tefera Meron Lakew, for hosting me and protecting me like your little sister. A big shout-out to Dr. Ilenia Murgia for her guidance and support during the early stages of my PhD journey. To Dr. Simone Di Prima, thank you for the great conversations, advice, and the unforgettable home party. And to my dearest friends Elisa, Francesca, “Regina” Ilaria, Bozin, and Peppe - you guys are simply the best!

To my Swiss family, heartfelt thanks to Feiko, Niels, Dominik, Marceline, Adeline, and Kim for your kindness and unwavering support. Your motivation and energy inspired me every day, and working alongside such talented people taught me to be tougher, stronger, and braver. I’m also grateful to Christof and Patrick for their valuable help during fieldwork. Thank you all for many unforgettable memories we created together, especially in the fieldworks. Working with you has truly brought out the best in me, and I’ve grown into a better version of myself thanks to your support, inspiration, and encouragement.

Ha My NGO
PhD course "Agricultural Sciences" Cycle XXXVII - Università degli Studi di Sassasi


I am immensely grateful to the University of Sassari (UNISS) for its foundational support and for providing the infrastructure and academic environment that enabled the successful completion of my PhD. The university's commitment to research and academic excellence played a great role in shaping this work. I also extend my thank to the School of Agricultural, Forest and Food Sciences (BFH-HAFL) for their generous financial support and fellowship, which significantly enhanced the depth, quality, and impact of my research.

Last but by no means least, I would like to express my deepest gratitude to my big family in Vietnam for their unwavering love and encouragement - a constant source of strength through this journey. To my husband, Hoang Anh Thai: thank you for walking this path with me and for your constant support. Enduring three years of long distance - always moving between Vietnam, France, Italy, and Switzerland - was never easy, but it granted us even more invaluable opportunities to grow, adapt, and discover new things together. One of the most remarkable milestones we shared along the way was our civil marriage in Toulouse, France, on 18 November 2023 - a joyful moment of love and commitment, shared with our families, friends, and the mayor, that added even greater meaning to this chapter in our lives.

As I was writing this thesis, I was carrying "a little bean" - my little, lovely Đậu Đậu - in my belly. She definitely leveled up the game, but at the same time, gave me even more strength and determination to finish my PhD. We wrote this work together. I cannot wait to welcome you into the world, to meet you and to accompany you soon!

Ha My NGO
PhD course "Agricultural Sciences" Cycle XXXVII - Università degli Studi di Sassasi

The first year of my PhD was particularly challenging due to the ongoing COVID-19 pandemic. Yet, I was fortunate to be surrounded by truly incredible people - more than I could have ever hoped for. This PhD journey has given me some of the greatest gifts: inspiring friends, unforgettable travels, countless new experiences, and, above all, a better version of myself.

To all those whose names may not appear here but who have nonetheless played a meaningful part in my PhD journey - your support, kindness, and presence have left a lasting impact. Each of you has, in your own way, contributed to the completion of this work, and for that, I am deeply and wholeheartedly grateful.

Thank you all for your unwavering support - it has really been the cornerstone of this achievement...

Contents

List of Figures

List of Tables

List of Abbreviations

ASL	**A**bove **S**ea **L**evel
CF	**C**arbon **F**raction
DBH	**D**iameter at the **B**reast **H**eight
DW	**D**ry **W**eight
kN	**k**ilo**N**ewton
MAP	**M**ean **A**nnual **P**recipitation
MAT	**M**ean **A**nnual **T**emperature
N	**N**ewton
NZ	**N**ew **Z**ealand
R^2	Coefficient of Determination
RAR	**R**oot **A**rea **R**atio
RBMw	**R**oot **B**undle **M**odel with **W**eibull survival function
RD	**R**oot **D**istribution
RDM	**R**oot **D**istribution **M**odel
RDW	**R**oot **D**ry **W**eight
RMSE	**R**oot **M**ean **S**quare **E**rror
RR	**R**oot **R**einforcement
RRM	**R**oot **R**einforcement **M**odel
SAE	**S**um of **A**bsolute **E**rrors
SSE	**S**um of **S**quared **E**rrors
sph	**s**tems **p**er **h**ectare
$\mathbf{W}_C$	**W**eight of **C**arbon content
$\mathbf{W}_{CO_2}$	**W**eight of **C**arbon dioxide

To those who is curious about my work ...

Chapter 1

Introduction

1.1 Background

Forest plays a vital role in providing a wide range of ecosystem services, including soil stabilization, erosion control, biodiversity conservation, and carbon sequestration. Among these, the stabilizing effect of tree roots against shallow landslides and soil erosion is especially important in mountainous and hilly regions, where rainfall-induced mass movements frequently threaten both infrastructure and ecosystems. In this situation, tree roots act as natural anchorages in the soil, enhancing the shear strength of the soil by forming an interconnected network that resists mechanical failure.

The mechanical contribution of roots to slope stability, commonly referred to as root reinforcement, has been demonstrated in numerous experimental and modeling studies. Root reinforcement is not only based on the type of tree species but also affected by a range of external factors, including tree size, planting density, stand structure, soil characteristics, and climate conditions. Even though several studies have been done to understand root-soil interaction at the local scale, the spatial quantification and upscaling of root reinforcement to the stand and catchment scale remains a scientific challenge.

Species such as *Populus deltoides* × *nigra* "Tasman" poplar, and *Cryptomeria japonica* have been recognized as valuable species for both ecological restoration and slope stability due to their fast growth, deep rooting systems, and adaptability to various climates. Poplars are widely planted in New Zealand for bioengineering applications, while *Cryptomeria* is a dominant silvicultural species in Japan and has been introduced into European reforestation and climate adaptation programs. However, the ecosystem services provided by these species, particularly their contribution to mechanical slope stabilization and belowground carbon storage across different site conditions, are still missing. A comprehensive dataset of root distribution and root reinforcement, especially at spatial and stand scales, remains a major scientific challenge due to the complex root system, site variability, and limited field data.

To address these gaps, recent advances in modeling techniques such as the Root Distribution Model (RDM), the Root Bundle Model with Weibull survival function (RBMw), and the Root Reinforcement Model (RRM) have been developed to simulate the spatial patterns of root biomass and mechanical reinforcement. These models, when supported by fieldwork and laboratory datasets, can enhance predictive capacity for ecological engineering, bio-stabilization strategies, and climate change adaptation planning. Moreover, with increasing global attention on climate change mitigation and sustainable development, forests are being recognized not only for their aboveground biomass but also for their potential to store significant amounts of carbon in the root systems and soil.

Nevertheless, quantifying belowground carbon stocks is still one of the big gaps in global carbon assessments. Traditional methods based on destructive excavation are labor-intensive, time-consuming, and often impractical at large scales. Thus, the integration of Root Distribution Model with carbon estimation frameworks presents a promising non-destructive approach to improve the accuracy of belowground biomass and carbon stock assessments.

This doctoral thesis aims to bridge the knowledge gap by combining field data, mechanical testing, and spatial modeling approaches to evaluate the role of tree roots in both slope stabilization and carbon sequestration. By examining multiple tree species across different geographical and environmental conditions, the work contributes to a more comprehensive understanding of how forest root systems function as both ecological engineers and carbon sinks, offering insights for bioengineering practices, forest planning, and climate policy frameworks.

1.2 Research objectives

The primary objective of this thesis is to contribute to filling the knowledge gap concerning the role of forests in mitigating shallow landslides, with a particular focus on the spatial distribution pattern and mechanical effects of tree root systems. While root reinforcement has been widely recognized as a key factor in enhancing slope stability, comprehensive data on root distribution, mechanical root properties, and root reinforcement capacity at the stand scale, especially under various tree densities and soil conditions, are still missing.

This PhD work specifically addresses the quantification of the spatial dynamics of root distribution and root reinforcement for two selected tree species (*Populus deltoides* x *nigra*, and *Cryptomeria japonica*), using a combination of field measurements, laboratory testing, and model approaches.

A further key objective of this thesis is to explore the use of the Root Distribution Model (RDM) as a non-destructive tool to estimate root biomass and belowground carbon storage. As global efforts to quantify forest carbon stocks intensify, particularly in the context of climate change mitigation and carbon trading frameworks, precise estimation of belowground carbon storage has become increasingly important.

In summary, the specific objectives of this research are:

1. To calibrate and validate models, including the Root Distribution Model (RDM), the Root Bundle Model with Weibull survival function (RBMw), and the Root Reinforcement Model (RRM) for predicting root distribution patterns and root reinforcement across different tree species under varying tree densities and environmental factors.

2. To quantify root distribution and mechanical properties of selected forest species through field excavations, tensile tests, and in-situ root pullout tests across diverse environmental conditions.

3. To investigate the compatibility of the same tree species in terms of root distribution and root reinforcement grown in different geographical and environmental contexts.

4. To assess the influence of tree size, soil depth, and stand density on root biomass, root distribution patterns, and root reinforcement capacity.

5. To apply the Root Distribution Model for estimating root biomass and carbon sequestration, contributing to the development of a non-destructive and accurate method for assessing belowground carbon storage capacity.

By achieving these objectives, this thesis aims to support the development of practical tools and scientifically grounded models for slope stability assessments, bio-engineering design, and carbon assessment in forest management.

1.3 Thesis structure

Chapter 1: Introduction

Objective: This chapter introduces the background, research objectives, and overall structure of this PhD thesis to provide the reader with a clear understanding of its scope and purpose.

Chapter 2: Literature Review

Objective: This chapter provides an overview of shallow landslides and the role of tree root systems in slope stabilization.

Chapter 3: Quantifying Forest Contributions to Slope Stabilization

Objective: This chapter presents to the reader the models applied throughout the thesis and describes the theoretical background, methodology, and function of each model.

Chapter 4: Analysis of Poplar's (Populus nigra ita.) Root Systems for Quantifying Bio-Engineering Measures in the case study of New Zealand Pastoral Hill Country

Objective: This chapter quantifies the spatial root distribution and root reinforcement of *Populus nigra* ita. to support the implementation of bio-engineering measures in a case study in New Zealand.

This chapter has been published on Forests (MDPI) as: *Ngo, H. M., van Zadelhoff, F. B., Gasparini, I., Plaschy, J., Flepp, G., Dorren, L., Phillips, C., Giadrossich, F., and Schwarz, M. (2023). Analysis of Poplar's (Populus nigra ita.) Root Systems for Quantifying Bio-Engineering Measures in New Zealand Pastoral Hill Country. Forests, 14(6), 1240.* https://doi.org/10.3390/f14061240 (last accessed: 09 September 2025).

Chapter 5: Assess the compatibility of spatial root distribution and root reinforcement of Cryptomeria Japonica D. Don between Switzerland, China and Japan

Objective: This chapter conducts a comparative analysis of root distribution and root reinforcement of *Cryptomeria Japonica* using datasets from different countries.

This chapter was submitted to Ecological Engineering in December 2024 but was declined as it was not considered appropriate for the journal's readership. The manuscript is currently being prepared for resubmission to another journal (status last checked: 09 September 2025).

Chapter 6: Analysis of poplar's (*Populus nigra ita.*) Root Systems for the Assessment of Ecosystem Services in New Zealand's Pastoral Hill Country

Objective: This chapter evaluates the performance of the Root Distribution Model in estimating root biomass and its associated carbon sequestration capability, contributing to ecosystem service quantification.

This chapter is being prepared as a manuscript for submission to a peer-reviewed journal. Status as of 09 September 2025: manuscript in preparation.

Chapter 7: Conclusion, Limitations, and Future Outlook

Objective: This chapter summarizes the main findings of the PhD research, discusses limitations and challenges encountered with the applied models, and outlines future research directions.

Chapter 2

Literature Review

2.1 Shallow landslides

In recent years, landslides have become a hot topic for scientists, engineers, governments, and residents around the world. Google search quickly presents 120,000,000 results with the term *landslide* when searching in March 2025. For researchers, the topic of landslides is popular due to its relation in a wide range of scientific disciplines, including sedimentology, oceanography, geomorphology, volcanology, seismology, glaciology, construction engineering, soil mechanics, climate change, eustasy, natural hazards, and petroleum exploration and production (Shanmugam and Wang, 2015).

The term "landslide" is defined variably across disciplines such as geology, engineering, and related fields, reflecting the complexity and multidisciplinary nature of landslide research. In this research, the term "landslide" denotes the downslope movement of a mass of soils, natural rock, artificial fills, and organic material under the influence of gravity, as well as the landform produced by such movement at varying rates (mm per year to tens of m per second) that may range from a few m^3 up to several km^3 on slopes with a gradient between 90 and less than one degree (Cruden and Varnes, 1996; Hungr, Leroueil, and Picarelli, 2014). Landslides are classified primarily based on the type of movement and secondarily on the type of material involved. Movement types are categorized into five main groups: fall, topple, slide, spread, and flow. A sixth category, known as complex slope movements, includes combinations of two or more of these primary types. The material component is also a key factor that influences the behavior of landslides and is classified as rock or engineering soil. The engineering soil is further divided into *soil*, which consists predominantly of fine-grained particles, and *debris*, which is dominated by larger, coarse fragments (Varnes, 1978).

Landslides occur on all continents and play an important role in landscape evolution, particularly in mountainous regions with steep terrain. These areas are especially prone to slope instability due to a combination of triggering factors, including (1) climate-related factors, (2) seismic activity, (3) volcanic activity, and (4) various human actions. Crozier, 2010 identified six key climate-related factors that influence local slope stability, which are (i) total precipitation, (ii) rainfall intensity, (iii) air temperature, (iv) wind speed and duration, (v) changes in weather systems, and (vi) broader meteorological variability.

Shallow landslides, often referred to as *soil slips*, are among the most frequent, widespread, and hazardous forms of slope instability, particularly in steep, mountainous regions subject to high-intensity rainfall. These downslope movements typically affect superficial soil layers (generally less than 2 meters thick) and volumes of displaced material reaching several hundred cubic meters, with scar areas ranging between 50 to 1000 m^2 (Campbell, 1975; Moser and Hohensinn, 1983; Ellen et al.,

1988; Crosta, 1998). Despite their relatively small soil volume, shallow landslides pose significant hazards due to their rapid onset (velocity of more than 9 m/s), unpredictability, frequent occurrence in large numbers during single storm events, and potential to evolve into destructive debris flows, therefore, causing considerable damages to infrastructure, transportation networks, agriculture, and human life (Ellen and Fleming, 1987; Ellen et al., 1988; Crosta, 1998; Campus et al., 1998; Sidle and Ochiai, 2006; Petley, 2012; Hungr, Leroueil, and Picarelli, 2014).

The initiation of shallow landslides is primarily driven by hydrological triggers, particularly intense or prolonged rainfalls. Shallow landslides commonly occur on steep slopes where a thin, permeable topsoil layer overlies a less permeable subsoil or bedrock (Sidle and Swanston, 1982). This vulnerable stratigraphic configuration creates conditions for water accumulation at the interface, raising pore water pressure, increasing the soil's specific weight, weakening apparent cohesion, reducing soil shear strength, and promoting failure (Caine, 1980; Sidle and Swanston, 1982; Fredlund, 1987; Iverson, Reid, and LaHusen, 1997; Montgomery et al., 1997; Ng and Shi, 1998; Iverson, 2000; Montrasio and Valentino, 2007; Crozier, 2010; Giannecchini, Galanti, and D'Amato Avanzi, 2012). Land-use change (Persichillo, Bordoni, and Meisina, 2017), forest fires (Gehring et al., 2019), road construction (Arbanas and Dugonjić, 2010), and snowmelt (Arghiuş et al., 2011; Trandafir et al., 2015; Chiarelli et al., 2023), which fluctuate the groundwater table, can contribute to slope destabilization. Geotechnical properties, including soil cohesion, permeability, internal friction angle, and soil thickness, are also main factors that influence a slope's susceptibility to failure (Wu and Sidle, 1995). Fine-grained soils, particularly those rich in silt or clay, exhibit low permeability and rapid loss of strength when saturated, making them especially prone to shallow landslides (Tamiru et al., 2024). In seismically active regions, earthquake is another important trigger for shallow landslides. Ground shaking can reduce soil cohesion, disrupt root structures, and induce rapid failure, especially on saturated slopes or those with weak subsoil layers (Keefer, 2002; Malamud et al., 2004; Sidle and Bogaard, 2016). The combination of seismic activity and heavy rainfall is particularly hazardous, often resulting in widespread slope failures during and after earthquake events (Yin, Wang, and Sun, 2009).

The spatial and temporal distribution of shallow landslides is controlled by quasi-static and dynamic variables. Quasi-static variables, such as geology, soil geotechnical properties, elevation, slope gradient, and topographic incision, determine the spatial susceptibility of slopes to failure. On the other hand, dynamic variables, including soil moisture content, root strength, rainfall intensity, and human activities, control the timing of failure (Wu and Sidle, 1995). Rainfall thresholds, defined by intensity and duration, have been proposed to predict the occurrence of landslides, although their application remains challenging due to the complex interactions between rainfall and slope conditions (Caine, 1980; Guzzetti et al., 2004).

Due to the fast and unpredictable nature of shallow landslides, early warning and hazard mitigation are particularly challenging (Campus et al., 1998; Van Westen, Castellanos, and Kuriakose, 2008). Traditional monitoring methods are often ineffective due to the lack of precursory signs, which requires probabilistic and spatially explicit approaches to hazard assessment. Effective risk management requires integrating detailed environmental, geotechnical, hydrological, and land-use data to forecast both the location and timing of potential failures (Van Westen, Castellanos, and Kuriakose, 2008; Corominas et al., 2014). Given climate change projections indicating an increase in the frequency and intensity of extreme rainfall events (Gariano et al., 2017), the development of reliable predictive tools for shallow landslides and risk mitigation has become increasingly urgent.

Their widespread occurrence and capacity for substantial damage make hazard assessment a critical component of sustainable land management, particularly in mountainous regions (Nadim et al., 2006; Guzzetti et al., 2008). A comprehensive understanding of their triggering mechanisms, geotechnical controls, and environmental influences is essential for improving hazard assessment and land-use planning in vulnerable regions. Looking forward, research priorities must address the compounding effects of climate change and anthropogenic activities to enhance predictive capabilities and community resilience. The development of more accurate forecasting methods and effective mitigation strategies will be crucial as extreme weather events become more frequent and human pressure on landscapes intensifies.

2.2 Role of the tree roots

Forests play a substantial role in protecting people, settlements, and resources against a broader spectrum of natural hazards in mountain environments, including erosion, floods, rockfalls, and avalanches (Sidle, 1985; Brang et al., 2001; Schwarz et al., 2010a; Teich et al., 2022; Moos et al., 2023). Their role in hazard mitigation varies with hazard type, forest structure, location relative to hazard zones (e.g., initiation, transition, or accumulation zones), and spatial scale (tree, slope, or catchment).

Mountain forests are particularly vital where human settlements are located in hazard-prone terrain. Without forest cover, large parts of regions such as the Alps would be uninhabitable due to increased exposure to natural hazards. Historical records from the Alps as early as the 13th century reflect local awareness of these protective functions. The earliest documented references to protective forests in the Alps date back to 1333 and 1480, highlighting their role in safeguarding settlements located downslope (Gerbore, 1997).

Forests offer protection against natural hazards in two broad ways: through indirect protection, which includes surface soil conservation and improving watershed conditions and air quality; and through direct protection, such as protecting people, safeguarding infrastructure, and utility corridors. Forests can provide both active protection (e.g., stabilizing erosion or flood initiation areas) and passive protection (e.g., buffering rockfalls or sediment movement). However, for dynamic processes like landslides or avalanches, passive protection is limited, and proactive forest management is essential.

The designation and active management of protection forests are critical to ensure that they retain their protective functions. Protection forests, which are managed specifically to reduce risk from natural hazards, require strategic interventions such as selective thinning and planting of deep-rooted species. Without regeneration or silvicultural attention, the protective function of these forests diminishes over time. In several countries, human activities within protection forests are currently restricted to preserve soil and water resources (Dorren et al., 2004).

2.2.1 Hydrological and Mechanical Effects of tree roots on Slope Stability

Historically, forests have been recognized as natural defenses against slope failures, floods, and avalanches. The stabilizing effect of tree roots on slopes in mitigating hydrogeomorphic hazards, particularly shallow landslides, is well established and operates through both hydrological and mechanical mechanisms. The effectiveness of forest cover in stabilizing slopes depends on its capacity to modulate subsurface water dynamics and reinforce soil structure through root networks.

From a hydrological perspective, suction, evapotranspiration, and infiltration govern soil water balance and runoff at the catchment scale, whereas root reinforcement serves as the key mechanical influence on slope stability at the local scale. Tree roots influence several key processes that collectively delay or prevent the saturation of the soil, a common trigger for shallow landslides.

- **Evapotranspiration and Root Water Uptake**: Tree roots regulate soil moisture through transpiration. They can adsorb soil moisture from the surrounding soil from distances up to three times the crown radius (Gray and Sotir, 1996). When precipitation exceeds evapotranspiration, its impact on soil moisture depletion is negligible. However, before and during moderate rainfall events, evapotranspiration can decrease soil moisture, allowing the soil to absorb more water. In shallow soils, even slight reductions in soil moisture can slow down critical pore pressure accumulation. Furthermore, root water uptake also generates matric suction, providing additional apparent cohesion and shear strength in unsaturated zones.

- **Infiltration and subsurface flows**: Root decay channels and macropores serve as preferential pathways, increasing vertical and lateral infiltration and allowing water to drain more quickly (Vergani et al., 2016; Balzano, Tarantino, and Ridley, 2019). However, these root pathways can also allow water to soak into the ground faster, which may increase the risk of landslides (Vergani et al., 2017b).

From a mechanical perspective, roots enhance soil strength by binding particles, increasing tensile resistance, and intersecting potential failure planes (DR, 1987; Dorren and Schwarz, 2016). Fine roots mobilize their tensile strength through soil-root interaction, while coarse roots contribute frictional resistance along shear planes (DR, 1987). The mechanical behavior of soil can be significantly altered by tree roots through several interrelated processes:

- **Soil reinforcement**: Tree roots serve as natural reinforcements for soil, significantly enhancing slope stability and mitigating the risks of shallow landslides. Root systems of plants enhance soil shear strength through both coarse and fine roots. Following Cohen and Schwarz (2017), there are three different mechanisms of root reinforcement:

(1) **Basal root reinforcement** occurs when roots penetrate the soil layers and cross potential shear planes, increasing the soil's shear strength and anchoring unstable layers to more stable subsoils. It is considered the most effective mechanism when present. However, in many cases, this reinforcement is absent because the failure surface lies below the rooting depth.

(2) **Lateral root reinforcement** operates along the lateral margins of the landslide. The effectiveness of this mechanism depends on the deformation behavior of the landslide mass. If the mass behaves as a rigid body, lateral root reinforcement may be activated simultaneously along all edges - contributing in tension, shear, and compression. In contrast, when differential deformation occurs, lateral root reinforcement is progressively mobilized - initially in tension at the crown, followed by compression at the toe as the landslide evolves. The magnitude of this reinforcement depends on the spatial distribution of the root network.

(3) **Root-induced soil stiffening** enhances the macroscopic stiffness of the rooted soil mass, enabling greater redistribution of stresses across the hillslope during small deformations. This mechanism increases the effects of the two above-mentioned mechanisms.

These reinforcement effects vary by tree species, root architecture, and soil conditions.

- **Buttressing effect**: Tree roots act like natural supports, forming arch-like structures that help resist sliding forces on slopes (Nilaweera and Nutalaya, 1999;

Coppin, Richards, et al., 1990). The interaction between adjacent root systems contributes to arching effects, distributing stress laterally.

- **Deep anchoring**: In upland terrains with shallow soils, roots can extend into rock cracks, providing substantial anchorage and improving overall slope stability (Hasenmueller et al., 2017; Li et al., 2007). This is especially relevant for species with vertical taproots or extensive deep-rooting systems that can bridge weak layers or embed in firm substrates.

- **Rock weathering**: Roots contribute to physical weathering by wedging into bedrock fractures or generating new ones, often in combination with chemical weathering processes (Hasenmueller et al., 2017; Pawlik, Phillips, and Šamonil, 2016). Over time, this can destabilize the rock masses but also enhance anchorage by increasing the depth of root penetration.

Among the aforementioned processes, root reinforcement has been the most extensively studied. Root systems enhance slope stability by reinforcing soil through mechanical interactions. Root reinforcement operates as a fiber-reinforced system where the soil is strong in compression but weak in tension, and roots complement this by being strong in tension but weak in compression. This complementary interaction forms a composite soil–root matrix, enabling stress transfer and improved resistance to shearing. The effectiveness of root reinforcement depends on several parameters: (1) Root morphology, (2) Topography, and (3) Tree age. In the aspect of root morphology, small roots tend to have higher tensile strength due to higher cellulose content, while larger roots contribute more anchoring depth. Root behavior during shearing also differs: fine roots tend to break in place, whereas coarse roots can be pulled out of the soil without breaking (Ennos, 1990). Therefore, a combination of dense fine roots in the top layer and coarse roots that penetrate deeply into potential shear surfaces is the most effective configuration for slope and riverbank stabilization (Reubens et al., 2007). In the aspect of topography, environmental conditions such as soil moisture, soil fertility, nutrient availability, and soil mechanical properties may alter cellulose deposition, affecting root tensile strength. Within the same species, roots from convex slope areas exhibited higher tensile strength than those in concave hollows (Hales et al., 2009). In the aspect of tree age, this factor also influences the root reinforcement level. Dazio, Conedera, and Schwarz (2018) found that over-aging chestnut trees had a negative influence on the root reinforcement, whereas coppiced stands had a positive effect on slope stability.

The influence of vegetation is highly site-specific, influenced by factors such as species type, root morphology, soil texture, and climate (DR, 1987; Schmidt et al., 2001; Glade, 2003). Numerous studies have confirmed the stabilizing role of vegetation, especially forests, and have shown that land use changes such as deforestation, agricultural expansion, forest fire, or intensive harvesting lead to a marked increase in shallow landslide frequency due to the loss of root cohesion and alteration in hydrological pathways, particularly once root systems begin to decay several years after forest removal (Ziemer, 1981; Sidle and Wu, 1999; Vergani et al., 2016; Vergani et al., 2017a; Gehring et al., 2019). The decline in root cohesion post-harvest can last for over a century in some forest types, reducing slope stability long after logging. Previous research has demonstrated a strong correlation between slope failures and timber harvesting on steep terrain, suggesting the need for further investigation into how changes in stand density influence root reinforcement dynamics.

Trees are vulnerable to natural disturbances such as beetle outbreaks, storms, and wildfires, as well as anthropogenic interventions including forestry production, tree felling, fire control strips, and species replacement. Following tree death, the soil root

reinforcement progressively declines due to the loss of mechanical strength and stiffness. Root decay can increase soil porosity and facilitate water infiltration, thereby intensifying weathering and potentially initiating shallow landslides (O'Loughlin, 1974; Sidle, 1992; Johnson and Wilcock, 2002; Reubens et al., 2007; Ammann et al., 2009). As evidenced by an event in the last decade in Tuscany, such large-scale die-offs, when followed by intense rainfall or rapid snowmelt, can significantly compromise slope stability and pose serious geomorphological hazards.

The role of roots in soil reinforcement has been studied for several decades through experiments, field campaigns, and modeling. However, the complexity and heterogeneity of vegetation-soil interactions, along with their rapid spatial and temporal variability, make their effects difficult to model at broader scales (Glade, 2003; Persichillo, Bordoni, and Meisina, 2017). Root reinforcement can be quantified using various approaches (Sidle and Ochiai, 2006; Giadrossich et al., 2013a): (1) laboratory tests of tensile or cutting strength on individual roots of varying diameters; (2) laboratory direct shear tests on root-soil samples; (3) in situ tests using cut boxes within root-soil zone; (4) laboratory tests of cutting strength opposed by a roots column; (5) uprooting tests on stumps or entire plants; (6) back-analysis of soil failures after storm events; (7) field root pullout tests.

The scientific literature has provided a substantial amount of site-specific data, emphasizing a wide spatial and temporal variability of root reinforcement. Modeling approaches have evolved significantly from early efforts in the late 1970s (Burroughs and Thomas, 1977; Waldron, 1977; Wu, McKinnell III, and Swanston, 1979) to more advanced methods (Cohen, Schwarz, and Or, 2011; Pollen and Simon, 2005; Schwarz, Giadrossich, and Cohen, 2013). Most models integrate root biomechanical properties with their density and spatial distribution, simulating root development over time using concepts such as the pipe model theory (Shinozaki et al., 1964a; Shinozaki et al., 1964c) and the static fractal branching at the single-tree scale (Tobin et al., 2007). Another widely applied empirical approach relates root diameter to biomechanical properties (Wu, McKinnell III, and Swanston, 1979). Some of these models upscale root reinforcement to the stand scale by assuming a decreasing root density with increasing distance from the tree stem (Schwarz, Lehmann, and Or, 2010). A widely applied model for quantifying root reinforcement is the Root Bundle Model with Weibull survival function (RBMw), developed by Schwarz, Giadrossich, and Cohen, 2013. This model assumes that the amount of force transmitted by roots relies on their deformation and follows the Weibull survival function, accounting for variability in root strength.

Forests that are specifically managed to mitigate natural hazards, such as shallow landslides and debris flows, are classified as protection forests. These forests enhance slope stability primarily through the mechanical reinforcement provided by tree root systems, which function as a natural barrier against slope failure. In mountainous regions, protection forests play a vital role in reducing geohazard risks to infrastructure, human settlements, and water resources. The extensive root networks not only increase soil shear strength but also minimize the kinetic energy of mobilized soil and debris, thereby mitigating the impact of downslope flows.

Effective management of protection forests, such as selective thinning, maintenance of the understory, and planting of tree species with strong root systems. These interventions are designed to optimize the stabilizing function of the forest while preserving essential ecological and hydrological services. Besides their key role in hazard mitigation, protection forests also offer a range of co-benefits, including carbon sequestration, biodiversity conservation, and the provision of recreational and cultural ecosystem services.

Given their critical ecological and safety functions, protection forests should be prioritized in land-use planning and hazard risk management. They also provide co-benefits such as carbon sequestration, habitat provision, and recreational space, which further justify their conservation and sustainable management.

In conclusion, tree roots play a critical mechanical role in stabilizing slopes. Studies in regions such as New Zealand, Alaska, and Japan have demonstrated that tree removal leads to a decline in root reinforcement, increasing landslide susceptibility. Forests provide a multifunctional stabilizing influence on slopes, with mechanical reinforcement from roots being the most critical in the context of shallow landslides. Understanding and quantifying these effects are essential for incorporating vegetation into landslide hazard models and for designing effective nature-based solutions for slope stabilization. Their inclusion in landslide models through well-calibrated mechanical parameters is vital for reliable hazard assessment and the development of effective bioengineering stabilization strategies.

2.2.2 Importance of tree roots for other ecosystem services

Tree roots are foundational to a wide range of ecosystem services that maintain ecological integrity and support human livelihoods. They contribute to soil stabilization, nutrient cycling, water regulation, and biodiversity support, which are essential for sustainable land management. Beyond stabilizing slopes, tree roots play a crucial role in supporting a wide range of ecosystem services.

1. **Soil Health and Structure**: Tree roots bind soil particles together, increasing the soil's structural integrity and resistance to erosive forces. This is particularly critical on steep slopes, where the absence of root systems can lead to rapid soil loss, landslides, and sedimentation in water bodies. By creating a dense network, roots anchor soil layers, thereby reducing topsoil erosion and maintaining productive land. Tree roots improve soil structure and porosity through root growth and decay, which leads to better water infiltration and retention. Roots also contribute to aggregate stability, essential for maintaining healthy soil profiles and minimizing surface erosion.

2. **Water Cycle Regulation**: Roots enhance water infiltration by creating pathways that direct surface water into the soil, replenishing aquifers, and reducing surface runoff. This process mitigates the risks of flooding and improves water availability during dry periods. Additionally, tree roots play a role in moderating the water table by drawing up groundwater through capillary action, a process particularly beneficial in drought-prone regions. Roots enhance infiltration of water and reduce surface runoff, facilitate deep percolation, thereby recharging aquifers, and increase evapotranspiration, which can reduce peak water flows and moderate the hydrological cycle. Forests with deep root systems also modulate groundwater levels and reduce flooding downstream by slowing and storing precipitation. Forests not only act as a means of anchoring surface soil and limiting erosion but also regulate water at the watershed scale and contribute to flood control and hydrological resilience. Their roles extend further into climate regulation, air quality enhancement, and biodiversity support.

3. **Nutrient Cycling and Soil Fertility**: Tree roots contribute to nutrient cycling by facilitating the decomposition of organic matter. They release root exudates that simulate microbial activity, which helps in breaking down complex organic compounds into forms usable by plants. Additionally, deep-rooted trees access nutrients from subsoil layers, bringing them to the surface and enriching the topsoil. This enhances soil fertility, supporting both natural ecosystems and agricultural productivity.

4. **Carbon Sequestration and Climate Regulation**: Tree roots sequester carbon both in their biomass and through organic matter accumulation in the rhizosphere (root zone). Their turnover contributes significantly to long-term soil carbon storage, thus playing a role in climate regulation. Forests play a dual role in the climate system: they mitigate climate change by sequestering carbon, yet contribute to it when degraded or destroyed. Conversely, climate change itself can drive forest degradation and loss, creating a feedback loop that further intensifies global warming. The Reducing Emissions from Deforestation and Forest Degradation (REDD+) mechanism, initiated under the United Nations Framework Convention on Climate Change (UNFCCC), represents the first global framework aimed at mitigating climate change through the forestry sector (Pistorius, 2012). Beyond efforts to prevent deforestation and forest degradation, REDD+ also encompasses forest conservation, sustainable forest management, and the enhancement of forest carbon stocks in developing countries.

5. **Biodiversity Support**: Root support diverse microbial communities, which play critical roles in ecosystem functioning. Fungal symbionts, such as mycorrhizae, increase the nutrient uptake capacity of trees and improve soil health. Roots also provide physical habitat for soil fauna like earthworms and insects, which further contribute to soil aeration, decomposition, and nutrient recycling. Root systems contribute to habitat complexity, supporting diverse microbial communities and interacting with fungi and other organisms through symbioses like mycorrhizal networks, which enhance nutrient cycling and plant health.

6. **Agricultural and Livestock Benefits**: In silvopastoral systems like those in New Zealand, poplars and willows provide fodder during droughts, offer shade and shelter for livestock, improving animal welfare and productivity, contribute to reduced wind erosion, and better microclimate control.

7. **Landscape Aesthetics and Recreational Value**: While more indirect, the role of roots in sustaining forest health and resilience supports the broader ecosystem functions that contribute to scenic value, tourism, and mental well-being.

Climate change and evolving land use patterns challenge the sustained effectiveness of protection forests. Increases in disturbance regimes and shifts in species composition may affect their protective capabilities, requiring adaptive forest management approaches to maintain resilience in the face of global change.

Carbon storage

Tree roots are integral to terrestrial carbon storage, playing a dual role in sequestering carbon both directly in their biomass and indirectly by contributing to soil organic matter. Roots absorb carbon dioxide through photosynthesis, storing it in their tissues as biomass. Unlike above-ground biomass, root systems are less susceptible to disturbances such as logging, wildfires, or storms, making them a more stable carbon pool.

Fine roots, which have a higher turnover rate, contribute to soil organic carbon through their decay, while larger roots store carbon over extended periods. Roots enhance soil organic carbon levels by promoting the accumulation of stable organic matter. Decomposing root material and root exudates contribute to the formation of humus, a stable form of organic carbon in the soil. This process is particularly significant in temperate and boreal forests, where cold conditions slow the decomposition of organic matter, leading to higher carbon retention in soils.

The carbon storage potential of tree roots is vital for mitigating climate change. Forests with deep-rooted species can sequester large amounts of carbon, reducing

atmospheric carbon dioxide levels and helping to offset greenhouse gas emissions. Restoration projects that focus on planting tree species with extensive root systems can enhance carbon sequestration, especially in degraded landscapes.

To maximize the carbon sequestration benefits of tree roots, sustainable forest management practices are essential. These include protecting old-growth forests, implementing agroforestry systems, and encouraging reforestation with native species. Maintaining healthy root systems in both forested and agricultural landscapes ensures the resilience of these carbon pools against disturbances like deforestation, land-use change, and climate-induced stressors.

References

Ammann, Martin et al. (2009). "Significance of tree root decomposition for shallow landslides". In: *For Snow Landsc Res* 82.79-94, p. 79.

Arbanas, Željko and Sanja Dugonjić (2010). "Landslide risk increasing caused by highway construction". In: *Proc. of the Interpraevent*, pp. 333–343.

Arghiuş, Viorel-Ilie et al. (2011). "The relation between the landslide activity and irregular rainfall and snowmelt in the Codrului Hills, Romania". In: *Environmental Engineering and Management Journal* 10.1, pp. 3–6.

Balzano, Brunella, Alessandro Tarantino, and Andrew Ridley (2019). "Preliminary analysis on the impacts of the rhizosphere on occurrence of rainfall-induced shallow landslides". In: *Landslides* 16.10, pp. 1885–1901.

Brang, Peter et al. (2001). "Forests as Protection from Natural Hazards". In: *The Forests Handbook*. John Wiley & Sons, Ltd. Chap. 3, pp. 53–81. ISBN: 978-0-470-75707-9. DOI: 10.1002/9780470757079.ch3.

Burroughs, Edward Robbins and Byron R Thomas (1977). *Declining root strength in Douglas-fir after felling as a factor in slope stability*. Vol. 190. Department of Agriculture, Forest Service, Intermountain Forest and Range ...

Caine, Nel (1980). "The rainfall intensity-duration control of shallow landslides and debris flows". In: *Geografiska annaler: series A, physical geography* 62.1-2, pp. 23–27.

Campbell, Russell H (1975). *Soil slips, debris flows, and rainstorms in the Santa Monica Mountains and vicinity, southern California*. Vol. 851. US Government Printing Office.

Campus, S et al. (1998). "Frane per mobilizzazione delle coperture detritiche". In: *Eventi alluvionali in Piemonte, Regione Piemonte, Torino*, pp. 266–287.

Chiarelli, Davide Danilo et al. (2023). "Modeling snowmelt influence on shallow landslides in Tartano valley, Italian Alps". In: *Science of the total environment* 856, p. 158772.

Cohen, D., M. Schwarz, and D. Or (2011). "An Analytical Fiber Bundle Model for Pullout Mechanics of Root Bundles". In: *Journal of Geophysical Research: Earth Surface* 116.F3. ISSN: 2156-2202. DOI: 10.1029/2010JF001886.

Cohen, Denis and Massimiliano Schwarz (2017). "Tree-root control of shallow landslides". In: *Earth Surface Dynamics* 5.3, pp. 451–477.

Coppin, Nick J, Ivor G Richards, et al. (1990). *Use of vegetation in civil engineering*. Ciria Butterworths.

Corominas, Jordi et al. (2014). "Recommendations for the quantitative analysis of landslide risk". In: *Bulletin of engineering geology and the environment* 73, pp. 209–263.

Crosta, Giovanni (1998). "Regionalization of rainfall thresholds: an aid to landslide hazard evaluation". In: *Environmental Geology* 35.2, pp. 131–145.

Crozier, Michael J (2010). "Deciphering the effect of climate change on landslide activity: A review". In: *Geomorphology* 124.3-4, pp. 260–267.

Cruden, D.M. and D.J. Varnes (1996). *Landslide types and processes*. Vol. Special Report 247. Transportation Research Board, Washington D.C., pp. 36–75. ISBN: 030906208X.

Dazio, Emanuele (Plinio Rinaldo), Marco Conedera, and Massimiliano Schwarz (2018). "Impact of Different Chestnut Coppice Managements on Root Reinforcement and Shallow Landslide Susceptibility". In: *Forest Ecology and Management*, pp. 63–76. ISSN: 0378-1127. DOI: 10.1016/j.foreco.2018.02.031.

Dorren, Luuk and Massimiliano Schwarz (2016). "Quantifying the stabilizing effect of forests on shallow landslide-prone slopes". In: *Ecosystem-Based Disaster Risk Reduction and Adaptation in Practice*, pp. 255–270.

Dorren, Luuk KA et al. (2004). "Integrity, stability and management of protection forests in the European Alps". In: *Forest ecology and management* 195.1-2, pp. 165–176.

DR, GREENWAY (1987). "Vegetation and slope stability". In: *Slope stability*, pp. 187–230.

Ellen, Stephen D and Robert W Fleming (1987). "Mobilization of debris flows from soil slips, San Francisco Bayregion, California". In.

Ellen, STEPHEN D et al. (1988). "Description and mechanics of soil slip/debris flows in the storm". In: *USGS Prof. Paper* 1434, pp. 63–113.

Ennos, A Roland (1990). "The anchorage of leek seedlings: the effect of root length and soil strength". In: *Annals of Botany*, pp. 409–416.

Fredlund, DG (1987). "Slope stability analysis incorporating the effect of soil suction". In: *Slope stability*, pp. 113–144.

Gariano, SL et al. (2017). "Assessing future changes in the occurrence of rainfall-induced landslides at a regional scale". In: *Science of the total environment* 596, pp. 417–426.

Gehring, Eric et al. (2019). "Shallow landslide disposition in burnt European beech (Fagus sylvatica L.) forests". In: *Scientific Reports* 9.1, pp. 1–11.

Gerbore, EE (1997). "I boschi nel medioevo". In: *Uomini e boschi in Valle d'Aosta*.

Giadrossich, F et al. (2013a). "Mechanical interactions between neighbouring roots during pullout tests". In: *Plant and soil* 367.1, pp. 391–406.

Giannecchini, Roberto, Yuri Galanti, and G D'Amato Avanzi (2012). "Critical rainfall thresholds for triggering shallow landslides in the Serchio River Valley (Tuscany, Italy)". In: *Natural Hazards and Earth System Sciences* 12.3, pp. 829–842.

Glade, Thomas (2003). "Landslide occurrence as a response to land use change: a review of evidence from New Zealand". In: *Catena* 51.3-4, pp. 297–314.

Gray, Donald H and Robbin B Sotir (1996). *Biotechnical and Soil Bioengineering Slope Stabilization: A Practical Guide for Erosion Control*. John Wiley & Sons: Hoboken, NJ, USA.

Guzzetti, Fausto et al. (2004). "Landslides triggered by the 23 November 2000 rainfall event in the Imperia Province, Western Liguria, Italy". In: *Engineering Geology* 73.3-4, pp. 229–245.

Guzzetti, Fausto et al. (2008). "The rainfall intensity–duration control of shallow landslides and debris flows: an update". In: *Landslides* 5, pp. 3–17.

Hales, TC et al. (2009). "Topographic and ecologic controls on root reinforcement". In: *Journal of Geophysical Research: Earth Surface* 114.F3.

Hasenmueller, Elizabeth A et al. (2017). "Weathering of rock to regolith: The activity of deep roots in bedrock fractures". In: *Geoderma* 300, pp. 11–31.

Hungr, Oldrich, Serge Leroueil, and Luciano Picarelli (2014). "The Varnes classification of landslide types, an update". In: *Landslides* 11.2, pp. 167–194.

Iverson, Richard M (2000). "Landslide triggering by rain infiltration". In: *Water resources research* 36.7, pp. 1897–1910.

Iverson, Richard M, Mark E Reid, and Richard G LaHusen (1997). "Debris-flow mobilization from landslides". In: *Annual Review of Earth and Planetary Sciences* 25.1, pp. 85–138.

Johnson, AC and Peter Wilcock (2002). "Association between cedar decline and hillslope stability in mountainous regions of southeast Alaska". In: *Geomorphology* 46.1-2, pp. 129–142.

Keefer, David K (2002). "Investigating landslides caused by earthquakes–a historical review". In: *Surveys in geophysics* 23, pp. 473–510.

Li, Shao-Cai et al. (2007). "Root anchorage of Vitex negundo L. on rocky slopes under different weathering degrees". In: *Ecological engineering* 30.1, pp. 27–33.

Malamud, Bruce D et al. (2004). "Landslides, earthquakes, and erosion". In: *Earth and Planetary Science Letters* 229.1-2, pp. 45–59.

Montgomery, David R et al. (1997). "Hydrologic response of a steep, unchanneled valley to natural and applied rainfall". In: *Water Resources Research* 33.1, pp. 91–109.

Montrasio, Lorella and Roberto Valentino (2007). "Experimental analysis and modelling of shallow landslides". In: *Landslides* 4, pp. 291–296.

Moos, Christine et al. (2023). "Mountain protective forests under threat? an in-depth review of global change impacts on their protective effect against natural hazards". In: *Frontiers in Forests and Global Change* 6, p. 1223934.

Moser, Manfred and F Hohensinn (1983). "Geotechnical aspects of soil slips in Alpine regions". In: *Engineering Geology* 19.3, pp. 185–211.

Nadim, Farrokh et al. (2006). "Global landslide and avalanche hotspots". In: *Landslides* 3, pp. 159–173.

Ng, Charles Wang Wai and Q Shi (1998). "A numerical investigation of the stability of unsaturated soil slopes subjected to transient seepage". In: *Computers and geotechnics* 22.1, pp. 1–28.

Nilaweera, NS and P Nutalaya (1999). "Role of tree roots in slope stabilisation". In: *Bulletin of engineering geology and the environment* 57, pp. 337–342.

O'Loughlin, Colin L (1974). "A study of tree root strength deterioration following clearfelling". In: *Canadian Journal of Forest Research* 4.1, pp. 107–113.

Pawlik, Łukasz, Jonathan D Phillips, and Pavel Šamonil (2016). "Roots, rock, and regolith: Biomechanical and biochemical weathering by trees and its impact on hillslopes—A critical literature review". In: *Earth-science reviews* 159, pp. 142–159.

Persichillo, Maria Giuseppina, Massimiliano Bordoni, and Claudia Meisina (2017). "The role of land use changes in the distribution of shallow landslides". In: *Science of the total environment* 574, pp. 924–937.

Petley, David (2012). "Global patterns of loss of life from landslides". In: *Geology* 40.10, pp. 927–930.

Pollen, Natasha and Andrew Simon (2005). "Estimating the Mechanical Effects of Riparian Vegetation on Stream Bank Stability Using a Fiber Bundle Model". In: *Water Resources Research* 41.7. ISSN: 1944-7973. DOI: 10.1029/2004WR003801.

Reubens, Bert et al. (2007). "The role of fine and coarse roots in shallow slope stability and soil erosion control with a focus on root system architecture: a review". In: *Trees* 21.4, pp. 385–402.

Schmidt, K M et al. (Oct. 2001). "The Variability of Root Cohesion as an Influence on Shallow Landslide Susceptibility in the Oregon Coast Range". In: *Canadian Geotechnical Journal* 38.5, pp. 995–1024. ISSN: 0008-3674. DOI: 10.1139/t01-031.

Schwarz, M, Peter Lehmann, and Dani Or (2010). "Quantifying lateral root reinforcement in steep slopes–from a bundle of roots to tree stands". In: *Earth Surface Processes and Landforms: The Journal of the British Geomorphological Research Group* 35.3, pp. 354–367.

Schwarz, M et al. (2010a). "Quantifying the role of vegetation in slope stability: A case study in Tuscany (Italy)". In: *Ecological Engineering* 36.3, pp. 285–291.

Schwarz, Massimiliano, Filippo Giadrossich, and Denis Cohen (2013). "Modeling root reinforcement using a root-failure Weibull survival function". In: *Hydrology and Earth System Sciences* 17.11, pp. 4367–4377.

Shanmugam, G and Yuan Wang (2015). "The landslide problem". In: *Journal of Palaeogeography* 4.2, pp. 109–166.

Shinozaki, Kichiro et al. (1964a). "A quantitative analysis of plant form-the pipe model theory: I. Basic analyses". In: *Japanese Journal of ecology* 14.3, pp. 97–105.

— (1964c). "A quantitative analysis of plant form-the pipe model theory: II. Further evidence of the theory and its application in forest ecology". In: *Japanese journal of ecology* 14.4, pp. 133–139.

Sidle, R and Hirotaka Ochiai (2006). "Processes, prediction, and land use". In: *Water resources monograph. American Geophysical Union, Washington* 525.

Sidle, Roy C (1985). "Factors influencing the stability of slopes". In: *Proceedings of the workshop on slope stability: problems and solutions in forest management. Gen. Tech. Rep. PNW-180. Portland, OR: US Department of Agriculture, Forest Service, Pacific Northwest Forest and Range Experiment Station*, pp. 17–25.

— (1992). "A theoretical model of the effects of timber harvesting on slope stability". In: *Water Resources Research* 28.7, pp. 1897–1910.

Sidle, Roy C and Thom A Bogaard (2016). "Dynamic earth system and ecological controls of rainfall-initiated landslides". In: *Earth-science reviews* 159, pp. 275–291.

Sidle, Roy C and DN Swanston (1982). "Analysis of a small debris slide in coastal Alaska". In: *Canadian geotechnical journal* 19.2, pp. 167–174.

Sidle, Roy C and Weimin Wu (1999). "Simulating effects of timber harvesting on the temporal and spatial distribution of shallow landslides". In: *Zeitschrift fur Geomorphologie* 43.2, pp. 185–201.

Tamiru, Mulatu et al. (2024). "Geotechnical analysis and stability assessment of a landslide event in Gera Woreda, Ethiopia". In: *Cogent Engineering* 11.1, p. 2405745.

Teich, Michaela et al. (2022). "Protective forests for ecosystem-based disaster risk reduction (eco-DRR) in the alpine space". In: *Protective forests as ecosystem-based solution for disaster risk reduction (eco-DRR)*. IntechOpen.

Tobin, B et al. (2007). "Towards developmental modelling of tree root systems". In: *Plant Biosystems* 141.3, pp. 481–501.

Trandafir, Aurelian C et al. (2015). "Geomechanics of a snowmelt-induced slope failure in glacial till". In: *Environmental Earth Sciences* 73, pp. 3709–3716.

Van Westen, Cees J, Enrique Castellanos, and Sekhar L Kuriakose (2008). "Spatial data for landslide susceptibility, hazard, and vulnerability assessment: An overview". In: *Engineering geology* 102.3-4, pp. 112–131.

Varnes, David J (1978). "Slope movement types and processes". In: *Special report* 176, pp. 11–33.

Vergani, Chiara et al. (2016). "Root reinforcement dynamics in subalpine spruce forests following timber harvest: a case study in Canton Schwyz, Switzerland". In: *Catena* 143, pp. 275–288.

Vergani, Chiara et al. (2017a). "Investigation of root reinforcement decay after a forest fire in a Scots pine (Pinus sylvestris) protection forest". In: *Forest Ecology and Management* 400, pp. 339–352.

Vergani, Chiara et al. (2017b). "Root reinforcement dynamics of European coppice woodlands and their effect on shallow landslides: A review". In: *Earth-science reviews* 167, pp. 88–102.

Waldron, LJ (1977). "The shear resistance of root-permeated homogeneous and stratified soil". In: *Soil Science Society of America Journal* 41.5, pp. 843–849.

Wu, Tien H, William P McKinnell III, and Douglas N Swanston (1979). "Strength of tree roots and landslides on Prince of Wales Island, Alaska". In: *Canadian Geotechnical Journal* 16.1, pp. 19–33.

Wu, Weimin and Roy C Sidle (1995). "A distributed slope stability model for steep forested basins". In: *Water resources research* 31.8, pp. 2097–2110.

Yin, Yueping, Fawu Wang, and Ping Sun (2009). "Landslide hazards triggered by the 2008 Wenchuan earthquake, Sichuan, China". In: *Landslides* 6, pp. 139–152.

Ziemer, RR (1981). "Roots and the stability of forested slopes". In: *In: Timothy RH Davies and Andrew J. Pearce (eds). Proceedings of the International Symposium on Erosion and Sediment Transport in Pacific Rim Steeplands, 1981 January 25-31, Christchurch, NZ Int. Assn. Hydrol. Sci. Pub. No. 132: 343-361.*

Chapter 3

Quantifying Forest Contributions to Slope Stabilization

3.1 Models for the Quantification of Root Distribution and Root Reinforcement

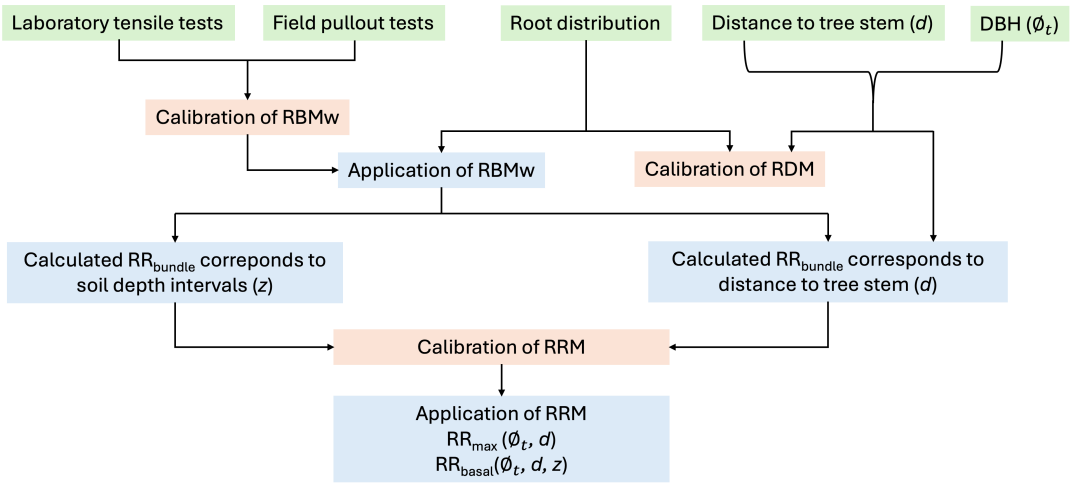

FIGURE 3.1: The framework applied in this study for predicting spatial variations of root distribution and root reinforcement.

Figure 3.1 exhibits the framework of models applied in this study to quantify the root distribution and root reinforcement of different tree species.

3.1.1 Root Bundle Model with Weibull survival function (RBMw)

Schwarz, Cohen, and Or, 2010 proposed a model called the Root Bundle Model (RBM) to model primarily the lateral root reinforcement. Assuming that individual roots behave as elastic–brittle fibers, the RBM estimates the pullout force of a root bundle as a function of displacement under displacement-controlled loading. As displacement increases, the force transmitted to each root rises, leading to progressive failure from the weakest to the strongest roots. The displacement at which maximum root reinforcement occurs is governed by the failure of the root diameter class that most strongly influences the mechanical behavior of the bundle.

The Root Bundle Model (RBM) enables estimating the complete force-displacement response of the root bundle and the total pullout work. Furthermore, it facilitates the

analysis of the progressive mobilization of root strength along the activation length throughout the pullout process, considering the effects of root-soil friction for each root within the bundle. The comprehensive characterization of the force-displacement behavior of root bundles under shear, tensile, and compressive loading is essential to understand the mechanisms that trigger shallow landslides. Moreover, it enables a more realistic representation of root mechanical effects in numerical models for slope stability analysis.

RBM accounts for variability in root mechanical properties solely as a function of diameter, assuming that roots within the same diameter class are mechanically homogeneous and mobilize the same maximum tensile force. However, previous studies have reported significant variability in mechanical properties even within a single diameter class. For a given diameter or narrow diameter range, differences in root anatomy and geometry can lead to variation in both the force and displacement at rupture. Factors such as root age, biochemical composition, and the environmental conditions in which roots develop can substantially influence root biomechanics (Hales et al., 2009).

To address this variability and investigate its effect on the mechanical behavior of root bundles, Schwarz, Giadrossich, and Cohen, 2013 introduced the Root Bundle Model with Weibull survival function (RBMw), an extension of the original RBM. Compared to RBM, RBMw incorporates a Weibull survival function to represent the probability distribution of failure among roots of the same diameter class, thereby allowing a more realistic simulation of progressive root breakage.

RBMw conceptualizes a root system as a collection of individual roots that act like a bundle of fibers. Each root in the bundle contributes to the overall soil reinforcement by resisting tensile forces when a slope is subjected to mechanical stress. The model evaluates the strength of the root-soil composite system by integrating the properties of individual roots, such as their tensile strength, diameter, and distribution in the soil.

The model incorporates a Weibull survival function to describe the probability distribution of root failure under increasing stress. The Weibull function is suitable for this application because it captures the variability in the strength and breakage characteristics of roots, allowing for a more realistic representation of root behavior under stress.

The Root Bundle Model with Weibull survival function is a widely used analytical framework in geotechnical and ecological engineering to quantify the mechanical reinforcement provided by tree roots in stabilizing soil. This model is particularly valuable in assessing the role of vegetation in slope stability and shallow landslide mitigation.

3.1.2 Root Distribution Model (RDM)

Root mechanical function is commonly classified based on diameter, differentiating between fine and coarse roots (Santantonio, 1990; Tobin et al., 2007). Fine roots, which are smaller than 2 mm in diameter, typically represent less than 5% of total tree biomass. Fine roots are part of the tertiary root system and account for more than 90% of the root system's water and nutrient absorption. The distribution of fine root biomass is influenced by the dynamic processes of root tip growth and death, which occur at a relatively high turnover rate (Majdi and Andersson, 2005; Børja et al., 2008). This turnover is modulated by local environmental conditions and seasonal variations (Johnsen, Maier, and Kress, 2005). Pregitzer et al., 2002 characterized the

life cycle of lateral fine roots as analogous to deciduous structures, comparable to leaves or needles.

Coarse roots (diameter > 2 mm) constitute approximately 15–25 % of the total tree biomass and are commonly categorized into four main classes: taproots, lateral roots, basal roots, and adventitious roots (sinker). These roots can be further classified as primary or secondary, with secondary roots developing from primary roots directly connected to the stem (Zobel, 2005). Coarse roots primarily serve structural functions, and their spatial distribution tends to be less influenced by below-ground competition. In certain cases, coarse roots of adjacent trees may form natural grafts, thereby contributing to root network stability and resilience (Fraser, Lieffers, and Landhäusser, 2005).

The spatial distribution of root diameters around a tree defines typical root architectures classified as one of three types: heart root system, plate root system, and tap root system (Kokutse et al., 2006). It is well known that the development and structure of root systems under natural conditions are controlled by both genetic characteristics and external factors operating in the rooting environment (Genet et al., 2008).

Root mass distribution around a tree is seldom symmetrical under most natural conditions due to heterogeneities in micro-topography, soil physical properties, distribution of nutrients, soil water, below-ground competition, light interception by the crown, soil temperature, site cultivation, prevailing wind direction, and soil movement (Coutts, 1989; Nicoll and Ray, 1996; Steele et al., 1997; Chiatante et al., 2002; Chiatante et al., 2003b; Nicoll et al., 2006; Reubens et al., 2007).

Measurements of root distribution around individual isolated trees revealed that fine-root biomass (FRB) decreases with increasing distance from the stem (Ammer and Wagner, 2005). The density of fine roots is assumed to be uniformly distributed in the lateral direction under a homogeneous forest canopy (Stober, George, and Persson, 2000; Puhe, 2003). The resulting homogeneous fine root density under a stand is due to the fact that overlapping root systems of neighboring trees may increase fine root density up to a maximum value sustainable by below-ground resources (Brisson and Reynolds, 1994; Casper, Schenk, and Jackson, 2003).

However, several studies reported spatial variations in fine root density (Bedeneau and Auclair, 1989; Müller and Wagner, 2003; Yanai, Park, and Hamburg, 2006) and total root biomass density (Genet et al., 2008), especially in tree stands where the growth is limited by extreme climatic factors or irregular canopy cover (Puhe, 2003). The distribution and amount of root mass also depend on the season (John, Pandey, and Tripathi, 2001). Tree density in a stand seems to be an important factor influencing the mean fine root biomass (Puhe, 2003; Børja et al., 2008).

At the scale of a single tree root system, Roering et al., 2003 has shown a strong correlation between tree stem diameter at breast height (DBH) and root zone effective radius, defined as the maximum distance from the stem where coarse roots are found. Typically, the lateral extent of a tree root zone is considered to be about 1 to 3 times its crown radius (Kuiper and Coutts, 1992; Drexhage and Gruber, 1998; Casper, Schenk, and Jackson, 2003; Gray and Barker, 2004; Johnsen, Maier, and Kress, 2005).

In addition to the lateral extent of a root zone, in some cases, the maximum rooting depth is another important factor for root reinforcement function. Root depth is often restricted by bedrock, porosity, moisture, soil structure, nutrients, and by climatic conditions (Tobin et al., 2007). Docker and Hubble, 2008 presented the results of root system architectural analysis and how the quantity of root material varies both with depth and lateral distance from the tree stem.

Mechanically important characteristics of root structure are branching order (Wang et al., 2006) and branching intervals along the root. The branching order decreases towards the origins of the root system (tree stem) as branches merge, defining branching points, with the distance between a pair of such points known as root branching distance.

Two types of branching geometry are often distinguished: either an apex that continues to grow straight and produces second-order lateral branches, or two terminal apices appear and replace the former apex at the tip of the root (Dupuy et al., 2005). While the tortuosity, the number and order of branches are important for the pullout resistance, the branching angle has only a limited influence.

Recognizing the labor-intensive and expensive process of detailed root distribution characterization, numerous empirical correlations have been developed to estimate root-related parameters using readily measurable above-ground tree traits. In the context of mechanical reinforcement, a key objective is to quantify the spatial frequency of roots across different diameter classes at various positions within a forest stand.

In this study, we applied the Root Distribution Model, developed by Schwarz et al., 2010a. The model proposes the use of simple morphogenetic parameters, including mean radial branching distance and root diameter "proportionality factor", to describe root system structure. These parameters are species-dependent and may vary significantly across tree taxa. The model is designed to estimate the three-dimensional distribution of root density across diameter classes (Figure 3.2), facilitating a more mechanistic representation of root reinforcement potential.

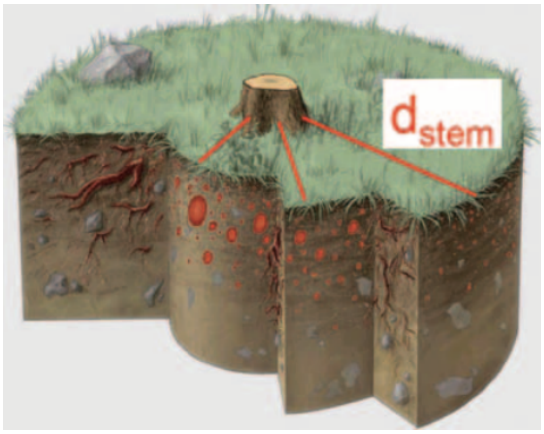

FIGURE 3.2: Illustration of lateral root distribution at three different distances from tree stem. Cite from paper of Schwarz et al. 2010 Schwarz, Lehmann, and Or, 2010.

The starting point for modeling root distribution is information regarding fine root distribution (<1.5 mm diameter). The distribution of root diameters associated with primary and secondary root systems is assumed to be strongly correlated with mean fine-root distribution and distance from the tree stem. The total number of fine roots associated with an individual tree may be estimated from the sapwood area, crown volume, or other tree properties (Schwarz et al., 2010a). This modeling approach involves a static fractal-branching model (Tobin et al., 2007) based on simple morphogenetic parameters, similar to those used by other models (Diggle, 1988; Lynch et al., 1997; Ozier-Lafontaine, Lecompte, and Sillon, 1999; Pagès et al., 2004).

The RDM simulates lateral root distribution only, without considering the vertical distribution. The calibration of the RDM is particularly useful for the application of models such as BankforNET (Gasser et al., 2019; Gasser et al., 2020; Perona et al., 2022), and for the modeling of hydraulic bank erosion influenced by riparian vegetation.

3.1.3 Root Reinforcement Model (RRM)

The root reinforcement was quantified as a function of tree dimensions and distance from the tree using the Root Bundle Model with Weibull survival function (RBMw). Based on the modeled root reinforcement values, Moos et al. (2016a) introduced a proxy variable for the root reinforcement of the nearest tree, assuming a gamma distribution. To quantify root reinforcement within a forest stand, the calculated maximum lateral root reinforcement, which is the peak of the force-displacement curve from RBMw, is correlated to the tree diameter at the breast height and the distance from the tree stem.

To upscale lateral root reinforcement to the stand scale, the following assumptions are applied (Schwarz, Cohen, and Or, 2012b; Dazio, Conedera, and Schwarz, 2018):

- The model does not take spatially differentiated root distribution along the slope gradient around a tree stem, as well as the concurrence of neighbor trees. It assumes that the roots are symmetrically distributed all around the tree.

- Trees are regularly distributed within the stand in a triangular lattice configuration.

- The minimum lateral root reinforcement is estimated by summing the contributions from overlapping root systems of adjacent trees.

Depending on the depth of the shallow landslide, lateral root reinforcement was computed as the cumulative sum from the soil surface to the depth of the potential failure surface.

The basal root reinforcement at the stand scale was also calculated using a gamma probability density function fitted to the measured vertical profile of root reinforcement, with data recorded at every 0.15 m interval. This approach is similar to the approach of Bischetti et al., 2007, who applied a gamma distribution to model the vertical distribution of Root Area Ratio.

3.2 Root Distribution Model in Biomass Estimation

A potential application of the Root Distribution Model is to estimate root biomass, which is a significant component of total tree biomass and hard to quantify, and the amount of carbon sequestered in the root system without excavating destructively. Estimating root biomass is vital for several reasons: (i) Carbon sequestration: Roots store a significant portion of terrestrial carbon, which contributes to climate change mitigation; (ii) Soil Health and Stability: Root biomass is directly linked to soil fertility and structural stability; (iii) Ecosystem Productivity: Root biomass reflects below-ground resource allocation, influencing overall plant growth and ecosystem functioning.

As global efforts to mitigate climate change intensify, accurately quantifying root carbon storage has become essential. Below-ground biomass, particularly coarse roots, comprises a substantial and often underestimated component of total forest carbon stocks. Unlike above-ground biomass, root-derived carbon is more stable and less susceptible to rapid turnover or disturbance, contributing significantly to long-term carbon sequestration in soils. As land-use strategies increasingly depend on

forest management for carbon offsetting, precise estimation of root biomass is essential for improving the accuracy of carbon budgets, informing sustainable silvicultural practices, and guiding ecosystem restoration efforts.

In Chapter 6, I discussed more details about the potential of applying the Root Distribution Model (RDM) in estimating root biomass and its capacity for sequestering carbon.

References

Ammer, Ch and S Wagner (2005). "An approach for modelling the mean fine-root biomass of Norway spruce stands". In: *Trees* 19, pp. 145–153.

Bedeneau, Max and Daniel Auclair (1989). "The study of tree fine root distribution and dynamics using a combined trench and observation window method". In: *Annales des sciences forestières*. Vol. 46. 3. EDP Sciences, pp. 283–290.

Bischetti, Gian Battista et al. (2007). "Root strength and root area ratio of forest species in Lombardy (Northern Italy)". In: *Eco- and Ground Bio-Engineering: The Use of Vegetation to Improve Slope Stability*. Springer: Berlin/Heidelberg, Germany, pp. 31–41.

Børja, Isabella et al. (2008). "Stand age and fine root biomass, distribution and morphology in a Norway spruce chronosequence in southeast Norway." In: *Tree physiology* 28.5.

Brisson, Jacques and James F Reynolds (1994). "The effect of neighbors on root distribution in a creosotebush (Larrea tridentata) population". In: *Ecology* 75.6, pp. 1693–1702.

Casper, Brenda B, H Jochen Schenk, and Robert B Jackson (2003). "Defining a plant's belowground zone of influence". In: *Ecology* 84.9, pp. 2313–2321.

Chiatante, Donato et al. (2002). "The influence of steep slopes on root system development". In: *Journal of plant growth regulation* 21, pp. 247–260.

Chiatante, Donato et al. (2003b). "Modification of root morphological parameters and root architecture in seedlings of Fraxinus ornus L. and Spartium junceum L. growing on slopes". In: *Plant Biosystems-An International Journal Dealing with all Aspects of Plant Biology* 137.1, pp. 47–55.

Coutts, MP (1989). "Factors affecting the direction of growth of tree roots". In: *Annales des sciences forestières*. Vol. 46. Supplement. EDP Sciences, 277s–287s.

Dazio, Emanuele (Plinio Rinaldo), Marco Conedera, and Massimiliano Schwarz (2018). "Impact of Different Chestnut Coppice Managements on Root Reinforcement and Shallow Landslide Susceptibility". In: *Forest Ecology and Management*, pp. 63–76. ISSN: 0378-1127. DOI: 10.1016/j.foreco.2018.02.031.

Diggle, AJ (1988). "ROOTMAP—a model in three-dimensional coordinates of the growth and structure of fibrous root systems". In: *Plant and soil* 105, pp. 169–178.

Docker, B B and T C T Hubble (Aug. 2008). "Quantifying root-reinforcement of river bank soils by four Australian tree species". en. In: *Geomorphology* 100.3-4, pp. 401–418. ISSN: 0169555X. DOI: 10.1016/j.geomorph.2008.01.009. URL: https://linkinghub.elsevier.com/retrieve/pii/S0169555X08000159.

Drexhage, Michael and Franz Gruber (1998). "Architecture of the skeletal root system of 40-year-old Picea abies on strongly acidified soils in the Harz Mountains (Germany)". In: *Canadian Journal of Forest Research* 28.1, pp. 13–22.

Dupuy, Laure et al. (2005). "A density-based approach for the modelling of root architecture: application to Maritime pine (Pinus pinaster Ait.) root systems". In: *Journal of Theoretical Biology* 236.3, pp. 323–334.

Fraser, Erin C, Victor J Lieffers, and Simon M Landhäusser (2005). "Age, stand density, and tree size as factors in root and basal grafting of lodgepole pine". In: *Canadian Journal of Botany* 83.8, pp. 983–988.

Gasser, Eric et al. (2019). "A review of modeling the effects of vegetation on large wood recruitment processes in mountain catchments". In: *Earth-Science Reviews* 194, pp. 350–373.

Gasser, Eric et al. (2020). "A new framework to model hydraulic bank erosion considering the effects of roots". In: *Water* 12.3, p. 893.

Genet, Marie et al. (Oct. 2008). "Root Reinforcement in Plantations of Cryptomeria Japonica D. Don: Effect of Tree Age and Stand Structure on Slope Stability". In: *Forest Ecology and Management* 256.8, pp. 1517–1526. ISSN: 03781127. DOI: 10.1016/j.foreco.2008.05.050.

Gray, Donald H and David Barker (2004). "Root-soil mechanics and interactions". In: *Riparian vegetation and fluvial geomorphology* 8, pp. 113–123.

Hales, TC et al. (2009). "Topographic and ecologic controls on root reinforcement". In: *Journal of Geophysical Research: Earth Surface* 114.F3.

John, Babu, Harendra N Pandey, and Radhey S Tripathi (2001). "Vertical distribution and seasonal changes of fine and coarse root mass in Pinus kesiya Royle Ex. Gordon forest of three different ages". In: *Acta Oecologica* 22.5-6, pp. 293–300.

Johnsen, K, C Maier, and L Kress (2005). "Quantifying root lateral distribution and turnover using pine trees with a distinct stable carbon isotope signature". In: *Functional Ecology* 19.1, pp. 81–87.

Kokutse, Nomessi et al. (2006). "3D numerical modelling and analysis of the influence of forest structure on hill slopes stability". In: *Interpraevent*. Universal Academy Press Tokyo, Japan, pp. 561–567.

Kuiper, LC and MP Coutts (1992). "Spatial disposition and extension of the structural root system of Douglas-fir". In: *Forest ecology and management* 47.1-4, pp. 111–125.

Lynch, Jonathan P et al. (1997). "SimRoot: modelling and visualization of root systems". In: *Plant and Soil* 188, pp. 139–151.

Majdi, Hooshang and Pål Andersson (2005). "Fine root production and turnover in a Norway spruce stand in northern Sweden: effects of nitrogen and water manipulation". In: *Ecosystems* 8, pp. 191–199.

Moos, Christine et al. (2016a). "How does forest structure affect root reinforcement and susceptibility to shallow landslides?" In: *Earth Surface Processes and Landforms* 41.7, pp. 951–960.

Müller, KH and S Wagner (2003). "Fine root dynamics in gaps of Norway spruce stands in the German Ore Mountains". In: *Forestry* 76.2, pp. 149–158.

Nicoll, BC et al. (2006). "The architecture of Picea sitchensis structural root systems on horizontal and sloping terrain". In: *Trees* 20, pp. 701–712.

Nicoll, Bruce C and Duncan Ray (1996). "Adaptive growth of tree root systems in response to wind action and site conditions". In: *Tree physiology* 16.11-12, pp. 891–898.

Ozier-Lafontaine, Harry, François Lecompte, and Jean François Sillon (1999). "Fractal analysis of the root architecture of Gliricidia sepium for the spatial prediction of root branching, size and mass: model development and evaluation in agroforestry". In: *Plant and Soil* 209.2, pp. 167–179.

Pagès, Loïc et al. (2004). "Root Typ: a generic model to depict and analyse the root system architecture". In: *Plant and soil* 258.1, pp. 103–119.

Perona, Paolo et al. (2022). "Tree root distribution modelling in different environmental conditions". In: *Ecological Engineering* 185, p. 106811.

Pregitzer, Kurt S et al. (2002). "Fine root architecture of nine North American trees". In: *Ecological monographs* 72.2, pp. 293–309.

Puhe, Joachim (2003). "Growth and development of the root system of Norway spruce (Picea abies) in forest stands—a review". In: *Forest ecology and management* 175.1-3, pp. 253–273.

Reubens, Bert et al. (2007). "The role of fine and coarse roots in shallow slope stability and soil erosion control with a focus on root system architecture: a review". In: *Trees* 21.4, pp. 385–402.

Roering, Joshua J et al. (2003). "Shallow landsliding, root reinforcement, and the spatial distribution of trees in the Oregon Coast Range". In: *Canadian Geotechnical Journal* 40.2, pp. 237–253.

Santantonio, Dan (1990). *Modeling growth and production of tree roots*. Timber Press, Portland, OR.

Schwarz, M., D. Cohen, and D. Or (2010). "Root-Soil Mechanical Interactions during Pullout and Failure of Root Bundles". In: *Journal of Geophysical Research: Earth Surface* 115.F4. ISSN: 2156-2202. DOI: 10.1029/2009JF001603.

Schwarz, M, D Cohen, and Dani Or (2012b). "Spatial characterization of root reinforcement at stand scale: theory and case study". In: *Geomorphology* 171, pp. 190–200.

Schwarz, M, Peter Lehmann, and Dani Or (2010). "Quantifying lateral root reinforcement in steep slopes–from a bundle of roots to tree stands". In: *Earth Surface Processes and Landforms: The Journal of the British Geomorphological Research Group* 35.3, pp. 354–367.

Schwarz, M et al. (2010a). "Quantifying the role of vegetation in slope stability: A case study in Tuscany (Italy)". In: *Ecological Engineering* 36.3, pp. 285–291.

Schwarz, Massimiliano, Filippo Giadrossich, and Denis Cohen (2013). "Modeling root reinforcement using a root-failure Weibull survival function". In: *Hydrology and Earth System Sciences* 17.11, pp. 4367–4377.

Steele, Sarah J et al. (1997). "Root mass, net primary production and turnover in aspen, jack pine and black spruce forests in Saskatchewan and Manitoba, Canada". In: *Tree physiology* 17.8-9, pp. 577–587.

Stober, C, E George, and H Persson (2000). "Root growth and response to nitrogen". In: *Carbon and nitrogen cycling in European forest ecosystems*, pp. 99–121.

Tobin, B et al. (2007). "Towards developmental modelling of tree root systems". In: *Plant Biosystems* 141.3, pp. 481–501.

Wang, Zhengquan et al. (2006). "Fine root architecture, morphology, and biomass of different branch orders of two Chinese temperate tree species". In: *Plant and Soil* 288, pp. 155–171.

Yanai, Ruth D, Byung B Park, and Steven P Hamburg (2006). "The vertical and horizontal distribution of roots in northern hardwood stands of varying age". In: *Canadian journal of forest research* 36.2, pp. 450–459.

Zobel, Richard W (2005). "Tertiary root systems". In: *Roots and soil management: Interactions between roots and the soil* 48, pp. 33–56.

Chapter 4

Analysis of Poplar's (*Populus nigra* ita.) Root Systems for Quantifying Bio-Engineering Measures in the case study of New Zealand Pastoral Hill Country

forests MDPI

Article

Analysis of Poplar's (*Populus nigra* ita.) Root Systems for Quantifying Bio-Engineering Measures in New Zealand Pastoral Hill Country

Ha My Ngo [1,2,*], Feiko Bernard van Zadelhoff [2,3], Ivo Gasparini [2], Julien Plaschy [2], Gianluca Flepp [2], Luuk Dorren [2], Chris Phillips [4], Filippo Giadrossich [1] and Massimiliano Schwarz [2]

1 Department of Agriculture, University of Sassari, Viale Italia 39A, 07100 Sassari, Italy; fgiadrossich@uniss.it
2 HAFL, Bern University of Applied Sciences, Länggasse 85, CH-3052 Zollikofen, Switzerland; massimiliano.schwarz@bfh.ch (M.S.)
3 Institute of Geography (GIUB), University of Bern, CH-3012 Bern, Switzerland
4 Manaaki Whenua-Landcare Research, Lincoln 7608, New Zealand
* Correspondence: hmngo@uniss.it

Abstract

Populus nigra ita. is an important tree species for preventing rainfall-triggered shallow landslides and hydraulic bank erosion in New Zealand. However, the quantification of its spatial root distribution and reinforcement remains challenging. The objective of this study is to calibrate and validate models for the spatial upscaling of root distribution and root reinforcement. The data were collected in a 26-year-old "Tasman" poplar stand at Ballantrae Hill Country Research Station in New Zealand. We assessed root distribution at different distances from the stem of four poplar trees and from eleven soil pits along a transect located in a sparse to densely planting poplar stand. 124 laboratory tensile tests and 66 field pullout tests on roots with diameters up to 0.04 m were carried out to estimate root mechanical properties. The results show that the spatial distribution of roots can be well predicted in trenches of individual tree root systems ($R^2 = 0.78$), whereas it tends to overestimate root

distribution when planting density was higher than 200 stems per hectare. The root reinforcement is underestimated within single tree root systems ($R^2 = 0.64$), but it performs better for the data along the transect. In conclusion, our study provided a unique and detailed database for quantifying root distribution and reinforcement of poplars on a hillslope. The implementation of these models for the simulation of shallow landslides and hydraulic bank erosion is crucial for identifying hazardous zones and for the prioritization of bio-engineering measures in New Zealand catchments. Results from this study are useful in formulating a general guideline for the planning of bio-engineering measures considering the temporal dynamics of poplar's growth and their effectiveness in sediment and erosion control.

Keywords: root reinforcement model; root distribution model; root bundle model; shallow landslides; poplar; forestry management

4.1 Introduction

New Zealand's pastoral hill country is a good example of how anthropogenic land use has altered geomorphological processes. Specifically, the extension of natural forests was reduced from about 85% prior to human habitation to 29% of land area nowadays (McGlone, 1989; Holdaway et al., 2017). Most of the pastoral hill country is used today for farming, grazing (mainly sheep and cows, and also deer). Within a few decades after the first arrival of Europeans in the middle of the 19^{th} century, the extensive forest clearance and conversion to pasture applied by the colonists lead to a dramatic increase of erosion (O'loughlin and Pearce, 1976; Beattie, 2003; Glade, 2003). Landslides have caused considerable loss of productive soil (Trustrum and De Rose, 1988; Schwarz et al., 2016a), water holding capacity, movement of sediment in streams and rivers, and decline in water quality (Rogers and Selby, 1980; Claessens et al., 2007). Studies have documented that soil productivity recovery from shallow landslide affected areas takes a long time (decades) and annual pastoral production is less than 80% of that of areas unaffected by landslides (Lambert, Trustrum, and Costall, 1984; Douglas, Trustrum, and Brown, 1986; Rosser and Ross, 2011).

New Zealand is a predominantly hilly and mountainous country. 69% area of the pit country (equals ca. 18 million hectares) are steeper than 12^o. This area then divided into "hill-land" with slopes from 12-28^o and "steep-land" with slopes exceed 28^o. 45% of the 6.3 million hectares in the North Island is soft rock and crushed soft rock terrain while another 23% is volcanic ash and loess-mantled terrain. The North Island hill country is dominated by shallow landslides and mass movement erosion. In contrast to the North Island, 56% of the 3.7 million hectares in the South Island is situated on hard rock terrain. The South Island is dominated by surface erosion hazards such as sheet erosion and soil slip erosion.

Before 1200 AD, around 85% of the nation was covered by forest (Blaschke, Trustrum, and DeRose, 1992). The rest was mostly alpine regions, coasts, and wetlands. After 1200 AD, the Polynesians, explored New Zealand and became the first native inhabitants of the islands. They were considered a contributor to forest removal by introducing agricultural practices to the primordial land with cutting and burning lowland forests on the plains, coasts or valley floors (Glade, 2003). Although such deforestation had irreversible ecological consequences, such as changes of local flora and fauna (McGlone, 1989), it did not generally affect the occurrence of landslides at the large scale (DeRose, Trustrum, and Blaschke, 1993).

Exotic fast-growing trees such as pines (*Pinus radiata*), willows (*Salix* spp.), and poplars (*Populus* spp.) have been widely introduced on pastoral hill country because of economic benefits including soil conservation, serve as fodder, shelter, and shade for livestock, lower wind speed, produce carbon credits, and generate timber production (McGregor et al., 1999 Jan 1; Parminter, Dodd, and Mackay, 2001 Jan 1; Glade, 2003). For example, shade belts in hot weather have been declared to boost reproductive performance and growth rates while decreasing the risk of hypothermia and death in lambs (Gregory, 1995). Indigenous species with a slower growth rate were not used in problematic areas (Van Kraayenoord, 1968). The most suitable and proven tree species were poplar (*Populus* spp.) and willow (*Salix* spp.) because they are (i) easy to reproduce vegetatively by means of cuttings, (ii) readily established from large poles in the presence of stock, (iii) easily transported and can be planted on steep hill country, (iv) grow quickly with 1 to 4 m per year in the first years, (v) tolerate wet soil conditions during long periods and do not affect pasture growth unless planted at narrow spacing or high density, (vi) possess an extensive and strong root system which is able to rapidly stabilize the soil mass (Van Kraayenoord, 1968; Wilkinson, 1999; Phillips, Marden, and Suzanne, 2014), (vii) obtain a high evapotranspiration rate so can remove a large amount of water from soil, (viii) obtain good capacity to recover from mechanical damage such as soil movements or stock impacts (Van Kraayenoord, 1968), (ix) provide shade, shelter, and quality fodder (especially during drought periods), (x) sequester carbon (Fang, Xue, and Tang, 2007; McIvor and Douglas, 2012), and lastly, (xi) may provide income for farmers with their timber.

In the present study, we focused on the effects of root distribution of *Populus deltoides x Populus nigra* "Tasman" poplar on pastoral hill country in New Zealand. "Tasman" poplar is one of the two clones of the most common poplar hybrid in New Zealand (McIvor, 2012). "Tasman" poplar, as well as "Veronese" poplar, are hybrids of the American (*Populus deltoides*) and the European (*Populus nigra*). However, the former is a male clone while the latter is a female one (Sulaiman, 2006). Tasman poplar has a narrower crown and acquires more water compared to Veronese poplar but is more resistant to rust. The incredible growth rate of these *Populus deltoides x P. nigra* hybrids was highlighted by McIvor et al. (2008). Although some studies have quantified the spatial distribution of roots in young trees (McIvor, 2012; Phillips, Marden, and Suzanne, 2014; Schwarz et al., 2016a), data and modeling for the quantification of older trees are missing. The present study aims to fulfill this research gap. Specifically, the objectives are to quantify the spatial root distribution and root reinforcement of 26-year-old Tasman poplars and apply analytical models for upscaling and implementing root reinforcement in geomorphological models.

4.2 Materials and Methods

4.2.1 Site description

Data were collected at Ballantrae Hill Country Research Station (40°18'57"S, 175°50'24"E) located in the Manawatu region, in the south of North Island (Figure 4.1). The elevation of the site is ca. 130 m ASL (Manaaki Whenua - Landcare Research 2019) and the terrain is slightly northeast facing. The climate is temperate: frosty winters and cool summers with the maximum 30°C on exceptional occasions. Details of our study site are shown in Table 4.1.

TABLE 4.1: Summary of study site characteristics (data from the LRIS Portal)

Variables	Description	Variables	Description
Region	Hard Rock Hill Country	Soil pH	5.5 - 7.5
Province	Eastern Soft Rock	Mean Erosion rate	2604 t/km^2/yr
Rock type	Sedimentary rocks	Mean annual soil temperature	11 - 15^{o}C
Soil texture	Silt loam	Topsoil gravel content	0 - 4 %

The site is steep to very steep developed on siltstone and banded mudstone, which are very loose to compact, with moderate to high (more than 1200 mm) rainfall events. Shallow landslides are the dominant erosion form and 1-10% of the area is affected by earthflows. The erosion rate recorded in 2001 was ca. 2604 t/km^2/yr. Soil pH ranged from 5.5 to 7.5. Potential maximum rooting depth is moderately deep from 0.6 to 1.19 m belowground.

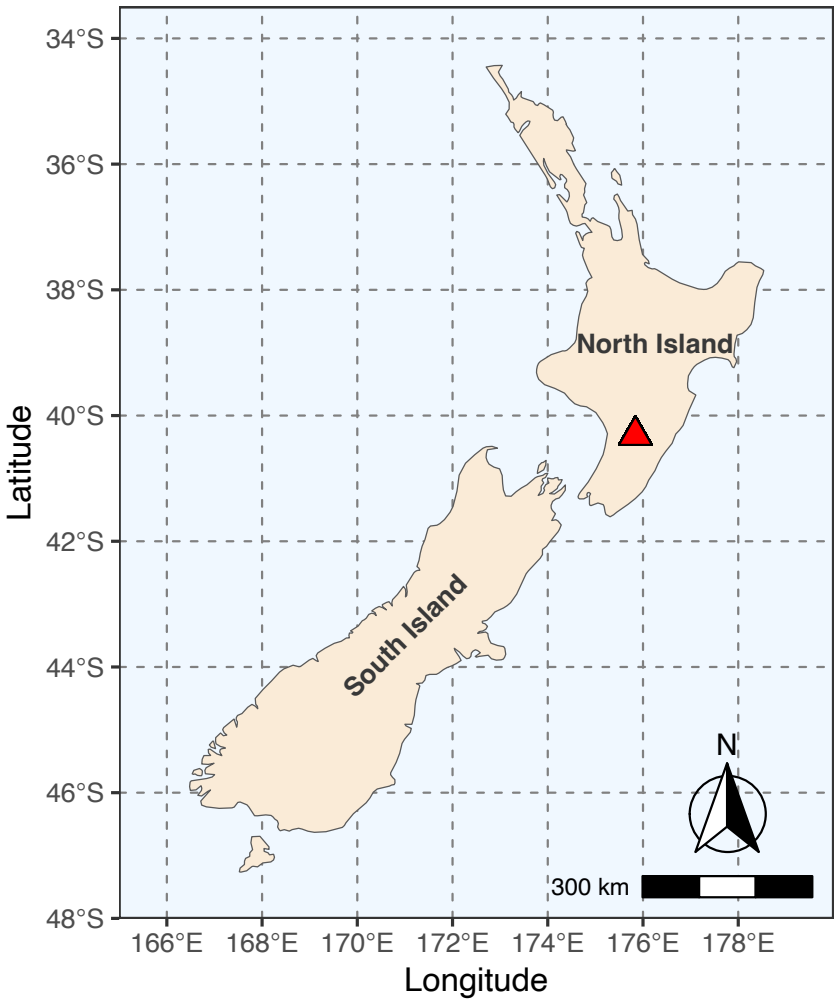

FIGURE 4.1: Location of the study site (presented as the red triangle) in New Zealand.

The poplar stand was 26 years old at the time when field measurements were made. The poles were distributed in a radial pattern (Nelder layout) (Figure 4.2). Tree spacing was about 3.5 m, corresponding to approx. 800 stems per hectare (sph) in the densest zone and up to 12.9 m (ca. 60 sph) in the sparsest one. Double circular trenches were excavated around four trees located in the sparse zone to recorded data on root distribution and root mechanical properties (Figure 4.2). The high soil clay content explains the low vertical permeability of the soil and the hydro-morphic characteristics (Figure 4.3). A total of 11 soil pits were also dug to quantify the effect of stand density on the root distribution of overlapping root systems.

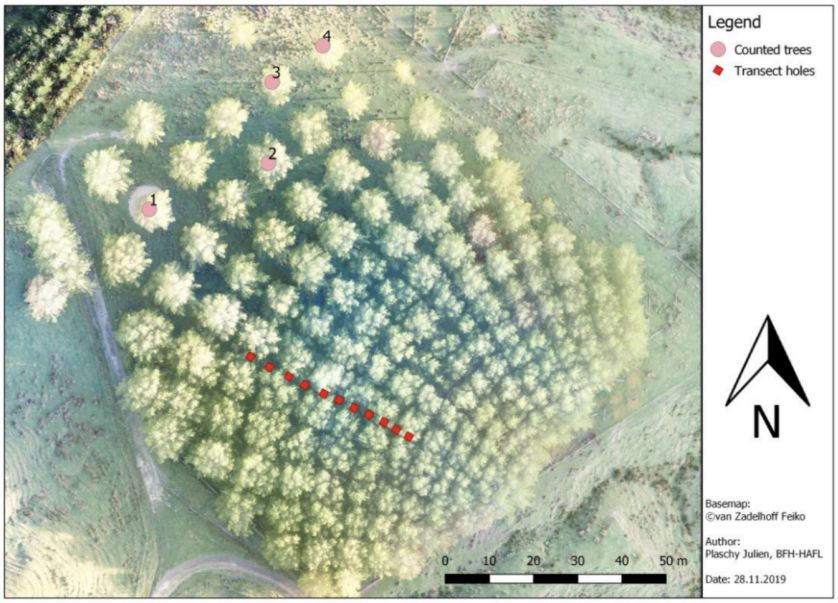

FIGURE 4.2: Overview of the tree stand, being a "nelder" planting trial. Trees from the wider spaced part of the stand were chosen to have less overlap between the root systems of neighbouring trees and are represented by pink dots. Transect pits are represented as red squares.

Root counting and measurement were conducted manually from 30 September - 8 November 2019. The study was divided into two parts with different objectives. Details on the methodologies are presented in the following sections.

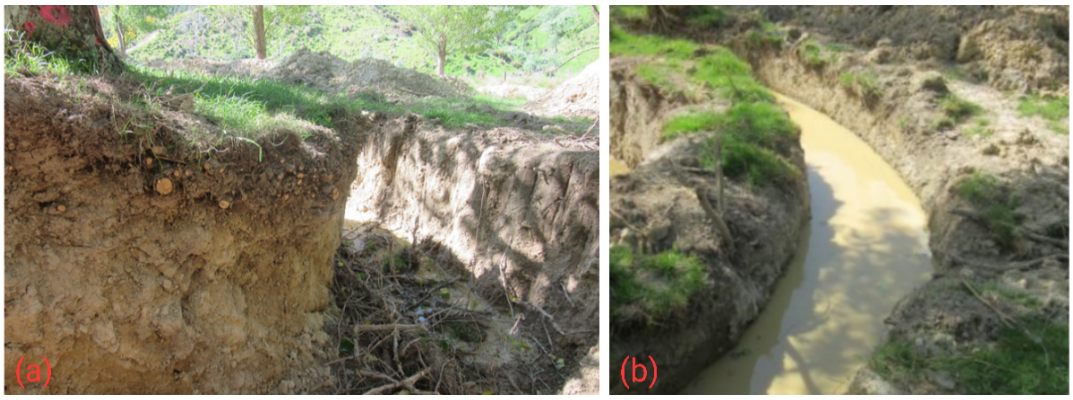

FIGURE 4.3: One of the trenches (a) before a rainfall event and (b) with more than 0.7 m water after 3 days without rain, indicating slow soil drainage.

4.2.2 Root distribution measurements

Individual tree measurements

To quantify the spatial root distribution at the single tree scale, we used the method similar to Giadrossich et al. (2020a). We selected four trees (Tree 1, 2, 3, and 4) in the sparsest part of the stand in order to minimize the influence from neighbouring trees, as shown in Figure 4.2, with DBH (Diameter at Breast Height) of 0.41, 0.42, 0.51, and 0.56 m, respectively. Two 360^o trenches around the stem, with a width and depth of approximately 1 m, were dug with an excavator. The distances from the middle of the tree stem to these trenches were 1.5 m, 2.5 m, 3.5 m, and 4.5 m . Trenches were divided into eight 45^o sectors. Sectors 1 and 8 were situated uphill. Each sector was separated into 7 depth layers [0-0.15 m], [0.15-0.30 m], [0.30-0.45 m], [0.45-0.60 m], [0.60-0.75 m], [0.75-0.90 m], and [0.90-1.05 m]. Living fine roots belonging to the sampled tree were counted and assigned to diameter class [0.5-1.5 mm], whereas living coarse roots were classified into 1 mm diameter classes [1.5-2.5 mm], [2.5-3.5 mm], [3.5-4.5 mm], and so on. The maximum recorded root diameter was 40 mm.

Transect measurements

To validate the upscaling of the model at the stand scale, eleven square pits were dug in the stand along a transect between two rows of trees as shown in Figure 4.2. Each pit had four soil faces, 1 m wide and 0.9 m deep. Roots were counted and recorded separately for each face (1-4) of each square pit in the same manner as for the circular trenches. All the surrounding trees' parameters within a distance of 30 times its DBH to the pit were recorded as they possibly affected the presence of roots in the pit. The transect pits are numbered from the sparsest zone (1) to the densest zone (11) (Table 4.2). The tree density around the pits was approximately 84 stems per hectare (sph) in the sparse zone and 770 sph in the dense zone.

TABLE 4.2: Tree distribution surrounding transect's pits. DBH refers to tree diameters measured at breast height; dist. is the distance of pit-tree.

Transect pit	No of surrounding trees	Mean dist. [m]	Min dist. [m]	Max dist. [m]	Average DBH [m]	DBH at min dist. [m]
1	8	10.5 ± 4.0	4.6	16	0.58	0.52
2	10	11.5 ± 4.2	6.2	16.3	0.57	0.57
3	11	10.5 ± 4.7	3.2	16.8	0.54	0.55
4	12	11.0 ± 3.7	5.9	14.5	0.53	0.54
5	11	10.2 ± 3.8	4.1	15.3	0.53	0.55
6	14	10.8 ± 3.8	5.1	17.1	0.52	0.46
7	15	10.5 ± 3.8	3.5	17.1	0.51	0.46
8	14	9.9 ± 3.7	4.8	15.9	0.51	0.46
9	15	9.8 ± 3.8	3.1	15.5	0.49	0.52
10	14	8.9 ± 3.1	4.5	12.7	0.48	0.47
11	16	9.0 ± 3.7	2.7	15.9	0.47	0.47

Root Area Ratio

The cross-sectional area of roots per area of soil profile, known as the root-area-ratio (RAR), is calculated for all trenches and transect's pits. The RAR is defined as

$$RAR = \sum_{i=1}^{n} \frac{A_{r,i}}{A_s} \tag{4.1}$$

where A_r is root cross section area [m^2] and A_s is soil area [m^2], i is the root diameter class, and n is the number of root diameter classes.

4.2.3 Root pullout tests

The mechanical properties of the root-soil interaction were tested by field pullout experiments as described in previous studies (Giadrossich et al., 2017a; Vergani et al., 2016; Vergani et al., 2017a; Vergani et al., 2017b; Dazio, Conedera, and Schwarz, 2018). Field root pullout testing is considered the most representative method to quantify root reinforcement when using the Root Bundle Model approach (RBMw) (Schwarz, Giadrossich, and Cohen, 2013). Trees used for the pullout tests were all in good health and were of similar DBH (0.4 m). Selected roots were carefully excavated to expose a sufficient length, anchored by threaded rods, and pulled towards the tree stem by a pullout device. The pullout device consists of an aluminium frame equipped with a steel rope winch and a crank handle. Force applied on the roots was measured

by a load cell with a nominal maximum load capacity of 2 tons. A total of 66 pullout tests and 124 laboratory tensile tests were performed.

4.2.4 Root distribution modeling

Root distribution is modeled using the Root Distribution Model (RDM) described by Schwarz, Lehmann, and Or (2010). The RDM estimates the number of roots in diameter class size i that cross a 1 m width vertical soil profile at a distance d from an isolated tree stem with the diameter at breast height (DBH, in [m]) ϕ_t following the equation:

$$N_{i,t}(d,\phi_t) = \begin{cases} D_{fr}\frac{[ln(1+\phi_{max})-ln(1+\phi_i)]}{ln(1+\phi_{max})}(\frac{\phi_i}{\phi_0})^{\beta}, & \text{with } d < d_{max} \text{ and } \phi_i < \phi_{max} \\ 0, & \text{otherwise} \end{cases} \quad (4.2)$$

d_{max} is the maximum rooting distance from the stem [m], D_{fr} is the density of fine roots (smaller than 1.5 mm) per horizontal meter, ϕ_i is the mean root diameter in class size i [m], ϕ_0 is a reference diameter (in this paper equal to 1 mm), ϕ_{max} is the maximum root diameter [m], and β is a constant exponent.

$$d_{max}(\phi_t) = \psi\phi_t \quad (4.3)$$

$$\phi_{max} = \frac{d_{max} - d}{\eta} \quad (4.4)$$

ψ is a proportionality constant, ϕ_t is the tree diameter at the breast height [m], and η is a dimensionless scaling coefficient.

The density of fine roots [0.5-1.5 mm] crossing a 0.9 m depth and 1 m width vertical soil profile at a given distance d from an isolated tree stem with DBH ϕ_t is calculated as:

$$D_{fr}(d,\phi_t) = [\frac{\mu(\phi_t^2\frac{\pi}{4})}{d_{max}2\pi d}](\frac{d_{max}-d}{d_{max}}), \text{ with } d < d_{max} \quad (4.5)$$

where μ is the pipe coefficient.

Model parameters μ, β, ψ, and η were calibrated by minimizing the Sum of Squares Errors (SSE) obtained as the difference between modeled and measured root distribution data.

The RDM simulates lateral root distribution only, without considering the vertical distribution. The calibration of the RDM is particularly useful for the application of models such as BankforNET (Gasser et al., 2019; Gasser et al., 2020; Perona et al., 2022), and for the modeling of hydraulic bank erosion influenced by riparian vegetation.

4.2.5 Root reinforcement calculations: from single root to root system

RBMw

The Root Bundle Model with Weibull survival function (RBMw) proposed in Schwarz, Giadrossich, and Cohen (2013), Dazio, Conedera, and Schwarz (2018), and Murgia et al. (2022) is used to quantify the reinforcement due to a root bundle. Root tensile force as a function of displacement and root distribution are two essential inputs of

the model. Applying in-situ data allows a better fit of the model calibration of the local field conditions (Giadrossich et al., 2017a), assuming that the pullout force of a single root is not affected by neighboring roots (Giadrossich et al., 2013a). A power-law relationship is used to fit the regression curve between maximum tensile force and root diameter:

$$F_{max}(\phi) = C(\phi)F_0\phi^{\alpha} \tag{4.6}$$

F_{max} is the maximum tensile force [N], ϕ is root diameter [m], F_0 is a constant, and α is an exponential parameter. Because the fitting curve overestimates the strength of roots with a diameter smaller than 5 mm in some cases, a cumulative normal distribution function (Equation 4.7) with values ranging from 0 to 1 is used to improve the model fit (Gehring et al., 2019).

$$C(\phi) = \frac{1}{2}[1 + erf(\frac{\phi - \phi_m}{\phi_{sd}\sqrt{2}})] \tag{4.7}$$

where ϕ_m and ϕ_{sd} are coefficients corresponding to the mean and standard deviation of the cumulative normal distribution.

An apparent secant spring constant was calculated by the ratio of maximum root pullout force over the displacement at root failure.

$$k = k_0\phi \tag{4.8}$$

where k is the spring constant [N/m], ϕ is the root diameter [m], and k_0 is a root spring constant scaling factor.

In the RBMw, the survival probability of each root diameter is calculated as a function of the normalized displacement, $\Delta x^*(\phi)$.

$$\Delta x^*(\phi) = \frac{\Delta x}{\Delta x^{fit}_{max}(\phi)} \tag{4.9}$$

The Weibull survival function is defined as below:

$$S(\Delta x^*) = exp[-(\frac{\Delta x^*}{\lambda})^{\omega}] \tag{4.10}$$

where ω is the Weibull shape factor and λ is the Weibull scaling factor. The parameters k_0, α, λ, and ω are calibrated using measured data from field pullout tests and tensile tests, by minimizing the Sum of Squared Errors (SSE).

The total root reinforcement of a root bundle is calculated as the sum of all tensile forces of roots in the bundle at different displacements. Lateral tensile root reinforcement is expressed in N/m, considering all the roots crossing a 1 m width vertical soil trench.

$$RR_{bundle}(\Delta x) = \sum_{\phi=1}^{\phi_{max}} n_\phi F(\phi_i, \Delta x) S(\Delta x^*_\phi) \tag{4.11}$$

The lateral root reinforcement of all soil trenches in the study area is calculated using the calibrated RBMw.

Root reinforcement at the root system scale

The maximum lateral root reinforcement RR_{max}, defined as the peak of the force-displacement curve resulting from the RBMw, is used to upscale the value of root

reinforcement from a single root to the root system scale. RR_{max} is calculated as a function of the tree DBH, ϕ_t [m], and the distance from the tree stem, d [m]. The function for the lateral reinforcement is assumed to follow the gamma density distribution Γ (Dazio, Conedera, and Schwarz, 2018; Gehring et al., 2019) as below:

$$RR_{max}(\phi_t, d) = \begin{cases} a \cdot \phi_t \cdot \Gamma(\frac{d}{\phi_t \cdot 18.5}; b, c), & \text{for } d < 18.5 \cdot \phi_t \\ 0, & \text{for } d \geq 18.5 \cdot \phi_t \end{cases} \tag{4.12}$$

where ϕ_t is tree size (DBH, in [m]), d is the distance from the tree stem [m], a is scaling factor, b is shape parameter, and c is rate parameter (Zadelhoff et al., 2022). The calibration of the parameters a, b, and c is achieved by minimizing the Sum of Squared Errors.

From the lateral root reinforcement RR_{max}, it is possible to calculate the basal reinforcement in accordance with Gehring et al. (2019) as below:

$$RR_{basal}(z) = RR_{max} \cdot \Gamma(z; z_\alpha, z_\beta) \tag{4.13}$$

where z is the soil depth, z_α and z_β are calibrated coefficients of the gamma density function using minimizing SSE.

This model does not take spatially differentiated root distribution along the slope gradient around a tree stem. It assumes that the roots are symmetrically distributed all around the tree (Schwarz, Cohen, and Or, 2012b; Dazio, Conedera, and Schwarz, 2018).

4.2.6 Statistic analyses and models validation

RDM, RBMw, and root reinforcement models were implemented in the open-source programming language R software. Cross-validation (Allen, 1974; Stone, 1974; Geisser, 1975; Yadav and Shukla, 2016) is used to estimate the generalization performance and to evaluate the proposed models. Cross-validation has been widely regarded as a standard method in model evaluation and selection (Hastie et al., 2009; Zhang and Yang, 2015). The data is split into train/test in the percentage ratio of 80/20. This partition has been commonly applied in various research fields for splitting data and independent accuracy assessment because it was proved to perform better for large datasets, avoid overfitting, achieve the best result as well as decrease computational time (Huang, Yang, and Wang, 2003; Lyons et al., 2018; Vrigazova, 2021; Rácz, Bajusz, and Héberger, 2021; Seidu et al., 2022). We then evaluated model performance through the Sum of Squares Errors (SSE), R^2, and the difference in normalised SSE between training and testing datasets to examine the model stability. This operation is repeated 30 times, changing training and testing datasets randomly, in order to prove the convergence of the results. The formula is similar to the Mean Bias Error (MBE) as below:

$$\overline{Var} = \frac{1}{n}\sum_{i=1}^{n}(N\_SSE_{train,i} - N\_SSE_{test,i}) \tag{4.14}$$

where $N\_SSE_{train,i}$ is normalised SSE of the training dataset, $N\_SSE_{test,i}$ is normalised SSE of testing dataset, n is the number of assessed loops, and $\overline{Var}$ is the mean variance between the two datasets.

4.3 Results

4.3.1 Root distribution measurements and modeling

Root distribution measurements of single root systems

The number of measured fine roots [0.5-1.5 mm] decreases with soil depth and also with the increase in distances from the stem in all trenches (Figure 4.4). Considering horizontal distribution, the greatest number of fine roots is recorded in the 1.5 m trench in all trees.

The largest changes in fine root frequency are observed between the 1.5 m and 2.5 m trenches around all trees, whereas the number of fine roots in the three farther distances does not change remarkably. In the first soil layer, the reduction of fine roots between the 1.5 m and 2.5 m trench of tree 1, 2, 3, and 4 are 61%, 61%, 51%, and 59%, respectively.

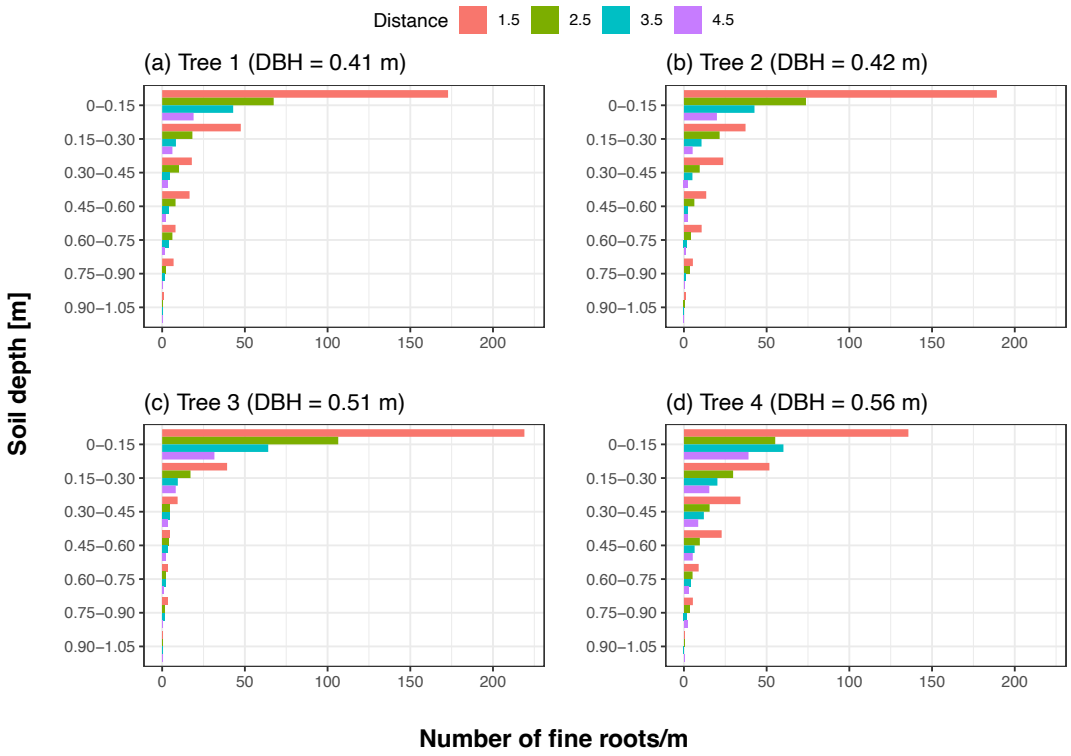

FIGURE 4.4: Mean measured number of fine roots [0.5-1.5 mm] of "Tasman" poplars in each soil depth of 1 m width at different distances 1.5 m (red color), 2.5 m (green color), 3.5 m (blue color), and 4.5 m (purple color) from stem with different DBH (a) 0.41 m, (b) 0.42 m, (c) 0.51 m, and (d) 0.56 m.

Considering the vertical root distribution, the number of fine roots is reduced dramatically by increasing soil depth. In the first trench, the total number of fine roots in the first soil layer is between 136 roots/m to 219 roots/m, decreasing down to 37 roots/m to 52 roots/m in the second layer.

Tree 3 exhibits the most fine roots in the first soil layer, however, fewer fine roots are present in deeper soil layers compared to other trees. Although the number of fine roots of the largest tree is the least in the nearest trench, it becomes the greatest in the farthest trench. In particular, fine roots of larger trees reaches deeper soil layers and expands further than smaller ones.

The amount of coarse roots has a similar pattern as fine roots, with decreasing trend from 1.5 m to 4.5 m distances (Figure 4.5). The majority of coarse roots is in the first 0.15 m soil layer. Tree 4 has the greatest number of coarse roots in both horizontal and vertical directions. In the horizontal direction, the number of coarse roots in tree 4 in the 4.5 m trench (presented as purple bars) is twice that of tree 1 and tree 2. There are huge gaps in the number of coarse roots from the 1.5 m to the 2.5 m trench in all trees, which reflected the pattern measured in the fine root distribution. Given coarse root density in the 0-0.15 m soil layer, the differences between the 1.5 m and 2.5 m trench in tree 1, 2, 3, and 4 are recorded to be 54%, 54%, 56%, and 56%, respectively.

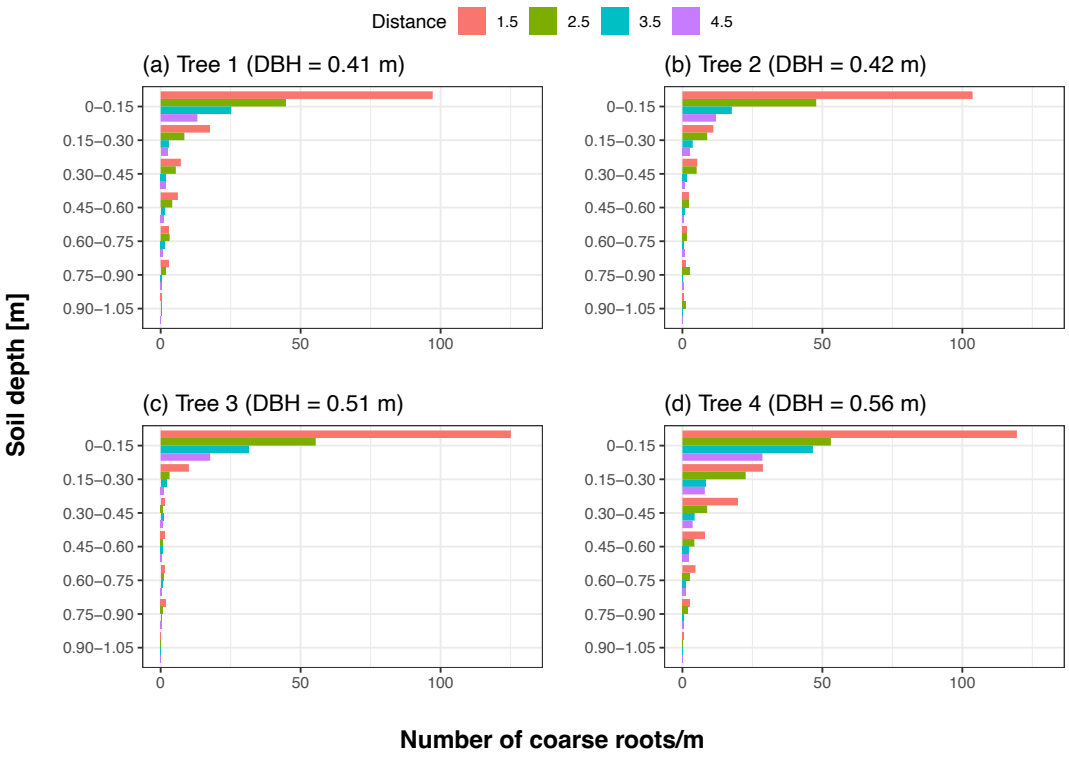

FIGURE 4.5: Measured number of coarse roots (> 1.5 mm) of "Tasman" poplars in each soil depth at different distances (1.5 m (red color), 2.5 m (green color), 3.5 m (blue color), and 4.5 m (purple color)) from the stem with different DBH (a) 0.41 m, (b) 0.42 m, (c) 0.51 m, and (d) 0.56 m

Table 4.3 presents the measured partition of three root categories: fine roots, 1.5-10.5 mm roots and > 10.5 mm roots at the first two soil layers and two nearest distances from the tree stem. Overall, fine roots comprise the greatest proportion of the total number of roots in all trees, followed by 1.5-10.5 mm root classes and roots > 10.5 mm.

TABLE 4.3: Measured composition of root classes: fine roots, 2-10 mm root class and > 10.5 mm roots at the first two soil depths and first two distances from the tree stem.

		1.5 m distance			2.5 m distance		
Tree	Depth	% fine roots	% 1.5-10.5 mm roots	% roots > 10.5 mm	% fine roots	% 1.5-10.5 mm roots	% roots > 10.5 mm
1	0-0.15	64	33	3	60	36	4
1	0.15-0.3	73	25	2	68	29	3
2	0-0.15	65	32	3	61	35	4
2	0.15-0.3	77	21	2	71	26	3
3	0-0.15	64	31	5	66	30	4
3	0.15-0.3	80	10	0.2	84	15	1
4	0-0.15	53	41	6	51	41	8
4	0.15-0.3	64	31	5	57	40	3

Root distribution modeling for single tree systems

The RDM was calibrated and validated with the collected in-situ data. Two types of data are required to calibrate the model; (i) the distribution of fine roots in relation to the distance from the stem, and (ii) the frequency of various diameter classes at different distances from the stem. The best-fitted parameters of the root distribution model for "Tasman" poplar are presented in Table 4.4. R^2 of two dataset were 0.78 and 0.85, suggesting the model fitted quite well with the measured data (Table 4.5). We repeatedly fitted the parameters of the model randomizing the splitting of the training and testing datasets with the proportion of 80/20 to evaluate the model stability; the results are presented in sector Appendix A.

TABLE 4.4: Calibrated parameters of the root distribution model.

Symbol	Parameter	Value
μ	Pipe coefficient	97056.03
β	Empirical exponent of coarse root density	-1.501547
η	Scaling coefficient for maximum root diameter at a distance	0.1319465
ψ	Proportionality constant for maximum root lateral extension	16.21262

TABLE 4.5: Summary table of the calibration and validation of the root distribution model. 80% of total measured data (n = 140) was applied to calibrate the model whereas 20% (n = 32) was used to validate the model. SSE is the sum of square errors, and R^2 is the coefficient of determination.

Dataset	**n**	**SSE**	R^2
Training	140	634.60	0.79
Testing	32	173.45	0.75
Trench	128	684.65	0.78
Pit	44	123.40	0.85

Figure 4.6 shows the fine root distribution of mean measured data and best-fitted modeled data considering different sizes of trees and various distances from the tree stems. The model underestimates fine root density in the first three trenches but well simulates it well in the farthest trench. The percentage errors between measured and modeled fine root density in the 1.5 m trench of the smallest to the biggest trees are 41%, 42%, 25%, and 10%. Similarly, the percentage errors between measured and simulated fine root density in the farthest trench are 33%, 23%, 17%, and 36%. Overall, our findings indicate that the root distribution model tends to underestimate the number of fine roots in all trees.

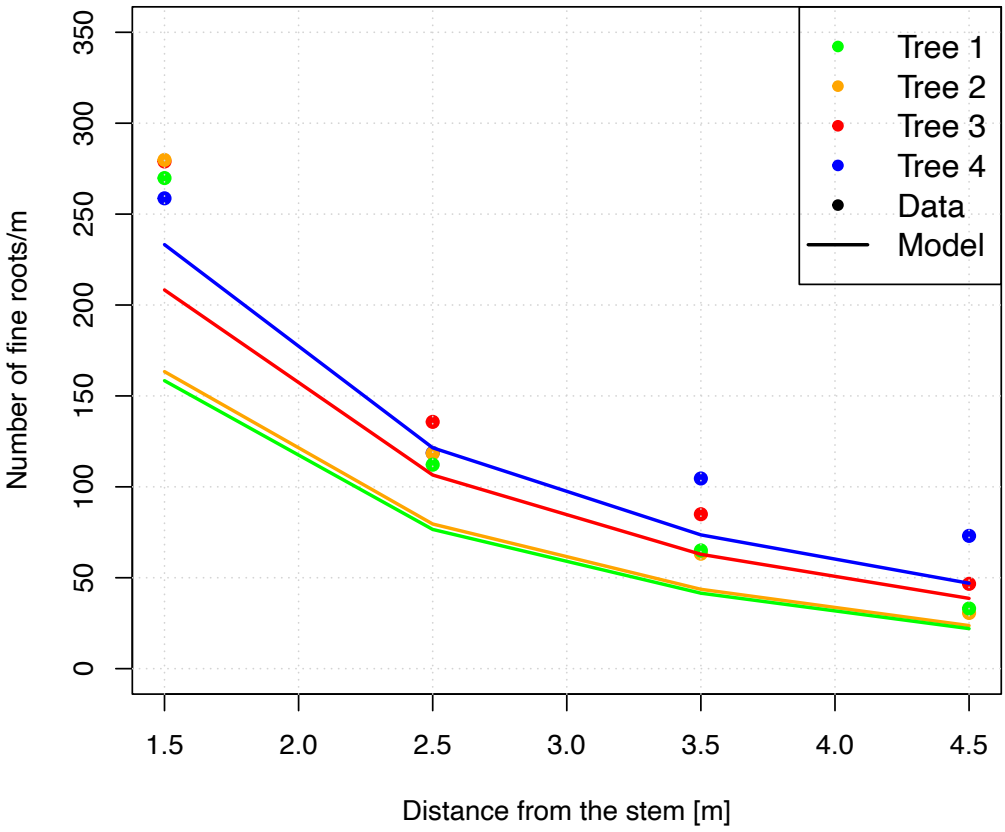

FIGURE 4.6: Mean measured (dots) and modeled (lines) number of fine roots per linear meter along the trenches (number/m), from four distances of 1.5 m, 2.5 m, 3.5 m, and 4.5 m from the four stems of "Tasman" poplars with different DBH. Tree 1 with 0.41 m DBH was presented in green, Tree 2 with 0.42 m DBH was indicated in orange, Tree 3 with 0.51 m DBH was exhibited in red, and Tree 4 with 0.56 m DBH was presented in blue.

The measured and modeled number of coarse roots from 1.5 to 10.5 mm diameter classes at each distance from the stem is presented in Figure 4.7. In general, the model tends to underestimate the abundance of coarse roots in all trenches of trees except from tree 3.

For the 10 mm class of root diameters, the differences between measured and predicted values in the 1.5 m trench from the smallest tree to the biggest tree are correspondingly 0.05, 0.13, 0.57, and -1.44 roots/m with simulated values higher than measured ones except from tree 4; whereas in 4.5 m trench, the variations are -0.17, -0.19, 0.11, and -0.47 roots/m, respectively with simulated values smaller than collected data in tree 1, 2 and 4. Therefore, the model exhibits a better estimation of coarse roots than fine roots. Generally, root distribution simulates the root density at each distance well with $R^2 = 0.78$.

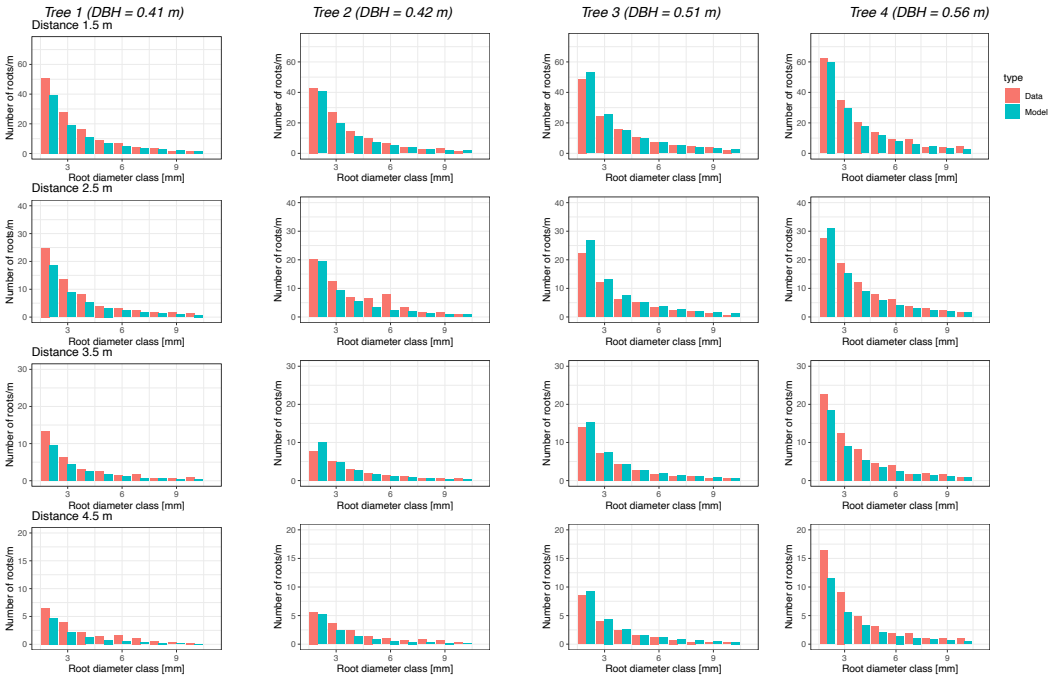

FIGURE 4.7: Measured (red bars) and modeled (blue bars) number of coarse roots in four poplar trees with different sizes at four distances of 1.5 m, 2.5 m, 3.5 m, and 4.5 m away from the stems. The red bars presented measured data whereas blue bars indicated simulated data.

Root distribution modeling at the stand scale

With the aim of validating our root distribution within a stand, we compared the simulated fine root abundance with measured data from four faces of the eleven soil pits in the transect. According to Figure 4.8, RDM performs well in the sparse zone in the stand (pits 1 to 5), whereas it tends to overestimate the number of fine roots in the pits situated in the denser zone (pits 6 to 11). In soil pit 1 and 2, which were located in the sparsest zone, the model estimates the number of fine roots with differences of 0.88 and 12 fine roots/m. In contrast, in pit 11, which was located in the densest zone, the modeled value is around 2.6 times greater than the measured one, reaching up to 204 fine roots/m while mean measured value is just ca. 79 fine roots/m. The percentage errors between the mean measured and modeled fine root density in each pit from sparse to dense zone are 1%, 17%, 94%, 0.1%, 17%, 45%, 42%, 87%, 175%, 83%, and 159%.

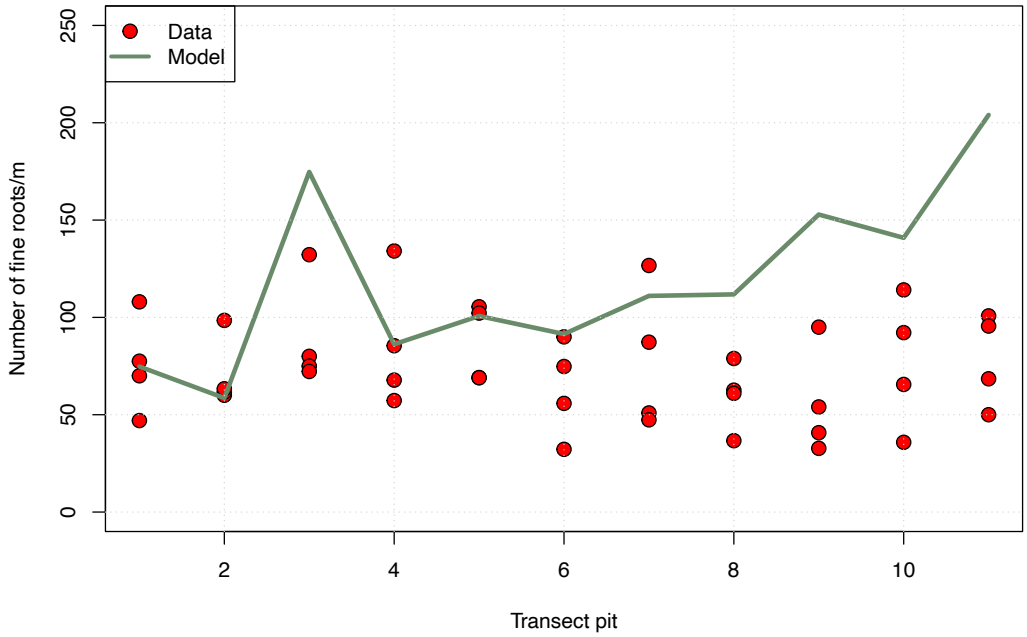

FIGURE 4.8: Comparison between measured and modelled number of fine roots in different transect pits (mean over the four soil faces). Red dots represent collected data at four soil faces of each pit; the green curve indicated the simulated average number of fine roots in 1 m width and 0.9 m depth of each pit.

Figure 4.9 compares the measured and modeled number of coarse roots in the transect of soil pits. Overall, the model overestimates the number of coarse roots, especially the 2 mm root class. The maximum and minimum variations between two types of data of the 2 mm root diameter class are recorded up to 32 roots in pit 11 and 0.72 roots in pit 1, respectively. The percentage errors of the predicted coarse root density compared to measured ones increase correspondingly from sparse to highly planting zone. We used the t-test to compare the means of two datasets and observed that the difference in number of roots in pit 1 between measured data (mean = 3.89) and simulated data (mean = 3.95) was insignificant ($t(58) = 0.017112$; $p = 0.9864$). The t-test performance on the comparison of measured and modeled root abundance in pit 11 showed that the number of roots simulated (mean = 10.80) was higher than measured values (mean = 4.06) but insignificant with a difference of ($t(38) = 0.91348$; $p = 0.3669$). Overall, the root distribution model performs well at the stand scale with $R^2 = 0.85$.

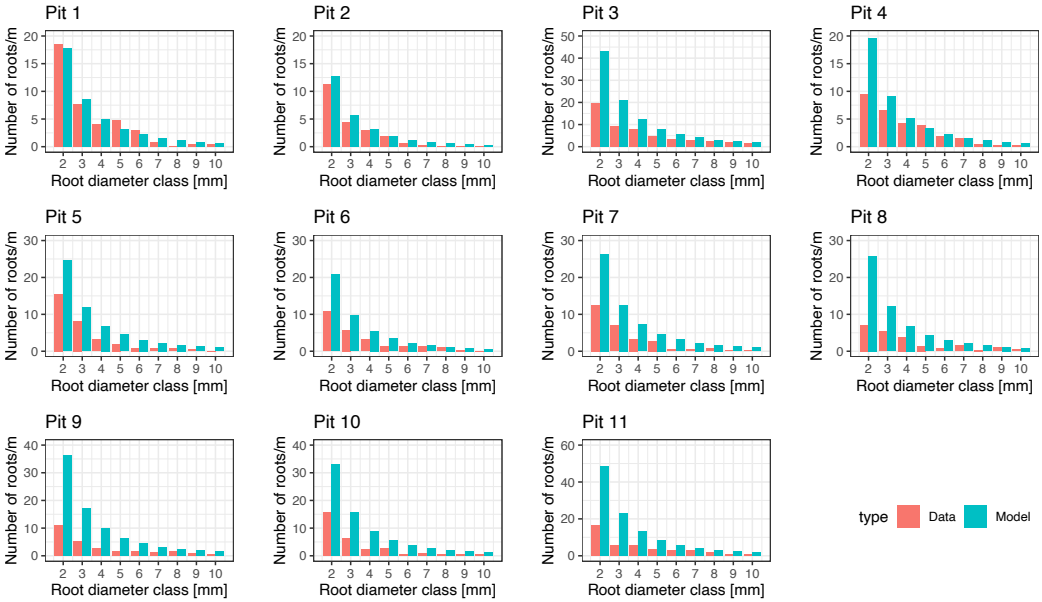

FIGURE 4.9: Comparison between measured and modeled number of coarse roots in root diameter class from 2 mm to 10 mm along the transect of soil pits in the stand (mean over the four vertical profiles of each pit).

4.3.2 Root Area Ratio

We calculated the cross-sectional area of roots per area of a soil profile (the root-area-ratio, RAR) at different distances from the stems.

Generally, most of the RAR is concentrated in the first 0.4 m soil depth and then decreases sharply close to 0 in all tree sizes, in accordance with the data on root distribution (Figure 4.10).

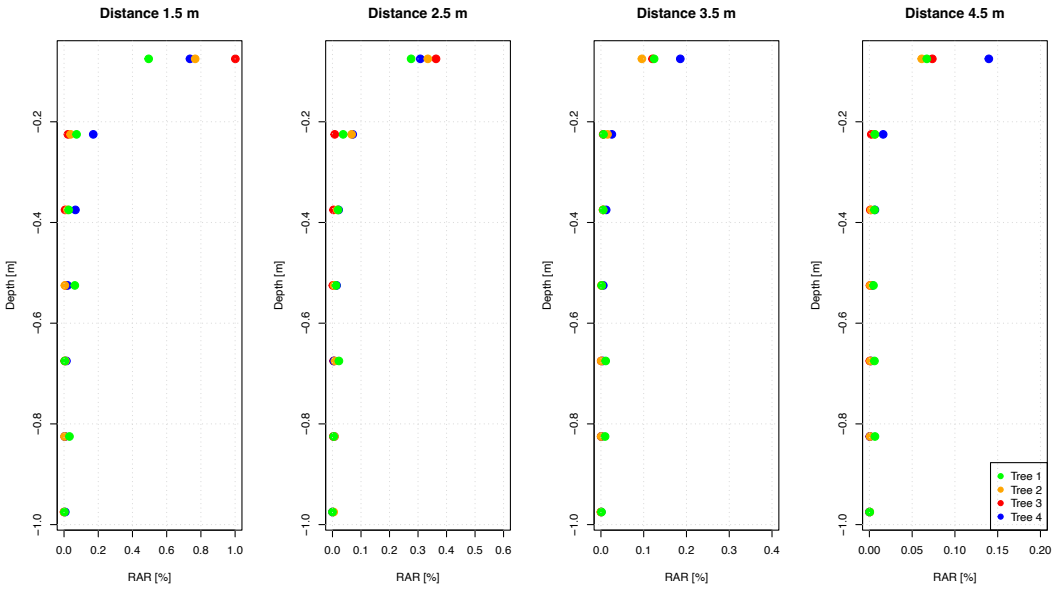

FIGURE 4.10: Correlations of measured RAR of four "Tasman" poplars with soil depth and distances from the stems. RAR values of tree 1 (DBH = 0.41 m) is represented in green dots, values of tree 2 (DBH = 0.42 m) is recorded in orange dots, values of tree 3 (DBH = 0.51 m) is indicated in red dots, and values of tree 4 (DBH = 0.56 m) is exhibited in blue dots.

Results of RAR exhibit great variation with different tree sizes and distances to the stem (Figure 4.11). Generally, RAR values decrease when the distance from the stem increases. In all single tree datasets, the maximum RAR values are recorded in the closest trench (1.5 m) ranging from 1.048% to 0.69%. For the 1.5 m trenches, the maximum RAR value is measured in Tree 3 with DBH of 0.51 m, and the minimum value is recorded in Tree 1 with DBH of 0.41 m. The biggest differences between measured and simulated RAR values are found to be at the first trench, especially in tree 2 with a residual up to 0.43%. At the distance of 4.5 m, the differences between the two datasets are not large with values of 0.08%, 0.05%, 0.02%, and 0.07% corresponding to the tree sizes from smallest to largest. Overall, the root distribution model tends to underestimate the RAR of all trees at all distances. However, the model performs better at 3.5 and 4.5 m distance from the stems.

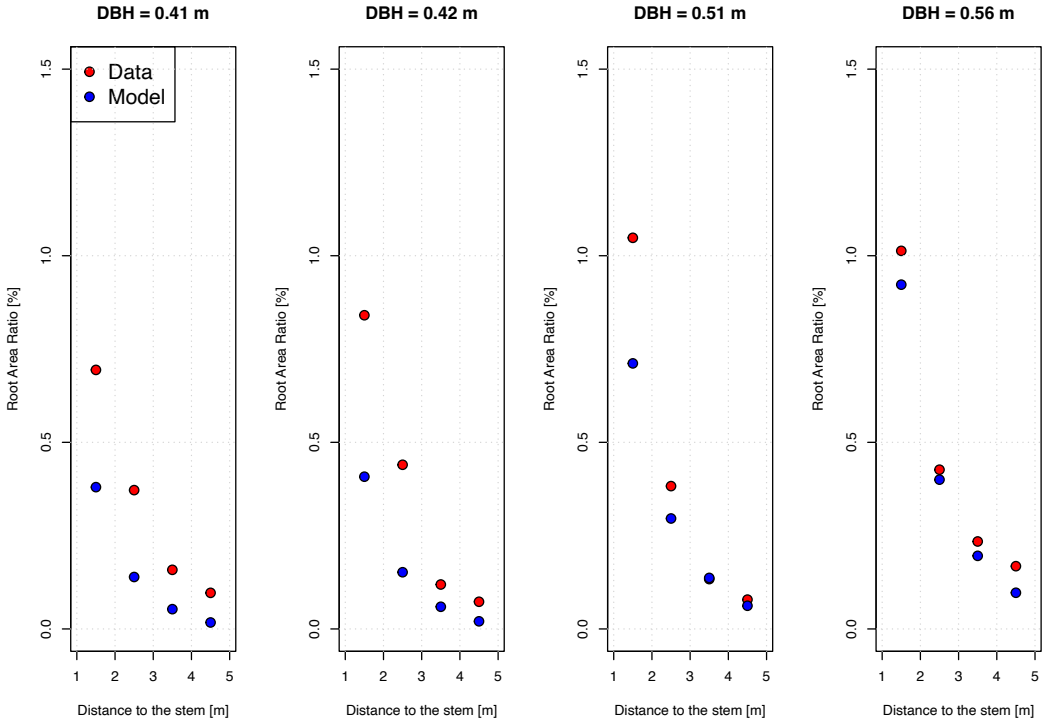

FIGURE 4.11: Comparison between measured (red dots) and simulated (blue dots) root-area-ratio (RAR) from different sizes of poplar trees at various trenches from the stems.

Along the transect of soil profiles, the biggest differences between collected and simulated RAR values are observed in transect pit 3, which is similar to the results of both fine and coarse root distribution (Figure 4.8, 4.9 and 4.12). The modeled RAR values are greater than the measured ones, even in pits located in the sparse zone. In contrast, the difference in RAR values between collected data and modeled is much smaller compared to the difference in fine root density in pit 11.

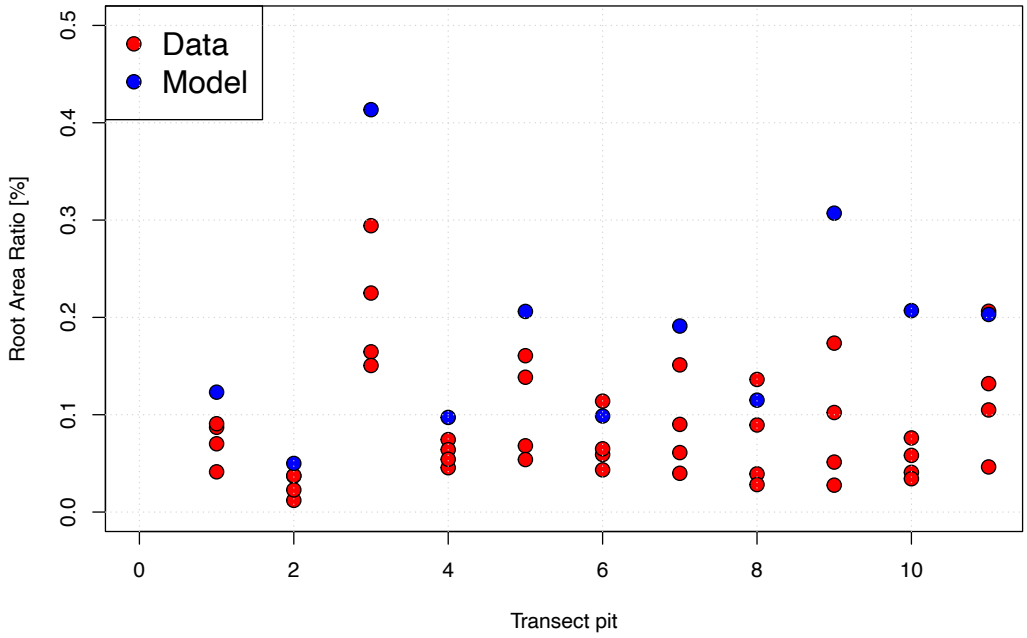

FIGURE 4.12: Comparison between measured (red dots) and simulated (blue dots) root-area-ratio (RAR) in various faces of transect's pits.

4.3.3 Root reinforcement upscaling

Root bundle model

The mechanical properties of poplar's roots were quantified using both laboratory tensile tests (124 tests) and pullout tests (66 tests) with root diameters ranging from 1.7 mm to 40 mm. Figure 4.13 shows all 190 collected data and presents a clear increase in maximum tensile force with increasing diameter. A shape increase in data variability can be observed in roots from 0.005 m to 0.01 m in diameter. However, with roots from 0.01 m and thicker, the rise appears to remain rather constant. The fitting correction with the cumulative normal distribution function (power-law fit + Survival curve) visibly diminishes residuals for small roots, especially roots smaller than 0.01 m. The $R^2 = 0.88$ suggests that the curve predicts the measured tensile forces well.

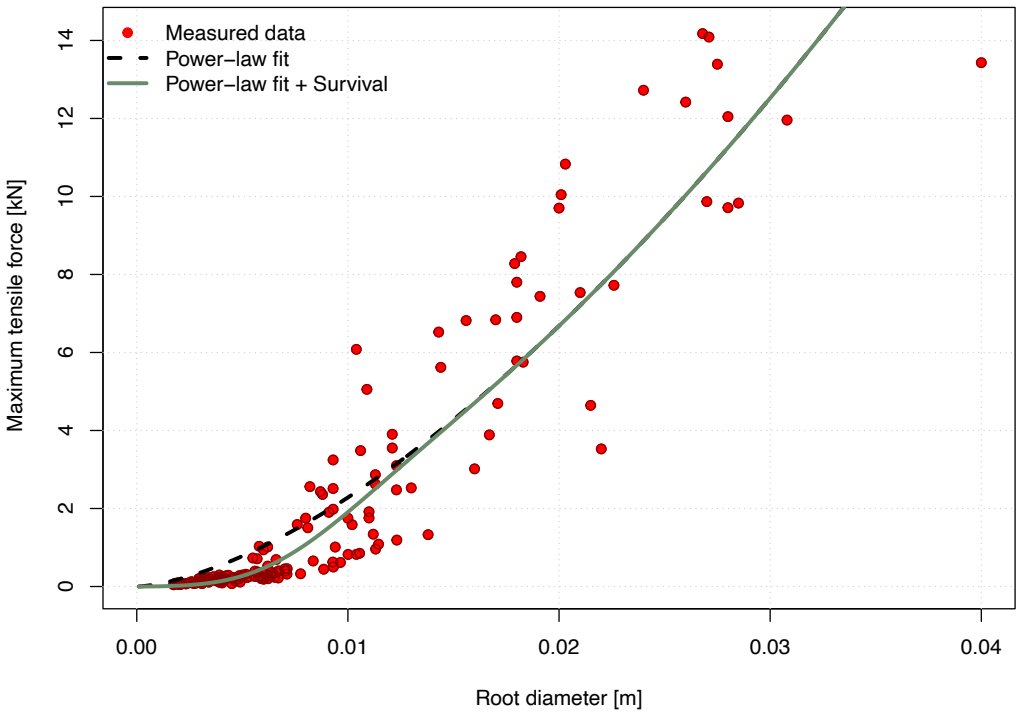

FIGURE 4.13: Maximum tensile force in relation to root diameter of "Tasman" poplars.

Figure 4.14 shows the survival function estimated from both root tensile tests in laboratory and pullout tests in-situ. The best-fitted Weilbull shape factor ω was 1.83 and the scaling factor λ was 1.53.

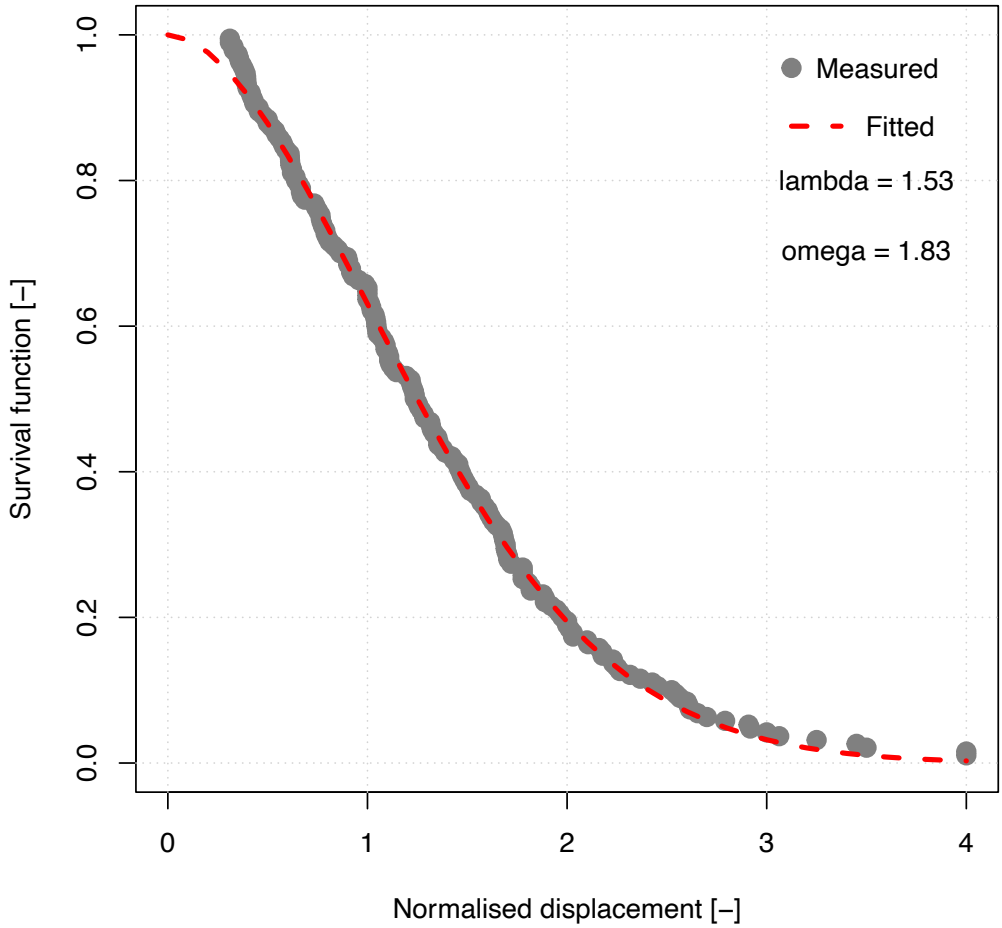

FIGURE 4.14: Survival function for collected data from both laboratory tensile test and pullout test. Grey dots are measurements. The red dashed line represents the best fit.

Table 4.6 summarizes the calibrated parameters of the root mechanical properties required for the root reinforcement quantification with the RBMw model of "Tasman" poplars.

TABLE 4.6: Calibrated parameters of the RBMw model.

Symbol	Parameter	Value
F_0	Root force scaling factor	2.9 x 10^6
α	Root force shape factor	1.55
k_0	Root spring constant scaling factor	9.7 x 10^6
λ	Weibull scaling factor	1.53
ω	Weibull shape factor	1.83
ϕ_m	Mean of cumulative normal distribution	0.00643
ϕ_{sd}	Standard deviation of cumulative normal distribution	0.00365

Root reinforcement as a function of distance and DBH

In general, lateral root reinforcement increases with increasing stem sizes and decreases with increasing distances from the stem. The coefficients fitted by the minimum Sum of Squared Errors in equation 4.12 are listed in tables 4.7 and 4.8. R^2 of the training and testing dataset are 0.60 and 0.69, respectively, indicating that the model performs reasonably well. Figure 4.15 compares measured (dots) and simulated (lines) lateral root reinforcement as a function of stem size (DBH) and distances from the stem.

TABLE 4.7: Calibrated parameters of the root reinforcement model.

Symbol	Parameter	Value
a	Scaling factor	41030.49
b	Shape parameter	0.9892003
c	Rate parameter	9.750829

TABLE 4.8: Summary table of the calibration and validation of the root reinforcement model. 80% of total measured data (n = 140) was applied to calibrate the model whereas 20% (n = 32) was used to validate the model. SSE is the sum of square errors, and R^2 is the coefficient of determination.

Dataset	n	SSE	R^2
Training	140	1157700	0.60
Testing	32	275801	0.69
Trench	128	1259770	0.64
Pit	44	173731	0.32

The results of the model show that a single tree with 0.6 m DBH is able to contribute to soil strength with a root reinforcement up to 64 kN/m in the 1.5 m trench and still provide up to 4.5 kN/m reinforcement at 4.5 m distance. However, a single tree with 0.4 m DBH can reach ca. 22 kN/m at 1.5 m distance and around 0.4 kN/m at 4.5 m distance from stem. Based on figure 4.15, there seems to be insignificant influence of DBH on the root reinforcement, especially from 2.5 m distance and upwards.

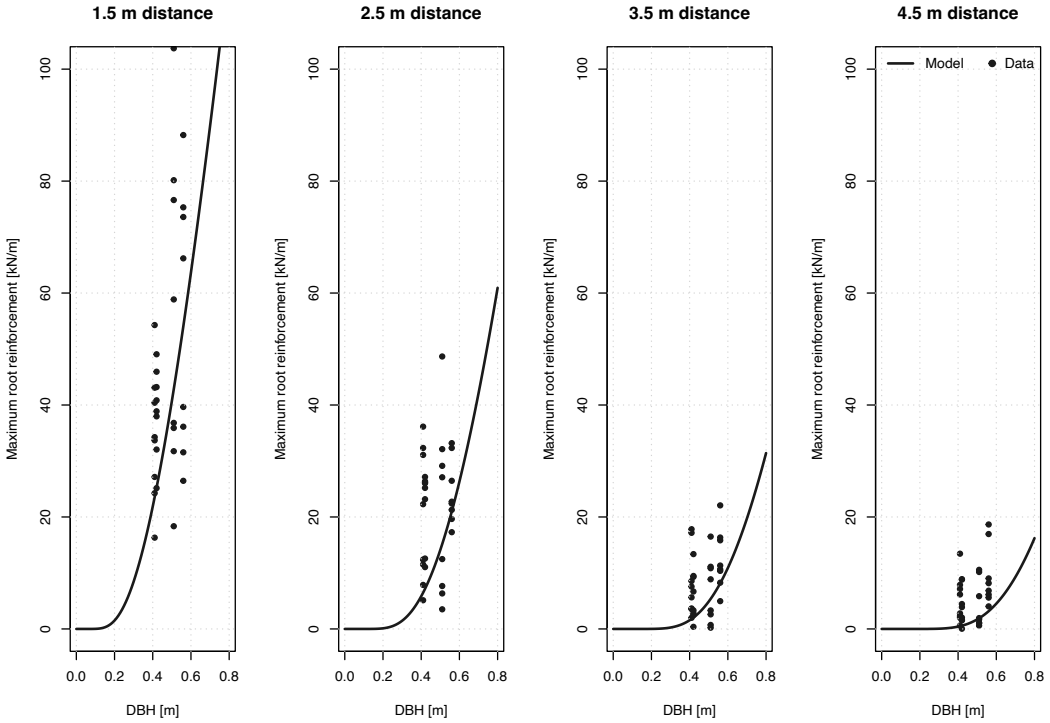

FIGURE 4.15: Maximum root reinforcement as a function of the tree DBH at four distances from the stem. Black dots represent measured root reinforcement calculated with RBMw while the black line indicates root reinforcement estimated with maximum lateral root reinforcement.

Figure 4.16 shows the residuals of the modeled lateral root reinforcement as a function of distance from the tree stem and the DBH. The data shows a higher variability of the residual near the tree stem and a decrease with increasing distance from the stem. The variability of residuals is similar between the DBH values. The greatest variations are up to 40 kN/m in the 1.5 m trench and 15 kN/m in the 4.5 m trench. The proportion of the positive values of residuals is higher than the negative ones, especially at greater distances from the tree stem. However, the mean values of variances from the closest to the farthest trenches were 9.4, 9.4, 4.03, 4.15 kN/m respectively, indicating a general underestimation of the model.

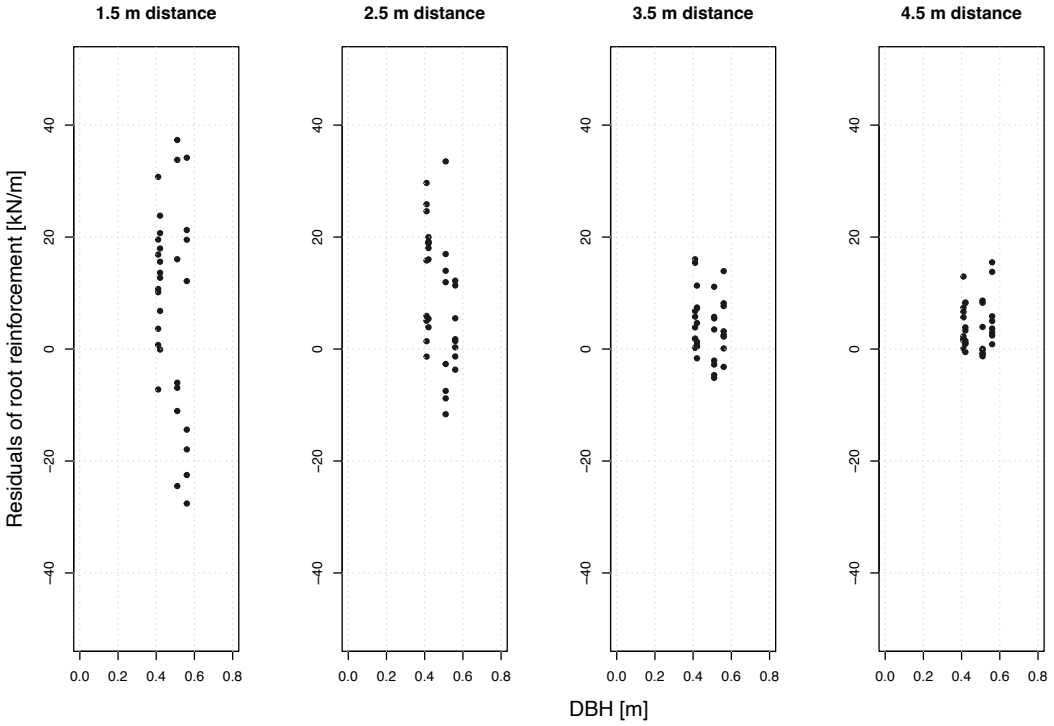

FIGURE 4.16: Residuals of the modeled lateral root reinforcement.

Along the transect, the modeled lateral root reinforcement values tend to be in good agreement with the measured ones. Only for the trenches with high tree density, the model tends to overestimate (Figure 4.17). Interestingly, the highest and lowest measured forces are in two neighbor pits in the low density part of the stand. The highest value is in the pit 3 (by the nearest distance between 2 trees), whereas the weakest one is in the pit 2 (by the farthest distances between 4 trees).

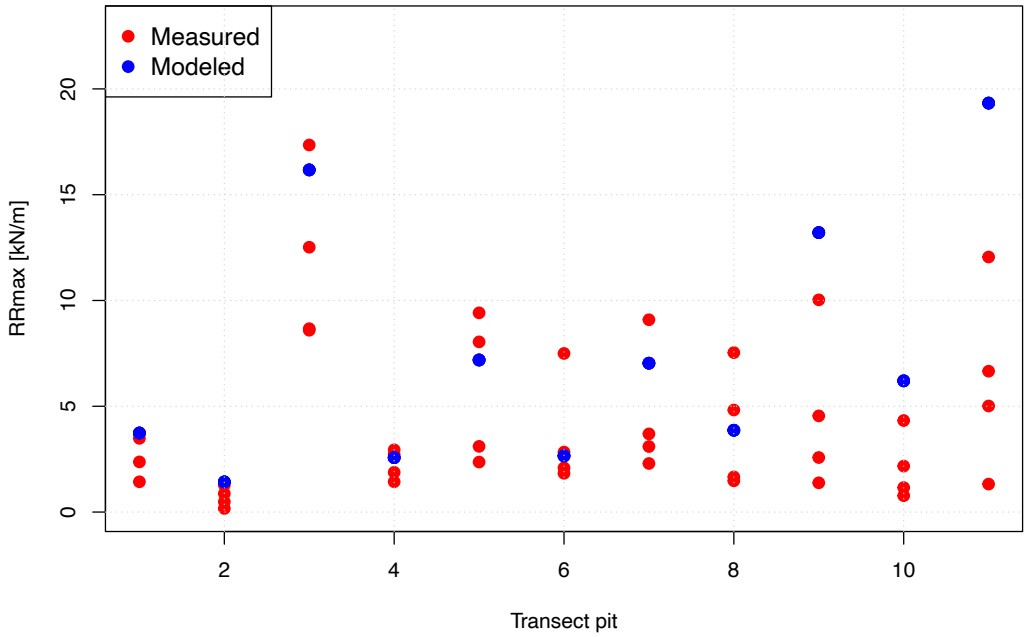

FIGURE 4.17: Comparison of the modeled (blue dots) and measures-based (red dots) values of root reinforcement along the transect of pits in the poplar stand. The modeled values are calculated for the center of the pits, whereas the measures-based values are calculated for each of the four profiles of the pits.

Vertical distribution of root reinforcement

Most lateral root reinforcement is concentrated within the first 0.30 m of soil depth, in both the trenches and transect pits. Equation 4.13 was calibrated with the measured data, shown with the red points and lines in Figure 4.18. The best-fitted values of the parameters are summarised in Tables 4.9 and 4.10 with an overall R^2 value of 0.99.

TABLE 4.9: Calibrated parameters of the root reinforcement model.

Symbol	Parameter	Value
Z_α	Shape parameter	1.151732
Z_β	Rate parameter	14.98385

Calibration and validation parameters of the model for the vertical distribution of root reinforcement (n = 172) with Z_α is the shape parameter, Z_β is the rate parameter, and SSE is the sum of square errors.

TABLE 4.10: Summary table of the calibration and validation of the root reinforcement model. 80% of total measured data (n = 140) was applied to calibrate the model whereas 20% (n = 32) was used to validate the model. SSE is the Sum of Square Errors, and R^2 is the coefficient of determination.

Dataset	**n**	**SSE**	R^2
Training	140	0.09	0.99
Testing	32	0.15	0.99
Trench	128	0.16	0.99
Pit	44	0.09	0.99

Within the first soil layer, the maximum root reinforcement value is measured up to 103.72 kN/m in the 1.5 m trench of Tree 3. The mean root reinforcement in each soil depth among the soil trenches are 17.12, 1.90, 0.80, 0.50, 0.34, and 0.30 kN/m, respectively. The strongest root reinforcement among transect pits is found to be 16.67 kN/m located in the first soil layer of pit 3. From 0.3 m and downwards, the basal root reinforcement decreases very rapidly. Among the second soil depths, the maximum root force is recorded in the first trench of Tree 4 with a value of 36 kN/m and in pit 11 with a value of 3.17 kN/m. At the average depth of 0.375 m, the strongest force is found in the first trench of the biggest tree - Tree 4 with values of 10.48 kN/m while at the depth of 0.525 m, the maximum force is recorded in the first trench of Tree 1 with 16.44 kN/m. From 0.6 m and downwards, the basal root reinforcement of all soil profiles is so weak that its contribution to soil strength would be insufficient. Unfortunately, we could not collect data from the roots under the stem. Vertical root distribution was recorded at 1.5, 2.5, 3.5, and 4.5 m from the stem. However, one pit was found to have a thick root of up to 100 mm running vertically. Such a root would have great influence on the basal root reinforcement, explaining the big variation of root reinforcement at the soil layer 0.8 m in pit data. According to Figure 4.18, most of the basal root reinforcement concentrates in the first soil layers and decreases sharply following deeper layers.

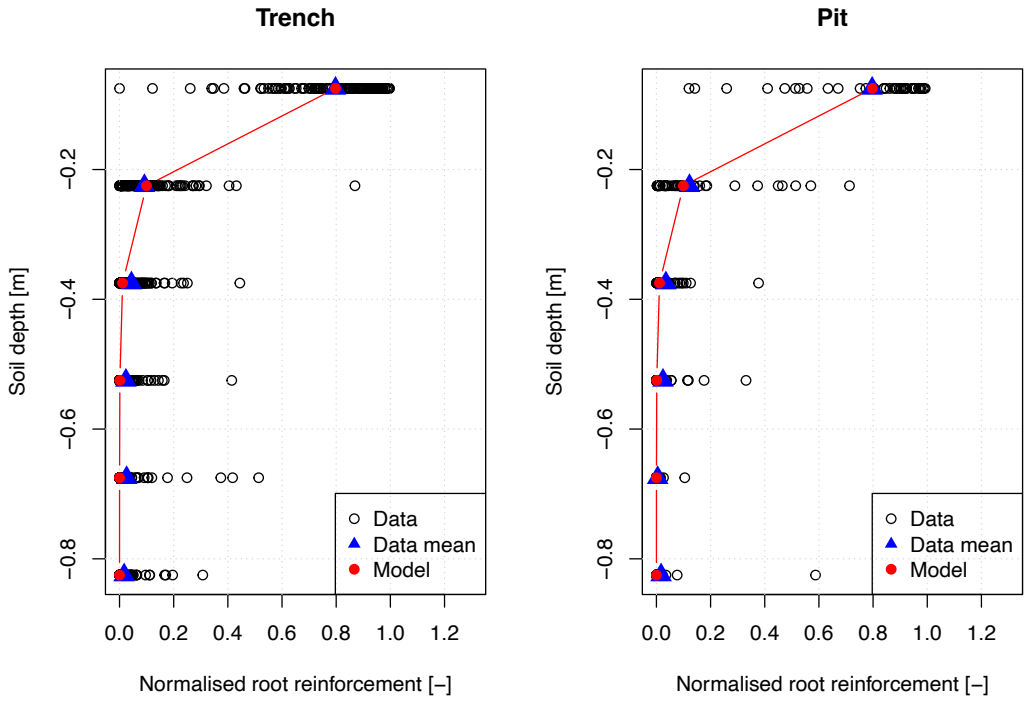

FIGURE 4.18: Normalised basal root reinforcement as a function of soil depth. Blank dots represent measured data, blue triangles represent mean measured normalised root basal reinforcement, and red dots show the modeled data.

4.4 Discussion

4.4.1 Distribution of the RAR

According to Gasser et al. (2020), the root-area-ratio is one of the key factors to quantify root mechanical and hydrological effects on soil strength on hydraulic bank erosion. In this study, the values of RAR increase with increasing DBH and decrease with increasing soil depth and distance from the tree stem. These results are similar to others reported in the literature (Bischetti et al., 2007; Abdi et al., 2010; Burylo, Hudek, and Rey, 2011; McIvor and Douglas, 2012). However, the values of RAR measured in this study are two orders of magnitude higher than the values reported for the same stand at the age of 9 years old. The DBH reported in Douglas et al. (2010) ranged between 0.173 and 0.192 m for tree densities of 84 and 770 sph, respectively. The values of RAR reported in Douglas et al. (2010) ranged between 0.00001 and 0.00003% at a distance of 0.9-1.8 m. These values are surprisingly low compared to the values reported by Zydroń, Gruchot, and Kluba (2019) for black poplars with RAR up to 0.44% and on average 0.225% for an 8-year-old tree at 0.5 m distance, grown in Poland. The values of RAR calculated in this study at age 26 years, in the same study area as Douglas et al. (2010), reach values that ranged between 0.02 to 1% at a distance of 1.5 m from trees with a DBH of 0.41-0.56 m (tree density of ca. 84 sph). This huge increment in RAR within 17 years reflects the rapid growth potential of poplar root systems.

The majority of the RAR is located in the first 0.4 m soil depth, confirming the results of similar studies on younger stands (Douglas et al., 2010; Zydroń, Gruchot,

and Kluba, 2019). In the specific case of the Ballantrae study area, the limitation in the vertical distribution of roots is mostly due to the type of soil, where the hydromorphological characteristics of the mineral horizons indicate a clear influence of water fluctuation. Additionally, other factors may contribute to confine the root distribution in the upper soil horizons, as discussed in Douglas et al. (2010). Nevertheless, some roots were measured at depths greater than 0.8 m too, as confirmed in Douglas et al. (2010) and Zydroń, Gruchot, and Kluba (2019) for younger trees.

The measured RAR values among different soil faces of the transect pits suggest that the root distribution can be greatly influenced by the distance to the nearest tree and its DBH more than the characteristics at stand scale. Roots with diameters ranging from 4-10 mm contribute the highest to the value of the RAR, as shown in other studies (Abdi et al., 2010). In comparison with pit 3 situated where tree density is lower (84 sph), pit 10 was located in an area of greater tree density (770 sph) and has much lower RAR values. This is probably due to the distance between the nearest tree and its DBH. This strong influence of the nearest tree is also confirmed by the model results. As observed from Table 4.2, pit 3 was 3.2 m far from a tree of 0.55 m DBH, whereas pit 10 was 4.5 m from a tree with a 0.47 m DBH. Moreover, pit 3 had a higher root density than pit 7, located at a similar distance to the nearest tree, but the tree size was smaller with 0.46 m in DBH. Similarly, pit 1 also shows a slightly higher value in RAR compared to pit 10 due to the DBH of the nearest tree. Other studies have shown that for the high planting density of younger trees, the influence of the DBH on root distribution is less dominant than in older plantations (Genet et al., 2006). Moreover, several studies have shown that measured root density distributions are affected by several factors such as tree species, climate, sampling time/season, soil type, land use management, and orientation of soil trenches (Turmanina, 1965; Gray and Sotir, 1996; Lindström and Rune, 1999; Operstein and Frydman, 2000; Genet et al., 2005; Al Afas et al., 2008a; Douglas et al., 2010). The differences in DBH values measured within the analysed 26-year-old poplar stand are clearly correlated with the stand density and thus with the competition for resources (light and nutrients). The initial size of the poles used for the plantation may also have had an influence, as discussed in Phillips, Marden, and Suzanne (2014) and Schwarz et al. (2016a). As observed in Table 4.2, the average DBH values of all trees decrease with increasing planting density, from 0.58 m in pit 1 to 0.47 m in pit 11. The results of the root distribution show that considering the influence of the tree dimension using the "pipe-theory" (Shinozaki et al., 1964b; Schwarz et al., 2010a) is an appropriate assumption for a single tree, less influenced by the concurrence of neighboring trees (such as in spaced planted tree conditions). However, the model seems to produce poorer predictions in the case of densely planted trees, due to stronger competition between neighbors. Future research needs to focus on how the influence of tree-neighbor competition in densely spaced trees induces a lateral and vertical optimisation of the roots occupancy, drifting the shape of the root system from a symmetrical-circular-like shape to an irregular one, defined by the position of the neighbor trees. This effect was previously discussed in Phillips, Marden, and Suzanne (2014), where root growth in densely planted poplar tends to occupy unplanted areas.

4.4.2 Spatial and temporal distribution of the root reinforcement, and its implication for shallow landslide stabilisation

Basal and lateral root reinforcement are the principal mechanisms that contribute long-term to the prevention of shallow landslides (Cohen and Schwarz, 2017). The results of this study show that basal root reinforcement is limited to the first 0.4

m depth, with low values extending deeper than 0.8 m (mostly near the tree stem), whereas lateral root reinforcement reaches values up to 20 kN/m at a 4.5 m distance from single isolated trees. Within the stand, the values of lateral root reinforcement are strongly influenced by the distance from tree stems and their dimensions, analogous to the observation made for the distribution of RAR. However, the model tends to overestimate root reinforcement for tree densities higher than 200 sph. Poplars would not normally be planted at densities higher than this in practice. Considering that for wide-spaced tree planting measures to control erosion, the tree density is usually less than 200 sph, the validated model can be applied for that condition. As discussed in Schwarz et al. (2016a), the optimum stand density for erosion control, carbon sequestration, and pasture productivity corresponds to a tree canopy cover of 30%, which corresponds to about 70 sph for a mean DBH of 0.3 m and to about 30 sph for a mean DBH of 0.53 m. This would lead to values of lateral root reinforcement near 0. In order to ensure sufficient root reinforcement, stem densities between 160 and 330 sph are needed, confirming the indication given in Schwarz et al. (2016a). Based on the result of this study, this range of stand density would guarantee a lateral root reinforcement between 1 and 16 kN/m for a mean DBH of 0.5 m in a triangular lattice of trees, following the approach described by Flepp et al. (2021).

The vertical distribution of root reinforcement determines the amount of basal root reinforcement. As previously discussed, the site conditions limit most of the roots on the first 0.4 m soil depth. It is documented that basal root reinforcement is significantly affected by the characteristics of the studied site and the depth of the potential shear plane of a landslide (Mao et al., 2015; Gehring et al., 2019). However, even a low value of basal root reinforcement at 0.5-1.0 m of perpendicular depth, corresponding to the thickness of most shallow landslides in NZ, may have a major contribution to slope stability. Especially considering that in correspondence with each tree stem, sinker roots as observed by McIvor et al. (2008) act locally as anchors transferring forces of the superficial root networks deeper in stable soil layers.

The temporal variation of root reinforcement may be mainly due to two types of processes: one is due to the dynamic of root distribution and mechanical properties during different seasons, and the second is due to the tree growth and stand dynamic over the years. McIvor et al. (2011) found that "Tasman" poplar has a significant reduction in fine-root length density during the dormant season, whereas coarse root distribution shows little change. Considering that, due to the fact that coarse roots dominate the contribution of root reinforcement (Schwarz et al., 2016a; Giadrossich et al., 2019), no significant seasonal changes are expected in root reinforcement where coarse roots are present. Little is known about the seasonal changes in the mechanical properties of poplar roots and more needs to be explored in future research, as discussed in Schwarz et al. (2016a). However, the fitting of the force-root diameter model shows a good agreement between the two different datasets. A clear positive correlation between maximum tensile force and root diameter is observed, similar to previous findings of poplars (Watson, McIvor, and Douglas, 2015; Zydroń, Gruchot, and Kluba, 2019), indicating that even in different growing conditions, different sampling seasons the obtained values are quite similar.

Over the years, tree root systems develop, increasing their capability to effectively stabilise soil on steep slopes. McIvor et al. (2008) concluded that poplar trees, which were situated on erosion-prone slopes, needed at least 5 years to obtain a structural root network sufficient to stabilise soil. The poplars analysed in the Ballantrae study site over the years (McIvor, 2012; Schwarz et al., 2016a), showed a considerable constant DBH-growth rate of about 0.019 m/year (slightly influenced by stand density).

Under this condition, a stand with a density of 100 sph (about 10 m distance between trees), would reach a minimum lateral root reinforcement in between the four or three neighbor trees of about 1.1-1.9 kN/m only after 30 years; whereas for a stand density of 250 sph (about 6 m distance between trees) after 30 years, the minimum lateral root reinforcement would reach values larger than 13 kN/m. An overview of the estimated minimum lateral root reinforcement as function of stand age is given in Table 4.11. These results are an important basis for the formulation of guidelines for the planning of erosion control measures using wide-spaced trees in New Zealand pasture hill country.

TABLE 4.11: Calculated dynamic of lateral root reinforcement (kN/m) for different stand densities, based on the results of this study. The results are calculated for the minimum expected value within a stand with squared (lower values) or triangular lattice (higher values), following the approach described in Zadelhoff et al. (2022)

Stand Density	**Distance between trees in a squared lattice**	**Root reinf. 10 years**	**Root reinf. 20 years**	**Root reinf. 30 years**
sph	m	kN/m	kN/m	kN/m
100	10.0	0	0 - 0.1	1.1 - 1.9
150	8.2	0	0.2 - 0.3	3.8 - 5.6
200	7.1	0	0.5 - 0.9	7.9 - 10.6
250	6.3	0	1.0 - 1.7	13.0 - 16.4

Compared to other tree species, the lateral root reinforcement of "Tasman" poplar results is greater within the first 1-2 m distance from stem than chestnut (*Castanea sativa*) (Dazio, Conedera, and Schwarz, 2018) or spruce (*Picea abies*) (Flepp et al., 2021). For the same tree size of 0.5 m, "Tasman" poplars had the highest root force in the first 3.0 m and rapidly reduced to about 1 kN/m at a 5.0 m distance. Among the three species, chestnut trees have the highest values of root reinforcement at the largest distances from the stem (Figure 4.19).

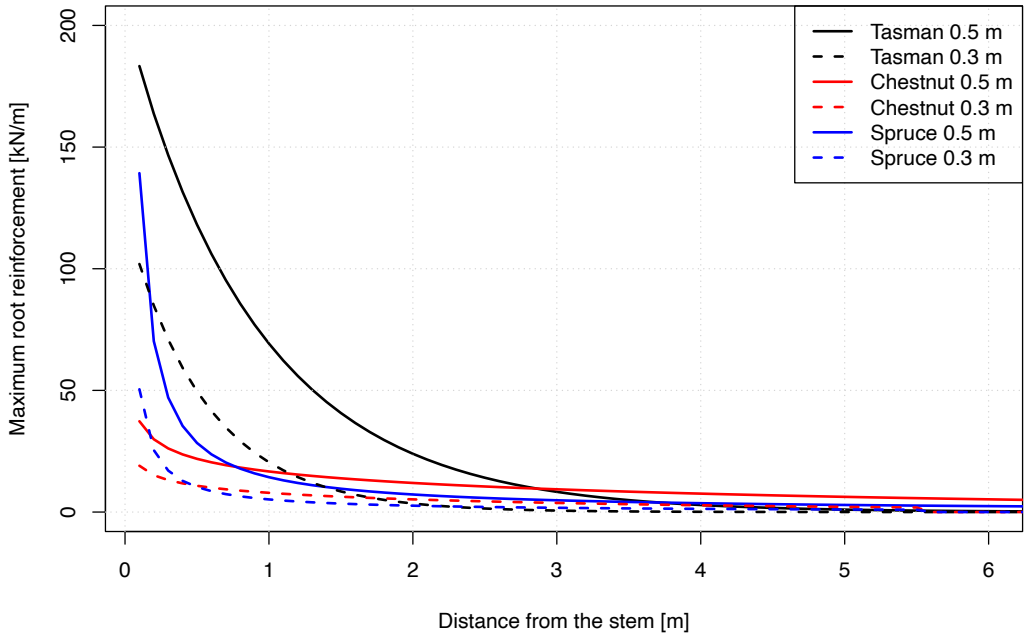

FIGURE 4.19: Compared maximum lateral root reinforcement of "Tasman" poplar with calibrated parameters from the present study, of chestnut coppices from the study of Dazio, Conedera, and Schwarz (2018), and spruce from the study of Flepp et al. (2021).

4.5 Conclusion

This study provides a unique and detailed dataset of root distribution and mechanical properties of "Tasman" poplar growing in the pastoral hill country in New Zealand. Moreover, numerical models for root and root reinforcement distribution have been calibrated and validated for the first time using a combination of single tree excavations and a transect along a gradient of stand densities. Additionally, 124 laboratory tensile tests were combined with 66 in-situ pullout tests to quantify the root pullout forces for root diameters up to 0.04 m.

The collected data extends the research from previous studies allowing for the quantification of the temporal dynamics of root distribution and reinforcement over 26 years of tree growth, considering different stem densities. In general, the high growth rate of the young trees is also confirmed in older trees and is reflected in the increment of root distribution and reinforcement as a function of the DBH. The results show that at least 20 years are needed to reach a minimum value of lateral root reinforcement at the stand scale, and at least 30 years are needed to reach root reinforcement sufficient to stabilise most of the shallow landslides depending on their disposition, as discussed in Schwarz et al. (2016a).

The applied root distribution model well estimates spatial root distribution in individual poplar trees ($R^2 = 0.78$) and within a stand with low density, whereas it tends to overestimate the number of roots in the stand with stem densities higher than 200 sph. We suggest improving root distribution model performance in dense stands by adding a threshold into the model to limit overestimation.

The lateral root reinforcement model has a trend of underestimating root force in individual trees ($R^2 = 0.64$), whereas it performs well along the transect in the stand with tree stem densities lower than 200 sph. The model also predicts the vertical distribution of root reinforcement well, which is mostly limited to the first 0.4 m of soil depth.

The results presented in this paper allow the implementation of the temporal and spatial distribution of root reinforcement in numerical models for the estimation of the effectiveness of different types of bio-engineering measures to reduce soil erosion due to hydraulic bank erosion and shallow landslides (Gasser et al., 2020; Zadelhoff et al., 2022; Schwarz et al., 2016a). Moreover, these tools are fundamental to develop strategies to prioritise interventions and optimise investments in green-based solutions at large spatial scales.

Further studies are needed to extend the application of the results, knowledge, and tools discussed in this paper for other plant species considering a wide range of environmental conditions, including the effects of climate change.

4.6 Appendices

Figure 4.20 displays boxplots of normalised SSE of 30 random generated combinations of training/testing datasets (80/20) for each proposed model. In Figure 4.20(a), the difference in normalised SSE between training and testing datasets fluctuated from ca. -187 to 283 N of cumulative root-force. Whereas for the testing dataset, the variability of the normalised SSE was higher. For maximum lateral root reinforcement, the difference varied greatly from $-6{\cdot}10^2$ kN/m to $4{\cdot}10^2$ kN/m; however, the mean value of differences was -1.242 kN/m (Figure 4.20(b)). Lastly, the residuals between modeled and measured values of basal root reinforcement varied from -253 N to 256 N. Nevertheless, the mean value of the residuals was just 4.7 N. The mean normalised SSE of all models were quite close to 0, suggesting that in general, the models converged to similar accuracy in the training as well as in the testing results.

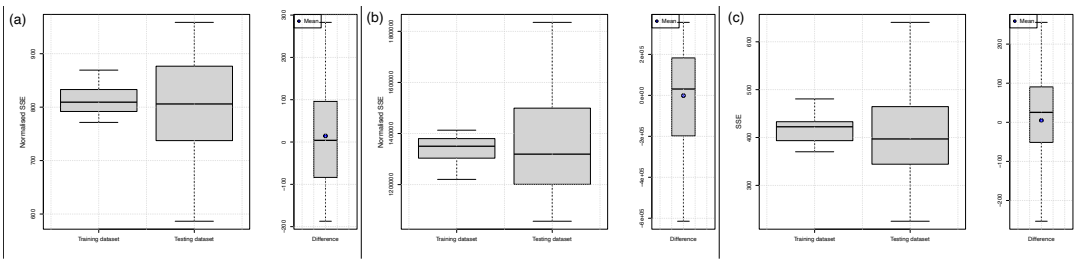

FIGURE 4.20: Normalised SSE of training dataset, testing dataset and residuals of (a) Root distribution model, (b) Lateral root reinforcement model, and (c) Basal root reinforcement model.

References

Abdi, Ehsan et al. (2010). "Quantifying the effects of root reinforcement of Persian Ironwood (Parrotia persica) on slope stability; a case study: Hillslope of Hyrcanian forests, northern Iran". In: *Ecological Engineering* 36.10, pp. 1409–1416.

Al Afas, N et al. (2008a). "Growth and production of a short-rotation coppice culture of poplar—IV: fine root characteristics of five poplar clones". In: *Biomass and Bioenergy* 32.6, pp. 494–502.

Allen, David M (1974). "The relationship between variable selection and data agumentation and a method for prediction". In: *technometrics* 16.1, pp. 125–127.

Beattie, James (2003). "Environmental Anxiety in New Zealand, 1840-1941: Climate Change, Soil Erosion, Sand Drift, Flooding and Forest Conservation". In: *Environ. Hist.* 9.4, pp. 379–392. ISSN: 09673407. URL: http://www.jstor.org/stable/20723453 (visited on 02/02/2023).

Bischetti, Gian Battista et al. (2007). "Root strength and root area ratio of forest species in Lombardy (Northern Italy)". In: *Eco- and Ground Bio-Engineering: The Use of Vegetation to Improve Slope Stability*. Springer: Berlin/Heidelberg, Germany, pp. 31–41.

Blaschke, Paul M, Noel A Trustrum, and Ron C DeRose (1992). "Ecosystem processes and sustainable land use in New Zealand steeplands". In: *Agriculture, ecosystems & environment* 41.2, pp. 153–178.

Burylo, M, C Hudek, and F Rey (2011). "Soil reinforcement by the roots of six dominant species on eroded mountainous marly slopes (Southern Alps, France)". In: *Catena* 84.1-2, pp. 70–78.

Claessens, L et al. (2007). "Modelling landslide hazard, soil redistribution and sediment yield of landslides on the Ugandan footslopes of Mount Elgon". In: *Geomorphology* 90.1-2, pp. 23–35.

Cohen, Denis and Massimiliano Schwarz (2017). "Tree-root control of shallow landslides". In: *Earth Surface Dynamics* 5.3, pp. 451–477.

Dazio, Emanuele (Plinio Rinaldo), Marco Conedera, and Massimiliano Schwarz (2018). "Impact of Different Chestnut Coppice Managements on Root Reinforcement and Shallow Landslide Susceptibility". In: *Forest Ecology and Management*, pp. 63–76. ISSN: 0378-1127. DOI: 10.1016/j.foreco.2018.02.031.

DeRose, RC, NA Trustrum, and PM Blaschke (1993). "Post-deforestation soil loss from steepland hillslopes in Taranaki, New Zealand". In: *Earth surface processes and landforms* 18.2, pp. 131–144.

Douglas, GB, NA Trustrum, and IC Brown (1986). "Effect of soil slip erosion on Wairoa hill pasture production and composition". In: *New Zealand journal of agricultural research* 29.2, pp. 183–192.

Douglas, Grant B et al. (2010). "Root distribution of poplar at varying densities on pastoral hill country". In: *Plant and Soil* 333.1, pp. 147–161.

Fang, Shengzuo, Jianhui Xue, and Luozhong Tang (2007). "Biomass production and carbon sequestration potential in poplar plantations with different management patterns". In: *Journal of environmental management* 85.3, pp. 672–679.

Flepp, Gianluca et al. (2021). "Temporal Dynamics of Root Reinforcement in European Spruce Forests". In: *FORESTS* 12, pp. 1–16.

Gasser, Eric et al. (2019). "A review of modeling the effects of vegetation on large wood recruitment processes in mountain catchments". In: *Earth-Science Reviews* 194, pp. 350–373.

Gasser, Eric et al. (2020). "A new framework to model hydraulic bank erosion considering the effects of roots". In: *Water* 12.3, p. 893.

Gehring, Eric et al. (2019). "Shallow landslide disposition in burnt European beech (Fagus sylvatica L.) forests". In: *Scientific Reports* 9.1, pp. 1–11.

Geisser, Seymour (1975). "The predictive sample reuse method with applications". In: *Journal of the American statistical Association* 70.350, pp. 320–328.

Genet, Marie et al. (2005). "The influence of cellulose content on tensile strength in tree roots". In: *Plant and soil* 278.1, pp. 1–9.

Genet, Marie et al. (2006). "Soil fixation by tree roots: changes in root reinforcement parameters with age in Cryptomeria japonica D. Don. plantations". In: *Interpraevent*. Citeseer, pp. 25–27.

Giadrossich, F et al. (2013a). "Mechanical interactions between neighbouring roots during pullout tests". In: *Plant and soil* 367.1, pp. 391–406.

Giadrossich, F et al. (2017a). "Methods to measure the mechanical behaviour of tree roots: a review". In: *Ecological engineering* 109, pp. 256–271.

Giadrossich, Filippo et al. (2019). "Large roots dominate the contribution of trees to slope stability". In: *Earth Surface Processes and Landforms* 44.8, pp. 1602–1609.

Giadrossich, Filippo et al. (2020a). "Minimum representative root distribution sampling for calculating slope stability in Pinus radiata D. Don plantations in New Zealand". In: *New Zealand Journal of Forestry Science* 50. DOI: 10.33494/nzjfs502020x68x.

Glade, Thomas (2003). "Landslide occurrence as a response to land use change: a review of evidence from New Zealand". In: *Catena* 51.3-4, pp. 297–314.

Gray, Donald H and Robbin B Sotir (1996). *Biotechnical and Soil Bioengineering Slope Stabilization: A Practical Guide for Erosion Control*. John Wiley & Sons: Hoboken, NJ, USA.

Gregory, NG (1995). "The role of shelterbelts in protecting livestock: a review". In: *New Zealand journal of agricultural research* 38.4, pp. 423–450.

Hastie, Trevor et al. (2009). *The elements of statistical learning: data mining, inference, and prediction*. Vol. 2. Springer: Berlin/Heidelberg, Germany.

Holdaway, Robert J et al. (2017). "Using DNA metabarcoding to assess New Zealand's terrestrial biodiversity". In: *New Zealand Journal of Ecology* 41.2, pp. 251–262.

Huang, S, Y Yang, and Y Wang (2003). "A critical look at procedures for validating growth and yield models". In: *W: Amaro A., Reed D., Soares P. [red.]. Modelling Forest Systems. CABI Publishing. Oxford Cambridge*. 2, pp. 271–293.

Lambert, MG, NA Trustrum, and DA Costall (1984). "Effect of soil slip erosion on seasonally dry Wairarapa hill pastures". In: *New Zealand journal of agricultural research* 27.1, pp. 57–64.

Lindström, Anders and Göran Rune (1999). "Root deformation in plantations of container-grown Scots pine trees: effects on root growth, tree stability and stem straightness". In: *Plant and soil* 217.1, pp. 29–37.

Lyons, Mitchell B et al. (2018). "A comparison of resampling methods for remote sensing classification and accuracy assessment". In: *Remote Sensing of Environment* 208, pp. 145–153.

Mao, Zhun et al. (2015). "Modelling and predicting the spatial distribution of tree root density in heterogeneous forest ecosystems". In: *Annals of botany* 116.2, pp. 261–277.

McGlone, Matt S (1989). "The Polynesian settlement of New Zealand in relation to environmental and biotic changes". In: *New Zealand journal of ecology* 12, pp. 115–129.

McGregor, E et al. (1999 Jan 1). "Silvopastoralism using tended poplars on New Zealand hill country: The opportunities". In: *New Zealand Grassland Association*. Vol. 61, pp. 85–89. DOI: 10.33584/jnzg.1999.61.2360.

McIvor, I R (2012). "New Zealand Poplar Commission National Report on Activities Related to Poplar and Willow Cultivation and Utilization 2008–11". In: A report prepared for 24th Session of the FAO International Poplar Commission in Dehradun, India.

McIvor, Ian et al. (2011). "Pastoral hill slope erosion in New Zealand and the role of poplar and willow trees in its reduction". In: *Soil erosion issues in agriculture*. InTech Rijeka, pp. 257–278.

McIvor, Ian R and Grant B Douglas (2012). "Poplars and willows in hill country-stabilising soils and storing carbon". In: *Advanced Nutrient Management: Gains from the Past-Goals for the Future* 25, pp. 1–11.

McIvor, IR et al. (2008). "Structural root growth of young Veronese poplars on erodible slopes in the southern North Island, New Zealand". In: *Agroforestry Systems* 72.1, pp. 75–86.

Murgia, Ilenia et al. (2022). "Modeling shallow landslides and root reinforcement: A review". In: *Ecological Engineering* 181, p. 106671.

Operstein, V and S Frydman (2000). "The influence of vegetation on soil strength". In: *Proceedings of the Institution of Civil Engineers-Ground Improvement* 4.2, pp. 81–89.

O'loughlin, CL and AJ Pearce (1976). "Influence of Cenozoic geology on mass movement and sediment yield response to forest removal, North Westland, New Zealand". In: *Bulletin of the International Association of Engineering Geology-Bulletin de l'Association Internationale de Géologie de l'Ingénieur* 13.1, pp. 41–46.

Parminter, I, MB Dodd, and AD Mackay (2001 Jan 1). "Economic analysis of poplar planting on steep hill country". In: *New Zealand Grassland Association*. Vol. 63, pp. 127–130. DOI: 10.33584/jnzg.2001.63.2447.

Perona, Paolo et al. (2022). "Tree root distribution modelling in different environmental conditions". In: *Ecological Engineering* 185, p. 106811.

Phillips, Chris J, Michael Marden, and Lambie M Suzanne (2014). "Observations of root growth of young poplar and willow planting types". In: *New Zealand Journal of Forestry Science* 44.1, pp. 1–12.

Rácz, Anita, Dávid Bajusz, and Károly Héberger (2021). "Effect of dataset size and train/test split ratios in QSAR/QSPR multiclass classification". In: *Molecules* 26.4, p. 1111.

Rogers, NW and MJ Selby (1980). "Mechanisms of shallow translational landsliding during summer rainstorms: North Island, New Zealand". In: *Geografiska Annaler: Series A, Physical Geography* 62.1-2, pp. 11–21.

Rosser, BJ and CW Ross (2011). "Recovery of pasture production and soil properties on soil slip scars in erodible siltstone hill country, Wairarapa, New Zealand". In: *New Zealand Journal of Agricultural Research* 54.1, pp. 23–44.

Schwarz, M, D Cohen, and Dani Or (2012b). "Spatial characterization of root reinforcement at stand scale: theory and case study". In: *Geomorphology* 171, pp. 190–200.

Schwarz, M, Peter Lehmann, and Dani Or (2010). "Quantifying lateral root reinforcement in steep slopes–from a bundle of roots to tree stands". In: *Earth Surface Processes and Landforms: The Journal of the British Geomorphological Research Group* 35.3, pp. 354–367.

Schwarz, M et al. (2010a). "Quantifying the role of vegetation in slope stability: A case study in Tuscany (Italy)". In: *Ecological Engineering* 36.3, pp. 285–291.

Schwarz, Massimiliano, Filippo Giadrossich, and Denis Cohen (2013). "Modeling root reinforcement using a root-failure Weibull survival function". In: *Hydrology and Earth System Sciences* 17.11, pp. 4367–4377.

Schwarz, Massimiliano et al. (2016a). "Modelling of root reinforcement and erosion control by 'Veronese'poplar on pastoral hill country in New Zealand". In: *New Zealand Journal of Forestry Science* 46.1, pp. 1–17.

Seidu, Jamel et al. (2022). "Impact of data partitioning in groundwater level prediction using artificial neural network for multiple wells". In: *International Journal of River Basin Management*, pp. 1–12. DOI: 10.1080/15715124.2022.2079653.

Shinozaki, Kichiro et al. (1964b). "A quantitative analysis of plant form-the pipe model theory: I. Basic analyses". In: *Japanese Journal of ecology* 14.3, pp. 97–105.

Stone, Mervyn (1974). "Cross-validatory choice and assessment of statistical predictions". In: *Journal of the royal statistical society: Series B (Methodological)* 36.2, pp. 111–133.

Sulaiman, Zulkefly (2006). "Establishment and silvopastoral aspects of willow and poplar: a thesis presented in partial fulfilment of the requirements for the degree of Doctor of Philosophy (Ph. D.) in Plant Science, Institute of Natural Resources, Massey University, Palmerston North, New Zealand". PhD thesis. Massey University, Palmerston North, New Zealand.

Trustrum, NA and RC De Rose (1988). "Soil depth-age relationship of landslides on deforested hillslopes, Taranaki, New Zealand". In: *Geomorphology* 1.2, pp. 143–160.

Turmanina, VI (1965). *The strength of tree roots*. Bull. Moscow Soc. Naturalists, Biol. Sec. 70, pp. 36–45.

Van Kraayenoord, C W (1968). "Poplars and willows in New Zealand with particular reference to their use in erosion control." In.

Vergani, Chiara et al. (2016). "Root reinforcement dynamics in subalpine spruce forests following timber harvest: a case study in Canton Schwyz, Switzerland". In: *Catena* 143, pp. 275–288.

Vergani, Chiara et al. (2017a). "Investigation of root reinforcement decay after a forest fire in a Scots pine (Pinus sylvestris) protection forest". In: *Forest Ecology and Management* 400, pp. 339–352.

Vergani, Chiara et al. (2017b). "Root reinforcement dynamics of European coppice woodlands and their effect on shallow landslides: A review". In: *Earth-science reviews* 167, pp. 88–102.

Vrigazova, Borislava (2021). "The proportion for splitting data into training and test set for the bootstrap in classification problems". In: *Business Systems Research: International Journal of the Society for Advancing Innovation and Research in Economy* 12.1, pp. 228–242.

Watson, Alex, Ian McIvor, and Grant Douglas (2015). "Live root-wood tensile strength of Populus × euramericana,'Veronese poplar'". In: *The New Zealand Poplar*, pp. 1–8.

Wilkinson, AG (1999). "Poplars and willows for soil erosion control in New Zealand". In: *Biomass and Bioenergy* 16.4, pp. 263–274.

Yadav, Sanjay and Sanyam Shukla (2016). "Analysis of k-fold cross-validation over hold-out validation on colossal datasets for quality classification". In: *2016 IEEE 6th International conference on advanced computing (IACC)*. IEEE, pp. 78–83.

Zadelhoff, Feiko Bernard van et al. (2022). "Introducing SlideforMAP: a probabilistic finite slope approach for modelling shallow-landslide probability in forested situations". In: *Natural Hazards and Earth System Sciences* 22.8, pp. 2611–2635.

Zhang, Yongli and Yuhong Yang (2015). "Cross-validation for selecting a model selection procedure". In: *Journal of Econometrics* 187.1, pp. 95–112.

Zydroń, Tymoteusz, Andrzej Gruchot, and Marcin Kluba (2019). "Spatial variability of reinforcement provided by juvenile root systems of black locust and black poplar". In: *Polish Journal of Environmental Studies* 28.5.

Chapter 5

Assess the compatibility of spatial root distribution and root reinforcement of *Cryptomeria Japonica D. Don* between Switzerland, China and Japan

Abstract

Root reinforcement is an important factor contributing to the mitigation of risk due to shallow landslides. Each forest species has its distinct root mechanical properties and root distribution patterns, leading to different reinforcing capacities. Japanese cedar (*Cryptomeria japonica*), a species native to Japan, has been widely planted for use of wood materials and is one of Japan's most important silvicultural trees. It also has been planted for climate change adaptation and biodiversity in different nations, including Switzerland. However, the ecosystem services provided by Cryptomeria forest stands remain challenging to quantify due to the limited amount of quantitative information. The aims of this study is to (1) quantify the spatial root distribution and mechanical properties of Cryptomeria roots, (2) quantify the 3-dimensional distribution of root reinforcement, and (3) compare above-mentioned properties between datasets from Switzerland and from Japan. We used unique dataset from China, Japan, and Switzerland of root distribution, root pullout tests, and tensile tests to calibrate models to upscale root reinforcement at the stand scale. Our findings demonstrated that the measured root distribution of Cryptomeria between Japan and Switzerland was similar for coarse roots (with diameters larger than 6 mm). However, the root distribution of roots with small diameters significantly differed between the forest stations. This suggests that the root distribution patterns vary based on the soil properties and climatic conditions of each study site. The relationship between root tensile force and root diameter showed that laboratory tests with small roots (less than 10 mm in diameter) can be combined with field pullout tests to obtain representative datasets for the calibration of root reinforcement models. Comparing trees with the same diameter, the maximum lateral root reinforcement in the Japanese stand was similar to the Swiss stand (range between 0-10 kN/m), with slightly higher values in Japan of about 2.4, 1.7, and 1.1 kN/m at the distance of 2.5, 3.5, and 4.5 m from the stem. For common stand conditions in Japan and in Switzerland, the minimum lateral root reinforcement ranged between 0 and 7 kN/m depending on the tree dimension (DBH) and stand density. Basal root reinforcement was distributed differently between Swiss and Japanese study sites. In Swiss sites, highest reinforcement values were found in the topsoil layer, while in Japanese sites, they were concentrated at greater depths

(between 0.15 and 0.45 m). For practical applications, our calibrated models can provide reliable estimates of root distribution and reinforcement at the stand scale, aiding in slope stability assessments.

Keywords: Root Reinforcement; Root Distribution; Cryptomeria japonica D. Don; Shallow Landslides; Forestry Management

5.1 Introduction

Vegetation has been demonstrated to play a substantial role in mitigating the risks of natural hazards in mountainous areas including landslides (Schwarz et al., 2010b), floods (Sakals et al., 2006), avalanches (Berger et al., 2013), debris flows (Sakals et al., 2006), and rockfalls (Dorren et al., 2007) by enhancing soil structure (Jastrow, Miller, and Lussenhop, 1998; Fattet et al., 2011), improving hydraulic conductivity (Stokes et al., 2014), and increasing soil strength through root systems (Gyssels et al., 2005). Root distribution patterns and root mechanical properties are considered the most important factors influencing the root reinforcement capacity (Wu, 1976; Wu, 2007; Marzini et al., 2023). For example, the maximum tensile force of the European Beech (*Fagus sylvatica* L.) (Gehring et al., 2019) differs from that of Norway Spruce (*Picea abies* L. H: Karst) (Vergani et al., 2017c), significantly influencing root reinforcement capabilities.

The selection of tree species for slope stabilization is normally based on qualitative evaluations such as previous experiences regarding habitat adaptation, availability, commercial availability, and above-ground characteristics, rather than the mechanical effects of roots (Watson and Marden, 2005). The contribution of root reinforcement to slope stability can be described through three distinct mechanisms (as shown in the Figure 5.1): (1) *Basal root reinforcement*: roots intersect the shear surface of the shallow landslides (the most effective), (2) *Lateral root reinforcement*: acts along the edges of shallow landslides during various triggering phases, and (3) *Soil mass stiffness*: roots enhance the apparent stiffness of the rooted soil mass (Cohen and Schwarz, 2017). Basal root reinforcement is most efficient when the shear plane of the shallow landslides is located within the rooting zones, normally at depths of less than 1 m in temperate regions, and potentially extending several meters deeper in tropical regions (Kim et al., 2017). On the other hand, lateral root reinforcement involves both root tension and compression within the unstable soil mass at its edges (Figure 5.1(c)). Previous studies have revealed that lateral root reinforcement is only effective in small shallow landslides with surface areas less than 1000 m^2, although this varies with slope angle and soil mechanical properties (Schwarz et al., 2010b). While there are several studies on the root properties of *Cryptomeria japonica*, there is still insufficient data to quantify the root reinforcement at the stand scale. This lack of information limits its practical application in decision support for the management of protective forests.

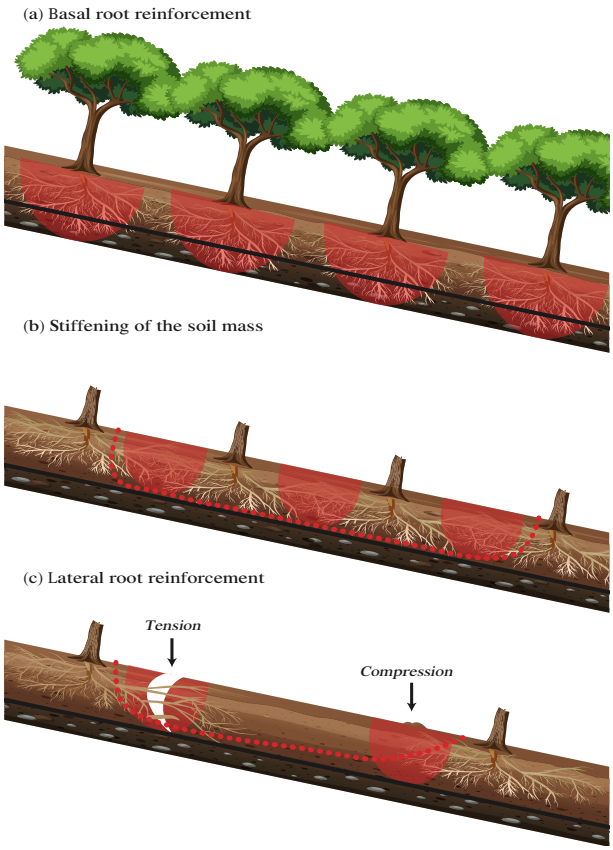

FIGURE 5.1: Three mechanisms of root reinforcement: (a) Basal root reinforcement, (b) Soil mass stiffness, and (c) Lateral root reinforcement. The solid black line indicates the shear surface of a shallow landslide (Modified from Giadrossich et al. (2013b)).

Cryptomeria japonica (Thunb. ex L.f.) D. Don, commonly known as Japanese cedar or Sugi, is a forest tree species extensively native to Japan and China, but it is also world-wide distributed. This species is one of the most important forest trees in Japan, both culturally and economically, constituting 44% of the country's man-made forests (Takahara et al., 2023). *Cryptomeria* is a monotypic genus, including only one species with two varieties: *japonica* and *sinensis*, the latter of which is native to China (Lima et al., 2021). It is a key species in ecological restoration in Southwestern China. According to Orwa (2009), Japanese cedar is a large evergreen conifer, typically reaching heights of 35-60 m and obtaining a bole diameter of 1-3 m at maturity. This species is both wind-tolerant and shade-tolerant, with frost resistance, and is commonly found in high-rainfall mountainous zones. *C. japonica* grows in free-draining, deep, rich, moist alluvial soils and prefers warm, sunny conditions. It is intolerant of poor nutrient soils and cold, dry environments. Japanese cedar has distinct characteristics such as reddish-brown bark, fibrous with vertical strips in its bark, needle-like leaves, light wood density, rapid growth, and susceptibility to drought due to higher photosynthetic and transpiration rates compared to other conifers (Kenzo et al., 2021; Lima et al., 2021).

The objectives of this study are to quantify the three-dimensional spatial root distribution and root mechanical properties of *C. japonica*, upscale the root reinforcement of *C. japonica* at the stand scale, and compare the root distribution patterns and root reinforcement capacities of this species across different regions. The detailed hypotheses of the study are explained below:

(1) Our first hypothesis is that the root system of *C. japonica* is similar between Japan and Switzerland in terms of spatial distribution and dimensions. This similarity could allow future studies to utilize existing root distribution data from previous research, thereby reducing the need for laborious and destructive field measurements.

(2) Various techniques have been performed to measure the mechanical characteristics of roots, including laboratory tensile tests and field pullout tests (Giadrossich et al., 2017b). Our second hypothesis is that there is no significant difference in the maximum breaking force for small root diameter ranges between the two measurement methods, allowing them to complement each other in creating a comprehensive database.

(3) Our third hypothesis is that the spatial distribution of root reinforcement of *C. japonica* trees of equal dimensions is similar between Japanese and Swiss forest stands.

5.2 Materials and Methods

The spatial root distribution pattern of Japanese cedar is estimated using the Root Distribution Model (RDM) (Schwarz, Cohen, and Or, 2012a), whereas the spatial root reinforcement is calculated using the Root Bundle Model with the Weibull survival function (RBMw) (Schwarz, Giadrossich, and Cohen, 2013) and the Root Reinforcement Model (RRM) (Moos et al., 2016b). The general framework of this study is illustrated in Figure 5.2.

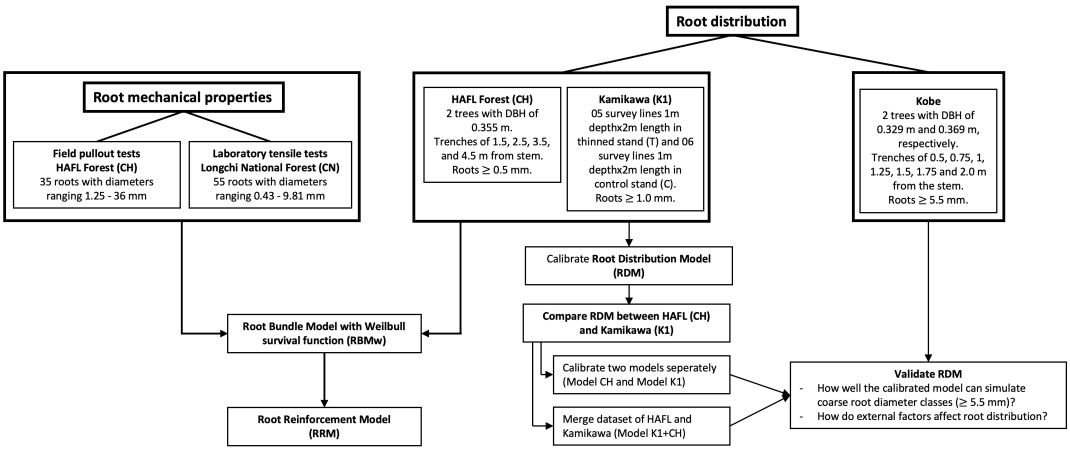

FIGURE 5.2: General framework of the present study.

The root distribution data utilized in this study was collected from three different sites: one site at HAFL Forest in Switzerland and two sites in Japan: (i) Kamikawa and (ii) Kobe (Yamase et al., 2018). Detailed information on each study site, including the methodologies and models used to assess the root distribution pattern of *C. japonica*, is presented in Table 5.1, and in Sections 2.1, 2.3 and 2.5.

Measured root distribution and root tensile force were used to calibrate the RBMw, which calculated the force-displacement curve and scaled up to spatial root reinforcement at the root system level using the RRM. Further details on root reinforcement are described in Sections 2.2, 2.4 and 2.5.

Site	Location	MAP (mm)	MAT (°C)	Soil condition	Stand density	Age (years)	Paper
HAFL, Switzerland (CH)	47°0'N, 7°28'E, 594m	1137	9.2	Acidified Cambisol	125 trees/ha	50	This study
Kamikawa, Japan (K1)	35°8'N, 134°4'E, 889m	1740	9.7	Andisol	723-1625 trees/ha	49	Yamase et al., 2019
Kobe, Japan	34°4'N, 135°1'E, 430m	1216	16.7	Cambisol	900 trees/ha	43	Yamase et al., 2018

TABLE 5.1: Summarized information on three fieldwork sites where the root distribution pattern of *Cryptomeria japonica* was measured.

5.2.1 Root distribution

Root distribution data were collected from HAFL Forest in Switzerland (CH), Kamikawa in Japan (K1), and Kobe in Japan. The methodologies were similar across all three locations: soil profiles were excavated, divided into 1 m wide sectors, and roots were counted. In HAFL Forest and Kamikawa, soil profiles were dug manually, recording all roots with diameters. In contrast, the fieldwork in Kobe utilized an air spade and focused only on coarse roots with diameters of 5 mm and above. A summary of the root distribution measurements is presented in Table 5.1.

Figure 5.3 shows the combination of fieldwork photos from the different sites: (a) and (b) show two candidate trees at HAFL Forest, (c) illustrates 2 m wide survey lines in Kamikawa, and (d) captures root system excavation in Kobe.

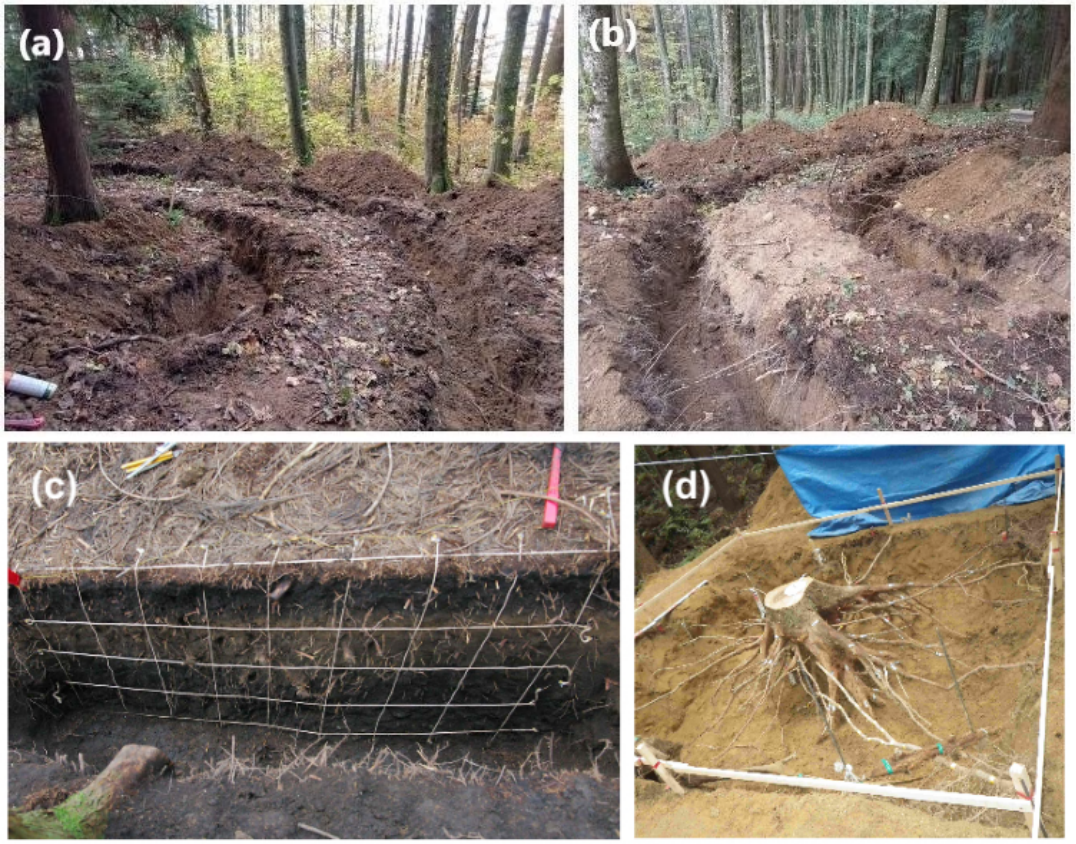

FIGURE 5.3: Trenches of two candidate trees: (a) Tree S1 and (b) Tree S2 at four distances (1.5, 2.5, 3.5, and 4.5 m from the stem) in HAFL Forest in Switzerland; (c) 2 m wide survey lines at the Kamikawa site; and (d) Tree excavation at the Kobe site, showing root counting at distances from 0.5 to 2.0 m from the stem.

Collected data from HAFL Forest in Switzerland

The root distribution of Japanese cedar was measured from two trees at HAFL Forest, behind the School of Agricultural, Forest and Food Sciences (BFH-HAFL), and named as Tree S1 and Tree S2. Both trees have the same diameter at breast height (DBH) of 0.355 m and are approximately 50 years old. The main criteria for selecting these candidate trees were: (i) isolated distance from neighboring trees to avoid overlap of root systems, (ii) absence of evident pathogens, and (iii) similar slope steepness and soil conditions between the two trees.

Four trenches were dug at distances of 1.5, 2.5, 3.5, and 4.5 m from each stem (Figure 5.3(a) and (b)). Roots were counted separately in each soil layer: [0-0.15 m], [0.15-0.30 m], [0.30-0.45 m], [0.45-0.60 m], and [0.60-0.75 m], and classified into diameter classes at 1 mm intervals starting from 0.5 mm: 1 mm [0.5-1.5 mm], 2 mm [1.5-2.5 mm], 3 mm [2.5-3.5 mm], and so on. In this study, fine roots are defined as roots with a diameter in the range of 0.5 to 1.5 mm, referred to as 1 mm root diameter class. For Tree S2, we were able to reach a depth of 0.75 m in the soil profile; however, for Tree S1, large rocks were present at a depth of 0.60 m. The soil type was identified as acidified Cambisol (WRB) (mean pH = 3.6) with increased clay content (24%) between 0.50 and 1 m depth, compared to the upper horizons, which contained 14-20% clay. The density of *C. japonica* trees in the area was approximately 125 trees per hectare.

The trenches covered a length corresponding to approximately 180° around the tree stems. In the first trench at a distance of 1.5 m from the stem, we measured root distribution across five 1 m width soil profiles. At greater distances of 2.5, 3.5, and 4.5 m from the stem, the number of measured 1 m width profiles increased to 6, 9, and 9 profiles, respectively. This excavation methodology has been applied in previous studies of various species such as *Pinus radiata* (Giadrossich et al., 2020b) and "Tasman" poplar (Ngo et al., 2023). In this study, "CH" refers to the samples collected from HAFL Forest in Switzerland.

Collected data from Kamikawa in Japan

A 49-year-old Japanese cedar forest, planted in 1963 in the Mineyama Highlands, Kamikawa, Hyogo, Japan (35°8'N, 134°4'E, 889 m a.s.l.), was selected for studying the root distribution of *C. japonica*. Thinning was carried out in 1995, 17 years before the fieldwork took place in 2008. The tree densities were approximately 723 trees per hectare in the thinning site and 1625 trees per hectare in the control site. The soil in this area developed from black volcanic ash. The average temperature was 9.7°C, and the maximum snow depth reached 1.50 m.

Five survey lines, each 2 m wide and 1 m deep, were excavated in the thinning site, while six survey lines of the same dimensions were excavated in the control site (Figure 5.3(c)). Each survey line was located between two trees, with one tree always fixed at a distance of 1 m from the stem. The slope gradient in this study area ranged from 5° to 15°. After excavation, the diameter and position of all roots within the survey lines were measured. Similar to the CH data, root distribution data from this site was analyzed by dividing the soil depth into layers of [0-0.15 m], [0.15-0.30 m], [0.30-0.45 m], and so on. However, the roots in this site were classified starting from 1.0 mm, unlike the CH data, which began at 0.5 mm. Roots were categorized into classes such as 1 mm [1-1.5 mm], 2 mm [1.5-2.5 mm], 3 mm [2.5-3.5 mm], and so on. Therefore, there is a difference in the real fine root quantities within this diameter class between the two study sites. Table 5.2 provides the exact location of each survey line corresponding to the target trees and adjacent trees. Data from this site are referred to as "K1" in the rest of the manuscript.

Site	Stand	ID	DBH_1 (m)	Dist_1 (m)	DBH_2 (m)	Dist_2 (m)
K1	Thinned	T_1	0.345	1.0	0.300	3.8
K1	Thinned	T_2	0.335	1.0	0.315	3.9
K1	Thinned	T_3	0.345	1.0	0.337	3.8
K1	Thinned	T_4	0.340	1.0	0.337	3.7
K1	Thinned	T_5	0.358	1.0	0.276	3.5
K1	Control	C_1	0.297	1.0	0.313	2.1
K1	Control	C_2	0.306	1.0	0.322	2.4
K1	Control	C_3	0.308	1.0	0.253	2.1
K1	Control	C_4	0.299	1.0	0.268	2.5
K1	Control	C_5	0.290	1.0	0.329	2.5
K1	Control	C_6	0.301	1.0	0.305	2.3

TABLE 5.2: Summary of information regarding the 11 survey lines in the K1 study site. DBH_1 refers to the diameter at breast height of the target tree, while Dist_1 indicates the distance from the survey line to the center of the target tree's stem. DBH_2 and Dist_2 are diameter at the breast height and distance from the survey line to the center of the adjacent tree's stem, respectively.

Collected data from Kobe in Japan

A field study on the root distribution of Japanese cedar was conducted in a 43-year-old forest at Futatabi park in the Rokko Mountains, Kobe, Hyogo, Japan (34°4'N, 135°1'E, 430 m a.s.l.) by Yamase et al. (2018). The mean annual temperature and precipitation recorded at the nearest meteorological station were 16.7°C and 1216 mm, respectively. The soil type was classified as brown forest soil and Cambisol (WRB), mainly consisting of weathered granite. The mean diameter at the breast height (DBH) of the trees was 0.329 m, with a stand density of 900 trees per hectare and the presence of understory vegetation including *Eurya japonica* and *Pleioblastus argenteostriatus f. glaber*.

The root systems of two *C. japonica* trees with diameters at breast height (DBH) of 0.329 m and 0.369 m were excavated at various distances from the stem: 0.50, 0.75, 1.00, 1.25, 1.50, 1.75, and 2.00 m, to a depth of 1 m using an air spade (Figure 5.3(d)). Information on coarse roots bigger than 5 mm, including root size and position, was recorded. Root diameters were measured in 0.1 mm units using a digital caliper. Similar to the CH data, measured roots in Kobe were classified into different root diameter classes for comparison, starting from 5.5 mm: 6 mm [5.5-6.5 mm], 7 mm [6.5-7.5 mm], 8 mm [7.5-8.5 mm], and so on. The volumetric water contents in the soil at depths of 0-0.1 m and 0.2-0.3 m were 37.9±2.3% and 26.9±6.5%, respectively (n=3). Detailed information about the study site and excavation methodology were described in Yamase et al. (2018).

5.2.2 Root mechanical properties

Collected data from Longchi National Forest in Southwestern China

The Longchi National Forest (located at 31°8'29"N, 103°34'30"E, 1829 m mean altitude) is an ecosystem conservation forest rich in subtropical alpine vegetation and situated at approximately 10 km from Dujiangyan City, on the western border of the

Sichuan Basin, serving as a transition zone between the Qingzang Plateau and the Chengdu plain. The local climate is characterized as moist semi-tropical, with distinct four seasons (Ma and Li, 2017). An average annual rainfall of 1135 mm makes this forest an ideal habitat for the growth of *C. japonica*. Summer months experience a high frequency of rainstorms, with intense rainfall occurring over short periods, and precipitation mainly occurs from May to September (Ma and Li, 2017). Field investigations were conducted in August.

Root samples from the Longchi National Forest were collected and tested using a laboratory tensile machine to observe their mechanical properties, as described in Mehtab et al. (2021). After being collected and preserved from the field, all root ends were fixed in the tensile machine with synthetic resin reinforcement to prevent slippage and damage when clamping in the test device. The root specimens were then stored in a refrigerator at 4°C for 48 hours. Prior to testing, root diameters were measured at the middle and both ends using an electronic Vernier caliper with an accuracy of 1/50 mm. A total of 55 root samples, with diameters ranging from 0.43 mm to 9.81 mm, were measured. Only straight roots with no anomalies were selected for testing. In this study, "CN" refers to the samples collected in the Longchi National Forest in China and measured using laboratory tensile tests.

Collected data from HAFL Forest in Switzerland

The study in Switzerland (47°0'N, 7°28'E, 594 m a.s.l.) was conducted behind the School of Agricultural, Forest and Food Sciences (BFH-HAFL). The study site is situated at the transition between the pre-alpine hills and the Swiss plateau. The climate is strongly influenced by both the Alps together with the Atlantic Ocean. In 2021, the average temperature and total precipitation recorded in the Bern region (553 m a.s.l) were 9.2°C and 1137 mm, respectively (MeteoSwiss, 2021), with approximately 55 mm of precipitation in February. Field investigations were carried out in January 2021. The C-horizons, rich in skeleton, were observed at depths of approximately 0.45 to 0.75 m. These un-weathered materials of these horizons originated from tertiary deposits of fluvial sediments.

Field pullout tests are considered the most representative measurements for applying the RBMw model and upscaling root reinforcement to the stand scale for slope stability models (Schwarz, Giadrossich, and Cohen, 2013; Giadrossich et al., 2017b). The primary advantage of field pullout tests is their potential to quantify root tensile behavior by considering the entire root-soil system. This includes changes in root diameter along the full root length (instead of small segments, as in laboratory tests), local changes in root direction, and root geometrical anomalies. Moreover, the influence of external factors such as soil moisture, soil type, soil-root friction, and soil confining pressure is also considered in these tests.

Following the methodology described by Giadrossich et al. (2017b), vertical trenches were excavated to perform root pullout tests on roots with diameters ranging from 1.25 to 36 mm, using a test speed of approximately 30 mm/min. A total of 35 pullout tests were carried out. In the trench face, soil was carefully removed to expose sufficient root length for each test. We removed bark to prevent root slippage during the anchoring and pulling process. A wire displacement sensor was positioned at a known distance from the trench face to measure displacement. Each root was pulled until either breakage or slippage occurred. Root diameters were measured at both the clamping and breaking points with a digital caliper. The tests were conducted under wet conditions. In this study, "CH" refers to samples collected from HAFL Forest in Switzerland.

5.2.3 Root distribution model

Root distribution at the stand scale is estimated based on the Root Distribution Model (RDM) proposed by Schwarz, Cohen, and Or (2012a). The model was originally developed to simulate lateral root distribution without accounting for vertical variations. Several modified versions have been proposed to estimate the root distribution of different forest species (Vergani et al., 2016; Schwarz et al., 2016b; Giadrossich et al., 2016). In this study, we followed the approach described in Giadrossich et al. (2016). The model estimates the quantity of roots in different root diameter classes i that cross a 1 m wide vertical soil profile at a distance d from an isolated tree stem with the diameter at breast height (DBH, in [m]) ϕ_t following the equation:

$$N_{i,t}(d,\phi_t) = \begin{cases} D_{fr}\frac{[ln(1+\phi_{max})-ln(1+\phi_i)]}{ln(1+\phi_{max})}(\frac{\phi_i}{\phi_0})^{\beta}, & \text{with } d < d_{max} \text{ and } \phi_i < \phi_{max} \\ 0, & \text{otherwise} \end{cases} \quad (5.1)$$

d_{max} is the maximum rooting distance from the stem [m], D_{fr} is the density of fine roots (ranging from 0.5 to 1.5 mm in this study) per horizontal meter, ϕ_i is the mean root diameter in class size i [m], ϕ_0 is a reference diameter (set to 1 mm in this study), ϕ_{max} is the maximum root diameter [m], and β is a constant exponent.

$$d_{max}(\phi_t) = \psi\phi_t \quad (5.2)$$

$$\phi_{max} = \frac{d_{max} - d}{\eta} \quad (5.3)$$

ψ is an empirical coefficient, ϕ_t is the tree diameter at the breast height [m], and η is a dimensionless scaling coefficient.

The density of fine roots crossing 1 m wide vertical soil profile at a given distance d from an isolated tree stem with DBH ϕ_t is calculated as:

$$D_{fr}(d,\phi_t) = [\frac{\mu(\phi_t^2\frac{\pi}{4})}{d_{max}2\pi d}](\frac{d_{max}-d}{d_{max}}), \text{ with } d < d_{max} \quad (5.4)$$

where μ is the pipe coefficient.

Model parameters β, ψ, η, and μ from equations 5.1, 5.2, 5.3, and 5.4 were calibrated by minimizing the Sum of Absolute Errors (SAE) obtained as the difference between the model prediction and the root distribution data, shown in Section 2.5.

The RDM assumes that the roots are symmetrically distributed all around the stem parallel to the slope.

The calibration of the model for the CH dataset was done considering a single tree, whereas for the K1 the interaction between the 2 neighbor trees has been considered, as listed in Table 5.2.

5.2.4 Root reinforcement model: from single root to a bundle of roots

In recent decades, various root reinforcement models has been developed to understand the mechanical role of roots in stablizing slope (Mao, 2022). In this study, we applied the Root Bundle Model with Weibull survival function and Root Reinforcement Model approach.

Root Bundle Model with Weibull survival function (RBMw)

The root distribution and root mechanical properties data were used to upscale root reinforcement through the Root Bundle Model with Weibull survival function approach (RBMw) as described in Dazio, Conedera, and Schwarz (2018), a modified version of the original model (Schwarz, Giadrossich, and Cohen, 2013), because this model considers the strength variability of roots within root diameter classes. The RBMw is a strain-step loading fiber bundle model that implements a Weibull survival function to consider the uncertainties caused by the mechanical and geometrical variability of roots. In each displacement step, individual roots contribute differently to the total reinforcement based on their apparent stiffness and tensile force. The model inputs include (i) force-displacement behavior measured by laboratory tensile tests and/or field pullout tests, and (ii) lateral root distribution across vertical cross-sections.

A power-law relationship is applied to the maximum root tensile force at failure F_{max} with respect to root diameter ϕ as shown below:

$$F_{max}(\phi) = C(\phi) \cdot F_0 \cdot \phi^{\alpha} \tag{5.5}$$

where F_{max} is the maximum root tensile force at failure [N], ϕ is root diameter [m], α is the power-law exponent, and F_0 is a pre-exponential factor.

A fitting correction is applied to address the overestimation of tensile force in small roots. The function is modified by adding a multiplier in the form of a cumulative normal distribution function (CDF) with values ranging between 0 and 1:

$$C(\phi) = \frac{1}{2}[1 + erf(\frac{\phi - \phi_m}{\phi_{sd}\sqrt{2}})] \tag{5.6}$$

where ϕ_m and ϕ_{sd} are coefficients corresponding to the mean and standard deviation of the cumulative normal distribution, respectively.

The secant spring constant of roots k [N/m] is calculated assuming linear-elastic behavior on the part of pulled roots (Schwarz, Giadrossich, and Cohen, 2013). Several modified versions have been applied to estimate the spring constant (Schwarz, Giadrossich, and Cohen, 2013; Giadrossich et al., 2016; Dazio, Conedera, and Schwarz, 2018). In this study, an apparent secant spring constant was computed by the ratio of maximum root pullout force over the displacement at root failure and then plotted as a linear curve in the relation to root diameter as below:

$$k(\phi) = k_0\phi \tag{5.7}$$

where k is the spring constant [N/m], ϕ is the root diameter [m], and k_0 is a constant parameter.

The progressive failure of the root bundle, caused by the variability in root-soil mechanical properties such as lignin vs. cellulose content, water content, fiber orientation, and heterogeneity in soil mechanical properties, is evaluated using a *Weibull survival function*. In the RBMw, it is hypothesized that the probability of root survival is a function of the normalized displacement and is described by the Weibull survival function parameter:

$$S(\Delta x^*) = exp[-(\frac{\Delta x^*}{\lambda})^{\omega}] \tag{5.8}$$

where S is the survival function, Δx^* is normalized displacement, ω is the Weibull shape factor, and λ is the Weibull scaling factor.

The normalized displacement Δx^* in a function of root diameter ϕ was computed as shown below:

$$\Delta x^*(\phi) = \frac{\Delta x}{\Delta x_{max}^{fit}(\phi)} \tag{5.9}$$

The root reinforcement as force (RR_{bundle}) of a bundle of roots as a function of displacement (Δx) is obtained by total force contribution from each root multiplied by the survival function (S) as shown below:

$$RR_{bundle}(\Delta x) = \sum_{i=1}^{i_{max}} n_i F(\phi_i, \Delta x) S(\Delta x_i^*) \tag{5.10}$$

where RR_{bundle} is the total root reinforcement of a bundle of roots per 1-m width of the trench in [N/m], Δx is the displacement (i.e., the distance over which the roots are stretched) in [m], n is the number of roots in a given root diameter class i, ϕ_i is mean root diameter of each root diameter class, i_{max} is the maximum root diameter class under consideration, and Δx_i^* is normalized displacement of each root diameter class.

The parameters of equations 5.5, 5.6, 5.7 and 5.8 including F_0, α, ϕ_m, ϕ_{sd}, k_0, λ, and ω are calibrated using the data from the laboratory tensile tests and/or field pullout tests and minimizing the Sum of Absolute Errors, shown in Section 2.5.

The aforementioned model assumes that neighboring roots or crossing roots do not affect the pullout force of a single root; therefore, each single root acts independently (Giadrossich et al., 2013a).

Root reinforcement: from the bundle of roots to the root system scale

The maximum lateral root reinforcement RR_{max}, defined as the peak of the force-displacement curve from the calibrated RBMw, is used to upscale the value of root reinforcement from a bundle of roots to the root system scale. RR_{max} is correlated to tree size ϕ_t (DBH, in [m]) and the distance from the tree stem d [m] as described in Moos et al. (2016b), using the following formula:

$$RR_{max}(\phi_t, d) = \begin{cases} a \cdot \phi_t \cdot \Gamma(\frac{d}{\phi_t \cdot 18.5}; b, c), & \text{for } d < 18.5 \cdot \phi_t \\ 0, & \text{for } d \geq 18.5 \cdot \phi_t \end{cases} \tag{5.11}$$

where a is scaling factor, the Gamma distribution with b is shape parameter, and c is rate parameter.

Basal root reinforcement is calculated from the calibrated RBMw and by using the Gamma distribution function fitted to the calculated distribution of root reinforcement (with measurements taken every 0.15 m) as shown below:

$$RR_{basal}(z) = RR_{max} \cdot \Gamma(z; z_\alpha, z_\beta) \tag{5.12}$$

where z is the soil depth, z_α and z_β are calibrated coefficients of the Gamma density function.

The parameters of equations 5.11 and 5.12 including a, b, c, z_α, and z_β are calibrated by minimizing the Sum of Absolute Errors (SAE), shown in Section 2.5.

The upscaling of lateral root reinforcement at the stand scale is based on following assumptions from Schwarz, Cohen, and Or (2012a), including (i) Root reinforcement is spatially distributed uniformly across the slope, and (ii) minimum lateral root reinforcement at the stand scale is computed as the sum of root reinforcement resulting from overlapping neighboring root systems.

5.2.5 Statistical Analysis

Different methods to calibrate Root Distribution Model

In previous studies, we calibrated the Root Distribution Model using a weighting function related to root tensile force (Ngo et al., 2023). Although coarse roots, especially those larger than 10 mm in diameter, are less frequent compared to fine roots, they play a crucial role in root reinforcement capacity. The weighting function improves the model's ability to better predict the quantity of big roots. However, the variation in the number of fine roots may increase, as their significance is less emphasized when the weighting function is applied.

In this manuscript, we test different methods to fit the Root Distribution Model. First, by comparing cumulative versus frequency analysis; and second, by evaluating the application of the weighting function related to root tensile force. The model fittings in this paper are carried out by minimizing the Sum of Absolute Errors (SAE), which as shown below:

$$SAE = \sum_{i=1}^{n} \sqrt{(y_i - \widehat{y_i})^2} \tag{5.13}$$

Calibrate models

All statistical analyses were performed using the R packages (R Core Team, 2018). We conducted a Student's t-test for each parameter of the Root Bundle Model (RBMw) to assess the differences in the *C. japonica* dataset between laboratory tensile tests conducted with CN samples and field pullout tests measured with CH samples. To evaluate the performance of the Root Distribution Model (RDM) and Root Reinforcement Model (RRM), we assessed their efficiency using the Sum of Absolute Errors (SAE) and Taylor Diagram (Taylor, 2001). Taylor Diagram visually summarizes multiple key statistical indices for model evaluation in a single diagram. The azimuth angle of the Taylor Diagram represents the Pearson correlation coefficient between the observed and predicted values, while the radial distance from the original point indicates the "normalized" standard deviation of the simulation relative to the measured values. Finally, the radial distance from the measured point reflects the RMSD (Root Mean Squared Deviation). Considering the general shape of the data distribution (many roots for fine roots and few roots for large diameter classes, meaning a long tail on one side of the data distribution), the interpretation of the Taylor Diagram is difficult and it is meant to give just a general view of model performances. The Pearson correlation term is the most appropriate to compare the performances of the RDM.

5.3 Results

5.3.1 Spatial root distribution of *Cryptomeria japonica*

Root distribution data at the HAFL Forest in Switzerland

In this section, we present the results of root distribution measurements from Switzerland, focusing on both horizontal and vertical distribution. In general, the root systems of the candidate trees exhibit a lateral extension exceeding 4.5 m and the data indicate that the majority of measured roots at the HAFL Forest are concentrated within the upper 0.15 m of soil depth.

The horizontal distribution of fine roots reveals a declining frequency as the distance from the tree stem increases. Similarly, the frequency of coarse roots also decreases with increasing distance from the stem. Figure 5.4 illustrates these trends, displaying data scaled to a 1-m width profile. The largest root sizes recorded at distances of 1.5, 2.5, 3.5, and 4.5 m from the two trees were 66 mm, 27 mm, 13 mm, and 13 mm, respectively. The root system of Tree S1 obtained more big roots compared to those of Tree S2.

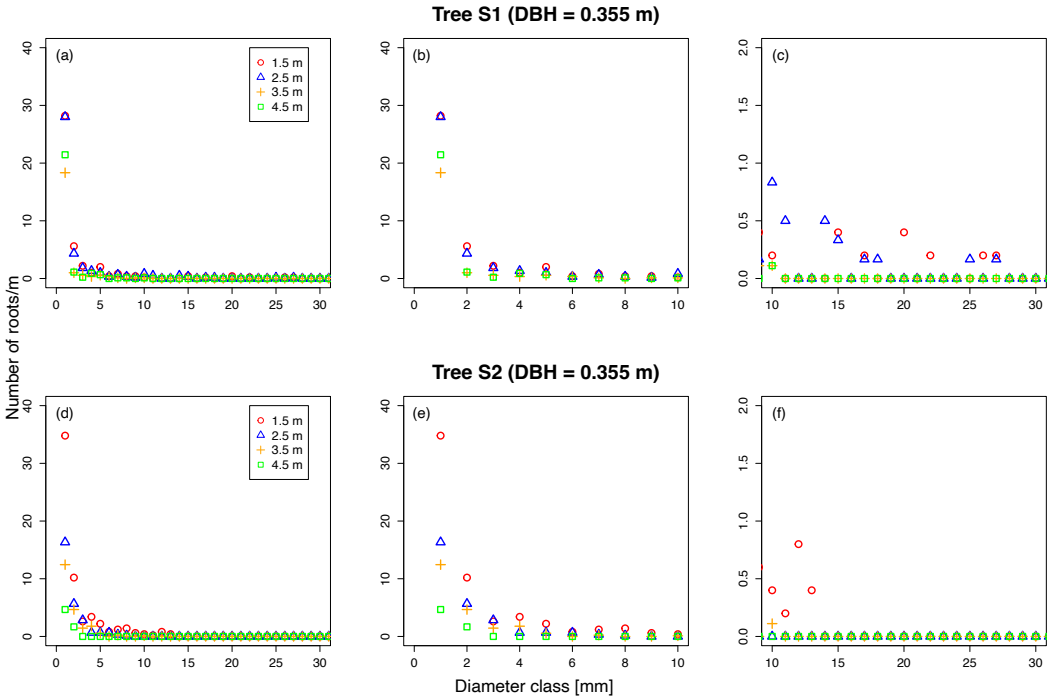

FIGURE 5.4: Mean values of measured horizontal root distribution per diameter class at various distances from the tree stem (as indicated in the legend), scaled for a soil profile of 1 m width and 0.75 m depth for the trees studied in Switzerland. The middle subplots (b) and (e) and right-hand subplots (c) and (f) display zoomed-in views of the corresponding left-hand subplots (a) and (d). The first row represents Tree S1, while the second row represents Tree S2.

The vertical distribution of roots indicates a decrease in root frequency with increasing soil depth, with all diameter classes being most abundant in the upper soil layer, specifically from 0 to 0.15 m. Roots with diameters greater than 30 mm were only observed in Tree S1 within the first soil layer of the first trench (Figure 5.5). In the depth range of 0 to 0.15 m, Tree S2 exhibited a greater total quantity of roots but had fewer roots with diameters exceeding 10 mm compared to Tree S1. The maximum root diameter recorded at this depth was 66 mm in Tree S1, whereas Tree S2 was only 13 mm. Closer to the stem, Tree S1 had larger root diameters even in the deeper soil layers compared to Tree S2. At a distance of 4.5 m from the stem (Figure 5.5(d) and Figure 5.5(h)), the root quantities in Tree S2 were lower than those in Tree S1 at all soil depths.

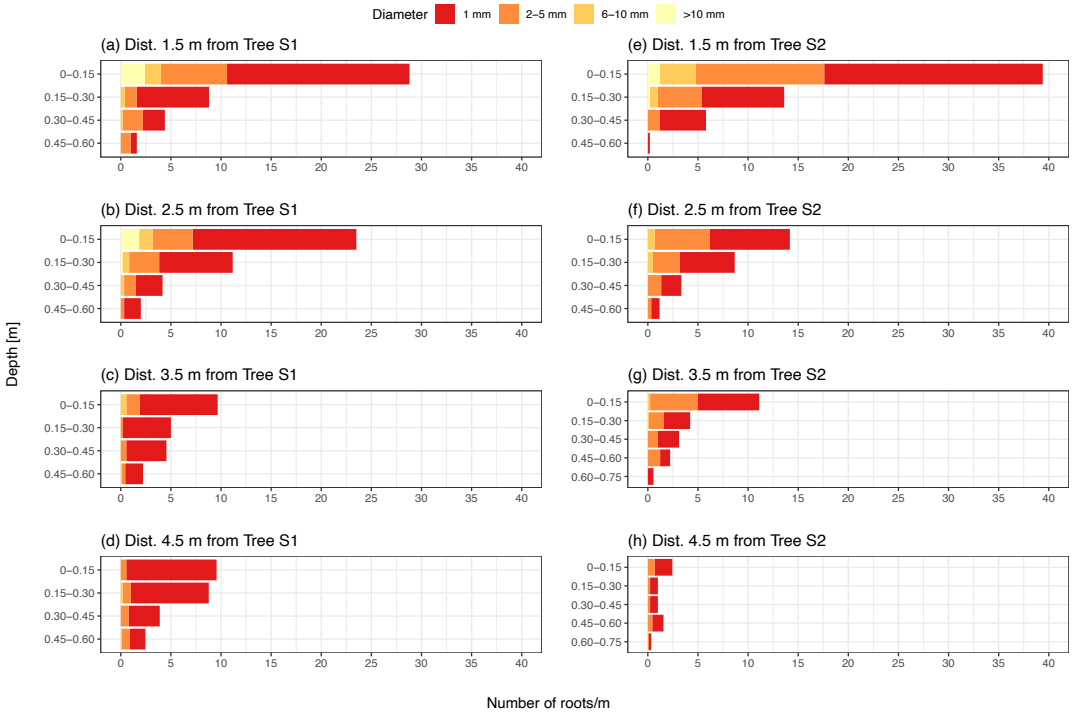

FIGURE 5.5: Vertical root distribution at varying distances from tree stem. The X-axis presents the mean number of roots measured, scaled to a 1-m width for each 0.15 m soil depth layer. Subplots (a), (b), (c), and (d) represent the mean number of roots per meter for Tree S1, while subplots (e), (f), (g), and (h) indicate the number of roots per meter for Tree S2. Root diameter classes are categorized as follows: 1 mm, 2-5 mm, 6-10 mm, and $>$ 10 mm.

Modelling of root distribution at the HAFL Forest in Switzerland

Different methods have been used to calibrate the Root Distribution Model (RDM). The comparison between measured fine roots and simulated fine roots using these three methods is shown in Figure 5.6. At a distance of 1.5 m from the stem, all methods fit within the range of measured values. However, at greater distances, all methods tended to underestimate the number of fine roots. Tree S1 exhibited a distinct pattern in fine root distribution, with a higher fine root frequency at 2.5 m compared to 1.5 m, and at 4.5 m compared to 3.5 m from the stem. The biggest difference in measured fine roots between the two trees was observed at a distance of 4.5 m from the stem, with a difference of 11 fine roots per meter.

The comparison between measured coarse roots and simulated coarse roots generated from the three models as well as summarized results of these three calibrated models are presented in the Appendix section: Figure 5.25 and Table 5.9.

Based on the performance of the three methods and the summarized results in Table 5.9, we selected the method that minimizes the Sum of Absolute Errors which results to be the one using the cumulative root number (CRN). The blue lines in Figure 5.6 illustrate the comparison between measured fine roots and simulated fine roots from this selected method. This model effectively predicted fine root quantities at a distance of 1.5 m, although it underestimated the number of fine roots at farther distances. The differences between the mean measured fine roots and simulated fine roots at distances of 1.5 m, 2.5 m, 3.5 m, and 4.5 m for Tree S1 were approximately 2, 14, 12, and 19 fine roots per meter, respectively. For Tree S2, the differences between

the mean measured fine roots and simulated fine roots at those same distances were approximately 4, 3, 6, and 2 fine roots per meter.

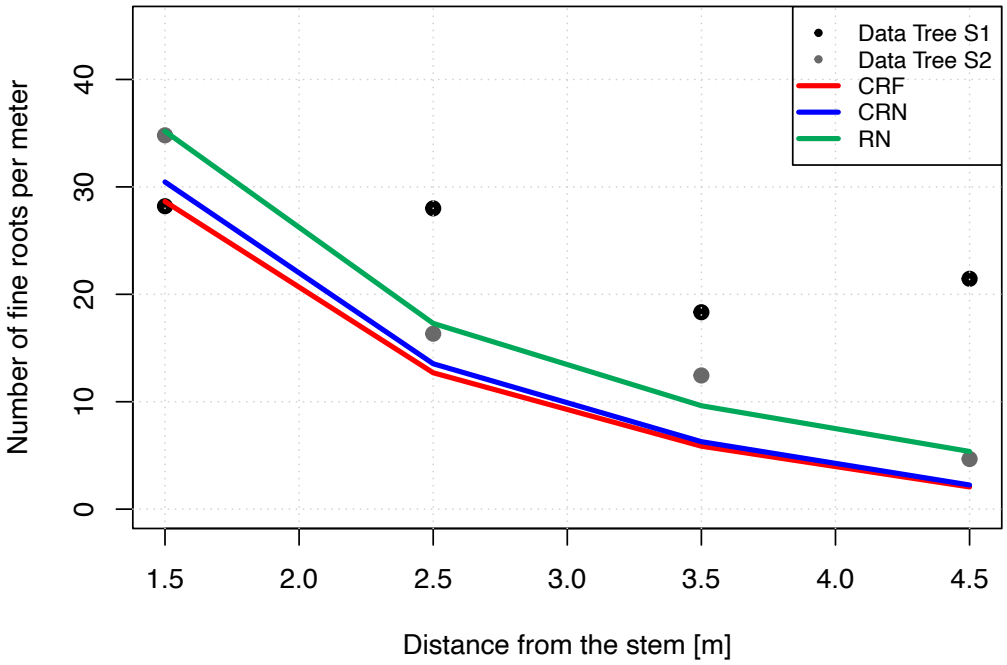

FIGURE 5.6: Comparison between measured and simulated fine roots using three calibration methods for the RDM to determine the best-fitted coefficients for the CH dataset. Black dots represent measurements from Tree S1, and gray dots represent measurements from Tree S2. CRF (red line) represents the calibrated model minimizing the SAE of cumulative root-force. CRN (blue line) represents the RDM calibrated by minimizing the SAE of cumulative root number. RN+CRF (green line) represents the RDM calibrated by combining root number and cumulative root-force conditions.

Even though Tree S1 and Tree S2 had the same size, were located in the same site, and were in the same health condition, the root frequency between the two trees was not identical. As illustrated in Figure 5.7, the presence of 10 mm diameter class roots was recorded up to a distance of 4.5 m from the stem in Tree S1; in contrast, only 2 mm diameter class roots were recorded at the same distance in Tree S2. In Figure 5.7, the red columns represent the mean measured root number per meter, while the black lines indicate the maximum and minimum measured root numbers for each root diameter class, and the blue columns display the simulated root numbers. At a distance of 1.5 m from the stem, the calibrated RDM overestimated the number of coarse roots in Tree S1 but underestimated the coarse root quantities in Tree S2. As the root size increased, the difference between the mean measured and simulated values decreased. At the distance of 2.5 m, the RDM well predicted the number of coarse roots in both trees. At 3.5 m from the stem, the calibrated model did not generate roots bigger than 6 mm, despite the observation of 10 mm roots in both trees. At a distance of 4.5 m from the stem, Tree S1 exhibited a maximum root number

of 8 roots per meter for the 2 mm diameter class. Additionally, a 10 mm diameter root was recorded at this distance in Tree S1. However, the calibrated model did not simulate any coarse roots at this distance, resulting in a general underestimation of coarse root frequency for individual trees at 4.5 m from the stem.

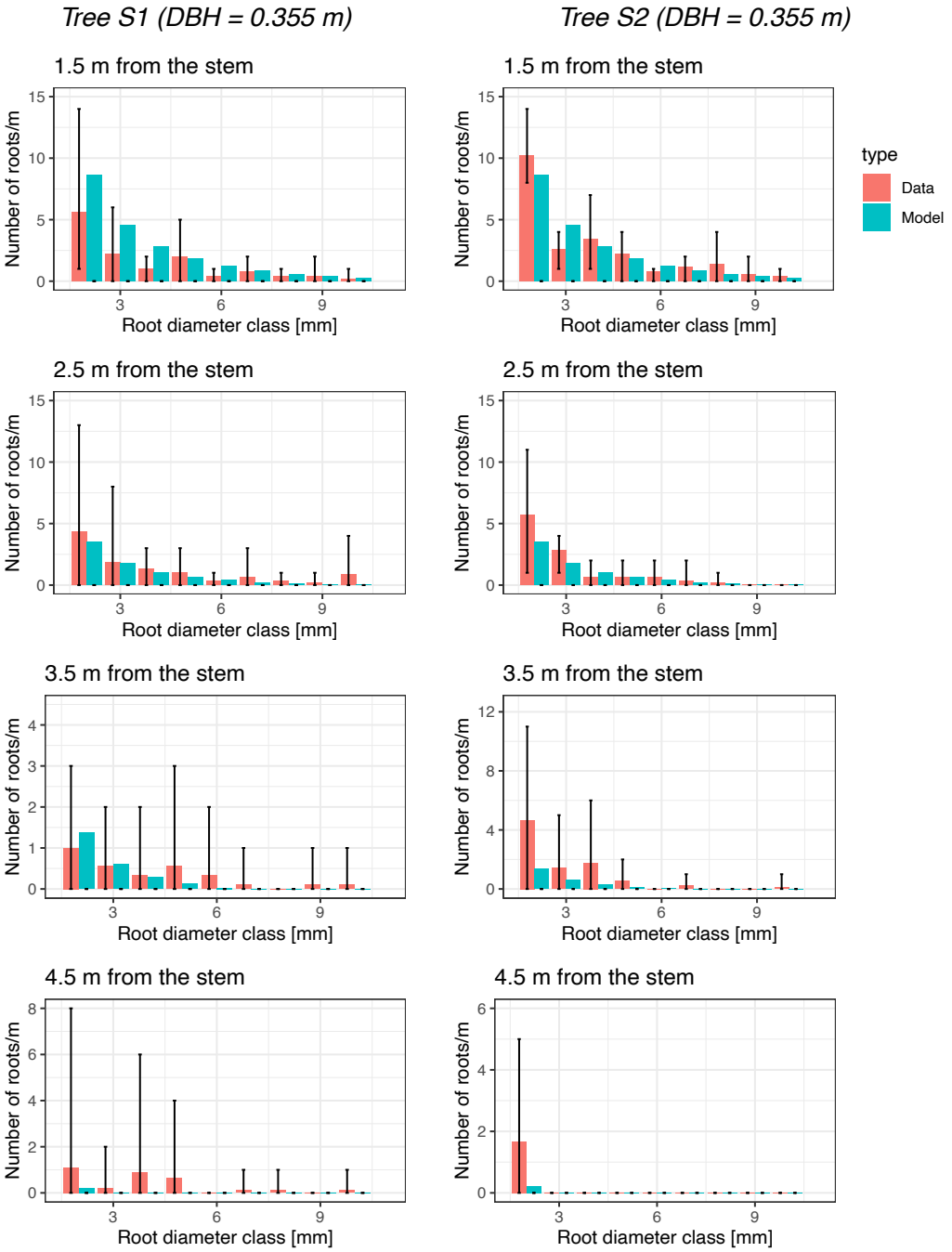

FIGURE 5.7: Comparison between measured coarse roots and simulated coarse roots fitted using the method of minimizing the Sum of Absolute Errors (SAE) of cumulative root number (CRN). The red columns represent the mean measured root number in 1-m width profiles, while the blue columns show the simulated root number from the model for the same profiles. The two ends of the black lines indicate the maximum and minimum measured root numbers per meter.

Root distribution data from Kamikawa in Japan

In this section, we present the results of root distribution measurements and modeling from Kamikawa site (K1) in Japan, focusing on both horizontal and vertical distribution. Given the sampling design of this dataset, the measurements are presented for each 1-m wide by 1-m deep soil profile and compared with the corresponding modeling results.

Figure 5.8 reveals significant differences in measured fine root numbers among profiles T4_1, T4_2, T5_1, T5_2, C1_1, and C1_2 compared to other profiles.

Similar to the CH dataset, the results from Table 5.9 indicate that the coefficient set generated from the CRN method was the best fit for calibrating K1 data. Figure 5.8 displays the comparison between the measured and simulated fine root numbers from the calibrated RDM for both the thinned (T) and unthinned-control (C) stands. The findings show that the fluctuation in measured fine root frequency across 22 survey lines was considerably larger than the simulated values.

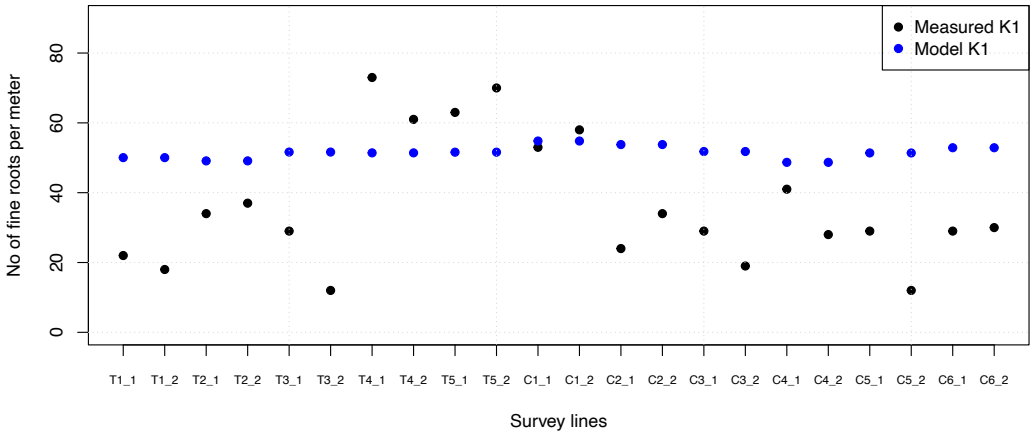

FIGURE 5.8: Number of fine roots per meter measured from 22 survey lines in K1 site in comparison with simulated number of fine roots from calibrated RDM using CRN method. The black dots represent measured values while blue dots represent simulated values.

Figure 5.9 shows the performance of the calibrated RDM in the thinned site. The model generally underestimates the number of coarse roots within the diameter range of 2 to 5 mm across most profiles, with a mean underestimation percentage of 33.52%. In contrast, for roots larger than 5 mm in diameter, the model performs better with an overestimation percentage of 18.44%.

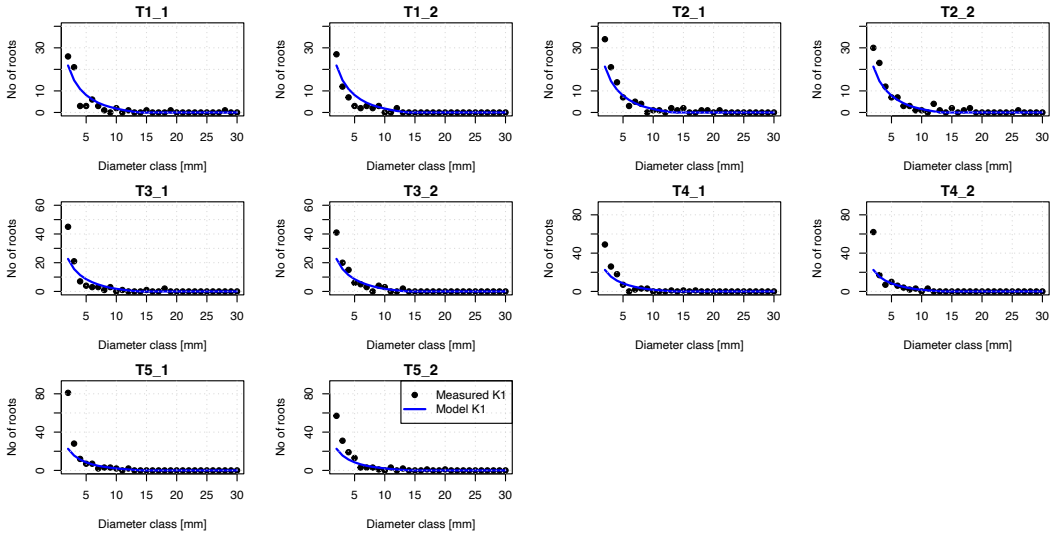

FIGURE 5.9: Root quantities in each coarse root diameter class measured from ten 1-m wide soil profiles in thinned forest in K1 site compared to simulated values of RDM. The black dots represent measured root numbers while the blue curves represent simulated root numbers from RDM.

The calibrated RDM exhibited different performance in the control site compared to the thinned stand. In general, the model tended to underestimate the quantity of 2 mm roots, with a percentage underestimation of 33.43%. Conversely, it overestimated the root frequency within the diameter range of 3 to 5 mm, with an overestimation percentage of 18.20%. For roots > 5 mm, the model simulated poorer in the control site than in the thinned site, resulting in an overestimation percentage of 30.96%.

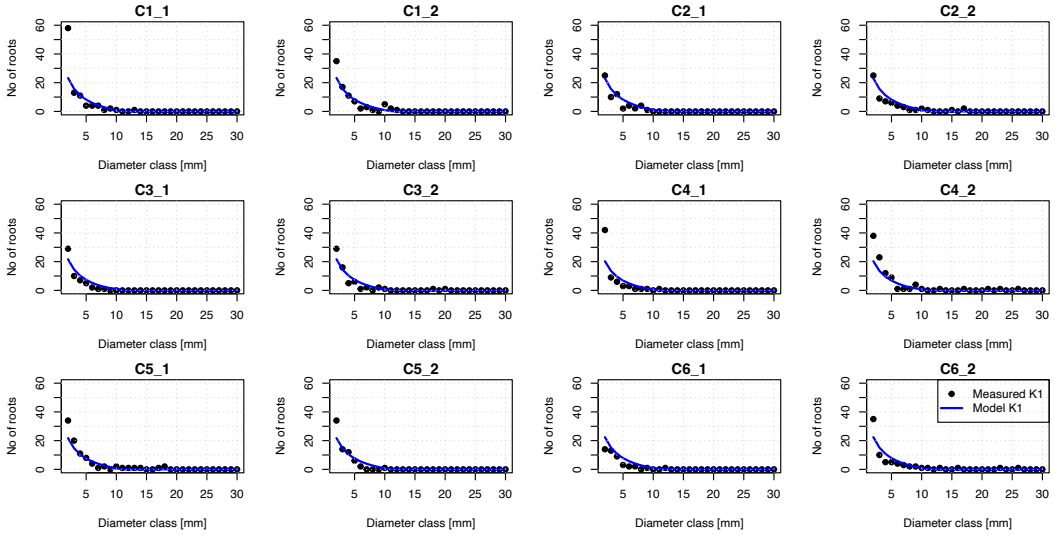

FIGURE 5.10: Root quantities in each coarse root diameter class measured from twelve 1-m width soil profile in control stand in K1 site compared to simulated values of RDM. The black dots represent measured root number while the blue curves represent estimated root distribution from RDM.

Compare root distribution data between Switzerland and Japan

To quantitatively evaluate how well the models simulate root distribution compared to observations and to assess the similarity between root distribution of *C. japonica* in Switzerland and Japan, we calibrated the RDM using a merged dataset from both the CH and K1 sites (referred to as Model K1+CH). Then, we compared the performance of three calibrated models (Model CH, Model K1, and Model K1+CH) against all combinations of measured datasets. The sum of absolute errors (SAE) (Table 5.3) and the Taylor Diagram are used to compare the performance of the models (Figure 5.14).

Model CH	μ=21573.35	ψ=15.08331	β=-1.05014	η=0.2899179			
	SAE_fr	SAE_cr	SAE_ar	SAE_crn	SAE_crf	SAE_rf	Profiles
CH data	621.9751	410.1329	1032.108	**28.99972**	157.3558	5979.593	58
K1 data	343.5232	1375.8388	1719.362	27.22777	152.8446	14600.51	22
K1+CH data	965.4982	1785.9708	2751.469	56.22749	310.2004	20580.1	80
Kobe data	-	141.1594	-	240.6244	536.4201	15029.56	14
Model K1	μ=42805.75	ψ=29.82645	β=-0.40036	η=0.660599			
	SAE_fr	SAE_cr	SAE_ar	SAE_crn	SAE_crf	SAE_rf	Profiles
CH data	530.6008	1081.1452	1611.746	68.92025	220.7381	12453.1	58
K1 data	457.6351	910.8129	1368.448	**16.14252**	135.3163	12877.45	22
K1+CH data	988.2359	1991.9581	2980.194	85.06276	356.0544	25330.54	80
Kobe data	-	428.1417	-	**236.9732**	532.1665	20760.46	14
Model K1+CH	μ=26173.24	ψ=15.00192	β=-0.57244	η=0.3052915			
	SAE_fr	SAE_cr	SAE_ar	SAE_crn	SAE_crf	SAE_rf	Profiles
CH data	599.7446	589.6924	1189.437	32.46714	156.4513	7483.003	58
K1 data	418.0102	963.0288	1381.039	19.14162	143.1854	12051.26	22
K1+CH data	1017.755	1552.722	2570.477	**51.60877**	299.6367	19534.26	80
Kobe data	-	326.4388	-	240.7348	537.3977	18665.96	14

TABLE 5.3: Results of the three calibrated root distribution models compared with measured datasets (including Kobe, which was not used for calibration). μ, ψ, β, and η are coefficients of Equations 5.1, 5.2, 5.3, and 5.4. SAE_fr refers to the Sum of Absolute Errors (SAE) for fine root number, SAE_cr refers to the SAE for coarse root number, SAE_ar refers to the SAE for all root numbers, SAE_crn represents the SAE for cumulative root number, SAE_crf represents the SAE for cumulative root force, and SAE_rf is the SAE for root-force. "Profiles" indicates the number of assessed profiles. Bold values indicate the models that performed the best for each dataset based on the minimum SAE of cumulative root number.

Based on Figure 5.11, the three models showed to well simulate root abundance at various distances in the CH site, particularly for coarse roots. From Figure 5.11(b), the biggest root residuals are in the range of 1 to 5 mm roots with Model CH tends to underestimate while Model K1 tends to overestimate root frequencies within this root diameter range. In particular, for the 2 to 5 mm root diameter class, at distances of 1.5 m and 2.5 m from the stem, Model K1 overestimated root abundance the most, with a total overestimation of 169.96%, while Model CH and Model K1+CH performed better, with overestimations of 4.48% and 101.36%, respectively. At 3.5

m from the stem, Model K1 performed better in estimating 2 mm roots for Tree S2, with an overestimation of 9.53%, compared to Model CH's underestimation of 70.69%. For the 3 mm root class and onwards, the percentage errors for Model CH, Model K1 and Model K1+CH compared to CH data, were 66.48%, 244.93%, and 36.28%, respectively. At 4.5 m from the stem, Model K1+CH performed the best in simulating coarse root frequency, with a percentage error of 88.18%. Overall, considering all root diameter classes and all four distances from the stem of the two *C. japonica* trees in the CH site, the percentage errors for Model CH, Model K1, and Model K1+CH were 30.95%, 55.27%, and 4.85%, respectively. This suggests that Model K1+CH showed the best performance in simulating root distribution for the two trees in the CH site, with an error percentage of less than 10%. Although Model CH and Model K1 were less accurate, they still performed well, with percentage errors below 100%. Overall, the Root Distribution Model well simulated the spatial root distribution patterns of two candidate trees in CH site.

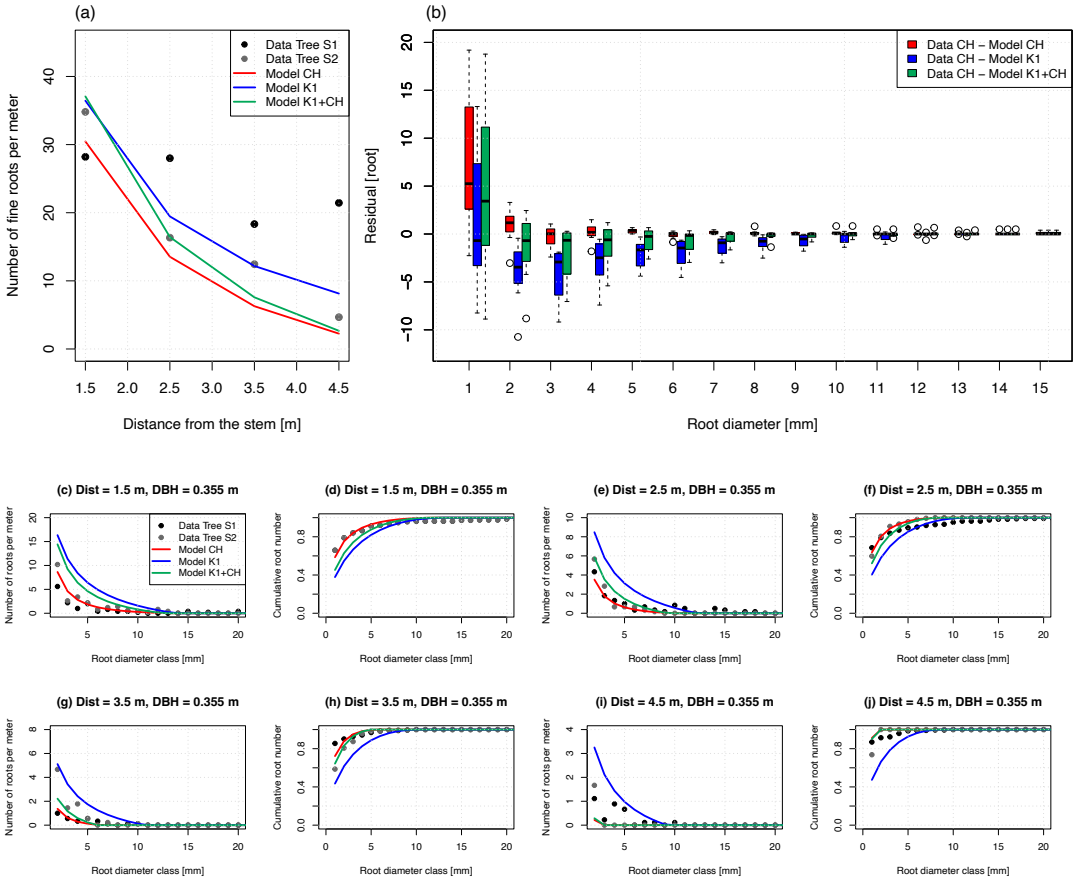

FIGURE 5.11: Comparison of root quantities and cumulative root number between measurements (Tree S1 as black dots and Tree S2 as gray dots) in CH site and three calibrated models (Model CH as red lines, Model K1 as blue lines, and Model K1+CH as green lines). Subplot (a) presents difference of fine root quantities from various datasets at different distances from the stem. Subplot (b) shows the root residual per meter in each root diameter class between measurement and models.

In the K1 site, as shown in Figure 5.12, the measured fine root numbers exhibited greater variability across different survey lines compared to the simulated values. From Figure 5.12(b), all three models (Model CH, Model K1, and Model K1+CH)

tended to underestimate the number of coarse roots, especially in the 2 to 5 mm root diameter class, with percentage errors of 70.52%, 22.55%, and 43.47%, respectively. As mentioned above, Model K1 better simulated the frequencies of roots bigger than 5 mm in the thinned stand than at the control stand. However, considering all coarse root diameter classes, these calibrated models (Model CH, Model K1, and Model K1+CH) performed better at simulating in the control site (with percentage errors of 67.58%, 3.38%, 35.76%, respectively) than in the thinned site (with percentage errors of 74.38%, 24.68%, and 46.52%, respectively). Even though Model K1 worked better than Model K1+CH in estimating the total root numbers, with percentage errors of 1.71% and 19.74%, respectively, Model K1+CH still performed well overall.

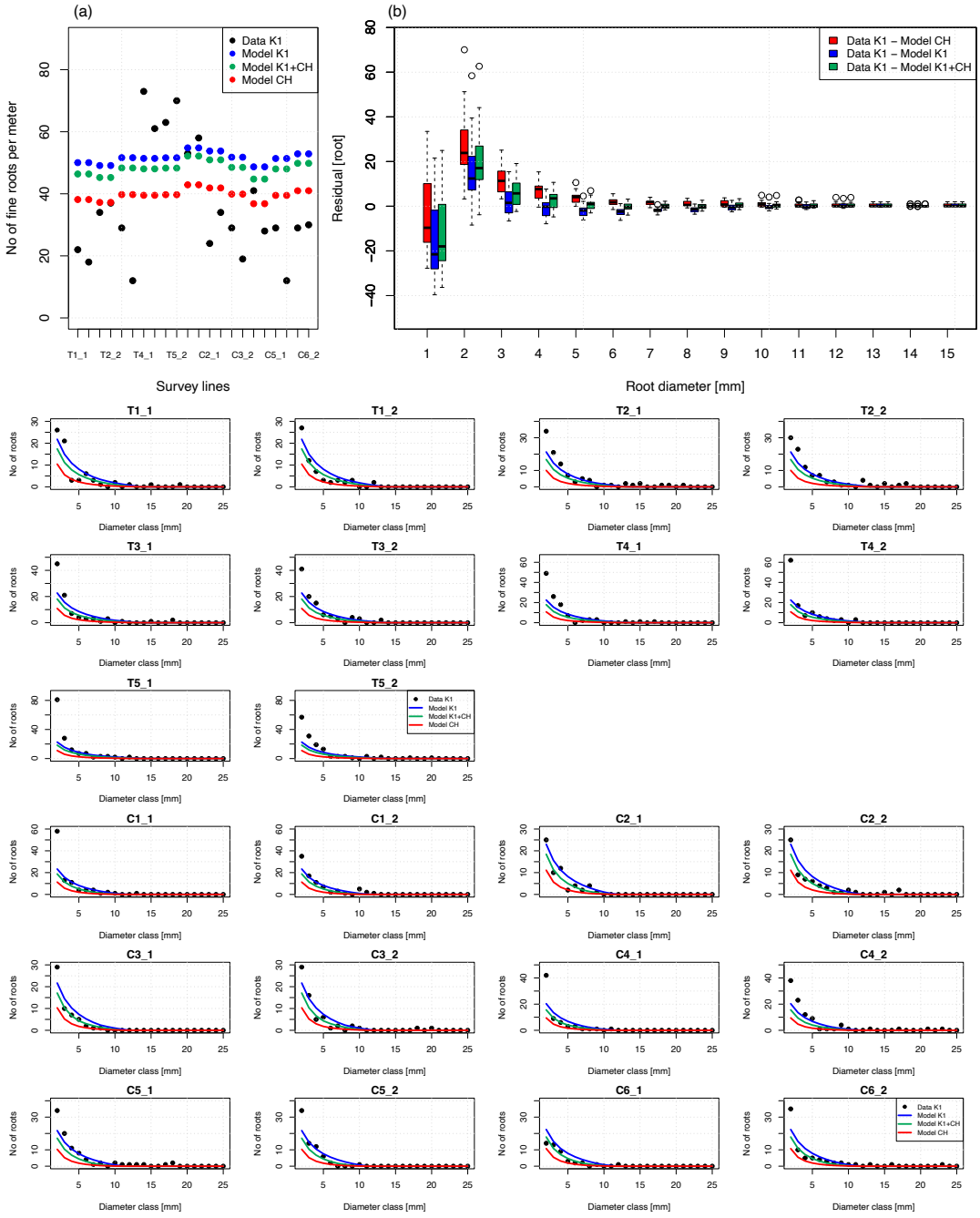

FIGURE 5.12: Comparison of (a) root quantities between measurements from the K1 site (Data K1) and three calibrated models: Model CH (red lines), Model K1 (blue lines), and Model K1+CH (green lines); (b) root residual per meter in each root diameter class between measurement and models. The upper plot displays the comparison for fine roots, while the smaller plots illustrate the comparison for root diameter classes of 2 mm and onwards.

We compared the results of Model K1, Model CH, and Model K1+CH in simulating the root distribution of two trees with diameters of 0.3 m and 0.4 m at various distances from the stem. We selected diameters of 0.3 m and 0.4 m because these sizes fall within the range of observed tree sizes in our study. Additionally, we assessed root distribution at distances ranging from 1.0 m to 4.5 m from the stem, as this range corresponds to the distances of our excavated trenches. The biggest difference

in root numbers between Model K1 and Model CH was observed at 1 to 5 mm root diameter classes. Model K1, calibrated with the measured K1 dataset, generated a higher root density compared to Model CH, particularly for the 1 to 10 mm root diameter classes. For instance, at a diameter at breast height (DBH) of 0.3 m and a distance of 1.5 m, Model K1 simulated 59.69% more roots than Model CH. As the distance from the stem increased, the percentage difference between the two models also increased.

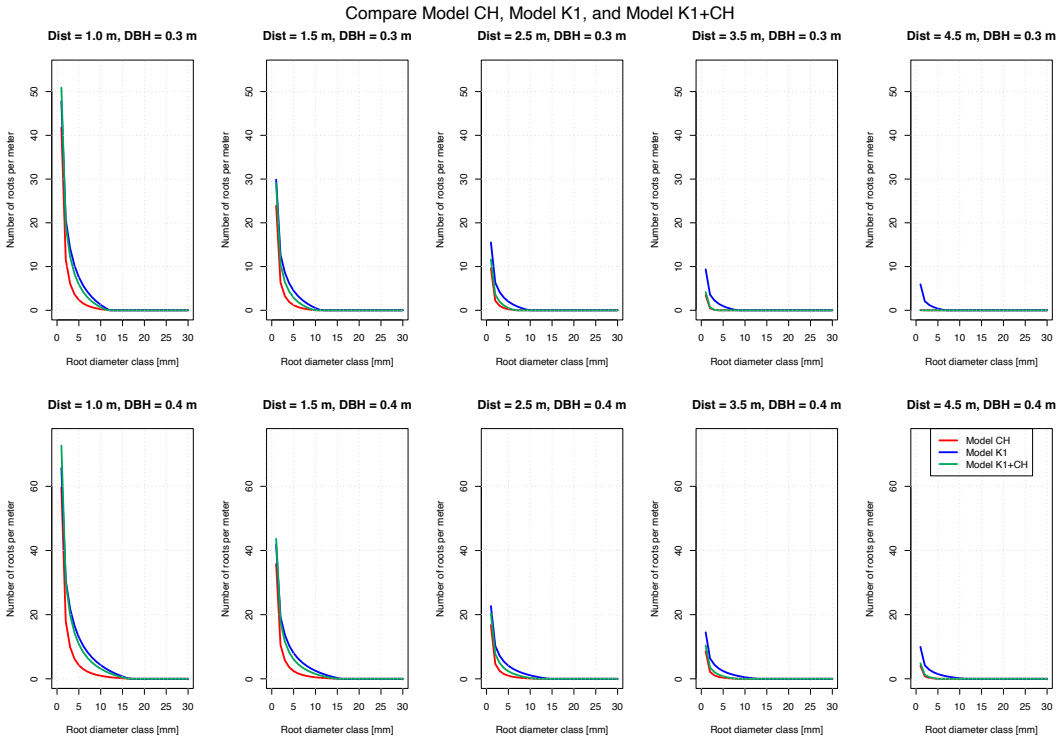

FIGURE 5.13: Simulated root distribution for Model CH, Model K1, and Model K1+CH at varying diameters at breast height and different distances from the tree stem. Red lines represent the performance of Model CH, blue lines indicate Model K1, and green lines exhibit the performance of Model K1+CH.

Based on Figure 5.14(a), the Taylor Diagram for the CH dataset demonstrates that all models effectively simulated root distribution in CH site with Pearson correlation coefficients of approximately 0.90 and a centered RMSD of 0.5. Out of three models, Model CH fits the best with measured CH dataset due to the highest value of Pearson coefficient and the smallest value of RMSD. Figure 5.14(b) illustrates the Taylor Diagram for the K1 dataset. Similarly, all three models simulated well root distribution, closely aligning with the measurements, with Pearson correlation coefficients in the range of 0.80 to 0.85, along with a centered RMSD of 0.6. Model K1 shows to simulate the root distribution the best with K1 measurements due to highest correlation and smallest RMSD value. The Root Distribution Model proves to be a good model for predicting root distribution in both sites.

Based on above-mentioned results, the root distribution patterns of *C. japonica* from CH site and K1 site are similar within the root diameter range of 6 mm and onwards. For root diameters smaller than 6 mm, the root frequencies are significantly different with percentage errors ranging between 10 and 170%.

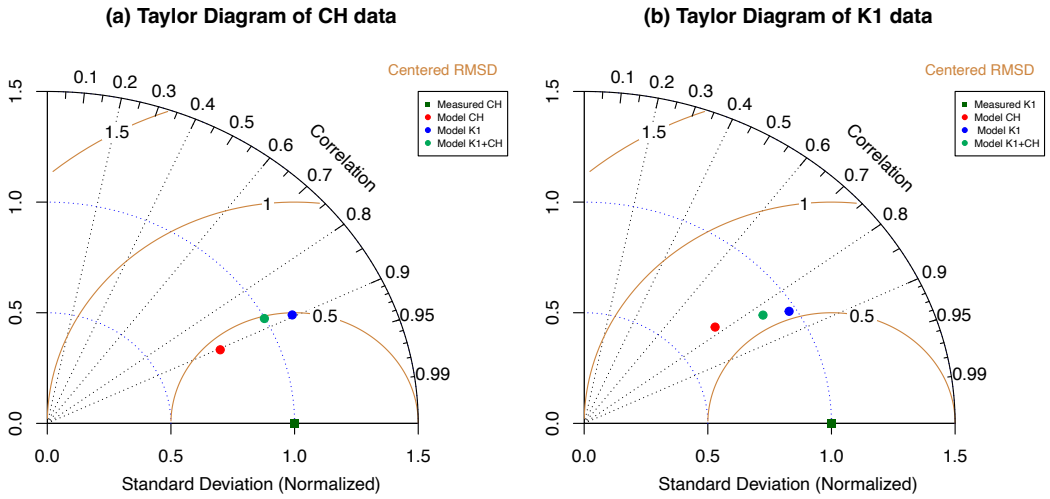

FIGURE 5.14: Taylor Diagram illustrating the predicted root distribution from various models for (a) the CH dataset and (b) the K1 dataset. Dark green squares represent measured values, the red point indicates Model CH, blue dots represent Model K1, and green dots refer to Model K1+CH.

Validate RDM with Kobe dataset

As shown in Table 5.3, columns SAE_fr and SAE_ar for the Kobe dataset were marked as NA because no data for roots with diameters between 1 and 5 mm was recorded at this site. Therefore, only the differences in root quantities from the 6 mm diameter class and above were calculated between the modeled and measured values for Kobe. SAE_crn is used as a coefficient for comparing the goodness of fit across different models. Based on this criterion, all three models have similar performances with SAE_crn values between 237 and 240.7.

The two candidate trees in Kobe were similar in size to the two candidate trees in the HAFL Forest, Switzerland. At a distance of 1.5 m from the stem, the maximum root diameters recorded for Tree 1 and Tree 2 at the Kobe site were 28.9 and 27.4 mm, respectively. In contrast, the maximum root diameter observed in the HAFL Forest was significantly larger, measuring 66 mm. Additionally, the number of coarse roots smaller than 15 mm in diameter was greater in Switzerland compared to Kobe.

Unlike other studied sites, the measured root data in Kobe did not exhibit a decreasing curve in root frequency relative to root size. Instead, at most distances, the Kobe data showed increasing curves in the number of roots within the 6 to 9 mm root diameter classes. When comparing the measured root numbers in the two Kobe trees with those in the two CH trees at a distance of 1.5 m, the root frequencies recorded in the CH trees were 1.7 up to 12.6 times higher than those in the Kobe trees for the 6 to 9 mm diameter range. For the 10 to 15 mm diameter class, the difference between the two datasets was small: for Tree Kobe_1, root residuals were 0.89 and 0.31 roots per meter compared to CH Tree S1 and CH Tree S2, respectively. In the same diameter range, the residuals between the measured root numbers of Tree Kobe_2 and CH Tree S1 and CH Tree S2 were 0.14 and 1.06 roots per meter, respectively.

Figure 5.15 and Figure 5.16 present a comparison among the three calibrated models (Model CH, Model K1, and Model K1+CH), the measured CH data (Tree S1 and Tree S2), and two candidate trees in the Kobe site (Tree 1 with a DBH of

0.329 m and Tree 2 with a DBH of 0.369 m). The results indicate that the calibrated RDMs well predict the root frequency in the diameter range of 10 to 15 mm in the Kobe site. The models tended to overestimate the number of coarse roots within the diameter range of 6 to 9 mm, while it underestimated the number of coarse roots bigger than 15 mm.

In particular, the total number of roots ranging from 6 to 9 mm at all 7 distances in Tree Kobe_1 and Tree Kobe_2 were 6 and 3 roots per meter, respectively. Model K1 generated approximately 132 roots per meter and 175 roots per meter for Tree Kobe_1 and Tree Kobe_2; Model K1+CH generated 97 and 134 roots per meter while Model CH simulated 34 and 46 roots per meter for Tree Kobe_1 and Tree Kobe_2. For total root numbers within the range of 10 to 15 mm at all the distances, the measured values were 11 and 10 roots per meter for Tree Kobe_1 and Tree Kobe_2, respectively. The generated values were 30 and 64 roots per meter for Model K1, 20 and 44 roots per meter for Model K1+CH, and 7 and 14 roots per meter for Model CH. For roots bigger than 15 mm, the total numbers measured at all distances from Tree Kobe_1 and Tree Kobe_2 were similar with 24 roots per meter. Only Model K1+CH and Model CH simulated roots bigger than 16 mm with very small values of 0.3 roots per meter for trees with DBH of 0.369 m. The biggest difference between measured and simulated root quantities was at 0.5 m distance from the stem and the difference decreased with the increasing distance from the stem. The maximum root diameter recorded at the Kobe site was 265 mm, which belonged to the soil trench located 0.5 m distance from the stem of Tree 2.

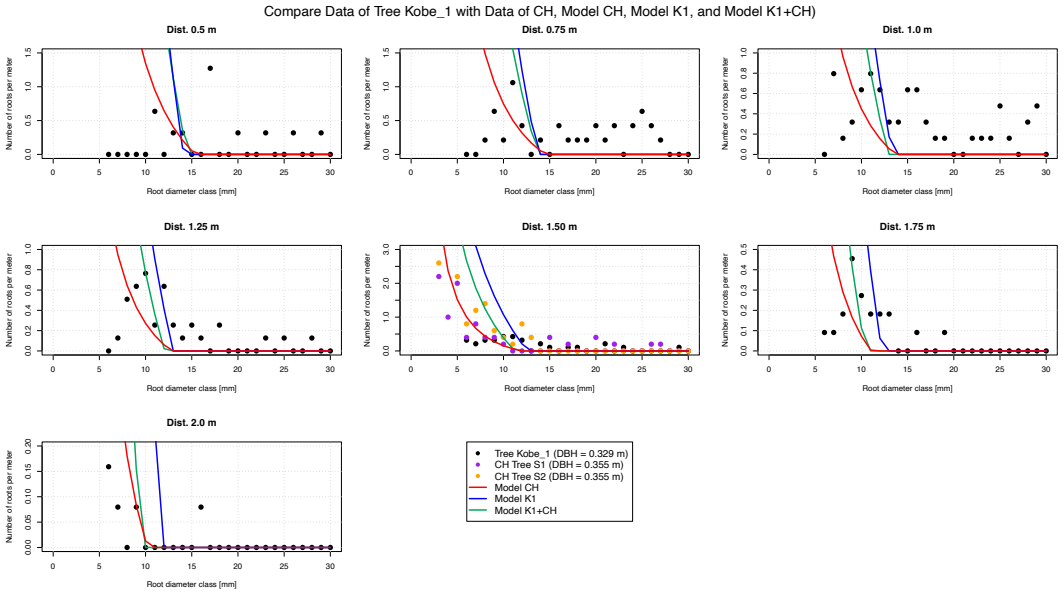

FIGURE 5.15: Validation of the performance of three Root Distribution Models against measured data from the CH dataset and the measured dataset of Tree 1 at the Kobe site in Japan. Black dots represent the measured data for Tree 1 at the Kobe site, while purple and orange dots correspond to the measured data for Trees S1 and S2 in the CH site, respectively. Red lines indicate Model CH, blue lines represent Model K1, and green lines refer to Model K1+CH.

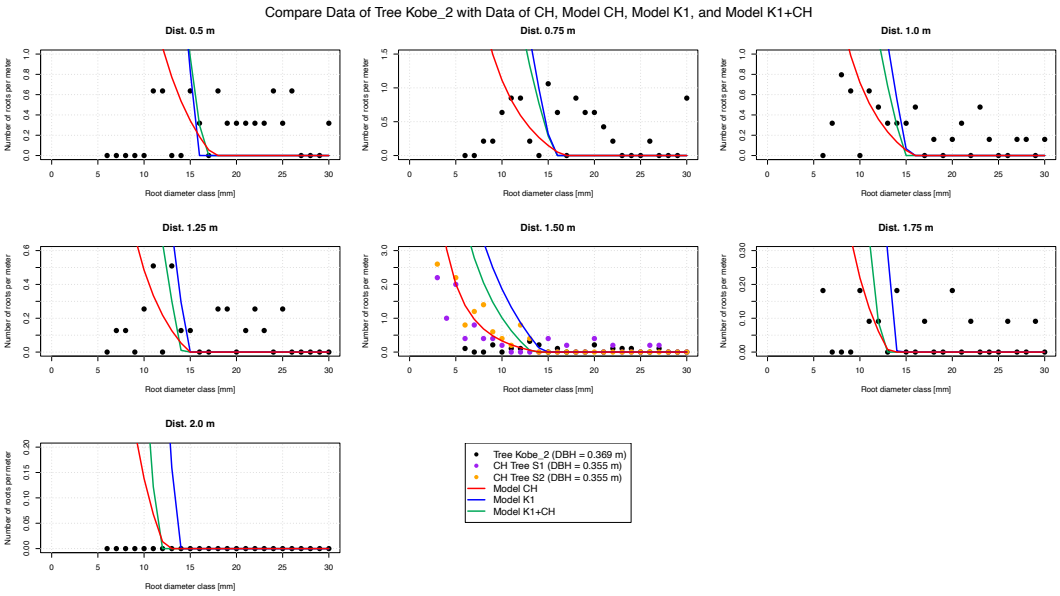

FIGURE 5.16: Validation of the performance of three Root Distribution Models against measured data from the CH dataset and the measured dataset of Tree 2 at the Kobe site in Japan. Black dots represent the measured data for Tree 2 at the Kobe site, while purple and orange dots correspond to the measured data for Trees S1 and S2 in the CH site, respectively. Red lines indicate Model CH, blue lines represent Model K1, and green lines refer to Model K1+CH.

5.3.2 Mechanical properties of roots

Root mechanical properties were analyzed by considering the maximum root pullout forces and their apparent secant spring constant (Schwarz, Giadrossich, and Cohen, 2013; Schwarz et al., 2015). Table 5.4 summarizes the equations relating root diameter to maximum tensile force/strength of *C. japonica* from previous studies and our research. Genet's study evaluated various tensile forces of *C. japonica* based on different species ages, categorizing them into juvenile plantations (9 years old), intermediate plantations (20 years old), and mature plantations (30 years old). We selected the output from the mature plantations in Genet's research for comparison, as the age of these stands was most close to that of our forest (Genet et al., 2008). The maximum diameter of tested roots from laboratory tensile tests was 9.81 mm, whereas the maximum diameter from field pullout tests was 42.8 mm.

Studies	No of samples	Min ϕ [mm]	Max ϕ [mm]	T.S.	Equation	R^2	Sampling time
Abe and Iwamoto (1986)	76	0.1	8.5	ex-situ	T_r (kg.f) $= 8.064 \cdot d^{1.447}$	0.81	-
Genet et al. (2008)	100	0.30	4.30	ex-situ	T_r (MPa) $= 31.9 \cdot d^{-0.41}$	0.36	July 2005
Yamase et al. (2019)	34	3.1	42.8	in-situ	$F_r = 15.69 \cdot d^{1.75}$	0.87	October 2012
HAFL Forest	35	1.25	36	in-situ	$F_r = C(\phi) \cdot 7.0 \cdot 10^5 \cdot d^{1.45}$	0.85	January 2021
Longchi Forest	55	0.43	9.81	ex-situ	$F_r = C(\phi) \cdot 4.6 \cdot 10^5 \cdot d^{1.36}$	0.77	August

TABLE 5.4: Summary of the relationship between root diameter and maximum tensile force (F_r) or tensile strength (T_r) of Japanese cedar (*Cryptomeria japonica*) from various studies.

Figure 5.17 illustrates the relationship between maximum tensile force and root diameter of *C. japonica*. The analysis of the root diameter - maximum force curve indicated an increasing trend in root tensile force with larger root diameters. The fitted power-law regression curve well simulated maximum tensile force for diameters smaller than 10 mm; however, it fluctuated significantly for bigger root diameters. The root tensile forces recorded by Abe and Iwamoto (1986) were greater than those in other studies. Both the in-situ CH dataset and the data collected from Yamase et al. (2019) showed no significant difference in root tensile force within the root diameter range of 1 to 10 mm. Similarly, both ex-situ tests from CN dataset and Genet et al. (2008) showed similar results. In the diameter range of less than 10 mm, laboratory tests measured higher root tensile forces than field pullout tests. However, the difference was insignificant. The mean tensile force for roots under 10 mm from the field pullout tests was 320.27 N, while from the laboratory tensile tests, the force was 373.89 N. The difference was not statistically significant, with a t-value of -1.37 and a p-value of 0.1731.

The difference between field pullout tests and laboratory tensile tests became more significant for roots bigger than 10 mm. This difference is due to the fact that no laboratory tests were conducted on roots bigger than 10 mm. By using the field pullout method, Yamase et al. (2019) conducted field pullout tests with root diameters up to 42.8 mm. In the Swiss study site, the assessed root diameters of the *C. japonica* ranged from 1.25 mm to 36 mm, with the lowest, highest, and mean values of maximum tensile force being 0.008 kN, 6.199 kN, and 0.948 kN, respectively.

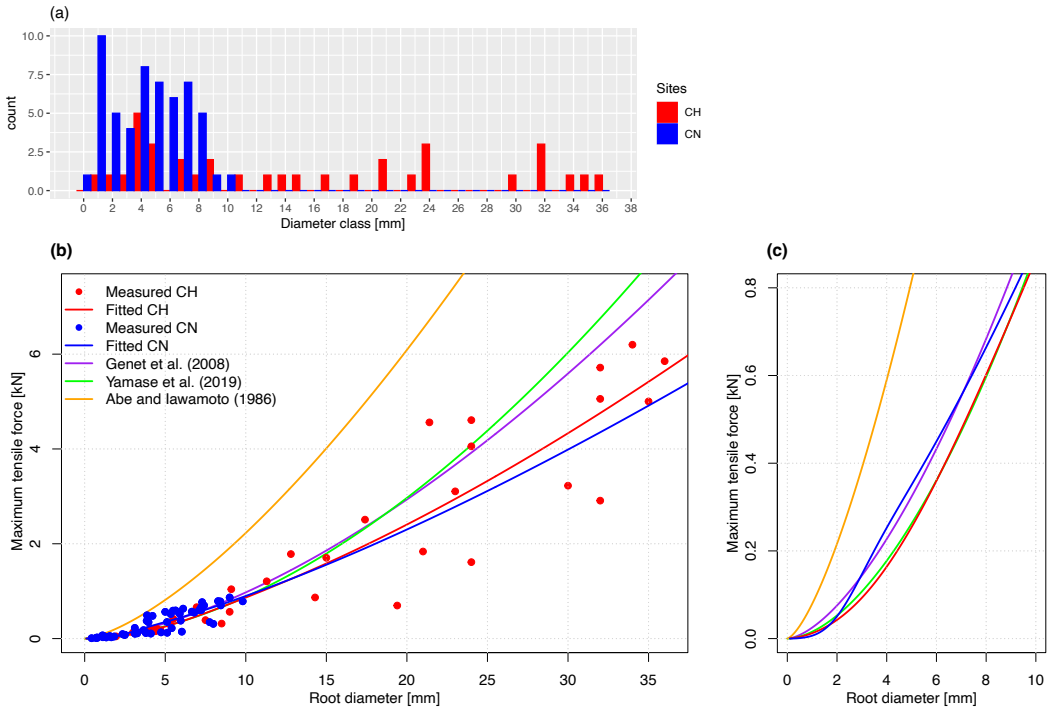

FIGURE 5.17: (a) Number of tested roots in each root diameter class [mm] from CH field pullout tests (red bars) and CN laboratory tensile tests (blue bars); (b) Power-law relationship between the maximum tensile force of *Cryptomeria japonica* trees as a function of root diameter, obtained from field pullout tests in Switzerland (solid red line) and laboratory tensile tests in China (solid blue line), compared with Genet et al. (2008) (solid purple line), Yamase et al. (2019) (solid green line), and Abe and Iwamoto (1986) (solid orange line). Data fitting in our studies follows Dazio, Conedera, and Schwarz (2018); (c) Zoom-in of subplot (b) with root diameters ranging from 0 to 10 mm.

As no laboratory tensile tests were conducted on roots bigger than 10 mm and no significant difference was observed between the CH and CN datasets for roots smaller than 10 mm, we merged these two measured dataset to obtain a comprehensive maximum tensile force - root diameter curve. This combined dataset was then used for calibrating the RBMw model. Figure 5.18 presents the power-law curve relationship between the merged dataset of root diameter and maximum tensile force.

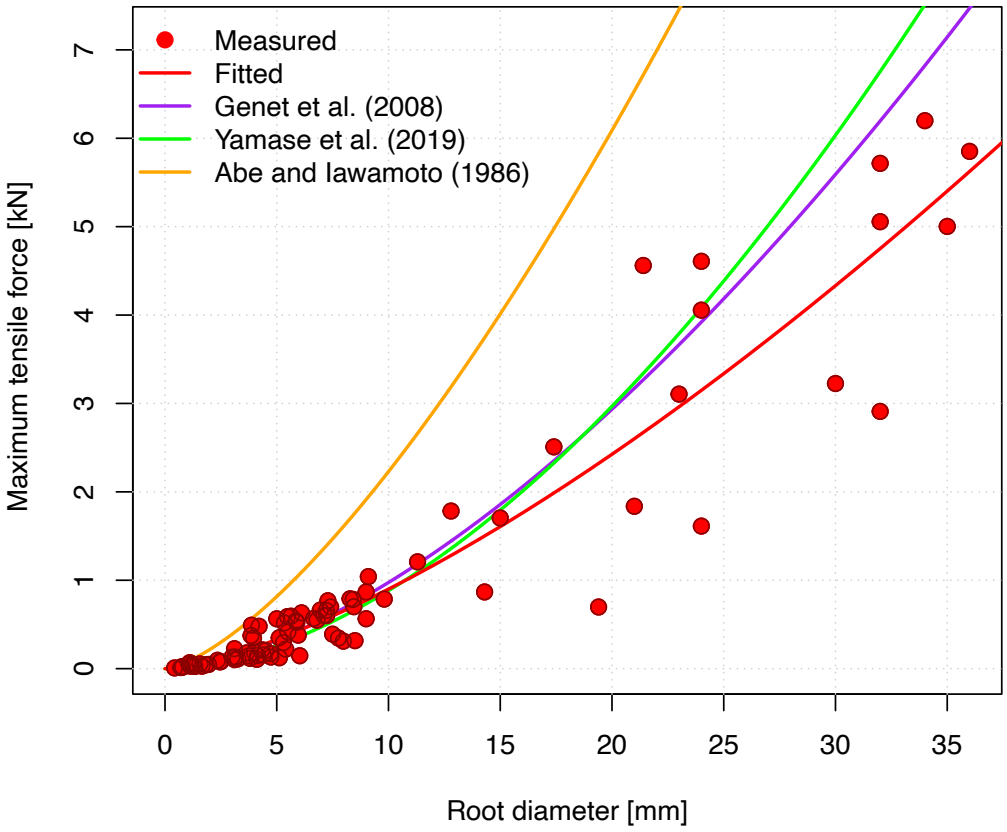

FIGURE 5.18: Maximum tensile force - root diameter curves from our merged dataset of CN and CH (shown in red color), from the study by Genet et al. (2008) (shown as purple line), from the study by Yamase et al. (2019) (shown as green line), and from the study by Abe and Iwamoto (1986) (shown as orange line).

Table 5.5 presents the best-fitted coefficients for the RBMw model of *C. japonica*.

Symbol	Parameter	Value	Unit
F_0	Root force scaling factor	$6.55 \cdot 10^5$	N
α	Root force shape factor	1.43	-
k_0	Root spring constant scaling factor	2128911.215	N/m
λ	Weibull scaling factor	1.251361072	-
ω	Weibull shape factor	2.46	-
ϕ_m	Mean of cumulative normal distribution	0.002	m
ϕ_{sd}	Standard deviation of cumulative normal distribution	0.001189115	m

TABLE 5.5: Best-fitted coefficients for the RBMw model of *Cryptomeria japonica*.

The variability of root mechanical properties is quantified using the Weibull distribution. The fitting of the Weibull distribution is shown in Figure 5.19. The fitted

model has a Weibull exponent of 2.46 and a Weibull scaling factor of 1.25. The R-squared value of the fit is 0.99, with a Sum of Absolute Errors of 2.06.

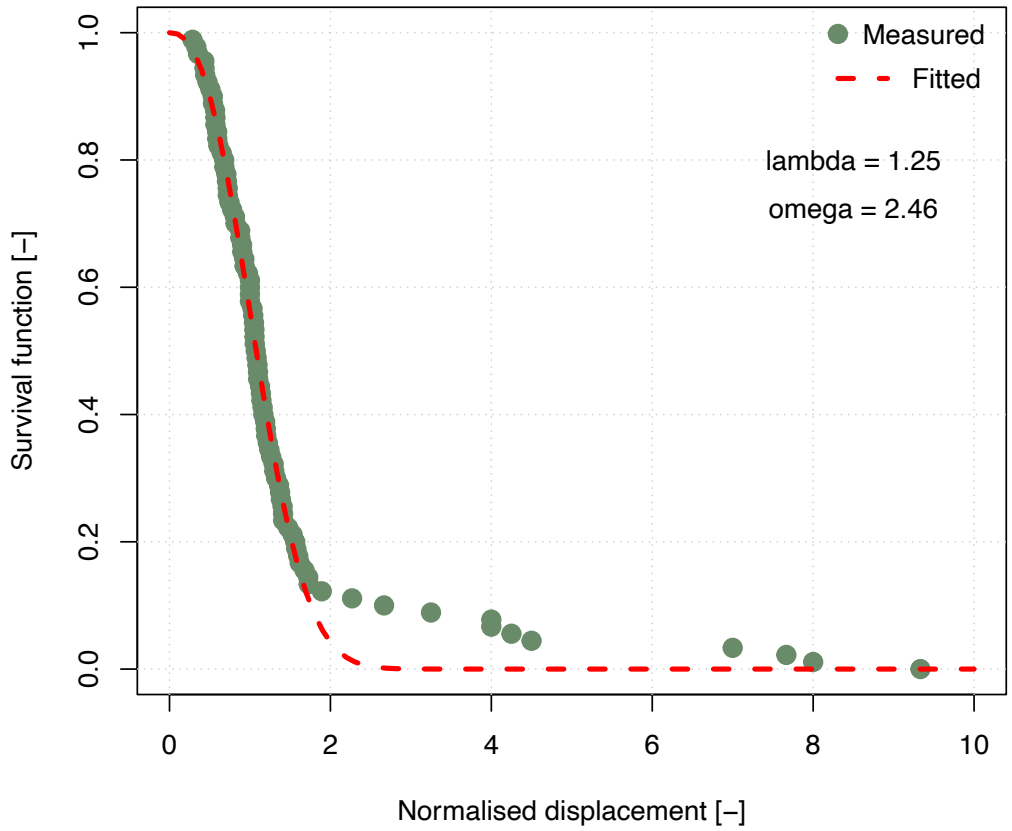

FIGURE 5.19: Fitted curves of survival function in relation to normalized displacement.

5.3.3 Root reinforcement

Lateral Root reinforcement

Figure 5.20 shows the bundle force at different trenches of the two *C. japonica* trees in both horizontal and vertical directions. It can be observed that the closest trench exhibited the highest force, while force decreased with increasing distance from the trees in both cases. For Tree S1, the bundle force in the 0 - 0.15 m layer reached up to 4.76 kN/m at a 1.5 m distance, then decreased to 1.98 kN/m at 2.5 m, and further to 0.21 kN/m at 3.5 m. Roots with diameters bigger than 30 mm were only found in the 1.5 m trench, and bigger roots contribute significantly more to root reinforcement due to the power-law relationship between root diameter and force. Similarly, in Tree S2, root bundle force weakened as the distance from the tree increased, with a maximum force of approximately 2.18 kN/m recorded at the 1.5 m trench. The large difference in root reinforcement between the 1.5 m trenches of the two trees is explained by root size; although Tree S2 had more roots, the largest root diameter was only 13 mm, whereas Tree S1 had a root with a diameter of 66 mm. At 4.5 m, root bundle reinforcement was relatively small compared to the other trenches.

In the vertical direction, the first soil layer 0 - 0.15 m played a crucial role as the primary contributor to root reinforcement in all trenches at the CH site. For Tree S1, this layer contributed the greatest root reinforcement among all soil layers at the trenches 1.5 m, 2.5 m and 3.5 m from the stem. However, unlike the other trenches, root reinforcement was highest in the second soil layer 0.15 - 0.30 m at the 4.5 m distance, with a value of 0.110 kN/m. The difference in root force between each soil layer also became smaller as the distance from the stem increased. For Tree S2, the highest root reinforcement in each trench was consistently recorded in the first soil layer, followed by the second soil layer. In the last trench, root reinforcement across all soil layers was less than 0.02 kN/m.

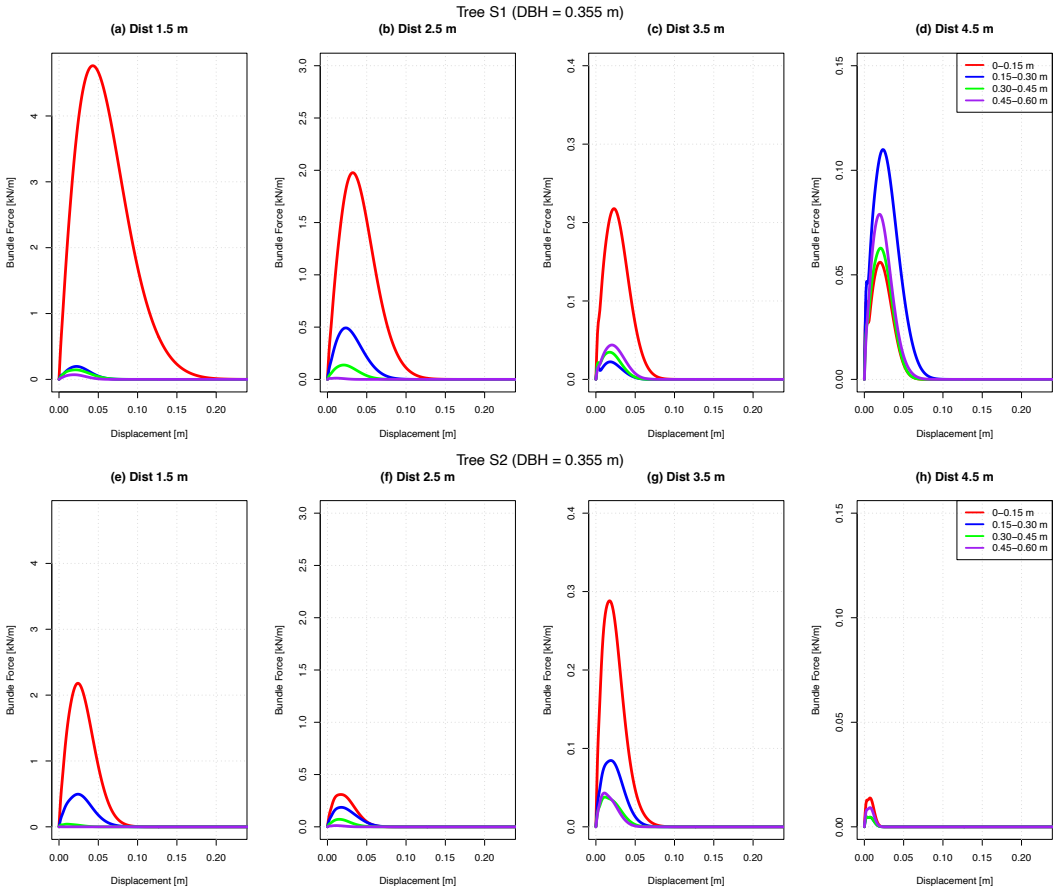

FIGURE 5.20: Root reinforcement per meter computed by RBMw as a function of displacement at distances of 1.5 m, 2.5 m, 3.5 m, and 4.5 m from the stem, based on field pullout tests in the HAFL Forest for Tree S1 (Sub-figures (a), (b), (c), (d), respectively) and Tree S2 (Sub-figures (e), (f), (g), (h), respectively). Root bundle force for the first soil layer (0 - 0.15 m) is represented by the red line, for the second soil layer (0.15 - 0.30 m) by the blue line, for the third soil layer (0.30 - 0.45 m) by green line, and for the forth soil layer (0.45 - 0.60 m) by the purple line.

We applied the measured root distribution data in combination with the calibrated RBMw model to calculate root reinforcement and determine the best-fitted coefficients for the Root Reinforcement Model (RRM). The calibrated values are summarized in Table 5.6.

Model CH	a = 40237.1	b = 0.4102142	c = 9.494713
	SAE_rf	No. profiles	
CH data	51817.04	58	
K1 data	82982.18	22	
K1+CH data	134799.2	80	
Model K1	a = 40055.71	b = 0.166209	c = 1.776659
	SAE_rf	No. profiles	
CH data	107544.8	58	
K1 data	57625.78	22	
K1+CH data	165170.6	80	
Model K1+CH	a = 49706.6	b = 0.4660286	c = 10.37495
	SAE_rf	No. profiles	
CH data	56790.38	58	
K1 data	64951.22	22	
K1+CH data	121741.6	80	

TABLE 5.6: Best-fitted coefficients of the Root Reinforcement Model for estimating maximum lateral root reinforcement. Coefficients a, b, and c are the calibrated parameters of the model. SAE_rf represents the SAE between the measured root-force and simulated root-force (unit: N); "No. profiles" refers to the number of profiles assessed at each site.

We assessed the differences in the maximum lateral root reinforcement in CH site between forces calculated by the RBMw model with the measured root distributions of two trees, compared to the predicted values using the RRM (shown in Figure 5.21). The nearest trench to the tree stem consistently exhibited the highest root reinforcement, with forces decreasing as the distance from the tree increased for both trees. Among 4 distances from the stem, the highest root reinforcement was observed at 1.5 m distance of a tree with 0.355 m DBH. At this distance, the mean measured root reinforcement was 3.89 kN/m, with values ranging from a minimum of 0.19 kN/m to a maximum of 10.09 kN/m. In comparison, Model CH estimated 4.54 kN/m, Model K1 estimated 6.40 kN/m, and Model K1+CH estimated 5.68 kN/m. The highest measured reinforcement at this distance was nearly twice as high as the estimates from the models. Compared to the mean measured root reinforcement, Model CH predicted the most accurately.

At a distance of 2.5 meters, the mean measured root reinforcement was 1.61 kN/m, with values ranging from a minimum of 0.10 kN/m to a maximum of 5.54 kN/m. Model CH estimated the root reinforcement at 0.79 kN/m, while Model K1 estimated a higher value of 3.19 kN/m, and Model K1+CH estimated root reinforcement at 0.89 kN/m. Therefore, Model K1+CH estimated the root reinforcement best at this distance.

At a distance of 3.5 m, the mean measured root reinforcement was 0.41 kN/m, with values ranging from a minimum of 0 kN/m to a maximum of 1.79 kN/m. Model CH and Model K1+CH both estimated the root reinforcement at 0.15 kN/m, while Model K1 provided a significantly higher estimate of 1.84 kN/m. As a result, Model CH and Model K1+CH predicted root reinforcement the best at this distance.

At 4.5 m distance, the root reinforcement was relatively small compared to other trenches. The mean measured root reinforcement at this distance was 0.19 kN/m, with values ranging from a minimum of 0 kN/m to a maximum of 2.23 kN/m. Model K1 provided the highest estimate at 1.14 kN/m, while both Model CH and Model

K1+CH estimated 0.03 kN/m. This indicates that while the measured root reinforcement reached up to 2.23 kN/m, the model estimates were significantly lower. The relatively low reinforcement at 4.5 m from the stem of a 0.355 m DBH tree suggests that root reinforcement at this distance may be negligible.

Overall, Model CH and Model K1+CH performed better but tended to underestimate the mean root reinforcement, while Model K1 overestimated it.

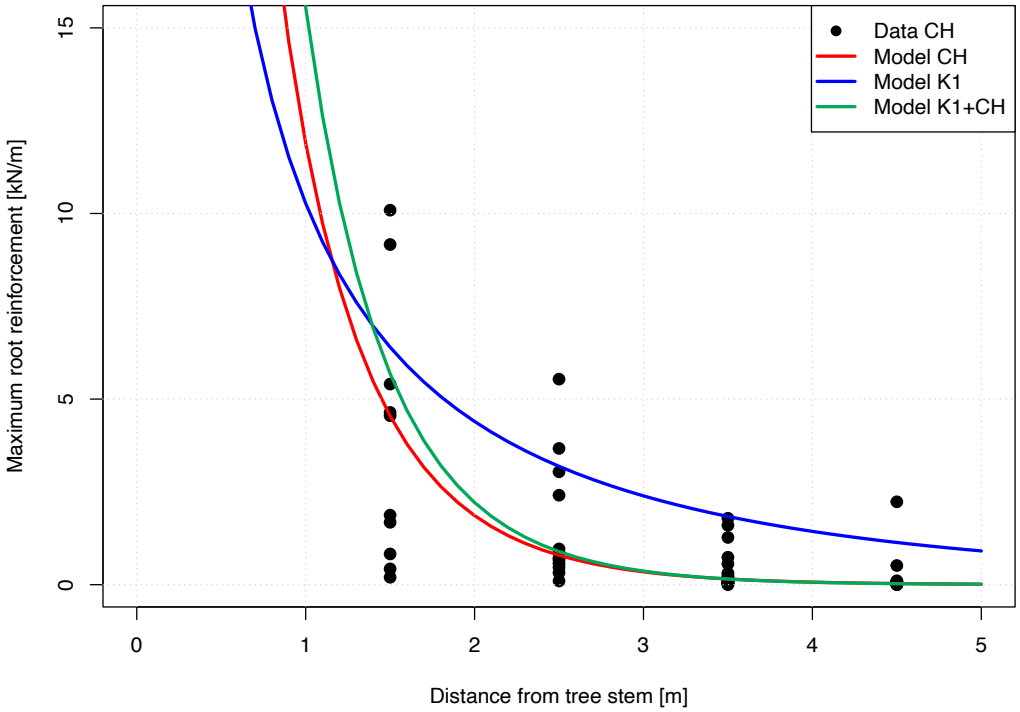

FIGURE 5.21: Maximum lateral root reinforcement of 0.355-m DBH trees in the HAFL Forest, Switzerland. The black dots represented measured root reinforcement whereas three lines represented three models as legend.

Figure 5.22 displays the difference in maximum lateral root reinforcement between the measurements and models predictions at the K1 site. Based on the results shown in Figure 5.22 and Table 5.6, the RRM calibrated with measured K1 data and the merged K1+CH data performed the best among the three models. The SAE between the measured root force in K1 and the simulated root force from Model K1 and Model K1+CH were 57.626 kN and 64.951 kN, respectively. This indicates that the differences in root force were approximately 2.619 kN and 2.952 kN per 1-m wide profile. For the simulation of Model K1+CH, the smallest difference between the measured root force and the simulated root force was 0.0028 kN/m (profile C6_1) and the biggest difference was 9.345 kN/m (profile T2_2).

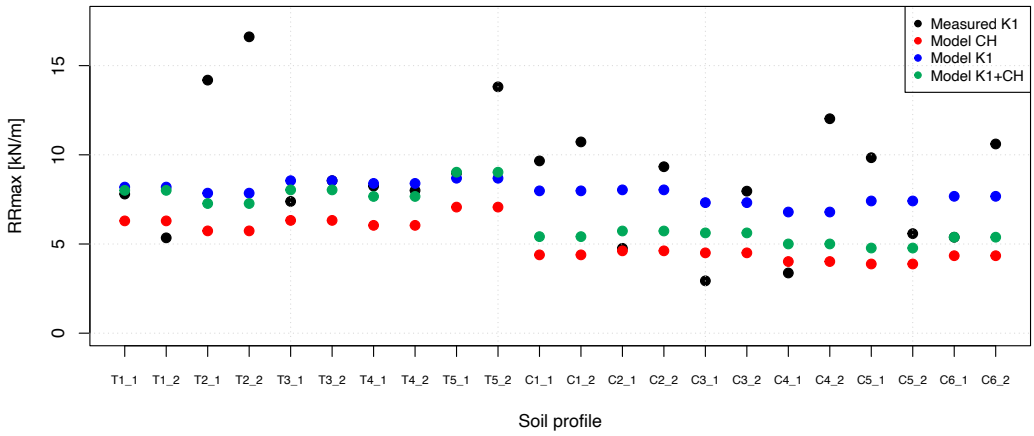

FIGURE 5.22: Maximum lateral root reinforcement for 22 survey lines, each 1 m wide, at the K1 site. The black dots represent the measured root reinforcement, whereas the three lines correspond to the predictions from the three models, as indicated in the legend.

Basal Root reinforcement

From lateral root reinforcement, we calibrated the coefficients to model the basal root reinforcement (Equation 5.12). Table 5.7 presents the best-fit coefficients for simulating basal root reinforcement.

Model CH	$z_\alpha = 0.933328$	$z_\beta = 6.093315$	
	SAE_nrf	R^2	No. profiles
CH data	0.093746	0.999999	58
K1 data	0.802567	0.338406	22
K1+CH data	0.269490	0.960967	80
Model K1	$z_\alpha = 1.829686$	$z_\beta = 4.573089$	
	SAE_nrf	R^2	No. profiles
CH data	0.729897	0.456638	58
K1 data	0.105699	0.948940	22
K1+CH data	0.520474	0.572178	80
Model K1+CH	$z_\alpha = 0.861826$	$z_\beta = 4.046038$	
	SAE_nrf	R^2	No. profiles
CH data	0.185757	0.991645	58
K1 data	0.598560	0.434978	22
K1+CH data	0.083988	0.986168	80

TABLE 5.7: Best-fit coefficients of the RRM for simulating basal root reinforcement. Coefficients z_α and z_β represent the parameters of the model. SAE_nrf is the SAE for normalized root reinforcement. R^2 indicates the coefficient of determination, and "No. profiles" refers to the number of profiles assessed at each study site.

Figure 5.23 presents the normalized basal root reinforcement profiles for different soil layers. A notable disparity in root reinforcement distribution between *C. japonica* trees in the HAFL Forest and the Kamikawa site was observed. In Switzerland,

the most substantial root reinforcement was concentrated in the topmost soil layer (0-0.15 m), with a gradual decline in strength with increasing depth. For the CH dataset, root reinforcement became negligible below 0.6 m. Conversely, the K1 data revealed that the strongest root reinforcement was anchored in the second (0.15-0.3 m) and third (0.3-0.45 m) soil layers, and the root system maintained a relatively high reinforcement capacity up to 0.8 m depth, unlike the CH data. As evidenced by the R^2 values in Table 5.7 and the trends depicted in Figure 5.23, the models demonstrated a satisfactory representation of basal root reinforcement across various soil depth horizons.

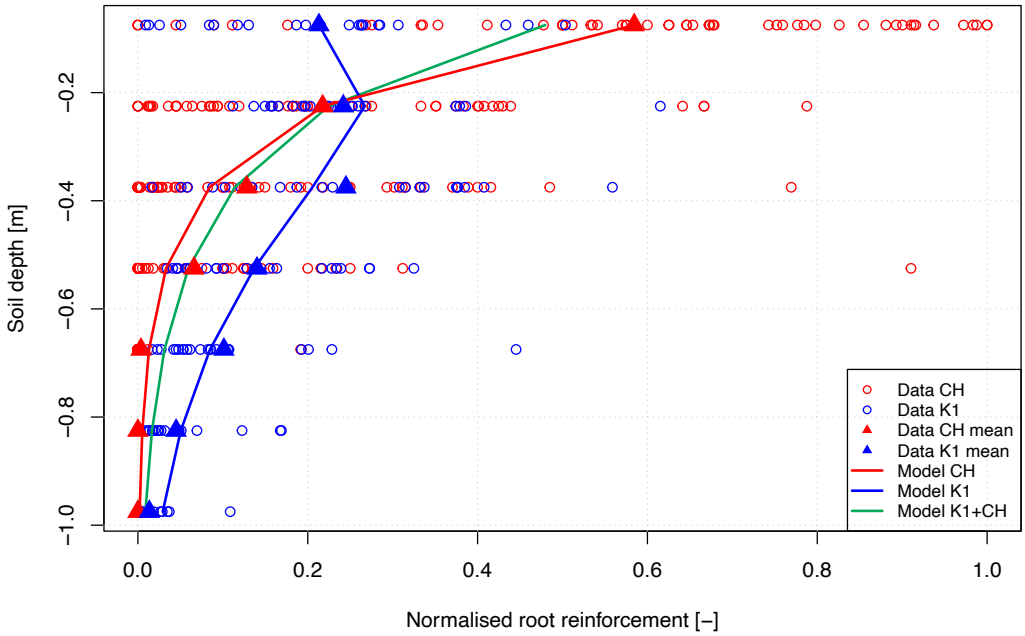

FIGURE 5.23: Normalised root reinforcement in relation to soil depth of *Cryptomeria japonica* was calculated by measured data and root reinforcement model. Dots refer to measured values, triangles present mean measured values, and solid lines refer to the simulated values from the models. The red color refers to CH site, blue color refers to K1 site and the green solid line represents the simulated normalised basal root reinforcement of Model K1+CH.

5.4 Discussion

5.4.1 Root distribution

The observed decreasing trend in root quantity with increasing distance from the stem has been previously documented in tree species such as *Picea abies* (Schwarz et al., 2012), *Castanea sativa* Mill. (Dazio, Conedera, and Schwarz, 2018), *Populus nigra* ita. (Ngo et al., 2023), and *Cryptomeria japonica* (Thunb. ex L.f.) D.Don (Liu et al., 2024). Liu et al. (2024) indicated that the root frequency and root size of Cryptomeria decreased with increasing distance from the trunk with an average DBH of 0.16 m in the Boshan Mountain in China. However, at the CH site, Tree S1 exhibited an atypical pattern with a higher number of fine roots at a distance of 4.5

m from the stem compared to 3.5. This difference with previous findings could be due to the influence of neighboring trees. Despite our efforts to select the most isolated candidate tree and to differentiate target roots from those of neighboring trees based on root morphology, root bark, and growth direction, it remains uncertain whether all fine roots counted at the 4.5 m distance originated from the target tree. Tree S2 had a higher number of fine roots and coarse roots than Tree S1; however, no roots larger than 30 mm in diameter were found in Tree S2, whereas a root with a 66 mm diameter was observed in Tree S1. The difference in the maximum root size between two trees may be due to the fact that trenches were excavated only along a 180^0 arc around each tree, rather than a full 360^0. Consequently, it is possible that the largest root of Tree S2 was located on the side not covered by the trenches, despite efforts to maintain consistent trenching direction for both trees to ensure the optimal conditions for comparison.

The vertical distribution of roots of Tree S2 extended up to 0.75 m depth while in Tree S1, we could not dig deeper than 0.60 m. At the CH site, the majority of observed roots were concentrated in the first soil layer (0-0.15 m depth). This pattern is consistent with findings in other forest species (Vergani et al., 2016; Ngo et al., 2023). Similarly, Genet et al. (2008) reported that half of the below-ground biomass in *C. japonica* stands was located between 0.1 and 0.2 below the soil surface. In contrast, Liu et al. (2024) observed the maximum root-area-ratio of *C. japonica* in the depth of 0.2-0.4 m.

At the Kamikawa study site, a consistent decreasing trend between root quantity and increasing root diameter class was observed across all 22 survey lines. A notable difference in the number of fine roots was observed between 6 survey lines (T4_1, T4_2, T5_1, T5_2, C1_1, and C1_2) and the other lines. This variation could be attributed to differences in soil properties among these lines. Another possible explanation could be due to the root overlap, although overlap is likely less significant than soil properties in influencing the maximum number of fine roots. In practice, when root overlap occurs, the root distribution pattern at the overlap point may be altered. Fine roots are unlikely to continue growing in the overlapping area due to competition for space and nutrients. The maximum number of fine roots per meter at the overlapping points may be interpreted from Figure 5.8. Although Dist_2 at the control site (1625 trees/ha) was shorter, ranging from 2.1 m to 2.5 m from the survey lines compared to Dist_2 at the thinned site (723 trees/ha) with a range of 3.5 m to 3.9 m (Table 5.2), the mean number of fine roots did not vary significantly. The fine root density ranged from 20 to 40 roots per meter, similar to the quantities recorded in the first trench of Tree S1 and Tree S2 in Switzerland. The variability in the number of roots with a diameter of 2 to 5 mm between the thinned and control sites (Figure 5.9 and Figure 5.10) is more likely attributable to differences in tree densities. In the thinned stand, individual trees may have a higher leaf area index, enabling faster growth and a higher demand for water and nutrients, leading to a more extensive root system. In contrast, in the control stand, greater competition among trees may result in a reduced root system.

We tested three different methods to calibrate the Root Distribution Model (RDM), using minimization of the Sum of Absolute Errors (SAE) of cumulative root number to determine the best-fit coefficients. If the primary objective is to calculate root reinforcement, it is recommended to minimize the SAE of cumulative root-force (CRF) during model calibration, as the precision of coarse root counts becomes more critical. Larger roots contribute significantly more to root reinforcement compared to fine roots; for example, a single 10 mm root can provide substantially greater reinforcement than fine roots (Giadrossich et al., 2019). However, cumulative root-force is not

the ideal calibration metric for models aimed at other purposes. For understanding root distribution patterns, fine root density, or calculating root biomass, it is more appropriate to calibrate the RDM by minimizing the SAE of cumulative root number (CRN).

The analysis of performance of the models (Figure 5.14) proves that the Root Distribution Model simulates well root distribution patterns at both sites (CH and K1). However, some limitations exist: (i) the model tends to underestimate the frequency of roots bigger than 6 mm at the CH site, (ii) the model is unable to express variations in fine roots between the two stands at the K1 site, and (iii) the model does not account for soil property variability. To improve its performance, a potential enhancement could be establishing a threshold related to the maximum number of fine roots per meter at overlap points. Additionally, incorporating more detailed measurements of environmental and site-specific variables such as soil heterogeneity, tree competition, or environmental influences that can affect root distribution patterns, as well as adding a threshold to better account for larger root sizes at varying distances from the stem could eventually improve the model's ability to simulate root distribution more accurately across a range of distances and root sizes.

Based on our analysis, the root distribution of *C. japonica* at the CH and the K1 sites was similar in the root diameter range of 6 mm and onwards. This suggests that the Root Distribution Model (RDM), calibrated with a combined dataset from both sites, could be applied to predict root distribution within this diameter range at other locations with similar conditions. Furthermore, it could serve as a useful data for comparing *C. japonica* root distribution across sites with more variability in soil and climatic conditions, helping to assess the similarity between different root classes and the sensitivity of root distribution patterns with various environmental factors. The calibrated RDMs from this study offer several practical applications: (i) extrapolate root frequency of *C. japonica* in the diameter range of 6 mm and onwards at sites with similar conditions to CH and K1 sites, reducing the need for destructive and labor-intensive root excavation, (ii) estimate the root biomass of *C. japonica* and its capability in sequestering carbon, and (iii) be implemented in other models, such as BankforNET, to assess the effects of vegetation on bank erosion.

While Taylor Diagram is often used to evaluate the performance of calibrated models, they have some limitations in the interpretation of root distribution modeling. The standard deviation and RMSD values can be biased towards fine roots and may fail to represent the variability in larger roots, even though the correlation coefficient remains a reliable indicator.

When validating the calibrated RDM with Kobe dataset, the measured data showed the best alignment with simulated root numbers from Model K1 based on the Table 5.3. The root distribution pattern for the 6 to 9 mm diameter range at Kobe differed from the other study sites with an increasing trend. Notably, Kobe was the only site where an air spade was used for soil excavation, and the compressed air may have removed several roots, potentially explaining the difference in this root diameter range. As a result, some data for roots in the 6 to 9 mm class may be missing at the Kobe site. For root diameters ranging from 10 to 15 mm, the difference in measured root frequency between the two Kobe trees and the two CH trees was insignificant.

From the study's outcome, we observed the similarity in root distribution patterns of *C. japonica* in the root range of 10 to 15 mm across three different sites. Apart from this root diameter range, the root distribution patterns were significantly different in the root classes between 3 and 10 mm. This difference could be due to the variations in soil properties and climate conditions between the study sites. The measured

numbers of coarse roots at Kamikawa and Kobe study sites were higher than at the HAFL Forest.

5.4.2 Root mechanical properties

As shown in Table 5.4, a limitation of ex-situ tensile tests is the testing of roots with diameters $\geq$ 10 mm. In Genet's studies, the tested root diameters for mature plantations ranged from 0.30 mm to 4.30 mm, while Abe and Iawamoto (1986) tested only roots with diameters smaller than 8.5 mm. Similarly, in our experiment, the *C. japonica* roots tested for tensile strength in a laboratory in China were limited to diameters between 0.43 mm and 9.81 mm. There was no restriction on maximum size of tested roots in field pullout tests as long as the safety is secured and force does not exceed load cell sensor capacity. For example, Yamase et al. (2019) tested roots with diameters ranging from 3.1 to 42.8 mm while field tests conducted at the CH site in Switzerland included roots with diameters ranging from 1.25 to 36 mm. On the other hand, laboratory tensile tests were able to conduct a larger quantity of samples compared to field pullout tests, likely because the field pullout apparatus requires transportation, setup, and manual operation, making it more labor-intensive than laboratory tensile tests.

As observed from Figure 5.19(c), the root tensile force measured by laboratory tensile tests was higher than that recorded by field pullout tests with the same root diameter. This finding is consistent with both studies of Tosi (2007) and Docker and Hubble (2008) that tensile force measured in the laboratory was greater than that observed in field measurements. This discrepancy in results may be attributed to the limited sample length used in laboratory testing. This can reduce the likelihood of encountering defects, while field pullout tests assess the root's full length, including potential weak points along its entire structure. In the study of Abe and Iwamoto (1986), Genet et al. (2008), and from Longchi Forest, no laboratory tests were conducted on roots $\geq$ 10 mm, leading to a lack of accuracy for bigger root diameters.

Yamase et al. (2019) also conducted field pullout tests on *C. japonica* but reported higher tensile forces than our results. The differences between field pullout tests for the same tree species were previously explained by several factors: (i) Tree age, (ii) Slope steepness, (iii) Tree location, with root tensile strength higher on uphill compared to downhill areas (Schmidt et al., 2001; Chiatante et al., 2003a; Norris et al., 2008), (iv) Measuring season, as root tensile strength tends to increase in winter compared to summer due to seasonal changes in root water content, (v) Soil properties, such as soil water content, which directly affects the root-soil friction (Schwarz, Cohen, and Or, 2011; Zhu et al., 2022), and (vi) Pullout direction, as roots pulled in the direction toward its originating stem. Pulling a root in the direction of its growth (from stem to root tip) can result in a significantly higher tensile force, which fails to represent the condition of breakage during the triggering of shallow landslides.

In our study, the candidate trees for pullout tests in both Japanese and Swiss sites were of similar age, at 49 and 50 years, respectively. The slopes at both sites were relatively gentle, ranging from 5° to 15°, minimizing the influence of slope steepness on the results. Furthermore, both research teams ensured that the pullout tests were conducted in the correct direction. Therefore, differences in soil properties provide the most appropriate explanation for the differences observed in the field pullout test results between the Swiss and Japanese sites. The study site of our research was acidified Cambisol, distinct from Andisol at the Kamikawa site. Cambisols have been reported to show bulk density values ranging between 1.09 and 1.70 g/cm^3 (Brahim,

Bernoux, and Gallali, 2012; Vopravil, Formánek, and Khel, 2021), while Andisols typically exhibit lower soil bulk density values (< 0.9 g/cm^3) which means very soft surface soils (Imaya, 2020). This might influence the potential for root breakage during pullout tests, leading to the differences in root tensile forces.

Our study confirmed that the tensile force required to break a root in the field, as measured by pullout tests, is consistently weaker than the tensile force obtained from laboratory tests on roots of the same diameter. However, the difference could be negligible with roots smaller than 10 mm. The p-value of the t-test comparing roots smaller than 5 mm was 0.886 (>0.05), with mean values of 146.61 N for the CH data and 155.16 N for the CN data. The similarity of these means, combined with the p-value, indicates no statistically significant difference between the two datasets. This suggests that the average tensile force of roots smaller than 5 mm, measured by both techniques, is comparable. This finding aligns with previous studies, including Tosi (2007), which reported similar outcomes and demonstrated that the differences between in-situ and ex-situ tests could be negligible for roots smaller than 5 mm. Furthermore, as reported in the Results section, the p-value of the t-test comparing roots smaller than 10 mm was 0.1731 (>0.05), with mean values of 320.27 N for the CH data and 373.89 N for the CN data, also suggesting the insignificant difference in tensile force of roots smaller than 10 mm measured by two methods.

Combining the facts that (1) it is challenging to test tensile force of roots ≥ 10 mm in the laboratory, (2) unlike laboratory tensile tests, field pullout tests are less suitable for very fine roots due to the challenges of anchoring during the test process and also laborious, and (3) the insignificant difference in root tensile force between two testing methods, we suggested to use both methods, and merge the data to complement each other and broaden the sample size for further studies.

Our study found that the relationship between maximum tensile force and root diameter in *C. japonica* closely resembled patterns observed in other tree species (Schwarz, Cohen, and Or, 2012a; Vergani et al., 2017a; Dazio, Conedera, and Schwarz, 2018). The regression curves of the measured dataset, as shown in Figure 5.19(b), indicated an overall increasing trend, demonstrating that root tensile force increases with bigger root diameters. Figure 5.24 illustrates the relationship between maximum tensile force and root diameter for the *C. japonica*, compared with other tree species studied through either field pullout tests or a combination of laboratory tensile tests and field pullout tests. These species include Ash (*Fraxinus excelsior* L.) (Schwarz, Cohen, and Or, 2012a), Norway Spruce (*Picea abies* (L.) Karst.) (Vergani et al., 2016), Scots pine (*Pinus sylvestris*) (Vergani et al., 2017a), Chestnut (*Castanea sativa* Mill.) (Dazio, Conedera, and Schwarz, 2018), European Beech (*Fagus sylvatica* L.) (Gehring et al., 2019), and Poplar (*Populus nigra* ita.) (Ngo et al., 2023). Each species exhibits varying root reinforcement capacities. Ash and Scot Pine roots have the weakest tensile forces, while "Tasman" Poplar shows the highest. For instance, a "Tasman" Poplar root with a diameter of 30 mm has a tensile force of approximately 12.6 kN, which is 2.92 times greater than that of *C. japonica* of the same diameter. Additionally, Figure 5.24(b) highlights that Chestnut roots exhibit the highest tensile force for diameters ranging from 0 to 3 mm, but are more average in strength for larger root sizes. Overall, *C. japonica* shows average tensile force capacity compared to these other forest species.

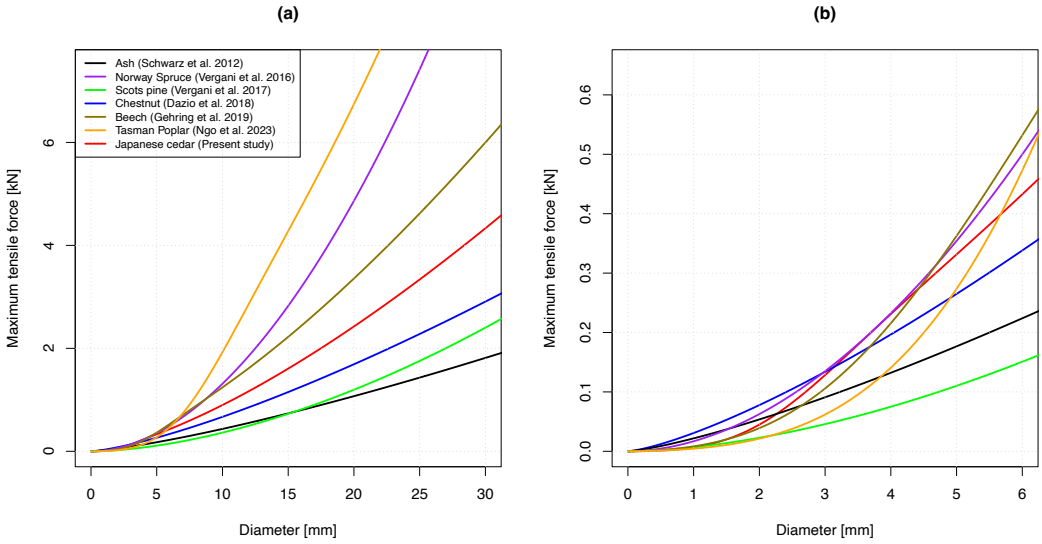

FIGURE 5.24: (a) Comparison of maximum root tensile force between Japanese cedar and other species recorded in previous studies that measured by field pullout tests or by the combination between laboratory tensile tests and field pullout tests. Subplot (b) in the right-hand is the zoom-in figure with root diameters ranging from 0 to 6 mm.

Table 5.8 summarizes the maximum tensile force in relation to root diameter for various European forest species based on findings from previous studies. This data provides a comparative analysis of the root tensile force across species, highlighting the variations in root reinforcement capacities depending on species and root size.

$F_{max} = F_0 \cdot \phi^{\alpha}$					
Species	Studies	F_0	α	Tested root range	R^2
Ash	Schwarz, Cohen, and Or (2012a)	21.8	1.3	up to 5.5 mm	0.67
Norway Spruce (control forest)	Vergani et al. (2016)	16.91	1.89	2 - 13 mm	0.56
Scots pine	Vergani et al. (2017a)	$1{\cdot}10^6$	1.72	up to 50 mm	0.9
Chestnut (*Castanea sativa* Mill.)	Dazio, Conedera, and Schwarz (2018)	$3.16{\cdot}10^5$	1.337	1 - 46 mm	0.68
Beech	Gehring et al. (2019)	C(ϕ_m=0.0031,ϕ_{sd}=0.0023)·909501	1.43	up to 25 mm	-
"Tasman" Poplar	Ngo et al. (2023)	C(ϕ_m=0.00643,ϕ_{sd}=0.00365)·$2.9{\cdot}10^6$	1.55	1.7 - 40 mm	0.88
Japanese cedar	Present study	C(ϕ_m=0.002,ϕ_{sd}=0.001189115)·$6.55{\cdot}\ 10^5$	1.43	0.43 - 36 mm	0.89

TABLE 5.8: Fitted maximum tensile force F_{max} [N] in relation to root diameters ϕ of different species recorded in previous studies measured by field pullout tests or by the combination of laboratory tensile tests and field pullout tests.

5.4.3 Root reinforcement

Maximum lateral root reinforcement is greatest when closest to the stem and decreases as the distance from the stem increases. There was a sharp decrease in root reinforcement between the 1.5 m and 2.5 m trenches despite a relatively small difference in the number of roots (Figure 5.5). This decline in root reinforcement with distance is due to the decreasing presence of large roots, which dominate near the stem and play a critical role in stabilizing the soil. As the distance from the tree increases, smaller roots become more prevalent, contributing more to overall reinforcement. For example, at a distance of 1.5 m from the stem of Tree S1, a single 66 mm root contributed 61.3% of the total bundle force, despite representing only 1.39% of the total root quantity (1 out of 72 roots recorded in the sector). Similar findings were reported by Yamase et al. (2019) and Giadrossich et al. (2019), where larger roots were shown to have a significantly higher impact on root reinforcement. Based on the measured root reinforcement of two trees at the CH site, the root reinforcement at a distance of 4.5 m from the tree stem is relatively small compared to other trenches.

At the K1 site, a distinct pattern was observed between the number of fine roots (black dots in Figure 5.8) and the measured maximum lateral root reinforcement across survey lines (black dots in Figure 5.22). This suggests that fine roots do not play a key role in determining the maximum lateral root reinforcement in K1 site. The two highest root reinforcement were recorded at survey lines T2_1 and T2_2, both were located in the thinned site while the root reinforcement was overall lower

in the control site. This could be due to the difference in the dimensions of the trees (the DBH of the thinned stand are about 0.05 m greater).

The comparison of the three models for predicting maximum lateral root reinforcement at varying distances from the two tree stems in the CH site shows that overall Model CH and Model K1+CH demonstrated good performance across the CH site. At the K1 study site, Model K1 exhibited the best performance with SAE of 2.619 kN for each 1-meter width survey line. The second-best calibrated model was Model K1+CH, which had a SAE of 2.952 kN per 1-meter width profile. All models tended to underestimate the root force across the survey lines. Overall, the RRM tends to underestimate the root reinforcement but better simulates maximum lateral root reinforcement in the individual tree than in a stand. The high variability of the root reinforcement of the single trenches confirms the finding of previous study, and highlights the need to include this characteristic in the calculation of slope stability (either as partial safety factor or as probability distribution). An example of this type of approach is illustrated in the SlideforNET manual (https://dev.slideformet.cosci-llc.com/).

There is a significant difference in the basal root reinforcement distribution of *C. japonica* between the CH site and the K1 site. Explanation for this difference in basal root reinforcement could be due to:

- Frequency and magnitude of the rainfall: Kamikawa has a mean annual precipitation of 1740 mm, higher than the mean annual rainfall in HAFL Forest with 1137 mm. Higher amounts of rain means more available water infiltrates in the deeper soil layer, creating a better environment for root growth in the deeper zone. In contrast, if the water cannot penetrate well into deeper layers, the root will concentrate in the topsoil horizon, where water availability is highest (Laio, D'Odorico, and Ridolfi, 2006).

- The amount of water is stored in the soil: The Andisol at the Kamikawa study site has high porosity, which allows it to retain a large amount of water. The high volumetric water content in the soils, measured at 67.8 ± 6.8% (0-0.10 m) and 64.8 ± 7.3% (0.20-0.30 m) in thinned stand, and 65.8 ± 5.3% (0-0.10 m) and 59.3 ± 6.0% (0.20-0.30 m) in the unthinned stand, highlights this unique soil property. With more water stored in the soil, the root system of *C. japonica* trees at the Japanese study site can develop deeper than at the Swiss site. Differences in groundwater levels may also influence coarse root development.

- Understory species: The roots of understory species could be another factor influencing the differences in the vertical rooting pattern of Japanese cedar between two study sites. The Kamikawa site may have more understory vegetation, and the roots of these plants might force the distribution of *C. japonica* roots in the deeper soil layers.

- Nutrient availability: The shallow rooting in the Swiss study site can be related to plant nutrient demands. *C. japonica* trees in Switzerland may be located in low productivity stands where nutrients are more available in the organic rich topsoil compared to deeper horizons. In the study of Hirano et al. (2017) Hirano, Tanikawa, and Makita, 2017 on fine roots of *C. japonica*, the biomass was larger and shallower at nutrient poor sites (soils with low acid buffering capacity, low base cations such as Ca, Mg and high Al) compared with nutrient rich sites (soils with high base cations such as Ca and Mg and low Al) (Hirano, Tanikawa, and Makita, 2017). The finding from the study of Hirano could relate to the difference in basal root reinforcement even though fine roots play less important role than coarse roots in root reinforcement.

- Soil type and grain size: This can affect root penetration and anchorage.

Overall, based on the results presented in Table 5.7 and illustrated in Figure 5.23, it was observed that the models effectively generated basal root reinforcement corresponding to each depth layer. The high R^2 values indicate a good correlation between the model predictions and the observed data, suggesting that the RRM accurately reflects the distribution of root reinforcement across different soil depths.

Although our study provided insights into the root mechanical properties of *C. japonica* and highlighted the spatial variability of root reinforcement of *C. japonica* across different study sites, several questions remain unanswered. There was a significant difference in root distribution between two candidate trees, which may be due to partial excavation of the root system. A 360^0 excavation could have led to more similar results. The root frequency was similar in the range of 10 to 15 mm across three sites while root frequency was significantly different in lower diameter ranges. Further research is needed to investigate the root reinforcement of *C. japonica* in relation to geographical mapping on slope stability. The findings from this study can inform further research on evaluating the impact of this species on slope and river bank stability, and contribute to formulate effective forestry management strategies.

5.5 Conclusion

To quantify and compare the spatial root reinforcement of Japanese cedar across different study sites, we measured root frequency at various soil depths and distances from tree stems at Swiss and Japanese locations, and assessed the root mechanical properties through both laboratory tensile tests and field pullout tests.

This study presents a comprehensive analysis of *C. japonica* root distribution and reinforcement. Our findings provide valuable insights for understanding root system dynamics in different environmental conditions and can be applied to various forestry management practices. The main conclusions of the study can be summarized as follow:

- Lateral Root Distribution: Statistical analysis revealed higher root number from 1 to 5 mm in Japanese study site than Swiss site and no significant differences in lateral coarse root distribution among the analyzed Cryptomeria japonica sites (6 mm and upwards).

- Vertical Root Distribution: Vertical root distribution varied considerably between Swiss and Japanese stands, likely due to differences in soil and climatic conditions.

- Root Distribution Modeling: The RDM accurately estimated root distribution for both Swiss and Japanese sites, as indicated by similar Pearson coefficients. No significant differences in root numbers across three sites were observed for root diameters between 10 and 15 mm.

- Root Mechanical Properties: Root mechanical properties varied significantly between forest stands. For roots larger than 20 mm, maximum field pullout force differed by approximately 20%. Extrapolating results from smaller diameter roots could lead to underestimates of root reinforcement.

- Data Merging: The datasets for laboratory tensile tests and field pullout tests showed strong overlap for root diameters between 0 and 10 mm. This supports the hypothesis that these datasets can be merged for calibrating the RBMw.

- Lateral Root Reinforcement: Measured lateral root reinforcement ranged from 0 to 10 kN/m in Swiss trees and 3 to 16 kN/m in Japanese stands.

- Basal Root Reinforcement: Basal root reinforcement differed significantly between Swiss and Japanese stands. In Swiss stands, reinforcement was concentrated in

the top 0.15 m of soil, while in Japanese stands, most reinforcement occurred between 0.15 and 0.45 m depth.

The high variability of root distribution and reinforcement highlights the importance of expanding data collection and international collaboration to improve our understanding of tree root systems and their role in environmental processes.

5.6 Appendices

Figure 5.25 compared the performance of three calibrated RDMs through number of coarse roots, cumulative root number, and cumulative root-force between measured and simulated values at different distances from the stems in CH dataset.

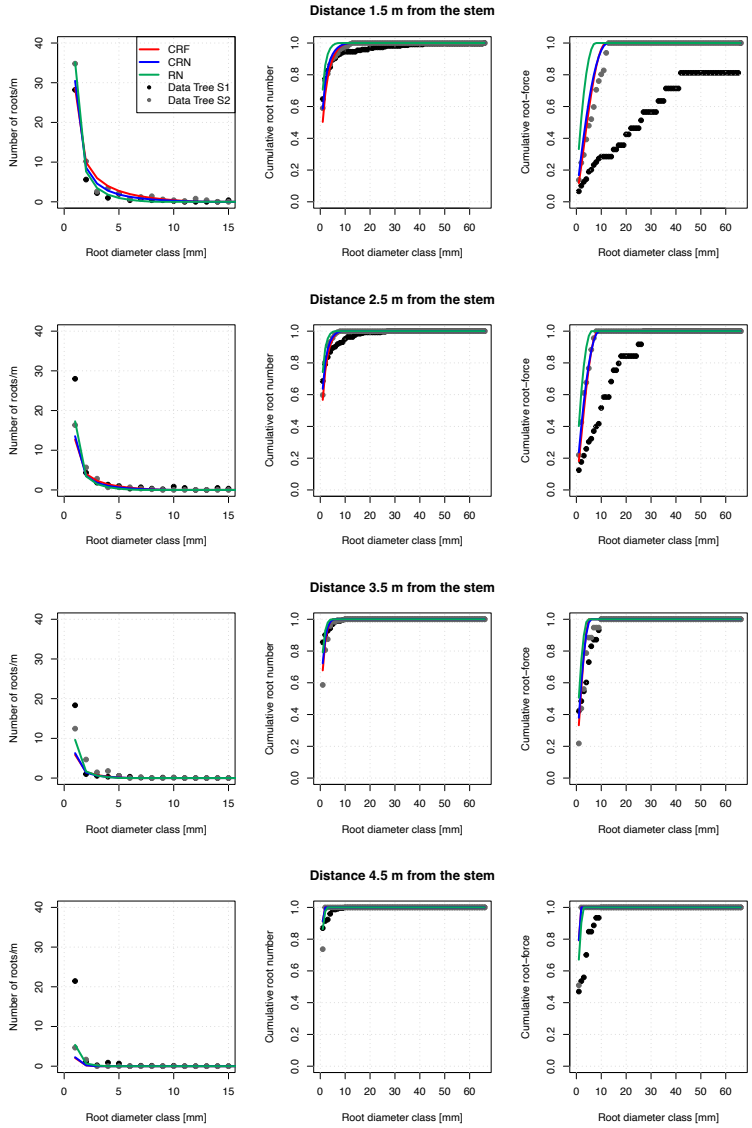

FIGURE 5.25: Comparison between measured and simulated root number, cumulative root number, and cumulative root-force from three methods to find the best-fitted coefficients for CH.

Model CH	μ	ψ	β	η	SAE_fr	SAE_cr	SAE_ar	SAE_crn	SAE_crf	SAE_rf	No. profiles
CRN	21573.35	15.08331	-1.05014	0.28992	621.98	410.13	1032.11	28.99	157.36	5979.59	58
CRF	20225.26	15.00997	-0.73386	0.30608	633.68	446.57	1080.26	30.15	156.08	4503.22	58
RN	29951.82	19.82105	-1.22056	0.66909	551.34	394.77	946.11	31.87	176.60	5680.57	58
Model K1	μ	ψ	β	η	SAE_fr	SAE_cr	SAE_ar	SAE_crn	SAE_crf	SAE_rf	No. profiles
CRN	42805.75	29.82645	-0.40036	0.66060	457.64	910.81	1368.45	16.14	135.32	12877.45	22
CRF	37421.59	29.89949	-1.47997	0.21070	389.94	1376.27	1766.21	22.19	117.85	16344.39	22
RN	47128.80	29.43846	-0.42443	0.81876	532.18	825.88	1358.06	19.83	151.37	11716.86	22
Model K1+CH	μ	ψ	β	η	SAE_fr	SAE_cr	SAE_ar	SAE_crn	SAE_crf	SAE_rf	No. profiles
CRN	26173.24	15.00192	-0.57244	0.30529	1017.76	1552.72	2570.48	51.61	299.64	19534.26	80
CRF	18278.09	15.02018	-0.55500	0.25759	965.00	1649.46	2614.46	54.47	294.17	20221.06	80
RN	24269.52	18.26657	-0.18150	0.55757	934.62	1577.74	2512.36	56.94	326.20	19473.56	80

TABLE 5.9: Results from three different methods to calibrate Root Distribution Model (RDM) and compare simulated data with measured data in each site. μ, ψ, β, and η are coefficients of Equations 5.1, 5.2, 5.3, and 5.4. SAE_fr is shortened for the Sum of Absolute Errors in fine root number. SAE_cr is shortened for the Sum of Absolute Errors in coarse root number. SAE_ar is shortened for the Sum of Absolute Errors in all root number. SAE_crn is the Sum of Absolute Errors of cumulative root number. SAE_crf is the Sum of Absolute Errors of cumulative root force. SAE_rf is the Sum of Absolute Errors of root-force. And No. profiles is the number of assessed profiles.

Figure 5.26 showed linear lines between measured root reinforcement and simulated root reinforcement of three calibrated models.

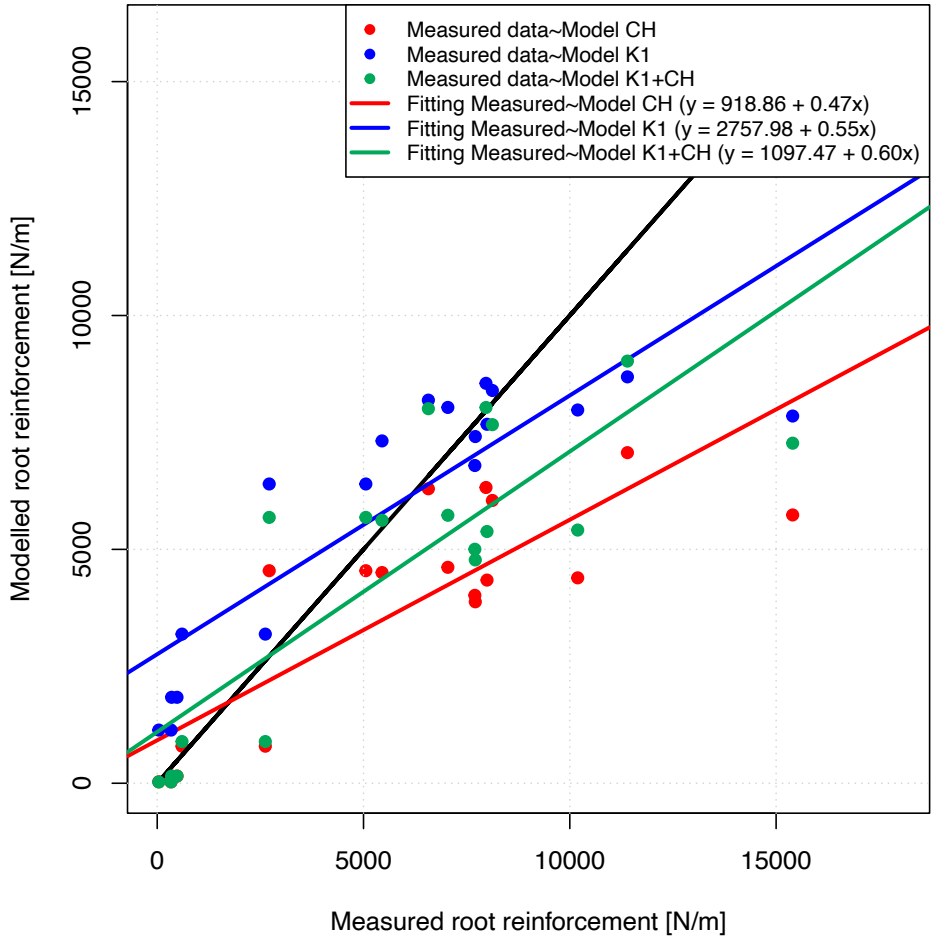

FIGURE 5.26: Comparison between measured root reinforcement in CH and K1 sites and modeled maximum lateral root reinforcement. The red color represented the fitting between measured root reinforcement and Model CH. The blue color represented measured root reinforcement versus Model K1. Green color symbolized the measured root reinforcement versus Model K1+CH.

References

Abe, Kazutoki and Masaru Iwamoto (1986). "An Evaluation of Tree-Root Effect on Slope Stability by Tree-Root Strength". In: *JOURNAL OF THE JAPANESE FORESTRY SOCIETY* 68.12, pp. 505–510. DOI: 10.11519/jjfs1953.68.12{_}505.

Berger, Frédéric et al. (2013). "Eco-engineering and protection forests against rockfalls and snow avalanches". In: *Management strategies to adapt alpine space forests to climate change risks*. IntechOpen.

Brahim, N, Martial Bernoux, and T Gallali (2012). "Pedotransfer functions to estimate soil bulk density for Northern Africa: Tunisia case". In: *Journal of Arid Environments* 81, pp. 77–83.

Chiatante, D. et al. (Jan. 2003a). "Modification of Root Morphological Parameters and Root Architecture in Seedlings of Fraxinus Ornus L. and Spartium Junceum L. Growing on Slopes". In: *Plant Biosystems - An International Journal Dealing*

with all Aspects of Plant Biology 137.1, pp. 47–55. ISSN: 1126-3504. DOI: 10.1080/11263500312331351321.

Cohen, Denis and Massimiliano Schwarz (2017). "Tree-root control of shallow landslides". In: *Earth Surface Dynamics* 5.3, pp. 451–477.

Dazio, Emanuele (Plinio Rinaldo), Marco Conedera, and Massimiliano Schwarz (2018). "Impact of Different Chestnut Coppice Managements on Root Reinforcement and Shallow Landslide Susceptibility". In: *Forest Ecology and Management*, pp. 63–76. ISSN: 0378-1127. DOI: 10.1016/j.foreco.2018.02.031.

Docker, B B and T C T Hubble (Aug. 2008). "Quantifying root-reinforcement of river bank soils by four Australian tree species". en. In: *Geomorphology* 100.3-4, pp. 401–418. ISSN: 0169555X. DOI: 10.1016/j.geomorph.2008.01.009. URL: https://linkinghub.elsevier.com/retrieve/pii/S0169555X08000159.

Dorren, Luuk et al. (2007). "State of the art in rockfall–forest interactions". In: *Schweizerische Zeitschrift fur Forstwesen* 158.6, pp. 128–141.

Fattet, M. et al. (Oct. 2011). "Effects of Vegetation Type on Soil Resistance to Erosion: Relationship between Aggregate Stability and Shear Strength". In: *CATENA* 87.1, pp. 60–69. ISSN: 0341-8162. DOI: 10.1016/j.catena.2011.05.006.

Gehring, Eric et al. (2019). "Shallow landslide disposition in burnt European beech (Fagus sylvatica L.) forests". In: *Scientific Reports* 9.1, pp. 1–11.

Genet, Marie et al. (Oct. 2008). "Root Reinforcement in Plantations of Cryptomeria Japonica D. Don: Effect of Tree Age and Stand Structure on Slope Stability". In: *Forest Ecology and Management* 256.8, pp. 1517–1526. ISSN: 03781127. DOI: 10.1016/j.foreco.2008.05.050.

Giadrossich, F et al. (2013a). "Mechanical interactions between neighbouring roots during pullout tests". In: *Plant and soil* 367.1, pp. 391–406.

Giadrossich, F et al. (2013b). "Stabilisation mechanisms of hillslopes due to root reinforcement". In: *Quaderni di Idronomia Montana* 31, pp. 353–362.

Giadrossich, F. et al. (Dec. 2017b). "Methods to Measure the Mechanical Behaviour of Tree Roots: A Review". In: *Ecological Engineering*. Soil Bio- and Eco-Engineering: The Use of Vegetation to Improve Slope Stability - Proceedings of the Fourth International Conference 109, pp. 256–271. ISSN: 0925-8574. DOI: 10.1016/j.ecoleng.2017.08.032.

Giadrossich, Filippo et al. (2016). "Modeling bio-engineering traits of Jatropha curcas L." In: *Ecological Engineering* 89, pp. 40–48.

Giadrossich, Filippo et al. (2019). "Large roots dominate the contribution of trees to slope stability". In: *Earth Surface Processes and Landforms* 44.8, pp. 1602–1609.

Giadrossich, Filippo et al. (Aug. 2020b). "Minimum Representative Root Distribution Sampling for Calculating Slope Stability in Pinus Radiata D.Don Plantations in New Zealand". In: *New Zealand Journal of Forestry Science* 50. ISSN: 1179-5395. DOI: 10.33494/nzjfs502020x68x.

Gyssels, G. et al. (June 2005). "Impact of Plant Roots on the Resistance of Soils to Erosion by Water: A Review". In: *Progress in Physical Geography: Earth and Environment* 29.2, pp. 189–217. ISSN: 0309-1333. DOI: 10.1191/0309133305pp443ra.

Hirano, Yasuhiro, Toko Tanikawa, and Naoki Makita (2017). "Biomass and morphology of fine roots in eight Cryptomeria japonica stands in soils with different acid-buffering capacities". In: *Forest Ecology and Management* 384, pp. 122–131.

Imaya, Akihiro (2020). "Classification of volcanic soils in the Soil Classification System of Japan and verification based on forest soils". In: *Soil Science and Plant Nutrition* 66.5, pp. 673–679.

Jastrow, JD, RM Miller, and J Lussenhop (1998). "Contributions of interacting biological mechanisms to soil aggregate stabilization in restored prairie". In: *Soil Biology and Biochemistry* 30.7, pp. 905–916.

Kenzo, Tanaka et al. (Aug. 2021). "Effects of Throughfall Exclusion on Photosynthetic Traits in Mature Japanese Cedar (Cryptomeria Japonica (L. f.) D. Don.)" In: *Forests* 12.8, p. 971. ISSN: 1999-4907. DOI: 10.3390/f12080971.

Kim, John H. et al. (2017). "Vegetation as a Driver of Temporal Variations in Slope Stability: The Impact of Hydrological Processes". In: *Geophysical Research Letters* 44.10, pp. 4897–4907. ISSN: 1944-8007. DOI: 10.1002/2017GL073174.

Laio, Francesco, Paolo D'Odorico, and Luca Ridolfi (2006). "An analytical model to relate the vertical root distribution to climate and soil properties". In: *Geophysical Research Letters* 33.18.

Lima, Ana et al. (Jan. 2021). "Variations in Essential Oil Chemical Composition and Biological Activities of Cryptomeria Japonica (Thunb. Ex L.f.) D. Don from Different Geographical Origins—A Critical Review". In: *Applied Sciences* 11.23, p. 11097. ISSN: 2076-3417. DOI: 10.3390/app112311097.

Liu, Jianping et al. (2024). "Experimental Study on the Effect of Root Content on the Shear Strength of Root–Soil Composite with Thick and Fine Roots of Cryptomeria japonica (Thunb. ex Lf) D. Don". In: *Forests* 15.8, p. 1306.

Ma, Yu and Caixia Li (Apr. 2017). "Research on the Debris Flow Hazards after the Wenchuan Earthquake in Bayi Gully, Longchi, Dujiangyan, Sichuan Province, China". In: *2017 International Conference on Advanced Materials Science and Civil Engineering (AMSCE 2017)*. Atlantis Press, pp. 166–170. ISBN: 978-94-6252-337-1. DOI: 10.2991/amsce-17.2017.36.

Mao, Zhun (2022). "Root reinforcement models: classification, criticism and perspectives". In: *Plant and Soil* 472.1-2, pp. 17–28.

Marzini, Lorenzo et al. (2023). "Influence of root reinforcement on shallow landslide distribution: A case study in Garfagnana (Northern Tuscany, Italy)". In: *Geosciences* 13.11, p. 326.

Mehtab, Alam et al. (Jan. 2021). "Scaling the Roots Mechanical Reinforcement in Plantation of Cunninghamia R. Br in Southwest China". In: *Forests* 12.1, p. 33. ISSN: 1999-4907. DOI: 10.3390/f12010033.

Moos, Christine et al. (2016b). "How does forest structure affect root reinforcement and susceptibility to shallow landslides?" In: *Earth Surface Processes and Landforms* 41.7, pp. 951–960.

Ngo, Ha My et al. (2023). "Analysis of Poplar's (Populus nigra ita.) Root Systems for Quantifying Bio-Engineering Measures in New Zealand Pastoral Hill Country". In: *Forests* 14.6, p. 1240.

Norris, Joanne E. et al. (Feb. 2008). *Slope Stability and Erosion Control: Ecotechnological Solutions*. Springer Science & Business Media. ISBN: 978-1-4020-6676-4.

Orwa, C (2009). "Agroforestree Database: a tree reference and selection guide, version 4.0". In: *http://www. worldagroforestry. org/sites/treedbs/treedatabases. asp*.

Sakals, Matt E et al. (2006). "The role of forests in reducing hydrogeomorphic hazards". In: *Forest Snow and Landscape Research* 80.1, pp. 11–22.

Schmidt, K M et al. (Oct. 2001). "The Variability of Root Cohesion as an Influence on Shallow Landslide Susceptibility in the Oregon Coast Range". In: *Canadian Geotechnical Journal* 38.5, pp. 995–1024. ISSN: 0008-3674. DOI: 10.1139/t01-031.

Schwarz, M., D. Cohen, and D. Or (2011). "Pullout Tests of Root Analogs and Natural Root Bundles in Soil: Experiments and Modeling". In: *Journal of Geophysical Research F: Earth Surface*, F02007 (14 pp.) ISSN: 2169-9003. DOI: 10.1029/2010JF001753.

Schwarz, M., D. Cohen, and D. Or (Oct. 2012a). "Spatial Characterization of Root Reinforcement at Stand Scale: Theory and Case Study". In: *Geomorphology* 171–172, pp. 190–200. ISSN: 0169-555X. DOI: 10.1016/j.geomorph.2012.05.020.

Schwarz, M. et al. (Mar. 2010b). "Quantifying the Role of Vegetation in Slope Stability: A Case Study in Tuscany (Italy)". In: *Ecological Engineering*. Special Issue: Vegetation and Slope Stability 36.3, pp. 285–291. ISSN: 0925-8574. DOI: 10.1016/j.ecoleng.2009.06.014.

Schwarz, Massimiliano, Filippo Giadrossich, and Denis Cohen (2013). "Modeling root reinforcement using a root-failure Weibull survival function". In: *Hydrology and Earth System Sciences* 17.11, pp. 4367–4377.

Schwarz, Massimiliano et al. (2012). "QUANTIFYING ROOT REINFORCEMENT IN PROTECTION FORESTS: IMPLICATIONS FOR SLOPE STABILITY AND FOREST MANAGEMENT". In: *the Interpraevent*, p. 12.

Schwarz, Massimiliano et al. (2015). "Root reinforcement of soils under compression". In: *Journal of Geophysical Research: Earth Surface* 120.10, pp. 2103–2120.

Schwarz, Massimiliano et al. (2016b). "Modelling of root reinforcement and erosion control by 'Veronese'poplar on pastoral hill country in New Zealand". In: *New Zealand Journal of Forestry Science* 46, pp. 1–17.

Stokes, Alexia et al. (Apr. 2014). "Ecological Mitigation of Hillslope Instability: Ten Key Issues Facing Researchers and Practitioners". In: *Plant and Soil* 377.1, pp. 1–23. ISSN: 1573-5036. DOI: 10.1007/s11104-014-2044-6.

Takahara, Hikaru et al. (2023). "Vegetation history of Cryptomeria japonica in Japan since the last interglacial period". In: *Ecological Research* 38.1, pp. 49–63.

Taylor, Karl E (2001). "Summarizing multiple aspects of model performance in a single diagram". In: *Journal of geophysical research: atmospheres* 106.D7, pp. 7183–7192.

Tosi, Matteo (July 2007). "Root Tensile Strength Relationships and Their Slope Stability Implications of Three Shrub Species in the Northern Apennines (Italy)". In: *Geomorphology* 87.4, pp. 268–283. ISSN: 0169-555X. DOI: 10.1016/j.geomorph.2006.09.019.

Vergani, Chiara et al. (2016). "Root reinforcement dynamics in subalpine spruce forests following timber harvest: a case study in Canton Schwyz, Switzerland". In: *Catena* 143, pp. 275–288.

Vergani, Chiara et al. (2017a). "Investigation of root reinforcement decay after a forest fire in a Scots pine (Pinus sylvestris) protection forest". In: *Forest Ecology and Management* 400, pp. 339–352.

Vergani, Chiara et al. (Feb. 2017c). "Root Reinforcement Dynamics of European Coppice Woodlands and Their Effect on Shallow Landslides: A Review". In: *Earth-Science Reviews* 167. DOI: 10.1016/j.earscirev.2017.02.002.

Vopravil, Jan, Pavel Formánek, and Tomáš Khel (2021). "Comparison of the physical properties of soils belonging to different reference soil groups." In: *Soil & Water Research* 16.1.

Watson, Alex J. and Michael Marden (2005). *Live Root-Wood Tensile Strengths of Some Common New Zealand Indigenous and Plantation Tree Species*.

Wu, T H (1976). "Investigation of Landslides on Prince of Wales Island, Alaska". In: *Geotechnical Engineering Report* 5.5, p. 106.

Wu, Tien H. (2007). "Root Reinforcement: Analyses and Experiments". In: *Developments in Plant and Soil Sciences*. Developments in Plant and Soil Sciences. Ed. by ALEXIA STOKES et al., pp. 21–30. DOI: 10.1007/978-1-4020-5593-5{_}3.

Yamase, Keitaro et al. (2018). "Ground-penetrating radar estimates of tree root diameter and distribution under field conditions". In: *Trees* 32, pp. 1657–1668.

Yamase, Keitaro et al. (Dec. 2019). "Estimating Slope Stability by Lateral Root Reinforcement in Thinned and Unthinned Stands of Cryptomeria Japonica Using Ground-Penetrating Radar". In: *CATENA* 183, p. 104227. ISSN: 03418162. DOI: 10.1016/j.catena.2019.104227.

Zhu, Jinqi et al. (2022). "Soil moisture and hysteresis affect both magnitude and efficiency of root reinforcement". In: *Catena* 219, p. 106574.

Chapter 6

Analysis of poplar's (*Populus nigra ita.*) Root Systems for the Assessment of Ecosystem Services in New Zealand's Pastoral Hill Country

Abstract

Understanding root biomass is essential for estimating carbon storage and assessing the ecological role of forest systems. This study quantified root biomass and carbon storage capacity in 26-year-old *Populus deltoides* × *nigra* "Tasman" poplar trees growing on a pastoral hill site in New Zealand. Four trees of varying sizes (DBH ranging from 41 to 56 cm) were fully excavated in a full 360^o radius at four distances from the stem: 1.5, 2.5, 3.5, and 4.5 m. The Root Distribution Model (RDM) was calibrated using the observed root distribution data and then applied to estimate root biomass, carbon storage, and CO_2 sequestration potential. Field measurements revealed that root biomass is positively correlated with tree diameter at breast height (DBH) and negatively with soil depth and distance from the stem. A generalized allometric equation was developed by combining measured data with previous studies at the same site and same species but different diameters, enabling reliable estimation of root dry weight across a wide DBH range. The model performed reliably for mature trees but underestimated biomass in smaller trees, likely due to missing root data near the stem, where the root density is highest, and also further than 4.5 m from the stem. The RDM presents a promising approach for non-destructive estimation of root biomass and belowground carbon stocks in forestry and agroforestry systems, contributing to the precision of carbon sequestration estimates for use in climate policy and carbon trading schemes.

Keywords: Root biomass; Root Distribution Model; Populus; Carbon storage; Forestry Management; Climate change mitigation

6.1 Introduction

New Zealand is a unique country with at least 40% of its land surface comprising steep hill below 1,000 m. These areas are commonly referred to as "New Zealand hill country" (Blaschke, Trustrum, and DeRose, 1992). A significant portion of New Zealand's pastoral farmland lies within this unstable hill country. To mitigate soil erosion, poplars are widely considered one of the most suitable tree species in these

landscapes (Wilkinson, 1999; Douglas et al., 2006; McIvor et al., 2008). Beyond erosion control, poplars offer additional benefits such as biomass production and potential contributions to climate change mitigation in New Zealand.

Poplars (*Populus* spp) are deciduous trees native to the Northern Hemisphere (Van Kraayenoord, 1968; Sulaiman, 2006) and were introduced to New Zealand by early Europeans settlers. The Tasman poplar (*Populus deltoides x P. nigra*) is one of the most common planted hybrids in the country (McIvor, 2012). Tasman poplar, as well as Veronese poplar, is an hybrid between the North American species eastern cottonwood (*Populus deltoides*) and the European black poplar (*Populus nigra*). Hybrids poplar often exhibit greater productivity than their parent species (Heilman and Stettler, 1985). They share mechanical properties with cottonwood but differ slightly from aspen (*Populus tremuloides*). In North America, hybrid poplars have widely replaced aspen in many structural panel products (Geimer and Crist, 1980; Zhou, 1990). Hybrid poplars are bred to enhanced disease resistance and increased wood fiber production under particular site conditions (Balatinecz and Kretschmann, 2001). Their rapid growth, extensive the moisture-loving and flood-tolerant, which made them a perfect choice for riparian agroforestry systems (Fortier et al., 2010). More than that, poplar is a fast-growing species with extensive radial root growth, which is of great advantage for hillslope soil stabilization (McIvor, Douglas, and Benavides, 2009). McIvor, Douglas, and Benavides (2009) discovered that a mass growth of 9.5 years old trees was more than 30 times higher than 5 year old ones. Hybrid poplar plantations are relatively fast accumulators of root biomass. Friend et al. (1991) discovered the rapid fine root development in the hybrid poplar plantation, which was probably thanks to the rapid growth capacity of the hybrid clones. As consequences, poplar is extremely well suited for rapid biomass production with its high photosynthetic competence and superior growth performance (Barigah et al., 1994). Poplar wood, as well as hybrid poplar wood, is generated into various products such as pulp and paper (Dickmann and Stuart, 1983; Laureysens et al., 2004), lumber, veneer and plywood (Terrasson and Valadon, 1995), composite panels, pallets, boxes, millwork, hockey sticks, furniture components, fruit baskets, containers, and chopsticks (Balatinecz and Kretschmann, 2001). Hybrid poplars obtain extra benefits, they are easy to propagate through vegetative cuttings and have wide habitats; therefore, closer to production and consumption industries. Hybrid poplars are genetically adjusted with higher quality traits for several specific products. In addition, hybrid poplars potentially become a major source of wood fiber and contribute greatly to energy supply in the next century (Balatinecz and Kretschmann, 2001). Intensive hybrid poplar plantation was thought to have rescued power companies during the energy crisis in the 1970s when petroleum was in short supply and petroleum prices kept increasing. After the crisis, European countries have paid a considerable attention in renewable energy topics (Vande Walle et al., 2007).

An extensive literature review demonstrated the important contribution of biomass in the future energy supply on a global scale (Berndes, Hoogwijk, and Broek, 2003). The European Union (EU) has promoted the strategy of utilizing biomass instead of fossil fuel to reduce climate change effects, secure energy supply, diversify energy sources (IEA, 2003) and lessen its dependence on exteral energy sources, e.g., the major oil-exporting and gas-exporting countries (EU commission, 2005; Gasol et al., 2007; Fischer et al., 2010). As estimation of tree biomass has become much vital during the last decades, there are a great number of researches on this topic. Botanists and foresters often have to deal with a various choices of biomass and plantation productivity estimation (Reed, 1989). Three most-used methods in principle are:

- Harvest entirely plots and subsequently extrapolate to a hectare (Klinge and Herrera, 1983; Klinge et al., 1975).
- Build a functional correlation between tree weight and other easily measured tree variables such as stem diameter at breast height (DBH), tree height (H), crown width (CW), tree age, and wood density (Jordan and Uhl, 1978; Saldarriaga et al., 1988; Overman, Witte, and Saldarriaga, 1994). Considering the regression equations between tree biomass and tree variables, in most cases, these relationship are exhibited under the form of linear regression $Biomass = a \cdot Tree\ Variable^b$ or log-transformed equation $log(Biomass) = a + b \cdot log(Tree\ Variable)$. As mentioned above, the most used tree variables are DBH, or DBH x H (Freedman, 1984). These above regressions do not only apply to estimate entire tree or plot but also tree components such as aboveground biomass, belowground biomass, branches, stumps, twigs, foliage, roots, and nutrients. To construct an equation, whole trees may be sampled by component, collecting each representative subsample is often more applied (Whittaker and Marks, 1975; Ruark, Martin, and Bockheim, 1987).
- Utilize published biomass allometric equations that obtained from populations of similar species in different locations or same locations if available.

Without a doubt, the most reliable procedure to determine tree biomass is harvesting and weighing of all trees or all their components in-situ, but it is destructive, laborious, costly and time-consuming. The first two methods are ideal to develop equations for small areas but then are not practical in several specific sites such as in scientific or protected natural areas - the most interesting places to study but cutting is forbidden. Transportation of samples out of remote areas are also restricted. In such cases, the third approach is the most optimal. It is the easiest, most economic, and also non-destructive (Campbell, Lieffers, and Pielou, 1985). There are several regressions from previous studies were constructed for this reason, also called as generalized biomass allometric equations, are effective within a region rather than a specific site (Young, Hoar, and Ashley, 1965; Kinerson and Bartholomew, 1977; Wiant et al., 1977; Goldsmith and Hocker, 1978; Pastor, Aber, and Melillo, 1984). Generalized allometric equations that ignored specific tree species performed well on tree biomass estimation except for branch and foliage biomass which need species-specific equations. Allometric models have been improved to meet the need of various targets in forest ecology and forest management.

It has been noted that equation including tree height (H) is more accurate in estimating biomass, especially foliage biomass, but at the same time more field work required (Pastor, Aber, and Melillo, 1984; Ruark, Martin, and Bockheim, 1987; Nilsson and Wasielewski, 1987; Ketterings et al., 2001). However, several researchers revealed that only DBH is adequate for local or regional biomass estimation (Honer, 1971; Crow, 1978; Gower, Kucharik, and Norman, 1999). Wang (2006) suggested applying DBH-only equations for most forest management purposes because (1) H is rarely used in practice (Pastor, Aber, and Melillo, 1984; Bond-Lamberty, Wang, and Gower, 2002; Martin et al., 1998), (2) H is much more difficult and time-consuming while less accurate to be estimated than DBH (Gower, Kucharik, and Norman, 1999), (3) adding H may introduce consequent variance due to a cumulative inaccuracy created by H measurements and then generate estimation errors at different subsequent prediction phase (Mowrer and Frayer, 1986). Wang (2006) found an increase of only $<4\%$ in R^2 by adding H as the second predator, which is not worth unless estimating components biomass as branch and foliage since the goal of all allometric equations

is as much accessible to all researchers as possible. Pontailler et al. (1997) noted that the power model predicted tree biomass better than the linear model.

Estimating precisely tree biomass remains a challenge due to the lack of unity in calculated results among published allometric models. Several generalized biomass prediction equations have been introduced for tropical forests (Brown, Gillespie, and Lugo, 1989; Overman, Witte, and Saldarriaga, 1994; Chambers et al., 2001; Chave et al., 2005) and for temperate forest (Ter-Mikaelian and Korzukhin, 1997; Martin et al., 1998; Wang, 2006). Published allometric regression models are mostly developed on a small quantity of trees and very few large diameter trees studied, therefore, not well representing the large-scale forest. In natural forests, allometric equations must be combined from various species to provide reliable biomass estimation. Otherwise, if the equation of a specific tree species is available, the biomass prediction of that particular species becomes more accurate (Litton and Boone Kauffman, 2008). These species normally obtain high value or essential for a research or forestry management plan.

In the present study, we focused on the root distribution and biomass of *Tasman poplar* on pastoral hill in New Zealand for ecosystem services. Several biomass estimates equations of poplars have been published (Pontailler et al., 1997; Brahim, Gavaland, and Cabanettes, 2000; Wullschleger et al., 2005; Dillen et al., 2007; Walle et al., 2007; Fang, Xue, and Tang, 2007; Al Afas et al., 2008b; Felix et al., 2008; Johansson and Karačić, 2011; Ajit et al., 2011; Parsapour et al., 2013; Truax et al., 2014; Fischer et al., 2014; Taeroe et al., 2015; Lupi et al., 2015; Verlinden, Broeckx, and Ceulemans, 2015; Heidari Safari Kouchi, Rostami Shahraji, and Iranmanesh, 2015; Zhang et al., 2016; Fortier et al., 2017; Headlee and Zalesny, 2019; Rebola-Lichtenberg, Schall, and Ammer, 2021). However, most of reported biomass equations for poplar trees are valid over smaller diameters than ones in our studies. For instance, Zhang et al. (2016) developed aboveground biomass equations for poplar plantations in Jiangsu Province of China with DBH ranged from 1.7 to 38.6 cm. Johansson and Karačić (2011) constructed a biomass equation for poplar trees in Sweden with the mean DBH over bark was 21.0 cm (range 4.9 - 44.7 cm). Taeroe et al. (2015) predicted biomass of *Populus trichocarpa* × *Populus maximowiczii* hybrid poplar clone in southern Scandinavia with DBH from 1.2 to 41 cm. Truax et al. (2014) developed clone-specific allometric relationships between DBH and leafless aboveground biomass production of 5 unrelated hybrid poplar clones with DBH ranged from 4.3 to 37.3 cm. Headlee and Zalesny (2019) used allometric biomass equations to describe woody aboveground biomass of 11 hybrid clones with mean DBH of 20 cm (range 8.9 - 34.2 cm) in the north-central USA. Accurately biomass estimations of large trees is crucial because large trees commonly account for a major portion of biomass in a given stand (Crow and Schlaegel, 1988; Gower, Kucharik, and Norman, 1999).

While above-ground biomass in poplar plantations has been widely studied around the world (Fang, Xue, and Tang, 2007; Fortier et al., 2010; Laureysens et al., 2004; Truax et al., 2012; Zabek and Prescott, 2006; Christersson, 2010), allometric equations available for belowground biomass estimation of these species are limited. Lodhiyal and Singh (1993) ordered biomass of each component of poplar tree: bolewood > branches > stump roots > foliage > bole bark > lateral roots > twigs > fine roots. One of the reasons that most former studies focused on the aboveground components of hybrid poplars is because of its high value and flexibility from an economic perspective. Different aboveground parts of hybrid poplars can generate various kinds of marketable products, e.g., branches and stems can be cut to produce bioenergy and particle boards; Stem wood can be used for pulp (Labrecque and Teodorescu, 2005; Yu et al., 2008; Balatinecz and Kretschmann, 2001; Fortier et al., 2010); In drought

pastures, the leaves and small branches of hybrid poplars can be pruned to become an economical livestock feed (McWilliam et al., 2004); Leaves and branches can be used for agricultural land fertilization (Singh and Sharma, 2007). Another reason is that belowground biomass estimates can require a laborious and time-costing effort. The techniques developed to quantify root morphology and biomass of hybrid poplars are effective but destructive and require a huge amount of labor (Friend et al., 1991). Three common schemes to estimate belowground biomass in general are:

- Whole tree root system excavation, so-called destructively harvested. The entire root system of the sample tree is excavated using a device, or manually digging, or combination approach.
- Soil excavation. In most cases, $1m^3$ of soil around the base of the sample tree was excavated. Obviously, several roots of the tree extend beyond 1 m but these roots are assumed to be compensated by roots from adjacent trees that expand into the excavated soil cube (Friend et al., 1991). Therefore, all the roots collected within the this $1m^3$ of soil were attributed to the sample tree. This technique is normally applied to young plantations. The volume of soil excavated depends on the size of the sampled tree.
- Excavated along roots. Radial roots were dry excavated, digging along the course followed by the roots in the soil, and the path of each root was plotted on graph paper (McIvor et al., 2008).
- Estimated by some theoretical proportion of aboveground values or total biomass of a tree.

The excavation of tree roots is very hard work, depending greatly on root morphology and soil conditions (Wang, 2006). A whole excavation provides priceless knowledge of correlations between root system and other factors such as soil properties, underlying rocks, steepness, and prevailing wind. Nevertheless, complete excavation is very laborious in complicated or tricky sites (McIvor, Douglas, and Benavides, 2009). The work of estimating precisely fine roots (<0.5 mm) is unrealistic.

Belowground biomass is accounted for approximately 25% of total biomass in forest ecosystems (Niklas and Enquist, 2002). Poplar root systems can represent approximately 25 - 35% of total plant biomass (Heilman, Ekuan, and Fogle, 1994; KS, 1996), this proportion can be higher (up to 63%) in juvenile trees (King, Pregitzer, and Zak, 1999; Yin et al., 2004; Oliveira et al., 2018). As trees increase in size, their root:shoot ratio tends to decrease. Although total root biomass was positively correlated with stand age, the increase was caused mainly by the increase in stump weight, whereas fine and coarse root mass did not vary (Ruark, Martin, and Bockheim, 1987).

In addition to biomass production, forests also contribute greatly to the global carbon cycle and climate change. Forest biomass estimation is an vital step to quantify the carbon budget (Zhang et al., 2016). Hybrid poplar, thanks to its specific characteristics include fast-growing, high-yield and strong adaptability to environmental changes, is considered as a high efficient carbon sink and can be planted to compensate CO_2 emissions (Oelbermann, Voroney, and Gordon, 2004; Updegraff, Baughman, and Taff, 2004; Yemshanov and McKenney, 2008; Fortier et al., 2010; Zhang et al., 2016). Liu et al. (2010) revealed that the carbon sequestration of poplar trees is nearly 20 times higher than other tree species. Since tree biomass can be easily estimated with published allometric equations, converting tree biomass to carbon

storage capacity through multiplying by the ratio of CO_2 to C could be the most ideal and reliable approach to estimate weight of carbon dioxide sequestered over large areas.

In the case of New Zealand, poplars are qualified for carbon credits under the New Zealand Government Emissions Trading Scheme (ETS) providing the planted area exceeds one hectare, and trees are sufficiently close to reach 30% of canopy cover (McIvor and Douglas, 2012). At maturity (DBH > 30 cm), 78 SPH "Tasman" poplars would be required to achieve 30 % canopy cover. The New Zealand Government has chosen the Emissions Trading Scheme (ETS) as the most economical method to evaluate greenhouse gas emissions with the aim of declining greenhouse gases emission in New Zealand. Within the New Zealand ETS system, New Zealand Units (NZUs) are used as a mean for trading. One NZU allows to discharge one tonne of carbon dioxide or of other greenhouse gases. Agroforestry systems such as hybrid poplar have a high potential to store carbon in both above- and below-ground biomass (Tufekcioglu et al., 2003), with biomass carbon storage ability of poplar buffers being largely affected by site fertility (Fortier et al., 2010).

In the present study, we focused on the root distribution of Tasman poplars, applied RDM to assess its biomass and carbon storage capacity in New Zealand pastoral hillcountry.

6.2 Materials and Methods

6.2.1 Site description

FIGURE 6.1: Location of the study site shown as a red star in New Zealand.

Data was collected at Ballantrae Hill Country Research Station (40°18'56"S, 175°50'23"E) in the region of Manawatu, locating in the south of the North Island (Figure 6.1). This region is commonly known for pastoral production. The elevation is approximately 130 m ASL (Manaaki Whenua - Landcare Research 2019). The terrain tends to incline (4-15^o) towards northeast. The study region is regulated by temperate climate with frosty winters and cool summers. Average monthly precipitation is between 50 and 80 mm. It is an ideal condition for tree growth and cultivation.

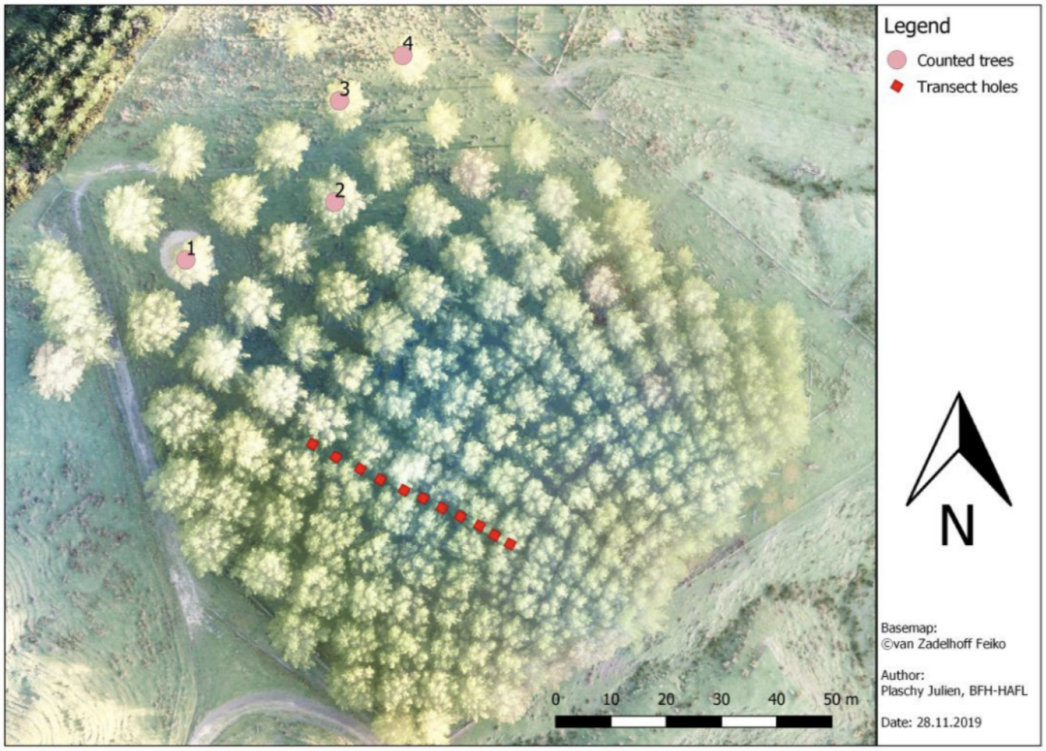

FIGURE 6.2: Overview of the tree stand. Trees from the more spaced part of the stand have been chosen for root counting in order to have less overlap between the root systems of neighboring trees.

The studied Tasman poplar stand was 26 years old. The poles were distributed in a radial disposition (Figure 6.2). Tree spacing was around 6 m in the densest zone (SE) and up to 14 m in the sparsest one (NW). Four trees located in the sparse zone were excavated to obtain root mechanical properties and root distribution.

Root counting and measurement were conducted from the 30th of September 2019 to the 8th of November 2019. The study were divided into two parts with different objectives. Detailed methodologies were presented in the following sectors.

6.2.2 Individual tree measurements

To quantify the spatial root distribution of a single tree scale, we selected four trees (Tree 1, 2, 3, and 4) with different DBH in the sparsest part of the stand as shown in Figure 6.2 to avoid the overlapping of neighbouring tree root systems and then dug two 360^o trenches of 0.9 meter depth with an excavator. The distances from the middle of the tree stem to these trenches were 1.5 m, 2.5 m, 3.5 m, and 4.5 m as shown in the Figure 6.3. Trenches were divided into 8 sectors of 45^o each. The first and the last sectors were situated in uphill. Each sector was separated into 7 depth layers [0-15 cm], [15-30 cm], [30-45 cm], [45-60 cm], [60-75 cm], [75-90 cm], and [> 90 cm]. Living fine roots coming from identified trees were counted and put in diameter class [0-1.5 mm] whereas living coarse roots were classified into 1-mm diameter class such as 1 mm [1.5-2.5 mm], 2mm [2.5-3.5 mm], 3 mm [3.5-4.5 mm], and so on. Collected data were applied to calibrate and validate the Root Reinforcement Model and Root Distribution Model.

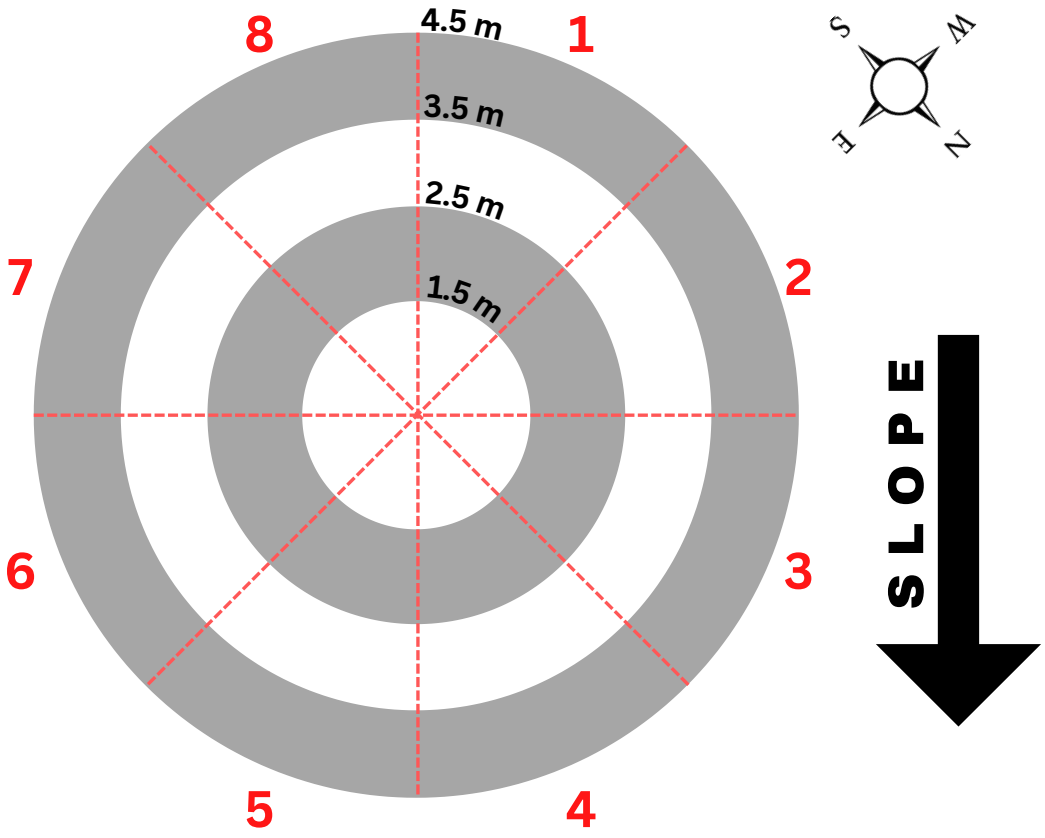

FIGURE 6.3: Schematic representation of the trenches (in grey) with the different sectors and distances.

6.2.3 Root distribution modeling

Root Distribution Model (RDM) described by Schwarz, Lehmann, and Or (2010) was applied to estimate the number of roots in diameter class size i that cross 0.9-m depth and 1-m width vertical soil profile at a distance d from an isolated tree stem with diameter at the breast height (DBH) ϕ_t following the equation:

$$N_{i,t}(d,\phi_t) = \begin{cases} D_{fr}\frac{[ln(1+\phi_{max})-ln(1+\phi_i)]}{ln(1+\phi_{max})}(\frac{\phi_i}{\phi_0})^{\beta}, & \text{with } d < d_{max} \text{ and } \phi_i < \phi_{max} \\ 0, & \text{otherwise} \end{cases} \quad (6.1)$$

d_{max} is the maximum rooting distance from the stem, D_{fr} is the density of fine roots (smaller than 1.5 mm) per horizontal meter, ϕ_i is the mean root diameter in class size i, ϕ_0 is a reference diameter (in this paper equals to 1 mm), ϕ_{max} is the maximum root diameter, and β is a constant exponent.

$$d_{max}(\phi_t) = \psi\phi_t \quad (6.2)$$

$$\phi_{max} = \frac{d_{max} - d}{\eta} \quad (6.3)$$

ψ is a proportionality constant, ϕ_t is the tree diameter at the breast height, and η is a dimensionless scaling coefficient.

The density of fine roots (< 1.5 mm) crossing a 0.9-m depth and 1-m width vertical soil profile at a given distance d from an isolated tree stem with diameter at the breast height (DBH) ϕ_t is calculated as:

$$D_{fr}(d, \phi_t) = [\frac{\mu(\phi_t^2 \frac{\pi}{4})}{d_{max} 2\pi d}](\frac{d_{max} - d}{d_{max}}), \text{ with } d < d_{max} \tag{6.4}$$

μ is a pipe coefficient.

Aforementioned parameters of the model μ, β, ψ and b were calibrated by minimizing the Sum of Squares Errors obtained as the difference between modeled and measured root distribution data. RDM simulated only lateral root distribution without considering vertical variations.

RDM in the studied stand has been calibrated and validated in previous paper (Ngo et al., 2023). Calibrated values of μ, β, ψ and b are 97056.03, -1.50155, 0.1319465, and 16.21262, respectively. We used these values to calculate root biomass and root carbon storage capacity of Tasman poplars.

6.2.4 Root Area Ratio

First, we measured each root cross-sectional area at a given soil profile i, based on the number of roots in each root diameter class:

$$A_i = \sum_{j=1}^{m} N_{i,j} \cdot \pi(\frac{d_j}{2})^2 \tag{6.5}$$

where A_i is root area of soil profile i, $N_{i,j}$ is the number of roots in root diameter class j at soil profile i, d_j is root diameter of root diameter class j, and m is number of root diameter classes.

To calculate Root-Area-Ratio (RAR), knowing as the ratio between root area and soil area at soil profile i:

$$RAR_i = \frac{A_i}{A_s} \tag{6.6}$$

where A_i is root area [m^2] at soil profile i and A_s is cross-sectional soil area [m^2] of soil profile i.

6.2.5 Root biomass calculation

Measured root biomass We obtained measured root distribution at four distances from the stem: 1.5m, 2.5m, 3.5m, and 4.5 m. We considered the distance from the first trench to the stem is L_0 (in m) whereas distance between each further trench is L (in m). In our case, L equals to 1 m. Root volume within the first assessed distance from the stem is computed following cylinder shape, while we calculated root volume from 2.5 m to 4.5 m distances as the sum of volumes of different truncated cones. The total measured root fresh volume of a tree (MRV, in m^3) from stem to distance of 4.5 m will be calculated following the equations:

$$MRV = A_1 \cdot L_0 + \sum_{j=1}^{n-1} \frac{L_j}{3} \cdot (A_j + A_{j+1} + \sqrt{A_j \cdot A_{j+1}}) \tag{6.7}$$

where MRV is the total measured root fresh volume, $A_1 \cdot L_0$ is the root volume from the stem to the first trench (1.5 m). We assumed that the root distribution was constant in the first 1.5 m from the stem. A_j, A_{j+1} is the root area of successive

trenches apart from first trench while L_j is the distance between j and $j+1$. For measurement data, L_j equals to 1 m.

Estimated root biomass We used the Root Distribution Model (RDM) to generate the number of roots within each root diameter class in a 1-m wide and 0.90-m deep soil profile at specific radial distances from the stem. Based on these estimates, we calculated the root quantities at successive distances and calculated the estimated root fresh volume (ERV, in m^3) for the entire root system of a tree. To estimate root biomass, we applied a radial integration of root cross-sectional area using a discretized representation of the root distribution. The integration was performed using a 1-m step size (L = 1m), which corresponds to the field sampling resolution using in trench-based root data collection. This approach ensures reliable comparison between model performance and empirical observations.

$$ERV = A_1^m \cdot L_0 + \sum_{j=1}^{n-1} \frac{L_j}{3} \cdot (A_j^m + A_{j+1}^m + \sqrt{A_j^m \cdot A_{j+1}^m}) \tag{6.8}$$

where $A_1^m \cdot L_0$ is the root volume from the stem to the first trench. L_j is the distance between trench j and $j+1$. A_j^m and A_{j+1}^m are root areas at trench j and $j+1$ from the stem.

Root fresh volume (RV, in m^3) was then converted to root dry weight (DW, in kg). Johansson and Hjelm (2012) found the mean basic dry density for Poplar stands of 0.313 g/cm^3, equals to 313 kg/m^3. The basic density was computed as ratio between dry weight and fresh volume. Therefore, to calculate root dry mass (DW, in kg):

$$DW = RV \cdot 313 \tag{6.9}$$

6.2.6 Carbon storage calculation

The carbon storage in root systems of each poplar trees was calculated by multiplying root dry biomass with carbon fraction (CF). The carbon content of tree remains quite constant across various species with the range from 42% to 50% (Schlesinger, 1997; Magnussen and Reed, 2004; Fang, Xue, and Tang, 2007; Wauters et al., 2008; Rana et al., 2010; Behera and Mohapatra, 2015). It has traditionally been assumed that the carbon content of dry biomass of a tree was 50% (Brown and Lugo, 1982; Roy, Mooney, and Saugier, 2001; Grace, 2004; Chojnacky, Heath, and Jenkins, 2014). On the other hand, Kirby and Potvin (2007) suggested this value equaled 47% for trees. In this study, we calculated carbon content of tree root (W_C) by simply taking a conversion fraction of 0.50 (default value given by OECD and lEA (1996) and IPCC (2006)) multiply with root biomass value (DW).

$$W_C = DW \cdot CF \tag{6.10}$$

where W_C is the carbon content and DW is dry root biomass.

To estimate the amount of CO_2 sequestration (kg), the carbon content was then multiplied by the ratio of CO_2 to C which equals to 44/12.

$$W_{CO_2} = \frac{44}{12} \cdot W_C \tag{6.11}$$

where W_{CO_2} is the weight of carbon dioxide sequestered in trees (kg).

Estimated values of stored CO_2 from measurement and from RDM were then compared with the amount of sequestered CO_2 calculated by the published allometric regression models from previous studies.

6.2.7 Statistic analyses

Both RBMw and RDM were implemented in R software and can be downloaded at the following link: www.ecorisq.org/openFTP/Schwarz.zip.

6.3 Results

6.3.1 Root Distribution Measurements and Modeling

Measured Root Distribution Four Tasman poplar trees with different DBH ranging from 0.41 m to 0.56 m was sampled to observed the distribution pattern of fine roots and coarse roots on pastoral hill country. Two circular trenches around each tree were excavated. Figure 6.4 and Figure 6.5 showed the difference in root distribution of all trees in upslope and downslope. The root distribution in upslope is the mean root quantity per meter of sector 1 and sector 8; while for downslope, root number per meter is calculated as the mean value of root distribution between sector 4 and sector 5 (Figure 6.3).

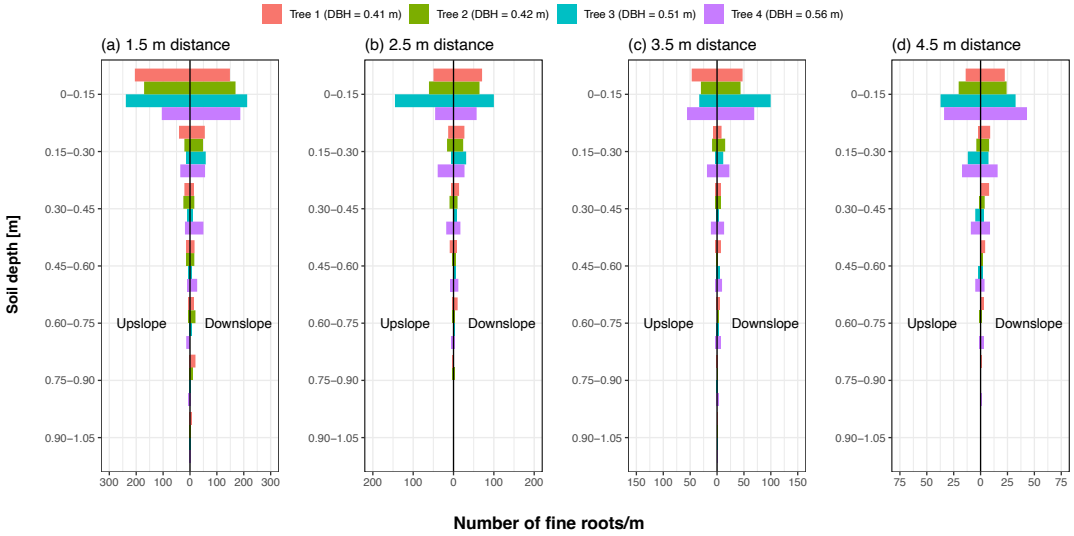

FIGURE 6.4: Measured number of fine roots (< 1.5 mm) in 1-m width and 1.05-m depth soil profiles from four Tasman poplars with DBH of 0.41 m (red bars), 0.42 m (green bars), 0.51 m (blue bars), and 0.56 m (purple bars) at different distances from the stems. Number of fine roots for upslope is the mean value of root quantity between sector 1 and sector 8, whereas number of fine roots for downslope is calculated as mean values between sector 4 and sector 5.

As observed in Figure 6.4, the number of fine roots correlated negatively with soil depth and with distances from the stem in all trees. Considering horizontal direction, the highest number of fine roots was recorded in the nearest trench. At this distance, three smaller trees have more fine roots in uphill than downhill while the biggest poplar tree showed more abundant fine roots in downhill direction. In other distances, the number of fine roots then tends to be more abundant in downslope compared to upslope.

Considering vertical direction, the number of fine roots decreased rapidly corresponding to the soil depth and fluctuated greatly. In 0 - 0.15 m soil layer, 0.51 m DBH tree showed more fine roots in uphill compared to downhill in all distances except 3.5 m far from the stem. In the same soil layer, tree 4 always showed higher number of fine roots downslope compared to upslope. In contrast, other two smallest poplar trees had the same root distribution patterns with more fine roots in downhill profile than uphill one from 2.5 to 4.5 m distance while higher number of fine roots in upslope compared to downslope at 1.5 m from the stem. Among four sampled trees, tree 3 and tree 4 tended to obtain the greatest number of fine roots. In 0.15 - 0.30 m soil depth, we observed clealier that number of fine roots is higher in downslope than upslope, except for tree 3 at 4.5 m from the stem. In both 0.30 - 0.45 m and 0.45 - 0.60 m soil layers, the biggest tree (DBH = 0.56 m) showed to have highest fine root numbers than other trees. Below 60 cm soil depth, the number of fine roots was insignificant in all trees. Only tree 4 has fine roots in the soil layer of 0.75 - 0.90 m at the distance 3.5 and 4.5 m from the stem, showing the extensive root system as the largest tree.

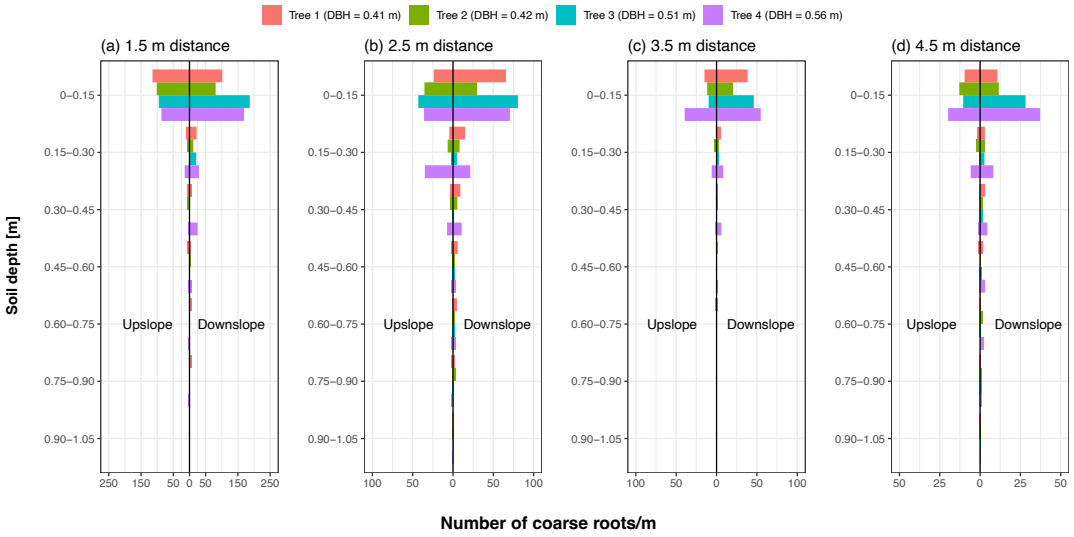

FIGURE 6.5: Measured mean number of coarse roots of four Tasman poplars in each soil depth at different distances of 1.5 m, 2.5 m, 3.5 m, and 4.5 m from the stem in both upslope (sector 1 and sector 8) and downslope (sector 4 and sector 5).

Similarly, coarse roots (> 1.5 mm) in Tasman poplars decreased with lower depth and farther from the stem. Considering horizontal direction, the amount of coarse roots of all trees fluctuated greatly between upslope and downslope, especially tree 3 and tree 4. In the two smallest trees, coarse roots were more abundant in the uphill sector in the first trench but then gradually grew towards downhill. On the contrary, both two biggest trees exhibited higher coarse roots abundance in downslope than upslope at all distances from the stem. At 4.5 m distance, it could be clearly seen the positive correlation between number of coarse roots and the size of the trees.

Considering vertical side, majority of coarse roots was recorded above 0.6 m soil depth. Within the first soil layer, we observed that when the root system of a Tasman poplar expands further, it tends to grow downward. A distinguished pattern was observed from tree 4 in the second soil layer that the number of coarse roots upslope was twice higher than downslope in the 2.5 m distance. Similar to fine roots, number of coarse roots is also higher downslope compared to upslope with depth below 0.15

m. At the farthest trench, only tree 3 and tree 4 showed to have root system at deep soil layers from 0.60 to 0.90 m. The number of coarse roots is shown to be negligible in the deepest soil layer for all four poplar trees.

Modeled Root Distribution The study of Ngo et al. (2023) calibrated and validated the Root Distribution Model with collected in-situ data of Tasman poplars from the same stand. In the present study, we utilized the calibrated RDM with the established best-fitted coefficients to calculate root-area-ratio (RAR) and root biomass.

TABLE 6.1: Best-fitted parameters of Tasman poplars for the Root Distribution Model. μ is the pipe coefficient, β is the empirical exponent of coarse root density, η is the scaling coefficient for maximum root diameter at a distance, ψ is the proportionality constant for maximum root lateral extension, SSE is the Sum of Square Errors, and R^2 is the coefficient of determination.

Dataset	**n**	μ	β	η	ψ	**SSE**	R^2
Tree trenches	128	97056.03	-1.5015	0.1319465	16.21262	684.65	0.78

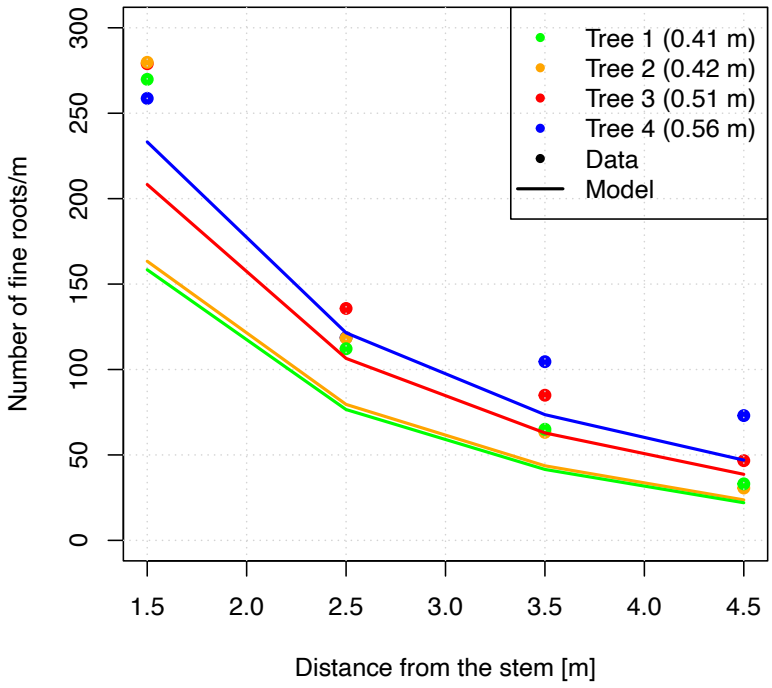

FIGURE 6.6: Measured (dots) and modeled (lines) number of fine roots of four Tasman poplars with different diameters at four distances of 1.5 m, 2.5 m, 3.5 m, and 4.5 m from the stem. Tree 1 (DBH = 0.41 m) was presented in green color, tree 2 (DBH = 0.42 m) was indicated with orange color, tree 3 (DBH = 0.51 m) was exhibited with red color, and tree 4 (DBH = 0.56 m) was presented in blue color.

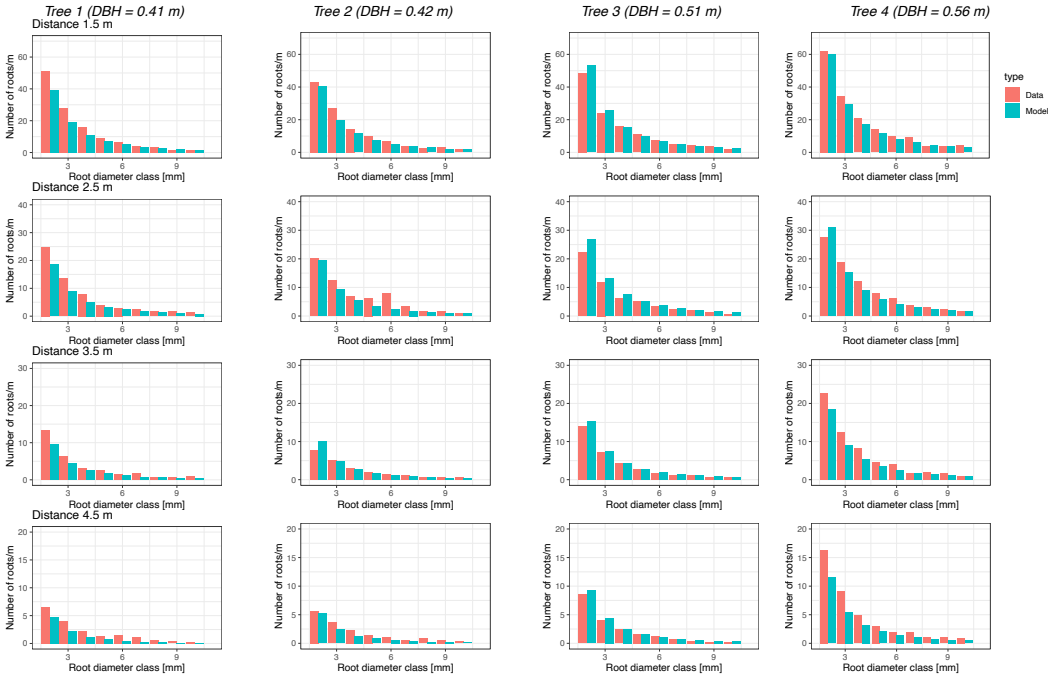

FIGURE 6.7: Measured (presented by red columns) and modeled (presented by blue columns) number of coarse roots of four Tasman poplar trees at four distances of 1.5 m, 2.5 m, 3.5 m, and 4.5 m from the stems.

The study of Ngo et al. (2023) demonstrated that with calibrated parameters, the number of fine roots was underestimated in all trees while the number of coarse roots fluctuated based on the size of sampled trees and distance from the stems between measured and simulated datasets. The variance between measured and modeled coarse root number in assessed 1 x 0.90-m profiles was not significant with $R^2 = 0.96$, however, it would be interesting to examine the difference in whole root system biomass.

6.3.2 Root Biomass and Carbon Storage

Root Biomass We calculated the root-area-ratio (RAR), which means the cross-sectional area of roots per area of a soil profile at different distances from the stems.

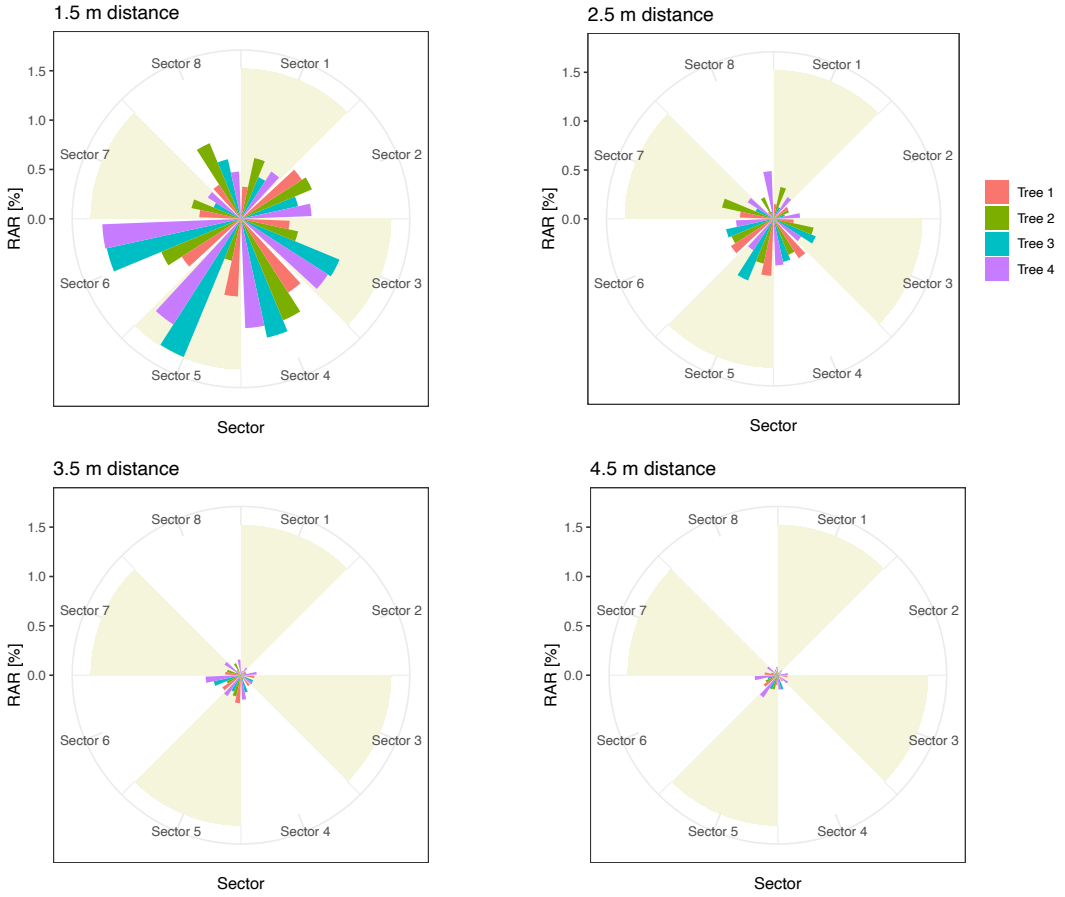

FIGURE 6.8: Measured RAR in 1m x 1.05m soil profiles of four Tasman poplar trees at different distances from the stems. Sector 1 and sector 8 located in the upslope direction while sector 4 and sector 5 located in the downslope.

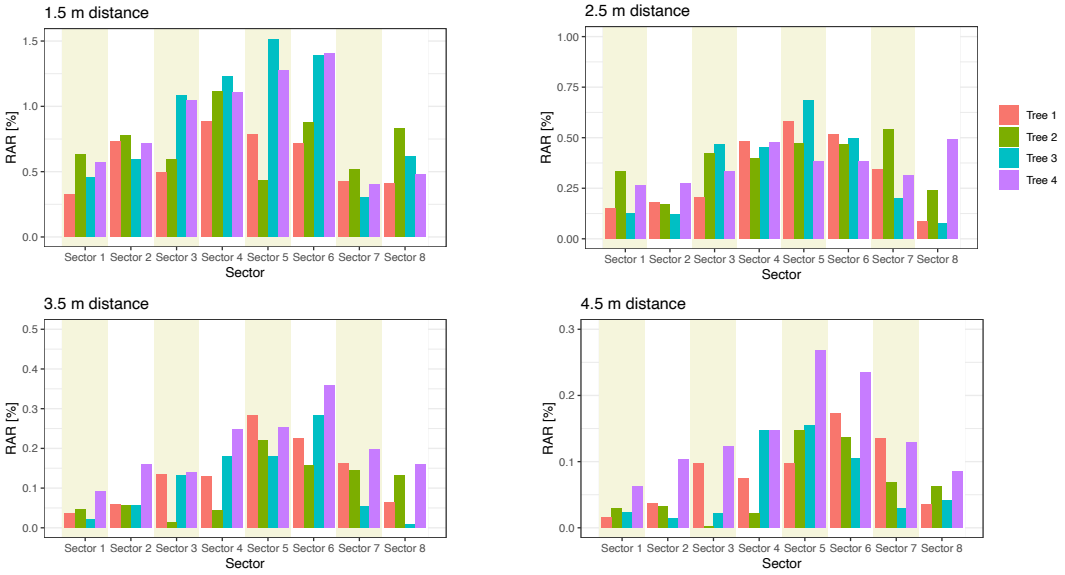

FIGURE 6.9: Measured RAR in 1m x 1.05m soil profiles of four Tasman poplar trees at different distances from the stems by sector.

It could be clearly observed that there was a significant gap in RAR between upslope and downslope. At distance of 1.5 m, two smallest trees exhibited the highest RAR in sector 4 whereas tree 3 and 4 showed the highest values in sector 5 and 6, respectively. At distance of 2.5 m, tree 1 and tree 3 showed highest RAR in sector 5 while the highest RAR of tree 2 and tree 4 is found in sector 7 and sector 8, respectively. The highest RAR value of tree 4 (DBH = 0.56 m) at the distance of 2.5 m from the stem is in sector 8 with 0.49%. At two nearest distances from the stem, tree 3 obtained the greatest RAR with ca. 1.51% and 0.68%, all found in sector 5. At two farther distances, the maximum RAR values of all trees are either located in sector 5 or sector 6. At two farthest distances, tree 4 showed highest RAR values with 0.36% and 0.27% in sector 6 and sector 5, respectively. On average, the RAR values in the nearest distance were approximately 21 times higher than of the 4.5-m trench. Figure 6.9 well indicated the root distribution of Tasman poplars in horizontal direction in a hillslope.

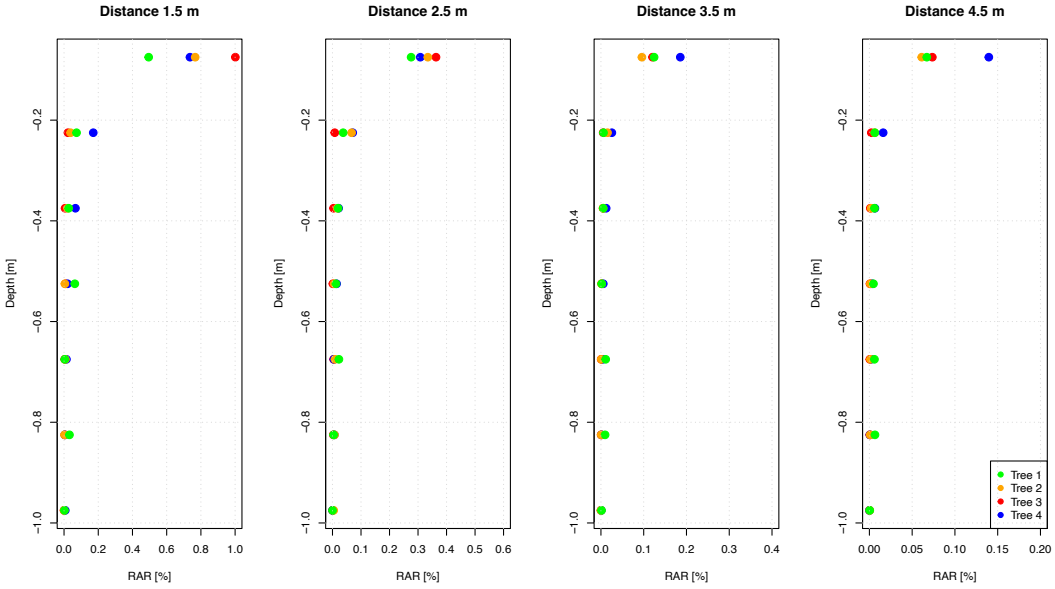

FIGURE 6.10: Correlations of measured RAR of four Tasman poplars with soil depth and distances from the stems. RAR values of tree 1 (DBH = 0.41 m) was represented in green dots, RAR values of tree 2 (DBH = 0.42 m) was shown in orange dots, RAR values of tree 3 (DBH = 0.51 m) was indicated in red dots, and RAR values of tree 4 (DBH = 0.56 m) was exhibited in blue dots.

Considering Figure 6.10, majority of poplar root was found in the first 0.6 m soil depth. RAR values below 0.6 m of all four trees were insignificant at every assessed distance. Within two closest trenches, tree 3 showed the highest RAR values in the first 0.15 m soil depth but then indicated to obtain lowest RAR values in the next soil layer. On the contrary, tree 4 showed more modest RAR values than tree 2 and tree 3 in the first soil layer but then obtained the greatest RAR in following depths. Within two farthest trenches, tree 4 had the highest RAR values in every layer, exhibiting the extensive root system of the biggest tree compared to smaller ones.

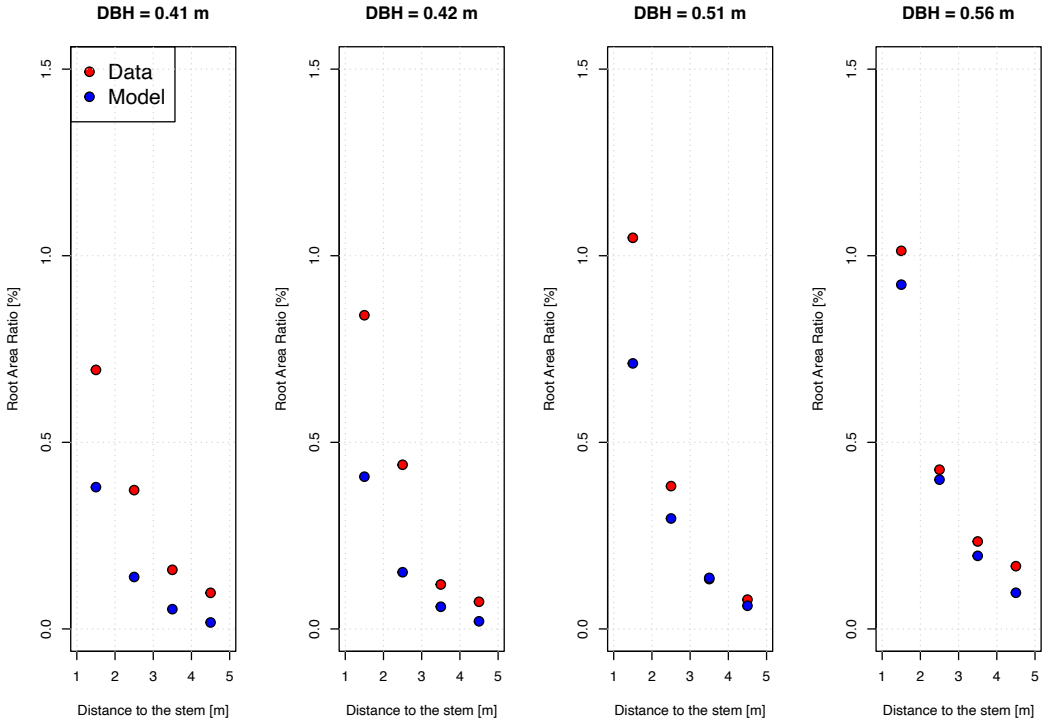

FIGURE 6.11: Comparison between measured (red dots) and simulated (blue dots) root-area-ratio (RAR) from RDM of 1 x 0.90 m profiles from different sizes of poplar trees at various trenches from the stems.

Figure 6.11 exhibited great variation of RAR values of different trees at various distances to the stem. RAR values decrease when roots grow further from the stem. At 1.5 m distance, the maximum measured RAR value was measured in tree 3 and the minimum one was recorded in the smallest tree. At 2.5 m distance, the highest measured RAR was found in tree 2 with approximately 0.44%. At 3.5 m and 4.5 m distances, the maximum RAR values were both found in tree 4 with 0.23% and 0.17%. In most of the cases, measured RAR values were higher than simulated ones. The biggest variances between measured and estimated RAR values were mostly observed at the first trench, especially in tree 2 with the difference up to 0.43%. The differences between measurement and model were getting smaller corresponding to further distances. The model performed better with two large trees than two small trees. At 4.5 m distance, the differences between two datasets were not notable with values of 0.08%, 0.05%, 0.02%, and 0.07% corresponding from the smallest tree to largest trees, showing that the RDM performed well at the distance of 4.5 m from the stem.

We then calculated root fresh volume and root dry weight of four sampled poplar trees following the equation 6.7, 6.8 and 6.9. The results were then recorded in the Table 6.2.

TABLE 6.2: Comparison of total root dry weight calculated from measurement (Equation 6.7) and from estimation (Equation 6.8) at different distances from the stem with $L_0 = 1.5$ m and $L = 1.0$ m.

ID Tree	DBH [m]	Distance from stem [m]	Measured DW [kg]	Estimated DW [kg]	Variance [kg]	Difference [%]
Tree 1	0.41	0 - 1.5	27.64035	15.13048	12.50987	45.27
		1.5 - 2.5	17.43308	8.041973	9.391107	53.86
		2.5 - 3.5	12.99183	4.645008	8.346822	64.24
		3.5 - 4.5	8.734574	2.261832	6.472742	74.12
		> 4.5	NA	0.9378279	NA	NA
Tree 2	0.42	0 - 1.5	33.47388	16.24537	17.22851	51.47
		1.5 - 2.5	20.87362	8.694396	12.179224	58.34
		2.5 - 3.5	12.94063	5.124411	7.816219	60.39
		3.5 - 4.5	6.572345	2.583028	3.989317	60.70
		> 4.5	NA	1.180093	NA	NA
Tree 3	0.51	0 - 1.5	41.73597	28.33663	13.39934	32.09
		1.5 - 2.5	22.15494	15.90493	6.25001	28.21
		2.5 - 3.5	12.3465	10.69893	1.64757	13.34
		3.5 - 4.5	7.24001	6.631052	0.608958	8.41
		> 4.5	NA	5.739708	NA	NA
Tree 4	0.56	0 - 1.5	40.34396	36.73694	3.60702	8.94
		1.5 - 2.5	22.77008	21.00396	1.76612	7.76
		2.5 - 3.5	16.65064	14.82841	1.82223	10.94
		3.5 - 4.5	13.95099	9.843695	4.107295	29.45
		> 4.5	NA	10.8376	NA	NA

Measured dry weight (DW) values beyond 4.5 m are marked as NA because root distribution was not assessed in situ beyond this distance from the stem.

For all trees, the estimated root dry weight values tend to underestimate the measured values, particularly within the distance of 3.5 to 4.5 m except Tree 3. The discrepancies are largest in Tree 1 and Tree 2, where relative differences between measured and estimated DW range from 45% to over 74%. Specifically, for Tree 1, the model underestimated DW in the 0 - 1.5 m distance by 45.27% and up to 74.12% in the 3.5 - 4.5 m range. A similar pattern is observed in Tree 2, where differences range between 51.47% and 60.70%. Variances ranging between 12.5 and 17.2 kg suggest that the model notably underestimates root biomass in areas closest to the stem, where root density is highest.

In contrast, Tree 3 and Tree 4 exhibit a higher level of consistency between measured and estimated DW values. Tree 3 shows a decreasing trend in difference from 32.09% to 8.41% across from the stem to 4.5 m range, suggesting improved model performance with increasing distance. Similarly, Tree 4 presents low differences across all distances, with percentage differences remaining below 30%, and as low as 7.76% in the 1.5 - 2.5 m range. These results highlight that the model tends to perform more accurately for trees with larger DBH, such as Tree 3 (0.51 m) and Tree 4 (0.56 m), than for those with smaller DBH like Tree 1 and Tree 2 (DBH = 0.41 and 0.42 m, respectively).

Beyond 4.5 m from the stem, measured data are unavailable (NA), and therefore,

model estimates in this range could not be validated. However, estimated DW values in this farthest distance remain relatively low across all trees (ranging from 0.94 to 10.84 kg), indicating a minor contribution of distant roots to the total root biomass.

Overall, these findings suggest that while the Root Distribution Model performs moderately well in predicting the general spatial pattern of root biomass, it tends to underestimate, particularly near the tree stem where root density is highest. This may be due to limitations in recording in-situ root distribution at this distance. However, the closer alignment observed in larger trees indicates that model performance may improve with increasing DBH.

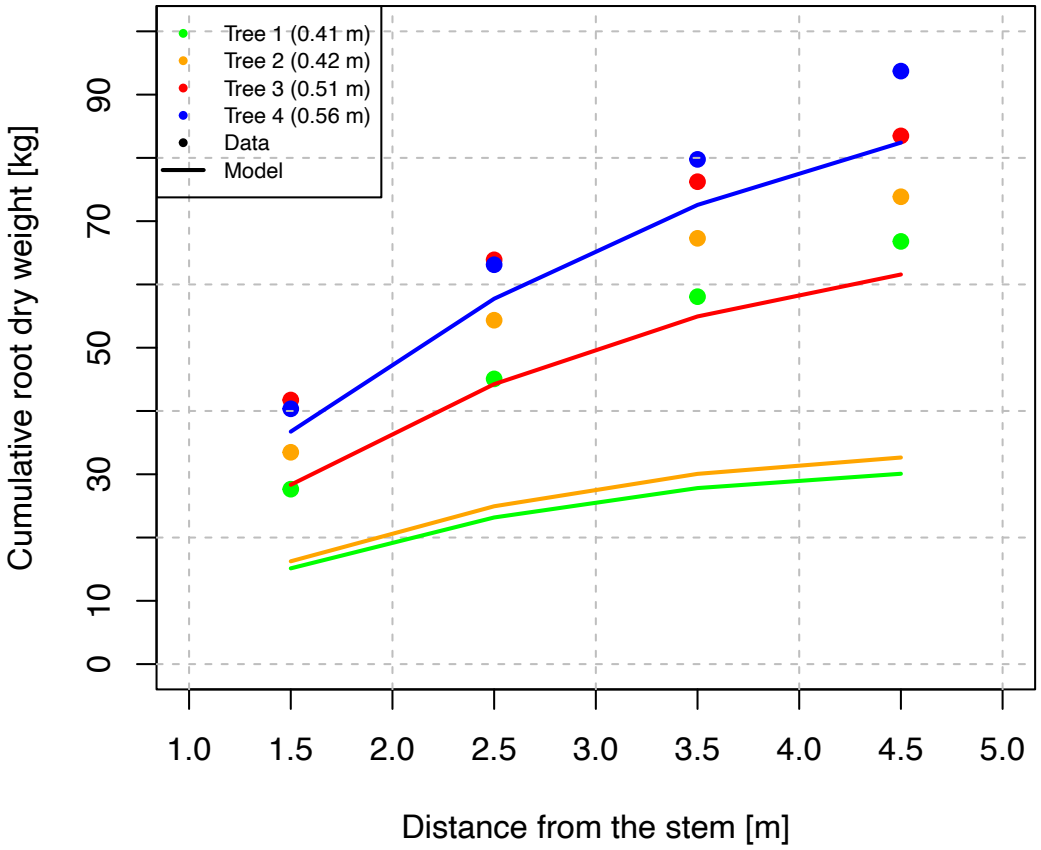

FIGURE 6.12: Comparison between measured and simulated cumulative root dry weight at different distances from the stem of four poplar trees.

Figure 6.12 presents the cumulative root dry weight as a function of the distance from the stem for four trees with varying diameters at breast height. Measured values are represented by colored points, while modeled values are shown as solid lines.

Across all trees, cumulative root dry weight increased with radial distance from the stem, reflecting the expected trend of root biomass distribution. Notably, the model closely generated the general pattern of the observed root dry weight curves, with particularly good prediction for Tree 4 (DBH = 0.56 m).

In contrast, Trees 1 and 2 (DBH = 0.41 and 0.42 m) showed significantly lower cumulative root dry weight throughout various distances. The model underestimated biomass in the farther zones (> 3.5 m) for these smaller trees but captured the overall trend.

When calculating root volume and biomass, we assumed a uniform root distribution within the first 1.5 m from the stem, due to the absence of in situ data in this zone. Beyond 1.5 m, root data were collected at 1-meter intervals, which likely introduced variability between the measured and actual root biomass. In contrast, estimated root dry mass was calculated continuously from the stem to the maximum rooting distance using the RDM.

Given the positive correlation between DBH and root biomass, larger trees exhibited higher total root dry mass. Table 6.2 presents the DBH values and corresponding total root dry weights for the sampled trees. The largest tree in the study was estimated to have accumulated up to 93 kg of root biomass.

Carbon Storage Tree size has been shown to play a major role in biomass variation and is commonly used as the variable in biomass allometric models (Gower, Kucharik, and Norman, 1999; Wang, 2006). DBH-only biomass equations are enough to satisfy biomass calculations of an individual tree and application in most of forest management purposes (Wang, 2006; Zhang et al., 2016).

TABLE 6.3: Table of total biomass and carbon storage of root system.

ID Tree	DBH [m]	Measured W_C [kg]	Estimated W_C [kg]	Measured W_{CO_2} [kg]	Estimated W_{CO_2} [kg]
Tree 1	0.41	33.39992	15.50856	122.4664	56.86472
Tree 2	0.42	36.93024	16.91365	135.4109	62.01672
Tree 3	0.51	41.73871	33.65563	153.0419	123.404
Tree 4	0.56	46.85784	46.6253	171.8121	170.9594

Table 6.3 presents the measured and estimated root carbon stocks (W_C) and their corresponding CO_2 equivalents (W_{CO_2}) for four Tasman poplar trees of varying diameters at breast height (DBH). Root carbon content was derived from dry biomass measurements and model estimates (Equation 6.10), while CO_2 equivalents were calculated using a standard conversion factor to reflect the amount of atmospheric carbon dioxide sequestered in the root system (Equation 6.11).

As expected, both measured and estimated root carbon values increased with tree size. Tree 4, with the largest DBH (0.56 m), exhibited the highest root carbon storage, with measured and estimated values of 46.86 kg and 46.63 kg, respectively. This corresponds to a CO_2 sequestration potential of approximately 172 to 176 kg, highlighting the substantial contribution of mature poplar trees to belowground carbon storage.

In contrast, Trees 1 and 2 (DBH = 0.41 and 0.42 m) stored much less, with measured CO_2 equivalents of 122.5 kg and 135.4 kg, respectively. The gaps between measured and estimated values were more significant in smaller trees. For instance, Tree 1 estimated W_C was only 15.5 kg compared to the measured 33.4 kg, equals to a 53.6% difference.

Despite this difference, model predicted more closely with measured values as tree size increased. For Tree 4, the model simulated quite well the observed root carbon with a difference of less than 0.5%.

6.4 Discussion

6.4.1 Root Distribution of Tasman poplars

The spatial distribution of fine and coarse roots in *Populus deltoides* x *nigra* "Tasman" reveals clear patterns shaped by both tree size and topographic position. Across all sampled trees, measured fine root abundance declined significantly with increasing soil depth and horizontal distance from the stem. Fine roots are mainly concentrated in the first soil layer and close to the stem, where nutrient availability and oxygen levels are highest.

In general, all four sampled trees exhibited a consistent pattern of higher fine root abundance in the downslope profile across all distances. This may reflect greater soil moisture accumulation or nutrient transport downslope, providing favorable conditions for root growth. Considering vertical distribution, the top soil layer (0 - 0.15 m) contained the highest density of fine roots, especially in larger trees.

As soil depth increased, the number of fine roots decreased rapidly, with roots below 0.60 m being minimal or absent in all trees except Tree 4. The detection of fine roots at 0.75 - 0.90 m soil depth in Tree 4, especially at greater distances from the stem (3.5 m and 4.5 m), suggesting that an extensively grown and vertically penetrating root system in the largest sample. This is consistent with the role of tree maturity and size in growing deeper and more wide root development.

Coarse roots followed a similar pattern of decreasing trend with both depth and distance from the stem. Similarly, in most of the cases, four trees displayed a dominance of coarse roots in the downslope direction at all distances, suggesting deeper anchorage and resource acquisition zones downslope. At the furthest trench (4.5 m), a strong positive correlation between coarse root abundance and tree size became evident, further supporting the relationship between tree biomass and root system development.

Similar to fine roots, most coarse roots were located in the upper 0.6 m of the soil profile. In the shallowest soil layer, the root system appeared to spread laterally before extending downward in larger individuals. A distinct pattern was observed in Tree 4, where coarse roots at 2.5 m distance from the stem were twice as abundant upslope than downslope in the second soil layer (0.15 - 0.30 m), potentially due to localized microtopographic or edaphic conditions. Deeper than 0.60 m soi depth, coarse roots were generally absent or present in negligible amounts, except in Tree 3 and Tree 4 at the farthest trench, again indicating a greater root system expansion in larger trees.

These findings confirm that root system architecture in Tasman poplars is strongly influenced by tree size, slope direction, and soil depth. The pattern that larger trees develop more extensive downslope and deeper root systems may imply adaptive responses to soil resource gradients, gravitational water flow, and mechanical support requirements. These patterns have important implications for understanding root-driven soil stabilization, water uptake strategies, and carbon storage potential in managed poplar plantations.

The calibrated Root Distribution Model underestimated number of fine roots across all sampled trees but predicted quite effectively spatial trends in coarse root distribution at soil profile scales.

6.4.2 Root Biomass of Tasman poplars

In this study, root biomass and carbon stocks of Tasman poplars of varying sizes were estimated on a pastoral hill site in New Zealand. The root-area ratio (RAR) is a key

parameter in assessing root reinforcement and soil stabilization. Our results showed that root biomass was positively correlated with tree diameter at breast height (DBH) and negatively correlated with both soil depth and distance from the stem. These patterns are consistent with the findings of Bischetti et al. (2007), Abdi et al. (2010), and Burylo, Hudek, and Rey (2011).

The majority of roots were concentrated within the upper 0.6 m of soil. In this surface layer, RAR exhibited significant variation across different tree sizes, but RAR values showed no notable difference in deeper layers. Considering the first soil layer, Tree 3 (DBH = 0.51 m) recorded the highest RAR values in the two closest trenches (1.5 m and 2.5 m), while Tree 4 (DBH = 0.56 m) had the highest RAR values at the 3.5 m and 4.5 m distances. The sharp decline in root density with increasing soil depth is likely attributable to the presence of bedrock and compacted subsoil at the study site.

This pattern contrasts with the findings of Genet et al. (2006), who reported higher RAR values in younger *Cryptomeria Japonica* trees compared to older ones, likely due to higher planting densities in younger stands. Root density is influenced by multiple factors, including tree species, climatic conditions, sampling time, soil type, land use practices, and root properties, as well as the spatial orientation of roots within the soil matrix (Turmanina, 1965; Gray and Sotir, 1996; Lindström and Rune, 1999; Operstein and Frydman, 2000; Genet et al., 2005; Al Afas et al., 2008a).

Although stand density did not appear to significantly influence total belowground biomass at the stand level, it had a notable effect on individual tree biomass. The Tasman poplars in this study provide a clear example: despite all trees being of the same age (26 years), those located in sparsely populated areas were substantially larger than those in high-density zones. The closer the trees stand together, the smaller sizes they are. This reflects the principle that denser stands suppress individual tree growth due to resource competition, as evidenced by DBH differences ranging from 41 cm in high-density areas to 56 cm in more open zones among the studied trees.

Field measurements indicated a mean dry biomass of 79.46 ± 11.70 kg/tree and an average carbon stock of 39.73 ± 5.85 kg/tree of a 26-year-old Tasman poplar stand. This corresponds to an estimate atmospheric CO_2 sequestration of approximately 145.68 ± 21.48 kg per tree. The biomass accumulation of Tasman poplars was found to be higher than that of other fast-growing and high-yielding species, such as Chinese fir and *Pinus sylvestris* var. *sylvestriformis* plantations (Liang et al., 2006).

Biological characteristics play a key role in explaining the gaps in biomass among different tree species of the same age or grown under similar site conditions (Liang et al., 2006). For instance, the aboveground biomass of 12-year-old *Populus × tomentosa* was considerably lower than that of 6-year-old *Populus × euramericana cv. I-72* in the same region of Shandong Province (Liang et al., 2006). Similarly, total biomass of *Populus euphratica oliv* has been shown to be substantially lower in drier and lower rainfall frequencies regions compared to more favorable environments (Chen and Li, 1984).

Table 6.4 summarizes several published DBH-only allometric equations developed specifically for the direct estimation of belowground biomass across various *Populus* species, locations, and age ranges.

The root biomass (RB) values predicted for a tree with DBH = 50 cm vary significantly depending on the model and its origin, ranging from as low as 31.43 kg to as high as 607.26 kg, reflecting differences in site conditions, species, and methodological approaches.

Among all models, Singh (1998), which is based on destructively sampled Populus deltoides trees in 1 m^3 in India (1.6 - 20.7 cm DBH), predicted the highest RB (607.26

kg with DBH of 50 cm) using separate logarithmic equations for stump, lateral, and fine roots. In contrast, McIvor et al. (2019) reported a much lower estimate (31.43 kg) for Veronese poplars in New Zealand, reflecting age-specific and local growth influence.

For allometric equations derived from similar species and sites to the current study (*Populus deltoides* × *nigra* in Ballantrae Hill Country in New Zealand), RB predictions ranged from 50.44 kg (McIvor et al., 2008) to 424.03 kg (McIvor, Douglas, and Benavides, 2009), depending on the DBH range and equation form. Notably, models with power functions (e.g., $RB = 0.0003 \cdot DBH^{3.62}$) yielded higher RB values than linear forms.

The present study developed two equations for *Populus deltoides* × *nigra* "Tasman" poplar trees aged 26 years, which estimated RB values of 83.42 kg (based on measurements) and 66.55 kg (from estimation of RDM) at DBH = 50 cm. These values lie within the middle to upper range of previously published equations.

Most of the published allometric equations were developed using field data from poplar trees with diameters below 30 cm, limiting their applicability to estimate root biomass of larger individuals. Applying these equations to estimate root biomass for trees with a DBH of 50 cm may, therefore, limit the precision of extrapolated estimates. Only a few studies, such as Das and Chaturvedi (2005), Wang (2006), Das et al. (2011), Johansson and Hjelm (2012), Chavan et al. (2022), and the present work, conducted experiments on trees with a broader DBH range larger than 40 cm and up to 56 cm, allowing for more accurate modeling of mature trees. These findings highlight the importance of developing and validating allometric relationships across a wider range of tree sizes, especially for productive, fast-growing species like *Populus* cultivated in forestry or agroforestry contexts.

Overall, the comparison emphasizes the importance of applying site- and species-specific allometric equations whenever possible. The wide variation in RB estimates for a DBH of 50 cm further illustrates the critical need for careful equation selection in carbon esimates and forest biomass modeling, particularly for mature trees in diverse environmental conditions.

Table 6.4: Summary of published DBH-only allometric equations to calculate belowground biomass of poplar species. RB is the dry root biomass.

Author	**Location**	**Species**	**DBH [cm] / Age**	**Allometric equations**	**R^2**	**RB of 0.5 m poplar [kg]**
Tandon et al. (1991)	India	*Populus deltoides*	3 - 11 years	$RB = 0.009386 \cdot (DBH)^{2.5917}$	0.95	237.52
Lodhiyal, Singh, and Singh (1995)	Central Himalaya, India	*Populus deltoides*	8 years	Stump roots = -3.7802 + 1.8910 · DBH Lateral roots = -3.3974 + 1.0080 · DBH Fine roots = -0.8636 + 0.1646 · DBH	0.934, 0.910, 0.623	145.14
Lodhiyal and Lodhiyal (1997)	Central Himalaya, India	*Populus deltoides*	4 years	Stump root = -0.3371 + 0.8813 · DBH Lateral root = -0.2485 + 0.4733 · DBH Fine root = -0.0444 + 0.0993 · DBH	0.971, 0.925, 0.777	72.06
Singh (1998)	Lucknow, India	*Populus deltoides*	1.6 - 20.7	ln(Stump root) = 2.16 · ln(DBH) + 2.71 ln(Lateral root) = 3.69 · ln(DBH) - 1.24 ln(Fine root) = 1.14 · ln(DBH) + 2.43	0.94, 0.95, 0.71	607.26
Das and Chaturvedi (2005)	Bihar, India	*Populus deltoides*	1.0 - 43.0	$RB = 69.105 \cdot [1 + \exp(3.273 - 0.077 \cdot DBH]^{-1}$	0.982	44.25
Wang (2006)	Heilongjiang, China	*Populous davidiana* Dode	2.8 - 41.3	$\log_{10}(RB) = 2.560 \cdot \log_{10}(DBH) + 1.025$	0.996	236.59
McIvor et al. (2008)	Ballantrae, New Zealand	*Populus deltoides* x *nigra* "Veronese"	8.4 - 21.3	$RB = 1.16 \cdot DBH - 7.56$	0.99	50.44

TABLE 6.4: Summary of published DBH-only allometric equations to calculate belowground biomass of poplar species. RB is the dry root biomass.

McIvor, Douglas, and Benavides (2009)	Ballantrae, New Zealand	*Populus deltoides* x *nigra* "Veronese"	18.9 - 29.0	$RB = 0.0003 \cdot (DBH)^{3.62}$	0.95	424.03
Das et al. (2011)	Bihar, India	*Populus deltoides*	1.80 - 42.30	$RB = 0.17 \cdot (DBH)^{1.38}$	0.97	37.59
Johansson and Hjelm (2012)	Sweden	*Populus* spp.	8.1 - 57.4	RB ($\geq$ 50 mm) $= 0.000010 \cdot (DBH)^{2.529000}$	0.80	66.94
Fortier et al. (2015)	Québec, Canada	*Populus deltoides* x *nigra*, *Populus canadensis* x *maximowiczii*, *Populus maximowiczii* x *balsamifera*	10.2 - 37.6	$RB = 0.1083 \cdot (DBH)^{1.6506}$	0.78	69.02
Fortier et al. (2017)	Québec, Canada	*Populus canadensis* x *maximowiczii*	7.3 - 29.5	$\ln(RB) = 1.50 \cdot \ln(DBH) - 1.69$	0.706	65.24
McIvor et al. (2019)	New Zealand	*Populus* x *euramericana* "Veronese"	19.5 - 40.2	Unpollarded: $RB = 0.11 \cdot (DBH)^{1.85}$ 12 years old: $RB = 6.26 \cdot (DBH)^{0.44}$	0.78, 0.92	181.80, 31.43
Chavan et al. (2022)	Hisar, India	*Populus* spp.	20.53 - 43.00	RB ($>$ 10 mm) $= 0.012 \cdot (DBH)^{2.537}$	0.92	245.17
Present study	Ballantrae, New Zealand	*Populus deltoides* x *nigra* "Tasman"	41.0 - 56.0	Measurement: $RB = 1.5817 \cdot DBH + 4.3339$ Model: $RB = 4.08 \cdot DBH - 137.45$	0.96, 0.99	83.42, 66.55

A sensitivity test was conducted to test the sensitivity of distance in the RDM in estimating root biomass. The results were recorded in the Table 6.5.

TABLE 6.5: Sensitivity of Estimated Dry Weight (DW) to variations in initial Distance L_0 and integration step size (distance) L in Equation 6.8 for a Tasman poplar with DBH = 0.51 m.

First distance L_0 (m)	**Distance L (m)**	**Estimated DW (kg)**
0.5	0.5	74.18
0.5	1.0	74.25
0.5	1.5	74.35
1.5	0.5	67.26
1.5	1.0	67.31
1.5	1.5	67.41

The estimated root dry weight (DW) was found to be sensitive to both the starting distance from the stem (L_0) and the integration distance (L) used in the Equation 6.8. These two parameters determine the extent of the root system captured and how accurately root area variation is represented across radial distances.

The starting distance (L_0) has a significant impact on the resulting biomass estimates. When L_0 = 0.5 m, the model includes the root dense zone immediately adjacent to the stem, where root density is typically highest. In contrast, initiating L_0 = 1.5 m excludes this high-density root zone closest to the stem (0.5 – 1.5 m), resulting in a significant decrease in the total estimated root volume. Consequently, simulations with L_0 = 0.5 m resulted in higher DW values (approximately 74 kg) than that at L_0 = 1.5 m (around 67 kg), highlighting the importance of including near-stem root zones in accurate biomass estimation.

The integration step distance L, while less influential than L_0, also affects the results due to its role in numerical precision. Smaller step sizes (L = 0.5 m) allow finer resolution of radial changes in root area, thereby providing more accurate volume estimates, particularly where root area decreases sharply with distance. Larger step sizes (L = 1.5 m) average over broader intervals and may smooth over important variations in root distribution. Nonetheless, the differences in estimated root dry biomass caused by changing L were relatively minor (such as 74.18 kg vs. 74.25 kg vs. 74.35 kg), suggesting that the model is numerically stable across realistic resolutions.

In summary, the dominant factor affecting DW estimates is L_0, which determines whether the model accounts for the high-density root zone closest to the stem. In contrast, variation in L primarily affects the integration accuracy but contributes slightly to overall differences. These findings highlighted the importance of aligning model setup with field sampling design and ensuring that critical root zones are captured in model-based volume and biomass estimations.

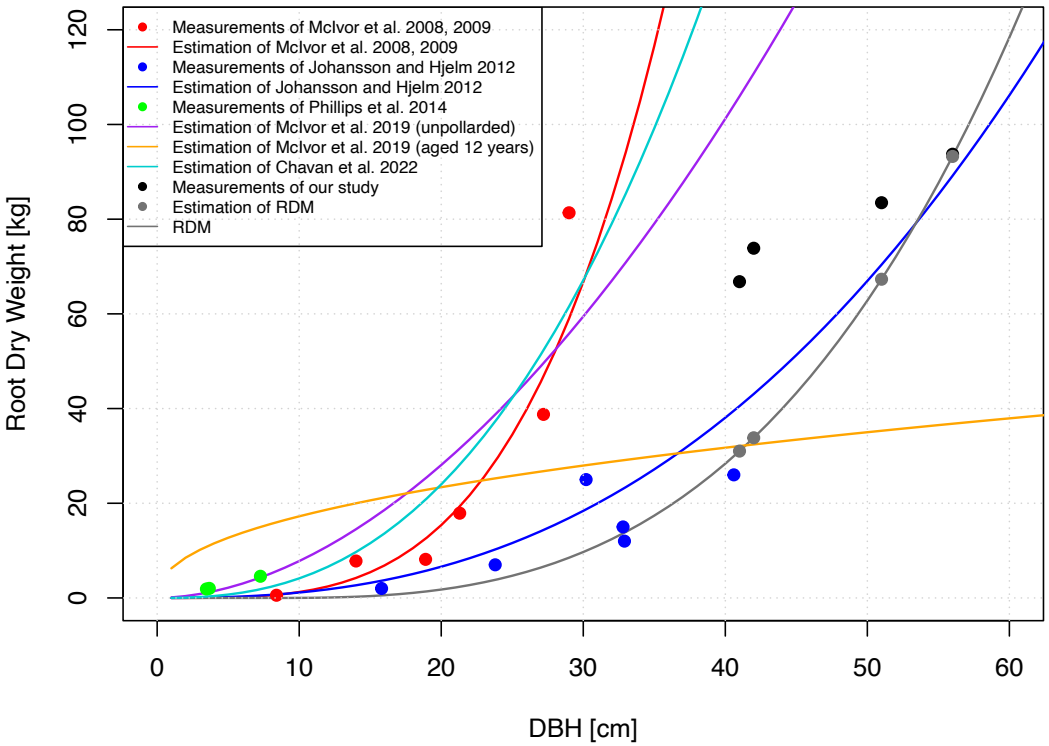

FIGURE 6.13: Comparison of Root Dry Weight versus diameter at breast height (DBH) across multiple studies and model estimations of poplar trees, including field measurements and Root Distribution Model (RDM) estimates from this study.

Figure 6.13 presents a comparison of root dry weight (DW) as a function of diameter at breast height (DBH) across several published studies, allometric equations, and field measurements, including the Root Distribution Model (RDM) developed in this study. All datasets except Johansson and Hjelm (2012) and Chavan et al. (2022) were conducted in New Zealand and focused on the same Populus hybrid (*Populus deltoides* x *nigra*), allowing for a meaningful cross-comparison under similar environmental and genetic conditions. Two studies, Johansson and Hjelm (2012) and Chavan et al. (2022), were conducted in different regions (Sweden and India, respectively), introducing additional variability due to environmental and methodological differences.

Among the New Zealand studies, McIvor et al. (2008), McIvor, Douglas, and Benavides (2009), Phillips, Marden, and Suzanne (2014), and McIvor et al. (2019) examined relatively young stands with root diameter $\geq$ 2 mm. However, their biomass estimations consistently higher than the measurements and simulations from our study. McIvor et al. (2019) data distinguished between pollarded and unpollarded trees; the pollarded model (orange curve) likely reflects growth suppression due to management, while the unpollarded curve (purple) shows a steeper biomass increase than our study.

Johansson and Hjelm (2012), despite being one of the two studies based outside New Zealand, aligns well with our field data and model estimates in the mature DBH range. Their study was conducted in Sweden on poplar stands of 16 - 23 years old and only counted roots with high diameter threshold ($\geq$ 50 mm), which may partially explain underestimation at smaller DBH compared to other studies. However, the close fit with our data at larger DBH suggests that either coarse roots dominate total biomass in mature trees or our measurement and simulation are underestimating the

entire root biomass.

Phillips, Marden, and Suzanne (2014), also conducted the root excavation in New Zealand, presents measured data on young trees with DBH below 10 cm and provides useful insight into early-stage root development. Their measurements (green dots) align well with the lower end of the findings from Johansson and Hjelm (2012) and McIvor datasets, reinforcing the validity of early growth patterns across studies. Although this dataset does not extend into the mature DBH range, it reinforces the reliability of the lower end of the RDM and allometric curves.

Chavan et al. (2022) established model-based estimates from poplar grown in India, with a observed root $>$ 10 mm. Their curve (cyan color) showed a steep increase in DW across the DBH range and tends to overestimate compared to both our results and the New Zealand-based datasets. This likely reflects a combination of regional site conditions, genetic differences in poplar species, and methodological difference (that do not count in roots smaller than 10 mm).

Our field measurements (black dots) and RDM estimates (gray dots and curve) show consistent growth patterns for mature trees, closely fit with findings of Johansson and Hjelm (2012) despite the differences in region and root diameter criteria. The alignment of the RDM with mature field data highlighted its reliability for non-destructive belowground biomass estimation. The model will perform better if data of root distribution from the stem to 1.5 m distance is collected.

Variations among studies can be attributed to differences in site location, tree age, management practices, species composition, and root diameter thresholds. Our results highlighted the strength of the RDM in capturing realistic root biomass patterns and reinforcing the importance of model calibration using context-specific measurements.

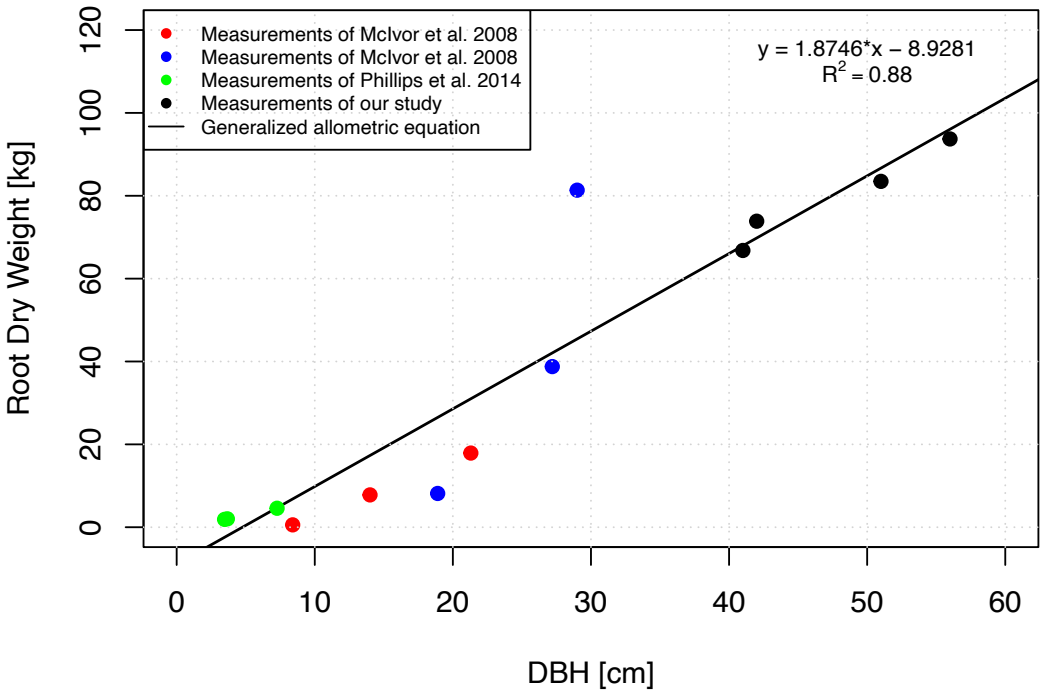

FIGURE 6.14: Relationship between diameter at breast height (DBH) and root dry weight (kg) based on measured values from studies of McIvor et al. (2008), McIvor, Douglas, and Benavides (2009), and Phillips, Marden, and Suzanne (2014), and our own measurements. The black line represents the generalized allometric equation derived from the combined data: y = 1.8746 · x – 8.9281 (R^2 = 0.88).

Figure 6.14 displayed the generalized allometric equations under the linear regression to calculate root dry weight (RDW) corresponding to a range of diameter at the breast height from 3 to 60 cm. The regression analysis, which combined data from our study with published datasets by McIvor et al. (2008), McIvor, Douglas, and Benavides (2009), and Phillips, Marden, and Suzanne (2014), all of which investigated the same *Populus deltoides* x *nigra* at the same experimental site as our study, generated a generalized allometric equation for predicting root dry weight (RDW) from diameter at breast height (DBH):

$$RDW = 1.8746 \cdot DBH - 8.9281 (R^2 = 0.88) \quad (6.12)$$

This equation shows a strong linear relationship between DBH and RDW, explaining 88% of the observed variability across the combined dataset. As shown in Figure 6.14, the generalized model fits well across a wide DBH range (3 – 60 cm), enabling both small and large trees measured in different years. The close alignment of data from various sources along the fitted line showed the consistency in root biomass accumulation with tree size, despite temporal differences in sampling campaigns.

Our study contributed valuable data for the higher DBH range (41 – 56 cm), which is underestimated in most published allometries. In contrast, data from McIvor et al. (2008), McIvor, Douglas, and Benavides (2009), and Phillips, Marden, and Suzanne (2014) primarily covered smaller individuals. Integrating these datasets allowed the model to capture a more complete biomass trajectory across developmental stages. The strong agreement between datasets also suggested that root biomass in *Populus*

deltoides x *nigra* responds predictably to stem growth under consistent environmental and management conditions.

However, it is important to note that the measured values in our study likely underestimated the actual root biomass, as discussed previously. Root distribution data were not collected between the stem and 1.5 m distance, which is the zone known to contain the highest root density, either beyond 4.5 m from the stem, where roots still contribute to total biomass. These spatial gaps may bias the measured RDW downward, particularly for larger trees where extensive lateral roots are expected.

Despite these limitations, the generalized equation provides a practical and useful tool for estimating root biomass at the stand level, especially in contexts where site-specific or species-specific models are unavailable and also a reference for further studies. The broad DBH range and uniform site characteristics reinforce the reliability of the generalized equation for use in forestry, agroforestry, and carbon accounting applications involving *Populus* plantations.

6.4.3 Carbon Storage Capacity of Tasman poplars

The comparison of measured and estimated carbon storage (W_C) and CO_2 equivalent storage (W_{CO_2}) revealed a clear evidence that the RDM underestimated the root biomass values, especially in smaller trees, with progressively improved accuracy as DBH increases. For Tree 1 and Tree 2 (DBH = 0.41 and 0.42 m), the estimated W_C values are less than 50% of the measured values, resulting in substantial underestimations of W_{CO_2} by approximately 54%. This suggests that the model underestimated root biomass, and thus carbon stock, in smaller trees, potentially due to limitations in capturing the dense root abundance near the stem or underestimating fine root quantities.

In contrast, the model performed better in Trees 3 and 4 (DBH = 0.51 and 0.56 m). For Tree 3, estimated W_C is within 19% of the measured value, and for Tree 4, the model estimate nearly matches the measured value with only an approximately 0.4% difference in W_{CO_2}. These results are consistent with findings from biomass estimation (Figure 6.13) and further confirm that the Root Distribution Model (RDM) performs more accurately in larger trees.

The results highlighted the need for calibration and correction factors when applying the RDM to smaller individual and to capture better root distribution at close distance from the stem, while also demonstrating the model's strong reliability for estimating carbon stocks in mature trees where destructive sampling is impractical.

The model can serve as a tool for estimating belowground carbon stocks in mature plantations or unmanaged stands, where destructive excavation is often not doable. Our findings also strengthens the challenge in root carbon modeling: the balance between practicality and precision. While models like the RDM offer valuable, non-destructive alternatives to field excavation, their application in carbon estimating may require DBH class or site-specific calibration to ensure accuracy across tree sizes. Moreover, underestimation in smaller trees could lead to bias in stand-level or region-level carbon inventories if not properly accounted for.

Our estimation suggested the strong carbon storage and sequestration potential of *Populus deltoides* × *nigra* "Tasman". As expected, biomass production and carbon storage increase with tree size, with mature Tasman poplars showed a great potential in providing high biomass production and immobilizing carbon. Data indicated that a mature Tasman poplar tree, at approximately 26 years of age, can store over 170 kg of carbon dioxide in its root system alone. This emphasizes the critical role of belowground biomass in long-term carbon sequestration and supports the potential of

poplar plantations in broader climate mitigation strategies. The study demonstrated the species' value not only for high-yield biomass production but also for contributing to mitigate greenhouse gas by slowing the rate of atmospheric CO_2 accumulation, and decelerate the rate of global warming. The development and management of Tasman poplars play a significant role in the terrestrial carbon cycle. Given their high carbon storage capacity, including root systems, these trees may offer strategic value in international climate negotiations - serving as a carbon sink resource for nations with extensive forested areas in the context of global carbon trading or offset schemes.

Finally, these results highlighted the potential for incorporating adaptive correction factors or integrating fine root dynamics into the existing model. By improving the representation of root structure in young trees, especially in high-resolution carbon accounting efforts such as REDD+ or national greenhouse gas inventories, the reliability of belowground biomass estimates could be significantly enhanced.

6.4.4 Limitations of the Root Distribution Model in estimating Root Biomass

While the Root Distribution Model (RDM) demonstrated strong reliability in estimating belowground carbon stocks in mature trees, particularly where destructive sampling is impractical, several limitations of the model in estimating root biomass must be acknowledged.

First, with calibrated parameters, the number of fine roots was consistently underestimated across all trees, while the number of coarse roots fluctuated depending on tree size and distance from the stem. This suggests the model may not accurately represent the distribution of fine roots, which contribute significantly to carbon storage but are influenced by local environmental variability.

Second, the model underestimated root biomass and associated carbon and CO_2 equivalent storage in smaller trees, especially in areas closest to the stem, where root density is highest. This is likely due to both modeling assumptions and the lack of fieldwork data within the first 1.5 meters from the stem, a critical zone for root biomass accumulation that was not recorded in field measurements.

Comparison between measured and modeled root biomass also showed that differences decreased with increasing distance from the stem, indicating that the model performed better at predicting root distribution farther from the stem. In general, the model worked moderately well in predicting the general spatial pattern of root biomass but underestimation near the stem remains a critical limitation. This likely due to practical challenges in recording in-situ root distributions in high-density zones, compounded by the model's sensitivity to the parameter L_0, which governs the inclusion of this zone in biomass calculations. Although variations in distance (L) between farther trenches had relatively minor impacts, the dominant factor affecting dry root weight estimates was the starting trench L_0. If L_0 is positioned too far from the stem, the model omits the most-dense region, leading to substantial underestimation. Thus, proper alignment between model structure and field sampling design is essential.

Lastly, while the RDM offers a practical, non-destructive alternative for belowground biomass estimation, its broader application across DBH classes and stand conditions may require site-specific or DBH-class calibration. Without such corrections, stand- or region-level carbon inventories risk underestimation of root carbon stocks, especially in younger or smaller individuals.

6.5 Conclusion

This study provided new knowledge and understanding of "Tasman" poplar root distribution in pastoral hill country in New Zealand as well as the performance of the Root Distribution Model in estimating root biomass of poplar trees with different sizes. A similar distribution pattern of fine roots and coarse roots across all four poplar trees was observed with more roots downslope compared to upslope. Horizontally, root quantities reduced when growing further from the stem. Vertically, most of the roots concentrated in surface soil layers, and beyond 0.60 m, the amount of roots is negligible. The larger the trees, the more extensive of its root system. The Root Distribution Model underestimated the number of fine roots while captured quite well the spatial distribution of coarse roots in all four sampled trees.

The Root Distribution Model (RDM) applied in this study offers a useful and non-destructive approach for estimating root biomass in *Populus deltoides* × *nigra* plantations. For estimating root biomass, the model effectively predicted the observed positive correlation between root biomass and tree size, as well as the negative correlation with both soil depth and distance from the stem. Calibrated with field site-specific data, the RDM successfully generates the spatial distribution of root biomass, particularly in mature trees. Although the absence of root distribution data between the stem and 1.5 m as well as beyond 4.5 m may lead to underestimation, the model remains reliable and informative. Its flexibility, capacity for integration with empirical measurements, and avoidance of destructive excavation make it a valuable tool for assessing belowground biomass and carbon stocks in forestry and agroforestry contexts. By integrating field data from both mature trees of our study and previously published studies at the same site, a generalized allometric equation was developed in this study to provide a reliable and practical approach for estimating root biomass of *Populus deltoides* × *nigra* across a wide range of tree sizes with strong predictive accuracy ($R^2 = 0.88$).

Similarly, the Root Distribution Model (RDM) proved effective for estimating belowground carbon stocks in mature "Tasman" poplar trees, aligning closely with measured values in larger individuals. However, the model underestimated carbon storage in smaller trees, highlighting the need for calibration or correction factors across different DBH. Mature Tasman poplars demonstrated substantial carbon sequestration potential, with a single 26-year-old tree storing over 170 kg of CO_2 in its root system. These findings highlighted the importance of root biomass in climate mitigation strategies and support the strategic role of poplar plantations in carbon offset initiatives.

Further studies are needed to improve the performance of the RDM in estimating root biomass, particularly by enhancing its accuracy in representing root density near the stem, where root abundance is typically highest. Its correction would bring model estimates closer to actual values. Addressing these limitations will certainly require additional fieldwork, especially focused on root distribution near the stem.

Despite these challenges, the RDM offers a promising tool for estimating belowground biomass and carbon stocks in forestry systems where destructive sampling is impractical. Its non-destructive characteristics make it particularly useful for long-term monitoring, large-scale forest inventories, and modeling efforts in managed and natural stands. In the context of climate change mitigation, the RDM supports more accurate assessments of carbon sequestration potential, especially in mature plantations with high biomass accumulation.

By contributing to improved belowground carbon accounting, the model holds promise for integration into national greenhouse gas inventories, REDD+ frameworks,

and voluntary or compliance-based carbon credit systems. As the demand for precise and verifiable carbon data grows, particularly for root biomass which remains a major source of uncertainty in terrestrial carbon models, tools like the RDM are critical for closing knowledge gaps. Future improvements of the model will further enhance its utility, ensuring more practical, reliable estimates to support climate policy, forest management, and global carbon offset initiatives.

References

Abdi, Ehsan et al. (2010). "Quantifying the effects of root reinforcement of Persian Ironwood (Parrotia persica) on slope stability; a case study: Hillslope of Hyrcanian forests, northern Iran". In: *Ecological Engineering* 36.10, pp. 1409–1416.

Ajit et al. (2011). "Predictive models for dry weight estimation of above and below ground biomass components of Populus deltoides in India: Development and comparative diagnosis". en. In: *Biomass and Bioenergy* 35.3, pp. 1145–1152. ISSN: 0961-9534. (Visited on 10/17/2022).

Al Afas, N et al. (2008a). "Growth and production of a short-rotation coppice culture of poplar—IV: fine root characteristics of five poplar clones". In: *Biomass and Bioenergy* 32.6, pp. 494–502.

Al Afas, Najwa et al. (2008b). "Dynamics of biomass production in a poplar coppice culture over three rotations (11 years)". In: *Forest Ecology and management* 255.5-6, pp. 1883–1891.

Balatinecz, John J and David E Kretschmann (2001). "Properties and utilization of poplar wood". In: *Poplar Culture in North America* Part A, pp. 277–291.

Barigah, TS et al. (1994). "Photosynthesis, leaf area and productivity of 5 poplar clones during their establishment year". In: *Annales des sciences forestières*. Vol. 51. 6. EDP Sciences, pp. 613–625.

Behera, Manoj Kumar and Nilima Priyadarshini Mohapatra (2015). "Biomass accumulation and carbon stocks in 13 different clones of teak (Tectona grandis Linn. F.) in Odisha, India". In: *Current World Environment* 10.3, pp. 1011–1016.

Berndes, Göran, Monique Hoogwijk, and Richard Van den Broek (2003). "The contribution of biomass in the future global energy supply: a review of 17 studies". In: *Biomass and bioenergy* 25.1, pp. 1–28.

Bischetti, Gian Battista et al. (2007). "Root strength and root area ratio of forest species in Lombardy (Northern Italy)". In: *Eco- and Ground Bio-Engineering: The Use of Vegetation to Improve Slope Stability*. Springer: Berlin/Heidelberg, Germany, pp. 31–41.

Blaschke, Paul M, Noel A Trustrum, and Ron C DeRose (1992). "Ecosystem processes and sustainable land use in New Zealand steeplands". In: *Agriculture, ecosystems & environment* 41.2, pp. 153–178.

Bond-Lamberty, B, C Wang, and ST Gower (2002). "Aboveground and belowground biomass and sapwood area allometric equations for six boreal tree species of northern Manitoba". In: *Canadian Journal of Forest Research* 32.8, pp. 1441–1450.

Brahim, Mohammed Ben, André Gavaland, and Alain Cabanettes (2000). "Generalized allometric regression to estimate biomass of Populus in short-rotation coppice". In: *Scandinavian Journal of Forest Research* 15.2, pp. 171–176.

Brown, Sandra, Andrew JR Gillespie, and Ariel E Lugo (1989). "Biomass estimation methods for tropical forests with applications to forest inventory data". In: *Forest science* 35.4, pp. 881–902.

Brown, Sandra and Ariel E Lugo (1982). "The storage and production of organic matter in tropical forests and their role in the global carbon cycle". In: *Biotropica*, pp. 161–187.

Burylo, M, C Hudek, and F Rey (2011). "Soil reinforcement by the roots of six dominant species on eroded mountainous marly slopes (Southern Alps, France)". In: *Catena* 84.1-2, pp. 70–78.

Campbell, John S, Victor J Lieffers, and EC Pielou (1985). "Regression equations for estimating single tree biomass of trembling aspen: assessing their applicability to more than one population". In: *Forest ecology and management* 11.4, pp. 283–295.

Chambers, Jeffrey Q et al. (2001). "Tree damage, allometric relationships, and above-ground net primary production in central Amazon forest". In: *Forest ecology and management* 152.1-3, pp. 73–84.

Chavan, SB et al. (2022). "Estimating biomass production and carbon sequestration of poplar-based agroforestry systems in India". In: *Environment, Development and Sustainability* 24.12, pp. 13493–13521.

Chave, Jérôme et al. (2005). "Tree allometry and improved estimation of carbon stocks and balance in tropical forests". In: *Oecologia* 145.1, pp. 87–99.

Chen, BH and HQ Li (1984). ") Study on biomass of natural diversifolious poplar plantations in river Talimu, Xinjiang, Western China". In: *For Sci Technol Xinjiang* 3, pp. 8–16.

Chojnacky, David C, Linda S Heath, and Jennifer C Jenkins (2014). "Updated generalized biomass equations for North American tree species". In: *Forestry* 87.1, pp. 129–151.

Christersson, Lars (2010). "Wood production potential in poplar plantations in Sweden". In: *Biomass and Bioenergy* 34.9, pp. 1289–1299.

Crow, Thomas R and Bryce E Schlaegel (1988). "A guide to using regression equations for estimating tree biomass". In: *Northern Journal of applied forestry* 5.1, pp. 15–22.

Crow, TR (1978). "Biomass and production in three contiguous forests in northern Wisconsin". In: *Ecology* 59.2, pp. 265–273.

Das, DK and OP Chaturvedi (2005). "Structure and function of Populus deltoides agroforestry systems in eastern India: 1. Dry matter dynamics". In: *Agroforestry systems* 65, pp. 215–221.

Das, DK et al. (2011). "Predictive models for dry weight estimation of above and below ground biomass components of Populus deltoides in India: Development and comparative diagnosis". In: *Biomass and bioenergy* 35.3, pp. 1145–1152.

Dickmann, Donald I and Katherine W Stuart (1983). "The culture of poplars in Eastern North America." In.

Dillen, Sophie Y et al. (2007). "Effects of environment and progeny on biomass estimations of five hybrid poplar families grown at three contrasting sites across Europe". In: *Forest Ecology and Management* 252.1-3, pp. 12–23.

Douglas, GB et al. (2006). "Interactions between widely spaced young poplars (Populus spp.) and introduced pasture mixtures". In: *Agroforestry Systems* 66, pp. 165–178.

Fang, Shengzuo, Jianhui Xue, and Luozhong Tang (2007). "Biomass production and carbon sequestration potential in poplar plantations with different management patterns". In: *Journal of environmental management* 85.3, pp. 672–679.

Felix, Erika et al. (2008). "Biomass production of hybrid poplar (Populus sp.) grown on deep-trenched municipal biosolids". In: *ecological engineering* 33.1, pp. 8–14.

Fischer, Günther et al. (2010). "Biofuel production potentials in Europe: Sustainable use of cultivated land and pastures. Part I: Land productivity potentials". In: *Biomass and bioenergy* 34.2, pp. 159–172.

Fischer, Milan et al. (2014). "Biomass productivity and water use relation in short rotation poplar coppice (Populus nigra x P. maximowiczii) in the conditions of Czech Moravian Highlands". In: *Acta Universitatis Agriculturae et Silviculturae Mendelianae Brunensis* 59.6, pp. 141–152.

Fortier, Julien et al. (2010). "Biomass and volume yield after 6 years in multiclonal hybrid poplar riparian buffer strips". In: *Biomass and Bioenergy* 34.7, pp. 1028–1040.

Fortier, Julien et al. (2015). "Plastic allometry in coarse root biomass of mature hybrid poplar plantations". In: *BioEnergy Research* 8, pp. 1691–1704.

— (2017). "Allometric equations for estimating compartment biomass and stem volume in mature hybrid poplars: General or site-specific?" In: *Forests* 8.9, p. 309.

Freedman, B (1984). "The relationship between the aboveground dry weight and diameter for a wide size range of erect land plants". In: *Canadian Journal of Botany* 62.11, pp. 2370–2374.

Friend, Alexander L et al. (1991). "Quantification of two-year-old hybrid poplar root systems: morphology, biomass, and 14C distribution". In: *Tree Physiology* 8.2, pp. 109–119.

Gasol, Carles M et al. (2007). "Life cycle assessment of a Brassica carinata bioenergy cropping system in southern Europe". In: *Biomass and Bioenergy* 31.8, pp. 543–555.

Geimer, Robert L and John B Crist (1980). "Structural flakeboard from short-rotation, intensively cultured hybrid Populus clones". In: *Forest*, pp. 42–48.

Genet, Marie et al. (2005). "The influence of cellulose content on tensile strength in tree roots". In: *Plant and soil* 278.1, pp. 1–9.

Genet, Marie et al. (2006). "Soil fixation by tree roots: changes in root reinforcement parameters with age in Cryptomeria japonica D. Don. plantations". In: *Interpraevent*. Citeseer, pp. 25–27.

Goldsmith, Leland J and Harold W Hocker (1978). *Preliminary small-tree aboveground biomass tables for five northern hardwoods*. 68. New Hampshire Agricultural Experiment Station, University of New Hampshire.

Gower, Stith T, Chris J Kucharik, and John M Norman (1999). "Direct and indirect estimation of leaf area index, fAPAR, and net primary production of terrestrial ecosystems". In: *Remote sensing of environment* 70.1, pp. 29–51.

Grace, John (2004). "Role of forest biomes in the global carbon balance". In: *The carbon balance of forest biomes*. Taylor & Francis, pp. 19–45.

Gray, Donald H and Robbin B Sotir (1996). *Biotechnical and Soil Bioengineering Slope Stabilization: A Practical Guide for Erosion Control*. John Wiley & Sons: Hoboken, NJ, USA.

Headlee, William L and Ronald S Zalesny (2019). "Allometric relationships for aboveground woody biomass differ among hybrid poplar genomic groups and clones in the North-Central USA". In: *BioEnergy Research* 12.4, pp. 966–976.

Heidari Safari Kouchi, A, T Rostami Shahraji, and Y Iranmanesh (2015). "Comparison of allometric equations to estimate the above-ground biomass of Populusalba species (Case study; poplar plantations in Chaharmahal and Bakhtiari province, Iran)". In: *Caspian Journal of Environmental Sciences* 13.3, pp. 237–246.

Heilman, Paul E, Gordon Ekuan, and D Fogle (1994). "Above-and below-ground biomass and fine roots of 4-year-old hybrids of Populus trichocarpa× Populus

deltoides and parental species in short-rotation culture". In: *Canadian Journal of Forest Research* 24.6, pp. 1186–1192.

Heilman, Paul E and RF Stettler (1985). "Genetic variation and productivity of Populus trichocarpa and its hybrids. II. Biomass production in a 4-year plantation". In: *Canadian Journal of Forest Research* 15.2, pp. 384–388.

Honer, TG (1971). "Weight relationships in open-and forest-grown Balsam Fir trees." In.

IPCC (2006). *2006 IPCC Guidelines for National Greenhouse Gas Inventories*. Accessed June 25, 2025. The Institute for Global Environmental Strategies (IGES). URL: https://www.ipcc-nggip.iges.or.jp/public/2006gl/.

Johansson, Tord and Birger Hjelm (2012). "Stump and root biomass of poplar stands". In: *Forests* 3.2, pp. 166–178.

Johansson, Tord and Almir Karačić (2011). "Increment and biomass in hybrid poplar and some practical implications". en. In: *Biomass and Bioenergy* 35.5, pp. 1925–1934. ISSN: 0961-9534. URL: https://www.sciencedirect.com/science/article/pii/S0961953411000535 (visited on 10/17/2022).

Jordan, CF and C Uhl (1978). "Biomass of a'tierra firme'forest of the Amazon Basin." In.

Ketterings, Quirine M et al. (2001). "Reducing uncertainty in the use of allometric biomass equations for predicting above-ground tree biomass in mixed secondary forests". In: *Forest Ecology and management* 146.1-3, pp. 199–209.

Kinerson, RS and I Bartholomew (1977). "Biomass estimation equations and nutrient composition of white pine, white birch, red maple, and red oak in New Hampshire." In.

King, John S, Kurt S Pregitzer, and Donald R Zak (1999). "Clonal variation in above- and below-ground growth responses of Populus tremuloides Michaux: influence of soil warming and nutrient availability". In: *Plant and Soil* 217, pp. 119–130.

Kirby, Kathryn R and Catherine Potvin (2007). "Variation in carbon storage among tree species: Implications for the management of a small-scale carbon sink project". In: *Forest Ecology and Management* 246.2-3, pp. 208–221.

Klinge, H and R Herrera (1983). "Phytomass structure of natural plant communities on spodosols in southern Venezuela: The tall Amazon Caatinga forest". In: *Vegetatio* 53, pp. 65–84.

Klinge, H et al. (1975). "Biomass and structure in a central Amazonian rain forest". In: *Tropical ecological systems: Trends in terrestrial and aquatic research*. Springer, pp. 115–122.

KS, PREGITZER (1996). "The structure and function of Populus root systems". In: *Biology of Populus and its implications for management and conservation*, pp. 331–354.

Labrecque, Michel and Traian I Teodorescu (2005). "Field performance and biomass production of 12 willow and poplar clones in short-rotation coppice in southern Quebec (Canada)". In: *Biomass and Bioenergy* 29.1, pp. 1–9.

Laureysens, Ilse et al. (2004). "Biomass production of 17 poplar clones in a short-rotation coppice culture on a waste disposal site and its relation to soil characteristics". In: *Forest ecology and management* 187.2-3, pp. 295–309.

Liang, Wan-jun et al. (2006). "Research advance of biomass and carbon storage of poplar in China". In: *Journal of Forestry Research* 17.1, pp. 75–79.

Lindström, Anders and Göran Rune (1999). "Root deformation in plantations of container-grown Scots pine trees: effects on root growth, tree stability and stem straightness". In: *Plant and soil* 217.1, pp. 29–37.

Litton, Creighton M and J Boone Kauffman (2008). "Allometric models for predicting aboveground biomass in two widespread woody plants in Hawaii". In: *Biotropica* 40.3, pp. 313–320.

Liu, WenGuo et al. (2010). "Research progress on physiologic and ecologic characteristics of poplar." In: *World Forestry Research* 23.1, pp. 50–55.

Lodhiyal, LS and Neelu Lodhiyal (1997). "Variation in biomass and net primary productivity in short rotation high density central Himalayan poplar plantations". In: *Forest Ecology and Management* 98.2, pp. 167–179.

Lodhiyal, LS and RP Singh (1993). "Biomass, productivity and litter fall in 9-year-old cottonwood plantation in tarai plains area of central Himalayas." In.

Lodhiyal, LS, RP Singh, and SP Singh (1995). "Structure and function of an age series of poplar plantations in central Himalaya: I Dry matter dynamics". In: *Annals of Botany* 76.2, pp. 191–199.

Lupi, Carlo et al. (2015). "Evaluating sampling designs and deriving biomass equations for young plantations of poplar and willow clones". In: *Biomass and Bioenergy* 83, pp. 196–205.

Magnussen, Steen and David Reed (2004). "Modeling for estimation and monitoring". In: *Knowledge reference for national forest assessments* 111.

Martin, Jonathan G et al. (1998). "Aboveground biomass and nitrogen allocation of ten deciduous southern Appalachian tree species". In: *Canadian Journal of Forest Research* 28.11, pp. 1648–1659.

McIvor, I R (2012). "New Zealand Poplar Commission National Report on Activities Related to Poplar and Willow Cultivation and Utilization 2008–11". In: A report prepared for 24th Session of the FAO International Poplar Commission in Dehradun, India.

McIvor, Ian et al. (2019). "Pollarding wide-spaced poplar trees on pastoral hillslopes alters root development". In: *Agroforestry Systems* 93.6, pp. 2227–2241.

McIvor, Ian R and Grant B Douglas (2012). "Poplars and willows in hill country-stabilising soils and storing carbon". In: *Advanced Nutrient Management: Gains from the Past-Goals for the Future* 25, pp. 1–11.

McIvor, IR, GB Douglas, and R Benavides (2009). "Coarse root growth of Veronese poplar trees varies with position on an erodible slope in New Zealand". In: *Advances in Agroforestry*. Springer, pp. 251–264.

McIvor, IR et al. (2008). "Structural root growth of young Veronese poplars on erodible slopes in the southern North Island, New Zealand". In: *Agroforestry Systems* 72.1, pp. 75–86.

McWilliam, Erica L et al. (2004). "The effect of different levels of poplar (Populus) supplementation on the reproductive performance of ewes grazing low quality drought pasture during mating". In: *Animal feed science and technology* 115.1-2, pp. 1–18.

Mowrer, H Todd and Warren E Frayer (1986). "Variance propagation in growth and yield projections". In: *Canadian Journal of Forest Research* 16.6, pp. 1196–1200.

Ngo, Ha My et al. (2023). "Analysis of Poplar's (Populus nigra ita.) Root Systems for Quantifying Bio-Engineering Measures in New Zealand Pastoral Hill Country". In: *Forests* 14.6, p. 1240.

Niklas, Karl J and Brian J Enquist (2002). "Canonical rules for plant organ biomass partitioning and annual allocation". In: *American Journal of Botany* 89.5, pp. 812–819.

Nilsson, Lars Owe and Daniel Wasielewski (1987). "Influence of fertilization in a natural Populus tremula stand". In: *Scandinavian Journal of Forest Research* 2.1-4, pp. 343–348.

OECD, IEA and IPCC lEA (1996). *IPCC guidelines for national greenhouse gas inventories*. Bracknell: IPCC.

Oelbermann, Maren, R Paul Voroney, and Andrew M Gordon (2004). "Carbon sequestration in tropical and temperate agroforestry systems: a review with examples from Costa Rica and southern Canada". In: *Agriculture, ecosystems & environment* 104.3, pp. 359–377.

Oliveira, Nerea et al. (2018). "Above-and below-ground carbon accumulation and biomass allocation in poplar short rotation plantations under Mediterranean conditions". In: *Forest Ecology and Management* 428, pp. 57–65.

Operstein, V and S Frydman (2000). "The influence of vegetation on soil strength". In: *Proceedings of the Institution of Civil Engineers-Ground Improvement* 4.2, pp. 81–89.

Overman, Johannes Petrus Maria, Hendrik Johannes Louis Witte, and Juan Guillermo Saldarriaga (1994). "Evaluation of regression models for above-ground biomass determination in Amazon rainforest". In: *Journal of tropical Ecology* 10.2, pp. 207–218.

Parsapour, Mohammad Kazem et al. (2013). "Allometric equations for estimating biomass in four poplar species at Charmahal and Bakhtiari province". In: *Iranian Journal of forest and poplar Research* 21.3, pp. 517–528.

Pastor, John, John D Aber, and Jerry M Melillo (1984). "Biomass prediction using generalized allometric regressions for some northeast tree species". In: *Forest Ecology and Management* 7.4, pp. 265–274.

Phillips, Chris J, Michael Marden, and Lambie M Suzanne (2014). "Observations of root growth of young poplar and willow planting types". In: *New Zealand Journal of Forestry Science* 44.1, pp. 1–12.

Pontailler, JY et al. (1997). "Linear and non-linear functions of volume index to estimate woody biomass in high density young poplar stands". In: *Annales des sciences forestières*. Vol. 54. 4. EDP Sciences, pp. 335–345.

Rana, Rumana et al. (2010). "FTIR spectroscopy, chemical and histochemical characterisation of wood and lignin of five tropical timber wood species of the family of Dipterocarpaceae". In: *Wood Science and Technology* 44.2, pp. 225–242.

Rebola-Lichtenberg, Jessica, Peter Schall, and Christian Ammer (2021). "Biomass production in mixed short rotation coppice with poplar-hybrids (Populus spp.) and black locust (Robinia pseudoacacia L.)" In: *GCB Bioenergy* 13.12, pp. 1924–1938.

Reed, David D (1989). "Discussion Paper Responses: Response to Study of Production Functions for Modeling Forest Biomass: An Area for Research". In: *Forest Science* 35.3, pp. 853–855.

Roy, Jacques, Harold A Mooney, and Bernard Saugier (2001). *Terrestrial global productivity*. Elsevier.

Ruark, Gregory A, George L Martin, and James G Bockheim (1987). "Comparison of constant and variable allometric ratios for estimating Populus tremuloides biomass". In: *Forest science* 33.2, pp. 294–300.

Saldarriaga, Juan G et al. (1988). "Long-term chronosequence of forest succession in the upper Rio Negro of Colombia and Venezuela". In: *The Journal of Ecology*, pp. 938–958.

Schlesinger, William H (1997). "Biogeochemistry: an analysis of global change." In.

Schwarz, M, Peter Lehmann, and Dani Or (2010). "Quantifying lateral root reinforcement in steep slopes–from a bundle of roots to tree stands". In: *Earth Surface Processes and Landforms: The Journal of the British Geomorphological Research Group* 35.3, pp. 354–367.

Singh, Bajrang (1998). "Biomass production and nutrient dynamics in three clones of Populus deltoides planted on Indogangetic plains". In: *Plant and Soil* 203, pp. 15–26.

Singh, Baljit and KN Sharma (2007). "Nutrition and growth of wheat–sorghum rotation in soils amended with leaf litter of trees before planting of wheat". In: *Agroforestry systems* 71.1, pp. 25–34.

Sulaiman, Zulkefly (2006). "Establishment and silvopastoral aspects of willow and poplar: a thesis presented in partial fulfilment of the requirements for the degree of Doctor of Philosophy (Ph. D.) in Plant Science, Institute of Natural Resources, Massey University, Palmerston North, New Zealand". PhD thesis. Massey University, Palmerston North, New Zealand.

Taeroe, Anders et al. (2015). "Allometric biomass, biomass expansion factor and wood density models for the OP42 hybrid poplar in southern Scandinavia". In: *BioEnergy Research* 8.3, pp. 1332–1343.

Tandon, VN et al. (1991). "Organic productivity and mineral cycling in plantations of Populus deltoides in tarai region of Uttar Pradesh." In.

Ter-Mikaelian, Michael T and Michael D Korzukhin (1997). "Biomass equations for sixty-five North American tree species". In: *Forest Ecology and Management* 97.1, pp. 1–24.

Terrasson, D and A Valadon (1995). "The market for poplar wood." In.

Truax, Benoit et al. (2012). "Yield in 8 year-old hybrid poplar plantations on abandoned farmland along climatic and soil fertility gradients". In: *Forest ecology and management* 267, pp. 228–239.

— (2014). "Biomass and volume yield in mature hybrid poplar plantations on temperate abandoned farmland". In: *Forests* 5.12, pp. 3107–3130.

Tufekcioglu, A et al. (2003). "Biomass, carbon and nitrogen dynamics of multi-species riparian buffers within an agricultural watershed in Iowa, USA". In: *Agroforestry systems* 57.3, pp. 187–198.

Turmanina, VI (1965). *The strength of tree roots*. Bull. Moscow Soc. Naturalists, Biol. Sec. 70, pp. 36–45.

Updegraff, Karen, Melvin J Baughman, and Steven J Taff (2004). "Environmental benefits of cropland conversion to hybrid poplar: economic and policy considerations". In: *Biomass and bioenergy* 27.5, pp. 411–428.

Van Kraayenoord, C W (1968). "Poplars and willows in New Zealand with particular reference to their use in erosion control." In.

Vande Walle, Inge et al. (2007). "Short-rotation forestry of birch, maple, poplar and willow in Flanders (Belgium) II. Energy production and CO2 emission reduction potential". In: *Biomass and Bioenergy* 31.5, pp. 276–283.

Verlinden, MS, LS Broeckx, and R Ceulemans (2015). "First vs. second rotation of a poplar short rotation coppice: Above-ground biomass productivity and shoot dynamics". In: *Biomass and Bioenergy* 73, pp. 174–185.

Walle, Inge Vande et al. (2007). "Short-rotation forestry of birch, maple, poplar and willow in Flanders (Belgium) I—Biomass production after 4 years of tree growth". In: *Biomass and bioenergy* 31.5, pp. 267–275.

Wang, Chuankuan (2006). "Biomass allometric equations for 10 co-occurring tree species in Chinese temperate forests". In: *Forest Ecology and Management* 222.1-3, pp. 9–16.

Wauters, Jean-Baptiste et al. (2008). "Carbon stock in rubber tree plantations in Western Ghana and Mato Grosso (Brazil)". In: *Forest Ecology and Management* 255.7, pp. 2347–2361.

Whittaker, Robert H and Peter L Marks (1975). "Methods of assessing terrestrial productivty". In: *Primary productivity of the biosphere*, pp. 55–118.

Wiant HV, Jr et al. (1977). "Tables and procedures for estimating weights of some Appalachian hardwoods." In.

Wilkinson, AG (1999). "Poplars and willows for soil erosion control in New Zealand". In: *Biomass and Bioenergy* 16.4, pp. 263–274.

Wullschleger, Stan D et al. (2005). "Phenotypic variation in growth and biomass distribution for two advanced-generation pedigrees of hybrid poplar". In: *Canadian Journal of Forest Research* 35.8, pp. 1779–1789.

Yemshanov, Denys and Daniel McKenney (2008). "Fast-growing poplar plantations as a bioenergy supply source for Canada". In: *Biomass and Bioenergy* 32.3, pp. 185–197.

Yin, Chunying et al. (2004). "Morphological and physiological responses of two contrasting poplar species to drought stress and exogenous abscisic acid application". In: *Plant Science* 167.5, pp. 1091–1097.

Young, HE, Leigh Hoar, and Marshall Ashley (1965). "Weight of wood substance for components of seven tree species." In.

Yu, Qibin et al. (2008). "Variation in mechanical properties of selected young poplar hybrid crosses". In: *Forest Science* 54.3, pp. 255–259.

Zabek, LM and CE Prescott (2006). "Biomass equations and carbon content of aboveground leafless biomass of hybrid poplar in Coastal British Columbia". In: *Forest Ecology and Management* 223.1-3, pp. 291–302.

Zhang, Chao et al. (2016). "Developing aboveground biomass equations both compatible with tree volume equations and additive systems for single-trees in poplar plantations in Jiangsu Province, China". In: *Forests* 7.2, p. 32.

Zhou, D (1990). "A study of oriented structural board made from hybrid poplar. Physical and mechanical properties of OSB." In.

Chapter 7

Conclusion, Limitations, and Future Outlook

7.1 Conclusion

This thesis provides new and comprehensive insights into the spatial dynamics of root distribution, root reinforcement, and carbon storage potential of forest tree species, particularly *Populus deltoides* x *nigra* "Tasman" poplar and *Cryptomeria japonica* across different environmental conditions. Through extensive fieldwork and laboratory testing, we improved, calibrated, and validated the RDM, RBMw, and RRM models, which generate root system functions for applications in bioengineering and climate change mitigation.

Findings from the New Zealand case study revealed that Tasman poplars developed extensive root systems, with both lateral and vertical distributions playing a significant role in slope stabilization and carbon sequestration. Spatial root distribution was positively correlated with tree size (DBH), but decreased with increasing soil depth and distance from the stem. By combining laboratory tensile tests and field pullout tests, this research effectively quantified root mechanical properties and calibrated the RBMw and RRM models for individual trees and at the stand scale. With field root distribution data across tree trenches and soil pits along a transect under various stand densities, we improved and calibrated RDM. These models reliably predicted root reinforcement and root biomass, particularly in the sparse stand ($<$ 200 stems per hectare) and with mature individual poplars. RDM well predicted root distribution in individual poplar trees with a density zone $<$ 200 sph and overestimated the number of roots in the dense zone $>$ 200 sph. Lateral root reinforcement model underpredicted root force in individual "Tasman" poplar trees, whereas it performed well in soil pits located in zone $<$ 200 sph. In all cases, RRM well generated basal root reinforcement. Our study in New Zealand revealed that at least 20 years are needed to reach the minimum value of lateral root reinforcement at the stand scale, and at least 30 years are required to reach root reinforcement sufficient to stabilize most of shallow landslides, depending on their disposition.

A comparative analysis of *Cryptomeria japonica* across different locations revealed distinct differences in root distribution and root reinforcement between Swiss and Japanese studied sites. While coarse root distribution remained comparable, notable differences were observed in fine root distribution and basal root reinforcement between the two sites. In Swiss forests, most root reinforcement was concentrated in the first soil layer, whereas in the Japanese stands, it was mainly located in 0.15 - 0.45 m soil depth, extending to deeper depths. Merging datasets from field root pullout and laboratory tensile tests is recommended, providing a more comprehensive and accurate dataset for calibrating the RBMw.

Furthermore, the RDM proved to generate good patterns in estimating belowground biomass and carbon stocks in "Tasman" poplar stands. A generalized allometric equation, developed by integrating our field data with existing data from the same species but covering a broader range of tree sizes at the same location, demonstrated strong predictive performance across a wide DBH range. A mature poplar tree can store over 170 kg in its root systems, highlighting the significant role of belowground biomass in long-term carbon sequestration strategies.

7.2 Limitations

Despite the promising results, several limitations of the models were identified during this work.

Root Bundle Model with Weibull survival function: Both field pullout and laboratory tensile tests predominantly focused on roots $\leq$ 40 mm in diameter. Laboratory tensile tests usually allow measurement of root mechanical properties for root diameters of up to 10 mm, as larger roots are challenging to test under laboratory conditions. In contrast, field pullout tests have limitations in testing the behavior of roots smaller than 2 mm due to equipment constraints, anchorage issues, and field setup. Additionally, testing large roots ($>$ 40 mm) in the field is very difficult due to the field setup, being labor-intensive and time-consuming. As a result, root behavior in larger diameter classes remains poorly quantified. To enhance the calibration and validation of the Root Bundle Model with the Weibull survival function, we recommend increasing the number of pullout tests involving larger roots and bundles of roots that include big roots, thereby observing maximum pullout force across a broad diameter range and supporting more accurate model validation, especially for applications involving slope stability and root reinforcement modeling.

Root Distribution Model: Despite its strengths in estimating spatial root distribution and root biomass patterns, the RDM overestimates the number of roots in poplar stands with densities of more than 200 stems per hectare. Moreover, the RDM underestimates root distribution in smaller trees and faces difficulty in estimating root density near the tree stem due to a lack of data in the most root-dense zones (0 - 1.5 m from the stem). Similarly, the lack of data beyond 4.5 m from the stem could lead to underestimated root biomass, especially in mature trees. A full excavation of individual trees is recommended to observe the entire root system and improve the model estimation. Calibration for different species, soil types, and stand structures remains essential. Another possible solution is adding a threshold to the RDM to better predict the fine root abundance.

Root Reinforcement Model: RRM tended to underestimate root force in individual trees and not predict well root reinforcement in densely populated stands ($>$ 200 sph), suggesting the need for density-dependent model calibration. The models were calibrated for specific tree species and sites; thus, their broader application requires further validation across diverse species and environmental settings.

7.3 Future Outlook

This research supports the development of advanced root modeling as a key tool in eco-engineering and forest-based climate solutions. Future studies are needed to focus on:

1. **Expanding Data Collection**: Additional field investigations are required to measure root distribution both near the stem (0 - 1.5 m) and at greater distances

beyond 4.5 m, to improve model performance and accuracy. Additionally, more data on different tree species and the influence of external factors such as soil properties, climatic conditions, etc., on root systems is also needed.

2. **Calibration Across Species and Locations**: Applying and validating the RDM, RRM, and RBMw models across a broader range of tree species, soil types, and climate conditions will enable more generalizable applications.

3. **Adding threshold to the model**: Integrating stand density thresholds and/or a threshold related to fine root distribution can significantly improve performance in mixed or dense plantations.

4. **Carbon Stock Assessment Integration**: The RDM has strong potential for integration into national and global carbon inventory frameworks. Future work should be conducted to improve and support its adaptation for monitoring, reporting, and verification systems under climate policy frameworks.

5. **Potential for Nature-Based Solutions**: The tools and findings from this thesis offer a foundation for prioritizing bio-engineering interventions and smart-targeting nature-based solutions for slope stabilization and erosion control at regional scales.

By addressing these directions, future research can enhance the predictive accuracy, scalability, and policy relevance of root system modeling in forest management and environmental engineering.

Data Availability Original datasets used in this thesis are available at:
`https://github.com/ngomy3006/root-data-poplar-cryptomeria`

This repository includes root distribution data, mechanical test results, and folder-level organization for Tasman poplars and *Cryptomeria japonica* trees, as used in the modeling and analysis described throughout this thesis. Access is granted upon request.